University of Southampton

Faculty of Engineering and Applied Science

Jet Noise Source Location

by

Stewart Alexander Lindsay Glegg

Thesis submitted for the degree of
Doctor of Philosophy in the
Institute of Sound and Vibration Research

January 1979

Quotation

"If your experiment needs statistics, you ought to have done a better experiment"

Lord Rutherford

To G.L.G.

LIST OF CONTENTS

List of Figures

LIST OF SYMBOLS

a_o	Speed of sound
$a_\omega(z)$	Distribution of sources within coherent region at freq.'ω'
B_e	Effective bandwidth of spectral window
B_eT	Product of B_e with length of signal received
$C_\beta(\alpha)$	Coherence of signals measured at α and β on polar arc
C_m	Coherence of signals measured at microphone m and ref mic.
$D_\omega(y,\alpha)$	Directionality of coherent region located at 'y'
$d(\alpha)$	Directionality of source distribution
E_m	Error in measured coherence at microphone 'm'
E	Typical value of E_m
f	Frequency in Hz
$G_{xy}(\omega)$	C.P.S.D. at freq. 'ω' between signals x and y
$I(\omega)$	Power spectral level of sources at freq.'ω'
K	Acoustic wavenumber = $2\pi/\lambda$
L	Aliasing length
M, M'	General integer variable, total number of microphones in half array (Sec. 3.6, 3.7.)
M_c	Convection Mach No.
M_w	Mach no. of wind
M_α	Resolved Mach of wind
m	Integer variable
N	General integer variable
N_L	Engine speed variable as % of maximum operational fan shaft speed.
NS	No. of samples in data block
$o(\ )$	Order function
$P_\omega(\alpha)$	Power spectral density at angle 'α' on polar arc at freq.ω.
$p(\alpha,t)$	Pressure fluctuations at 'α' on polar arc
$p_\omega(\alpha)$	Frequency component of pressure fluctuations at 'α' on polar arc
$Q_\beta(y)$	Source strength variable viewed from β
$Q(y)$	Source strength variable
$q(y,t)$	Source fluctuations as function of time at location 'y'
$q_\omega(y)$	Frequency component of source fluctuations at 'y'
$q_I(y)$	Source image at freq. 'ω'

R	Polar arc radius
$R_{\beta}(\alpha)$	C.P.S.D. at frequency 'ω' between signals at α and β on Polar arc
S	Standard deviation
t	Time variable (with subscripts)
T	Length of time averaging
$W(\ )$	Window function
$w(k\sin\alpha)$	Weighting function
x	Distance variable
y	Distance variable
$\bar{y},(y_1,y_2,y_3)$	Spatial cartesian vectors
$Y_e(M)$	Effective bandwidth of spatial data window
z	Distance variable
α	Angle on Polar arc
α_m	Aperture angle (max value of α in array)
β	Reference angle on Polar arc
Δ	Microphone spacing in$(\sin\alpha)$
λ	Acoustic wavelength
π	= 3.14159
τ	Time or time delay variable with subscripts
ϕ	Phase variable
ω	Angular frequency

UNIVERSITY OF SOUTHAMPTON

ABSTRACT

FACULTY OF ENGINEERING

INSTITUTE OF SOUND AND VIBRATION RESEARCH

Doctor of Philosophy

JET NOISE SOURCE LOCATION

by Stewart Glegg

This thesis describes the development of a technique which evaluates the relative strengths of noise sources on jet engines. At the outset the technique, known as Polar Correlation, had been shown to work in practice, and the purpose of this project was to refine it into a method suitable for general application.

In this thesis each aspect of this technique has been covered, starting with its theoretical background and concluding with its application to jet engines. Also included in this work is a discussion of the practical application of the technique, the development of data analysis systems, and experimental results on a number of different rigs.

The Polar Correlation technique samples the wavefield produced by a linear distribution of acoustic sources. From these measurements a resolution limited source image is obtained by inverting the wavenumber spectrum of the acoustic source distribution. The theoretical background to the technique, and the implications of the approximations which are required, are outlined in Chapter Two. The practical aspects of the technique and its application are described in Chapter Three. A major part of the work has been the development of data analysis systems which provide fast and efficient data reduction. Several different methods have been used and these are described in Chapter Four. The application of the technique to hot and cold model air jets, and full scale jet engines (specifically the Rolls Royce RB.211) are described in Chapters Five and Six.

In conclusion this technique has been used successfully for the location of jet noise sources at both full and model scale, and data analysis facilities for the technique have been established at both ISVR, Southampton University, and Rolls Royce Ltd,

CHAPTER 1: INTRODUCTION

1.1. INTRODUCTION

One of the major aspects of controlling the noise output from a complicated machine such as a jet engine is the evaluation of the areas to which noise reduction techniques can be most effectively applied. Only when the relative significance of each noise source is known can the most effective action be taken to reduce the overall noise output. While this is a very general problem which is significant in many applications of noise control, the work described in this thesis is limited to the evaluation of the noise sources on aero-engines. On a modern aero-engine there are several different sources of noise and several channels through which this noise may escape to the acoustic far field. For instance engine fan noise is transmitted either upstream and out of the engine inlet, or downstream and out of the by-pass duct exit, while combustion noise is emitted mainly by the hot core exhaust (see Figure 1.1). As well as these sources there also exists jet noise caused by the turbulent mixing of the jet exhaust with the outside medium. Determination of the relative levels of these sources permits the development engineer to concentrate acoustic treatment on those sources where the greatest net benefit is anticipated.

The simplest and most widely used technique of estimating the strengths of acoustic sources on jet engines is prediction and spectral analysis. If the spectral characteristics of each type of source can be predicted, then the measured frequency spectrum will show the level of each source. However this technique is limited to sources with known spectral characteristics, and it is only possible to differentiate between sources which do not contribute equally at a particular frequency. Although these methods have been used for many years in the aircraft industry, they are not very satisfactory because too much has to be assumed about the acoustic sources. Therefore there is a requirement for techniques which measure the relative strength of each source within a distribution at a specified frequency, without the necessity for the source characteristics to be known in advance. This thesis will describe a technique, known as Polar Correlation, which may be used to evaluate the relative strengths of sources along the axis of an aero-engine.

1.2. THE POLAR CORRELATION TECHNIQUE

Before reviewing the many different methods which have been used to evaluate sources of noise, the principle of Polar Correlation will be introduced. The noise sources on a jet engine emit acoustic waves which propagate into the acoustic far field, and the fluctuations at any point in this field are determined by the strength and distribution of acoustic sources on the engine. For example consider three simple harmonically fluctuating sources on a line as illustrated in Figure 3.1. The wavefield at a fixed instant in time for each source in isolation is illustrated on the left of this figure, and the overall wavefield is given by the sum of these three. The principle of source location on which Polar Correlation is based can be demonstrated by considering this simple model. Polar Correlation evaluates the source strength distribution by taking measurements on a polar arc of constant radius in the acoustic far field (see Figure 3.1). First consider the source at A in isolation: since this lies at the centre of the polar arc, at any fixed instant of time the fluctuating pressure on the polar arc will be constant, as illustrated by the top diagram on the right of Figure 3.1. However the waves from the source at B cross over the polar arc, and so at any fixed instant in time there will be a variation of pressure around the polar arc. This variation is shown on the right of Figure 3.1 and is found to be cosinusoidal as a function of the sine of the angle 'α'. Similarly for the source at C which lies further downstream from the polar arc centre. In this case the polar arc passes through more peaks and troughs of the wavefield and the variation of pressure as a function of $\sin(\alpha)$ yields a cosine wave of higher frequency.

When all three sources are radiating at the same time the total wavefield on the polar arc will be given by the sum of these three cosine waves, illustrated on the bottom right of Figure 3.1. However each cosine wave represents a term in the Fourier series which represents the total wavefield. The amplitude of each cosine wave is determined by the strength of the source, and the frequency by the location of the source. It is a relatively simple matter to solve this Fourier series to determine the strength and location of each source. In the more general case, sources are continuously distributed along the axis of an aero-engine, and therefore the Fourier series illustrated here, becomes a Fourier integral.

However in the case of aero-engines the acoustic sources are also randomly fluctuating, which means that the effective source strength at any frequency will vary with time. Therefore it is necessary to consider an averaged source strength. This may be obtained by considering the cross power spectral density* on the polar arc. This quantity is chosen because it retains the important phase relationships of the randomly fluctuating field which are required to evaluate the source distribution. It will be shown in Chapter 2 that there is a Fourier integral relationship between the distribution of source strength and the cross power spectral density in the acoustic far field. This integral relationship may be inverted numerically to yield a resolution limited image of the acoustic source distribution.

It should be noted that in principle only an "apparent" image of the source distribution can be obtained. The word "apparent" is used in this context because there are many different source distributions which can create the same acoustic far field. Therefore there are many different reconstructions which can be obtained from the same set of far field measurements, and the results which are obtained depend on the assumptions made about the source distribution. These assumptions constitute the model of the source distribution and the value of the reconstructed image depends on the accuracy of this model. This point will be considered in more detail in Chapter 2, and the rest of this chapter will describe some of the other methods of source location which have been used.

1.3. LITERATURE REVIEW

1.3.1. Sonar

The first engineering application of measuring acoustic waves to determine their source originated in the Great War with the development of sonar. This technique was developed by Solokov and its principle application is the detection of submarines. Like Polar Correlation, sonar techniques use an array of transducers to evaluate an acoustic wavefield. From these measurements the angle of arrival of the acoustic wave is estimated, and this yields the bearing of its

*The cross power spectral density is sometimes referred to as the cross spectral density in other texts.

source to the array; by using two arrays, two bearings are obtained and this enables the position of the source to be evaluated. Sonars can be either active or passive, the former relying on reflections of a reference acoustic signal, while the latter relies solely on the noise emitted by the target. There is a large amount of literature associated with sonar, and very sophisticated techniques have been developed to enhance resolution (e.g. Davids, Thurston and Mueser (1952), van Buren (1973)), and to reduce signal to noise ratios (Brown and Reynoulds (1959)). Although Polar Correlation and sonar have a great deal in common, their application is very different. In Polar Correlation it is the relative strengths of sources at approximately known locations which are required, while with sonar it is the detection of a single source in a noisy environment which is evaluated. Therefore in developing Polar Correlation to date, little use has been made of the more sophisticated techniques used in sonar analysis. However, there may be some aspects of sonar technology which can be used in the future to optimise the Polar Correlation technique.

1.3.2. Holography

Another method of source identification which has been developed is acoustic holography. This is a method of measuring the acoustic wavefield on a plane so that it may be reconstructed either optically or numerically to give an image of the sources contributing to the hologram.

In its active application holography is used to obtain the image of reflecting objects, which are illuminated using sound waves. However, in order to overcome resolution problems the size of the illuminated objects must be very much larger than the acoustic wavelength of the reflected sound. Therefore in most examples of this technique ultrasonic waves have been used (Mueller (1971), Aoki (1970), El-Sum (1969))

Passive holography has also been used in a number of applications. For instance a comprehensive study of vibrating plates using holographic methods was undertaken by Watson (1973). In his study Watson measured a microphone signal on a plane in the acoustic far field of the vibrating plate; this was then added to the signal used to drive the plate and the combination illuminated an intensity sensitive diode light on the back of the microphone. By scanning

the microphone over the hologram plane and photographing the diode light, an optical hologram was produced. Illuminating the hologram with laser light then gave the image of the field from the vibrating plate. Similar results have been reported by Greene (1969), who recorded the distribution of hologram intensity directly without recourse to optical processing.

Passive holography used to determine the location of a single source producing Gaussian noise is reported by MacDonald and Shulthesis (1968), and Hahn (1975). Also Uhea et al (1975) have reported using holography to identify the source of gear noise. However holography is very sensitive to signal/noise errors and so Sasaki et al (1977) have developed a more sophisticated method of signal processing using polyspectra. Numerical examples show this provides improved images but this method can only be applied to quasi-periodic sources.

From this review of holographic techniques it would appear that some of the major problems with source location on jet engines have not been attempted. First there is the practical problem of applying a holographic technique to a full scale jet engine on an open air test bed, and secondly the application of this method to source distribution with partial spatial coherence has not been investigated. These problems may result in limitations of the holographic technique, which could prove difficult to overcome.

1.3.3. Measurement of Jet Noise Source Distributions

One of the environmental noise problems of the last twenty years has been the effect of jet aircraft noise on the community close to airports, and this has resulted in a considerable amount of research into all aspects of jet engine noise. The mechanism which causes jet noise was originally explained by Lighthill (1952) in terms of the turbulent mixing process between the jet and the medium into which it exhausts. However to improve the understanding of jet noise it is useful to have some knowledge of the distribution of noise source intensity in the jet, and it is this objective which has inspired a number of investigations into the acoustic source distributions along model air jets.

Some of the earlier attempts to measure source distributions in jets have concentrated on evaluating various properties of the turbulence and relating these to the acoustic output by theoretical

considerations (see for example Dyer (1959), Maestrello & McDavid (1971)). However more recently a number of techniques have been developed which measure directly the distribution of source strength along both model and full scale jets, and in this section each of these methods will be reviewed.

a) Shields

The first attempts to measure the distribution of acoustic source strength within a jet from accoustic far field measurements alone utilised shields to eliminate part of the source distribution (Potter & Jones (1967), Bishop et al (1971)). The principle of this method relies on"what cannot be seen cannot be heard", which considering the discrepancy in wavelengths between optics and acoustics is perhaps an oversimplification. More recently, Damms (1977) has developed a theoretical interpretation of this type of measurement, and this has been applied to some data from the RB.211 engine (Beasley (1977)). The problem with this method is that the jet engine has to be modelled not only as a line source but also as a number of individual sources. The advantages of this technique are that first, the individual sources can be placed at locations where point sources are known to exist, thus theoretically giving infinite resolution and secondly, the directionality of each of these modelled sources can be evaluated. However there are also some major disadvantages: first, as the number of modelled sources are increased, the method used to calculate the source levels becomes numerically unstable and secondly, there is a major experimental problem in applying this method to a full scale jet engine. On the RB.211 a screen 28m long and 10m high was used in 26 different locations. This programme took several days to complete and required a number of engine runs. Compared with the microphone array techniques which have been used to obtain similar information on a single engine run, the shield technique would appear to have major practical disadvantages.

b) Causality Correlation

An ingenious technique of source location, known as Causality Correlation, has recently been developed by Siddon (1973). This technique has primarily been developed to measure jet noise sources although in principle it may also be used on other source mechanisms. To describe this technique it should be noted that the contribution

of an acoustic source to the far field intensity depends not only on the fluctuations of that source but also on its interference effects with other sources. Therefore to predict the acoustic far field from source measurements alone requires the evaluation of not only each source amplitude but also its cross-correlation with every other source. Attempts to measure this complete description of the sources in model air jets have never been successful because of the enormous measurement programme required and the fundamental difficulties of measuring the source strength. Therefore Siddon has proposed a method of source strength measurement which automatically includes the interference between each source.

The principle of Siddons technique is to cross-correlate source fluctuations with the acoustic far field signal. Since the far field signal includes contributions from all the sources within the distribution, all interference effects are automatically included, and the resultant correlation at the appropriate time delay specifies the effective radiated intensity of the source fluctuations being measured.

The advantage of this method is that it offers a direct link between a local region of the source and a specific far field observer, thus avoiding the resolution problem associated with the other far field methods. However,it should be noted that when considering the complete source distribution, probe measurements must be taken at intervals which are small compared with the acoustic wavelengths in order to account for interference effects, and to ensure integral closure (i.e. the integrated source intensity gives the far field level). There are also a number of quite severe practical problems which may offset the advantage of ideal resolution, in particular:-

i) Although the method offers at least an order of magnitude saving in experimental effort compared with source measurement alone, the level of effort required is still very appreciable and leads to a degree of detail beyond that required in all but the most fundamental research applications.

ii) Application of this technique requires a quite detailed knowledge of the noise producing mechanisms involved,since this determines the quantity to be measured by the source probe.

iii) The employment of a probe in the source region raises the problem of probe generated noise. The criterion for probe noise is particularly severe for causality correlation (see Siddon (1973)), since it must be negligible compared to that generated by the locally correlated source region in which the probe is located. This is a severe restriction and more seriously, there is no obvious experimental method of ensuring that it is obeyed. The probe noise could frequently be negligible compared to that produced by the total source region, while still being the dominant contributor in the locally correlated region in which it is placed. It is noted however that remote sensing devices, for example the Laser Doppler Velocimeter for velocity measurements, could eliminate this particular problem area.

iv) Finally it should be noted that the amplitude of the correlations to be measured will frequently be small, the average correlation coefficient being of the order of the reciprocal of the square root of the number of locally correlated regions contained in the total source array. Damms (1977) has also pointed out that they could also be appreciably smaller than this if a significant part of the 'source' signal is composed of the convection of a frozen pattern of fluctuations past the probe, as these will not contribute to the far field pressure.

In conclusion, it would appear that these difficulties make Causality Correlation unsuitable as a general purpose source location technique. Its application is probably restricted to specific research problems, but even here considerable care in its practical implementation is required if erroneous or misleading information is to be avoided.

c) Acoustic Mirrors

The first attempts to use the focusing properties of concave surfaces for source location in the context of aerodynamic noise appear to be those of Grosche (1968) and Chu et al (1972) (see also Grosche (1973)). The former used an elliptical mirror while the latter a parabolic one. The parabolic mirror focuses all rays arriving parallel to the mirror axis onto a microphone placed at the focal point. This is strictly only appropriate for a source at infinity, but it has been shown by Glegg (1975) that in practice this is not a severe restriction. It should be noted, however, that the parabolic

mirror can only locate the line (i.e. the mirror axis) on which the source must lie, and does not have resolution along this axis. However, the elliptical mirror focuses radiation from a source placed at one focal point to a microphone placed at the other. It therefore provides three dimensional focusing which can be an advantage.

The characteristic of acoustic mirrors which permits their use as source location devices is that the path length from the source at one focus to the microphone at the other, via the mirror surface, are equal. Thus if the amplitude and phase of wave emitted by the source is constant on the surface of a sphere centred on the source, all the rays will arrive at the microphone in phase and interfere constructively to yield a large signal. Alternatively, if the source does not lie on the focus, the rays reaching the microphone will have different path lengths and will interfere destructively, resulting in a smaller microphone signal.

However, the requirement for omnidirectional amplitude and phase restricts such techniques to evaluating the effective monopole source strength. It should be emphasised that this is a common feature of all far field source location techniques and is an example of the inherent non-uniqueness of the relationship between the acoustic far field and the source distribution (Ffowcs-Williams (1973), Kempton (1976)). However, the image of a source with directional characteristics similar to jet noise has been investigated by Glegg (1975) and it was shown that the effect of the directionality was not severe, merely degrading the resolution of the mirror.

While acoustic mirrors have been very successful as source location tools at model scale, there is a major practical problem in applying the same technique to full scale engines where the wavelengths of interest are very much longer. It may be shown that to obtain resolution of about 5 acoustic wavelengths, the mirror diameter must be about 50-75% of the customary far field measurement distance. On a full scale engine this could result in mirrors which are at least 10 m in diameter, and an accurate scanning mechanism for this mirror would obviously introduce major mechanical problems on an open air test site. Consequently acoustic mirrors have never been developed for full scale engine testing.

d) Microphone Arrays

Perhaps the major practical problem of using acoustic mirrors for source location on jets is their lack of applicability to different test rigs. A mirror is a large and expensive apparatus and has to be optimised for a particular application. Consequently there are major practical problems in designing and building a mirror which may be used on a number of test rigs at both model and full scale. As a result,microphone array techniques have been developed which provide equal ability to resolve sources as the mirror, and may be applied to many different rigs. In principle a microphone array technique is merely a simplification of the mirror. Rather than sample a segment of the wavefield and acoustically construct a source image, the microphone array samples the wavefield at specific points, and constructs the source image using signal processing techniques.

In the last five years a number of microphone array techniques have been developed specifically for the evaluation of jet noise sources. It would appear that the most widely applied of these techniques are the Acoustic Telescope (Billingsley and Kinns (1976)) and Polar Correlation (Fisher et al (1977)), while other techniques due to Parthasarathy (1974), Kinns (1976) and Maestrello and Liu (1976) have also been reported with a limited set of experimental results.

The Acoustic Telescope and Polar Correlation were developed concurrently at Cambridge University by Billingsley and Kinns, and at Southampton University by Harper-Bourne respectively, both under the sponsorship of Rolls Royce (1971) Ltd. Although these two techniques work on different principles, it has transpired that there is very little difference between the results which can be obtained using either technique. A detailed comparison by Damms (1977) concludes that theoretically there is no difference between these methods, and so the only advantages of one method over the other must result from practical considerations. In this respect each technique has its own advantages, which depend on the particular requirement of each test. The advantage of the Acoustic Telescope is its very fast data analysis which enables source distributions to be computed in real time; however it can only be applied using a specially developed mini-computer and it does not provide any intermediate storage medium between the microphone signals and the computed source distribution. Conversely

Polar Correlation requires a longer data analysis procedure but has the advantages of providing an intermediate data storage medium, and requiring less sophisticated data analysis systems.

The source location method used in the Acoustic Telescope relies on the same principle as sonar techniques. The Telescope consists of a linear array of equally spaced microphones in the acoustic far field, and may be focused onto a source in the distribution. The focusing is achieved by linearly summing the signals from each microphone in the array at the time delay appropriate to the acoustic propagation time from the source to each microphone. Therefore focusing is achieved in the same way as the acoustic mirror. The Polar Correlation technique however samples the signals in the acoustic far field in a similar way using microphones on a polar arc and utilises the relationship between amplitude and phase of these signals at specific frequencies to construct a wavenumber spectrum of the source distribution. Inverting the wavenumber spectrum provides an image of the source distribution. Since both techniques sample the wavefield using similar methods, a number of the principles developed in this thesis on wavefield sampling are equally applicable to both techniques.

In order to compare these two methods with other microphone array techniques the principle of each will be described and their limitations discussed.

i) Parthasarathys' Method: In this technique the signals from two microphones in the acoustic far field are cross correlated. Then by assuming that each source in the distribution is uncorrelated and produces pure white noise, the evaluated cross correlation gives the distribution of source strength intensity along the jet. The fallacy of this method lies in the assumptions made about the noise sources. Jet noise sources do not necessarily produce purely random white noise signals, and the source spectrum may vary along the axis of the jet. In principle this method is limited by these assumptions to very specific applications and the results presented (Parthasarathy (1974)) do not provide particularly well resolved source distributions.

ii) Binaural Source Location: This method was developed by Kinns (1976) and evaluates the centroid of a source distribution from the measured phase between two closely spaced microphones in the acoustic

far field. In common with other source location techniques this method assumes that the jet noise sources lie on the centre line of the jet, and in principle this method is the zero aperture limit of Polar Correlation. While this method locates the source centroid exactly (within the limitations of its source strength definition) it provides no resolution and therefore gives no information about the distribution of sources. Consequently it is of only limited application.

iii) Maestrellos' Method: This technique developed by Maestrello and Liu (1976) uses a microphone array similar to that of Polar Correlation, with microphones equally spaced on a polar arc in the acoustic far field. By cross correlating the signals between each microphone it is shown that there is a double wavenumber integral relationship between the measurements and the cross spectral density between sources in the distribution. This relationship will be demonstrated in the development of the theory pertaining to Polar Correlation in Chapter 2, and it is at this stage that the two methods diverge. In Polar Correlation the source strength is defined so that interference effects between sources are included in a single source strength definition, which reduces the relationship with the measurements from a double to a single wavenumber integral which may be inverted. In Maestrellos' method the double integral is solved using a curve fitting procedure. There are two criticisms of Maestrellos' work: first his analysis does not admit the existence of phase relationships between coherent sources, and this automatically excludes any convected source model of jet noise. Secondly, no analysis of measurement error sensitivity has been undertaken and according to Yardley (1974) this is likely to cause uncharacteristic errors in the numerical inversion procedures used to obtain source distributions.

1.3.4. Conclusion

In this section an attempt has been made to review all the relevant methods of acoustic source location. Specifically we are interested in methods which can be applied to the evaluation of sources on jet engines. Although there are many methods which have been applied to model scale jets, there are only two which have been used without major practical difficulties at both full and model scale:

these are the Acoustic Telescope and Polar Correlation. It has been shown that although these two techniques use different methods of analysis, they are capable of producing the same results and are subject to the same limitations. The choice of technique therefore depends on the requirements of a particular test.

In the following chapters, development work on the Polar Correlation technique will be described. However due to its close relationship with the Acoustic Telescope a number of the principles developed are equally relevant to both tehcniques, particularly those relating to the sampling of wavefields. It is hoped that this work will go some way to justify the claim that Polar Correlation is at present one of the two more sophisticated techniques for evaluating the distribution of source strength along jet engines.

CHAPTER 2: THE THEORY OF SOURCE LOCATION TECHNIQUES WITH PARTICULAR REFERENCE TO POLAR CORRELATION

2.1. INTRODUCTION

This chapter describes in detail the theoretical background to the Polar Correlation technique. However since this technique has a great deal in common with other source location techniques used to evaluate the source distributions on jet engines, a number of the theorems developed have a far more general application.

The basic restriction of source location methods which use one dimensional microphone arrays, such as Polar Correlation or the Acoustic Telescope (Billingsley & Kinns (1976)), is that the source distribution must be modelled as an effective line source. Therefore the starting point of this chapter is the solution to the wave equation which describes the acoustic field from such a distribution of sources. From this the principle of the wave number spectrum and its extension to Polar Correlation is developed.

One of the purposes of this chapter is to evaluate the significance of the assumptions and restrictions which are implicit in the application of Polar Correlation. These are discussed in terms of the evaluated source image, and the effects of axial resolution, aliasing lengths, and three dimensional effects are demonstrated. These effects are not solely a feature of Polar Correlation but are equally important in other methods of source location.

One of the inherent problems with any method of source location which uses measurements in the acoustic far field is the non-uniqueness of the results. This ambiguity arises because there are many different distributions of sources which cause the same acoustic far field; however from the far field information alone any source location technique can only define one apparent source distribution. This can be defined as the equivalent monopole source distribution, which may, in principle, be replaced by many other distributions of higher order multipole sources. At first sight this ambiguity might be considered so catastrophic that all far field source location techniques are rendered useless. However in practice the acoustic far field information is rarely the only information available. When undertaking an experiment of this type it is probable that the approximate location of each

source is known, and the information required is the relative level of each source within the distribution. To a certain extent this overcomes the ambiguity of the results since they may be checked against this additional information.

One of the problem areas of practical source location techniques is their application to randomly fluctuating sources with arbitary spatial coherence. This aspect is discussed in some detail and two different definitions of source level are developed. The first definition gives the effective source strength as seen by an observer at a reference position, and the second defines the relative strength of each region of coherent sources. The latter definition requires that each coherent structure is the same throughout the source distribution, and is therefore of limited application, whereas the former definition is more general but is also more difficult to both measure and interpret.

Finally it should be noted that this chapter is entirely of a theoretical nature and no attempt has been made to describe theorems in terms of their practical application. Therefore any reader who is only interested in applying this technique should immediately turn to Chapter Three, where the principles and application of this technique will be described without so much mathematical analysis.

2.2. THE WAVENUMBER SPECTRUM PRINCIPLE

The acoustic signal from a linear array of sources of strength $q(y,t)$ may be defined by the integral

$$p(\alpha,t) = \int_{-\infty}^{\infty} q(y,t - r/a_o)\, dy/r \qquad (2.2.1)$$

This is the well known solution to the wave equation in an acoustic field free from reflections; the pressure $p(\alpha,t)$ may be taken on a polar arc of constant radius R (see Figure 2.1) and the distance 'r' is defined as the propagation path length between the source at 'y' and the measurement point.

By taking the Fourier transform of both sides of this equation, a complex valued acoustic field strength is defined at the fixed frequency 'ω':

$$\tilde{p}_\omega(\alpha) = \int_{-\infty}^{\infty} \tilde{q}_\omega(y)\, e^{iKr}\, dy/r \qquad (2.2.2)$$

where $K = \omega/a_o = 2\pi/\lambda$.

At this stage it is convenient to note that in the acoustic far field, where the polar arc radius R is very much greater than the length of the source distribution L, the propagation path length can be approximated by $r = R - y\sin\alpha + o(\frac{y^2}{R})$; this is a fundamental approximation to all that follows and the effect of ignoring higher order terms in this series will be demonstrated later in this chapter.

Further, in the amplitude term of 1/r, the dependence on 'y' may be dropped altogether without any significant loss of accuracy, and the complex acoustic field is defined as

$$\tilde{p}_\omega(\alpha) = \frac{e^{iKR}}{R}\int_{-\infty}^{\infty} \tilde{q}_\omega(y)\, e^{-iKy\sin\alpha}\, dy \qquad (2.2.3)$$

This equation shows a Fourier transform relationship between the distribution of source strength and the complex pressure amplitude on the polar arc, and the quantity $\tilde{p}_\omega(\alpha)$ is known as the wavenumber spectrum of the source distribution $\tilde{q}_\omega(y)$. This suggests that by taking the inverse Fourier transform of $\tilde{p}_\omega(\alpha)$ as a function of '$K\sin\alpha$'*, it is possible to evaluate the distribution of source strength $\tilde{q}_\omega(y)$.

2.3. PHYSICAL PROBLEMS OF WAVENUMBER SPECTRA

It has been shown in the previous section that in principle the wavenumber spectrum may be used to evaluate the source distribution from measurements in the acoustic far field. However in practice there are several physical limitations which prevent an exact solution being obtained. These problems restrict the solution of the wavenumber spectrum so that at best only an apparent source image may be evaluated. This section will discuss the physical restrictions which are imposed, and their effect on the apparent source image.

a) Resolution

In order to evaluate the inverse Fourier transform of a function such as the complex acoustic field, $\tilde{p}_\omega(\alpha)$, it is necessary to measure this function between the infinite limits $-\infty < K\sin\alpha < \infty$. However this is physically impossible since measurements can only be made between the finite limits $-K\sin\alpha_m < K\sin\alpha < K\sin\alpha_m$ where $0 < \sin\alpha_m < 1$. In order to investigate the significance of this restriction, it is conven-

* (Note : 'K' is kept constant)

ient to multiply the acoustic field measurements by an arbitary weighting function which is zero outside the limits of the measurements. The infinite limits to the integral may then be used and the measurement restrictions are defined by the effects of the weighting function on the source image.

The measurable source image, $\tilde{q}_I(y)$, can therefore be calculated from the inverse Fourier transform of the acoustic field, $\tilde{p}_\omega(\alpha)$, multiplied by an arbitary weighting function $w(K\sin\alpha)$ which is zero outside the measurement limits of $\pm K\sin\alpha_m$:

$$\tilde{q}_I(z) = \frac{1}{2\pi}\int_{-\infty}^{\infty} \tilde{p}_\omega(\alpha)\, w(K\sin\alpha)\, e^{iKz\sin\alpha}\, d(K\sin\alpha) \qquad (2.3.1)$$

where $w(K\sin\alpha) = 0$ when $|K\sin\alpha| \geq K\sin\alpha_m$

A property of Fourier transforms is that the inverse transform of the product of two functions yields a convolution integral of the type (Churchill (1972), p.393)

$$\tilde{q}_I(z) = \frac{e^{iKR}}{R}\int_{-\infty}^{\infty} \tilde{q}_\omega(y)\, W(y-z)\, dy \qquad (2.3.2)$$

where $W(y)$ is the inverse Fourier transform of the weighting function $w(K\sin\alpha)$ and $\tilde{q}_\omega(y)\exp(iKR)/R$ is the inverse transform of the acoustic field $\tilde{p}_\omega(\alpha)$, as defined by equation 2.2.3.

This shows that the effect of the limited range of measurements and the choice of weighting function is to smooth the finer detail of the source image. Since the choice of weighting function is arbitary, the amount of smoothing on the source image can be controlled to a certain extent. For instance two typical weightings which may be used are the rectangular weighting and the Bartlett (triangular) weighting defined by:

$$\text{Rectangular:} \quad w(K\sin\alpha) = 1.0 \quad |K\sin\alpha| < K\sin\alpha_m \qquad (2.3.3)$$
$$= 0.0 \quad |K\sin\alpha| \geq K\sin\alpha_m$$

$$\text{Bartlett:} \quad w(K\sin\alpha) = 1 - \frac{|K\sin\alpha|}{K\sin\alpha_m} \quad |K\sin\alpha| < K\sin\alpha_m$$
$$= 0.0 \quad |K\sin\alpha| \geq K\sin\alpha_m$$

The source images of a simple point source using these weightings are shown in Figure 2.2, and the width of the main lobe in these images specifies the resolution of each window.

In order to demonstrate the dependence of the window function W(y) on the aperture angle 'α_m' and the wavenumber 'K', it is convenient to specify W(y) and the weighting function w(α) as Fourier transform pairs: i.e.

$$W(y) = \frac{1}{2\pi}\int_{-\infty}^{\infty} w(K\sin\alpha)\, e^{iKy\sin\alpha}\, d(K\sin\alpha) \qquad (2.3.4)$$

To eliminate the effect of the aperture angle it is useful to note that all weightings are functions of $K\sin\alpha / K\sin\alpha_m = x$, and so 2.3.4 may also be written as

$$W(y) = \frac{1}{2\pi} K\sin\alpha_m \int_{-\infty}^{\infty} w(x)\, e^{iKy\sin\alpha_m . x}\, dx \qquad (2.3.5)$$

where we have substituted $x = K\sin\alpha / K\sin\alpha_m$

Then by defining a normalised window function W_N which is independent of wavenumber 'K' and aperture angle 'α_m' and related to the weighting function by the Fourier Transform

$$W_N(y) = \frac{1}{2\pi}\int_{-\infty}^{\infty} w(x)\, e^{iyx}\, dx$$

it follows from 2.3.5 that

$$W(y) = K\sin\alpha_m \,.\, W_N(Ky\sin\alpha_m) \qquad (2.3.6)$$

This result, which shows that the window function depends upon $Ky\sin\alpha_m$, demonstrates that the resolution, or width of the main lobe, will be inversely proportional to $K\sin\alpha_m$. Also the peak level of the window will be proportional to $K\sin\alpha_m$ while the area beneath the curve remains independent of $K\sin\alpha_m$. Therefore good resolution is obtained using large aperture angles 'α'$_m$ and high frequencies so that '$K\sin\alpha$'$_m$ is large.

The weighting/window functions discussed above are identical to the weighting/window functions used in spectral analysis (Blackman and Tukey (1958)). There are many different types of these functions, and in general these have either large side lobes (e.g. the rectangular window in Figure 2.2) with a narrow main lobe or smaller side lobes (e.g. the Bartlett window Figure 2.2) with a broader main lobe. In this application the main requirement is for the best resolution without negative loops in the window function, and it was found that of the

standard window functions, the Bartlett most closely satisfied these criteria. Therefore the Bartlett window has been used as standard in all the source images presented in this thesis.

b) Aliasing

In order to evaluate the source image as defined by equation 2.3.1, it is necessary to measure the function $\tilde{p}_\omega(\alpha)$ as a continuous function of the wavenumber space variable 'Ksinα'. In practice however it is only possible to evaluate $\tilde{p}_\omega(\alpha)$ at a finite number of points in space. This effectively imposes a further physical restriction on the source image which may be defined as the aliasing problem. This problem applies not only to Polar Correlation, but to any scheme which uses discrete measurements in the acoustic far field.

In order to demonstrate this problem consider a measurement array which evaluates the field at equal locations Δ in 'sinα'. The complex field at the nth location is given by

$$\tilde{p}_\omega(n) = \frac{e^{iKR}}{R} \int_{-\infty}^{\infty} \tilde{q}_\omega(y)\, e^{-iKyn\Delta}\, dy$$

Alternatively this equation may be written as

$$\tilde{p}_\omega(n) = \frac{e^{iKR}}{R} \exp(iKLn\Delta) \int_{-\infty}^{\infty} \tilde{q}_\omega(y-L) e^{-iKyn\Delta}\, dy$$

By choosing $KLn\Delta = 2\pi n$, the term $\exp(iKLn\Delta)$ is unity, and it follows that the measurements $\tilde{p}_\omega(n)$ cannot differentiate between the source distributions $\tilde{q}_\omega(y)$, $\tilde{q}_\omega(y-L)$ ..... $\tilde{q}_\omega(y\pm mL)$. Therefore the source image calculated from the measurements $\tilde{p}_\omega(n)$ must be periodic with period 'L', and errors will occur if the source distribution is significant outside the limits $y = \pm L/2$, where L is defined by the spacing $L = \lambda/\Delta$ (since $K = 2\pi/\lambda$.)

c) Three Dimensional Effects

The model considered in Section 2.2 consisted of a linear array of sources on the y-axis. However in practice the type of source distributions to be considered are those from aero engines which have finite dimensions perpendicular to the y axis. Therefore it is necessary to consider the conditions under which the three dimensional source distribution may be considered.

Starting with the solution to the wave equation in three dimensions gives, on a polar arc of radius R, at the angle 'α' :

$$p(\alpha,t) = \iiint_{y_1 y_2 y_3} q'(\bar{y},\ t-r/a_o)\ dy_1\ dy_2\ dy_3/r \qquad (2.3.7)$$

By taking the Fourier transform with respect to time of this equation we obtain:

$$\tilde{p}_\omega(\alpha) = \iiint_{y_1 y_2 y_3} \tilde{q}'_\omega(\bar{y})\ e^{iKr}\ dy_1\ dy_2\ dy_3/r \qquad (2.3.8)$$

In the three dimensional case the far field approximation for the path length 'r' is given by

$$r = R - y_1 \sin\alpha - y_2 \cos\alpha + \ldots\ldots\ O(y^2/r)$$

and in the amplitude term 1/r, the y_1, y_2 dependence in this approximation may be ignored without significant loss of accuracy. Therefore equation 2.3.8 may be written:

$$\tilde{p}_\omega(\alpha) = \frac{e^{iKR}}{R} \iiint_{y_1 y_2 y_3} \tilde{q}'_\omega(\bar{y})\ e^{-iKy_1\sin\alpha - iKy_2\cos\alpha}\ dy_1 dy_2 dy_3 \qquad (2.3.9)$$

When the y_2 dimension is small such that $Ky_2 \ll 1$, then $\exp(-iKy_2\cos\alpha) = 1$ and an equivalent linear source strength may be defined as

$$\tilde{q}_\omega(y_1) = \iint_{y_2 y_3} \tilde{q}'_\omega(\bar{y})\ dy_2\ dy_3 \qquad (2.3.10)$$

such that

$$\tilde{p}_\omega(\alpha) = \frac{e^{iKR}}{R} \int_{y_1} \tilde{q}_\omega(y_1)\ e^{-iKy_1\sin\alpha}\ dy_1 \qquad (2.3.11)$$

which is equivalent to equation 2.2.3.

This demonstrates how the source distribution may be considered as a line source providing the dimensions in the y_2 direction are very much less than a wavelength so that $Ky_2 \ll 1$.

This condition may be relaxed slightly if the wavenumber spectrum is only evaluated over the limited range of $\pm K\sin\alpha_m$. In this case it is necessary that $Ky_2(1-\cos\alpha_m) \ll 1$ so that the integral

$$\iint_{y_2 y_3} q'_\omega(\bar{y})\ e^{-iKy_2\cos\alpha}\ dy_2$$

is independent of α over the range $-\alpha_m < \alpha < \alpha_m$. The effective linear source strength may then be defined as:

$$\tilde{q}_{\omega}(y_1) = \iint_{y_2 y_3} \tilde{q}_{\omega}'(y)\, e^{-iKy_2}\, dy_2\, dy_3 \qquad (2.3.12)$$

which is identical to 2.3.10 when $Ky_2 \ll 1$.

While this gives the condition under which the cross axis dimensions may be ignored, the effect of working outside these limitations will be discussed in a later section.

2.4. AMBIGUOUS SOURCE DISTRIBUTIONS

The relationships derived in the previous sections assume that the acoustic field may be described in terms of the solution to the wave equation:

$$p(\alpha, t) = \int_{-\infty}^{\infty} q(y, t - r/a_o)\, dy/r$$

However it has been emphasised by Ffowcs Williams (1973), (1974) that this solution is not unique, and there are many source distributions $q(y,t)$ which give the same acoustic field. This has been very concisely demonstrated by Kempton (1976) who has illustrated the equivalence of acoustic fields from a monopole source at 'y' and a multipole cluster at the origin 'y=0'. This follows from a Taylors series expansion of the acoustic field from the monopole of strength A(t): (see Kempton (1976))

$$\frac{1}{r} A(t-r/a_o) = \sum_{n=o}^{\infty} \frac{(R-r)^n}{n!} \frac{\partial^n}{\partial R^n} \left\{ \frac{1}{R} A(t-R/a_o) \right\} \qquad (2.4.1)$$

This series converges whenever $R > |R - r|$. In the acoustic far field terms of order $1/R^2$ may be ignored in the derivatives and in the expansion $R-r = y\sin\alpha + \ldots\ldots O(y^2/R)$. Therefore

$$\frac{1}{r} A(t-r/a_o) = \frac{1}{R} \sum_{n=o}^{\infty} \frac{(-y\sin\alpha/a_o)^n}{n!} \frac{\partial^n}{\partial t^n} A(t-R/a_o) \qquad (2.4.2)$$

Each term in this series is characteristic of a multipole of order 2^n and strength

$$\left\{ (-y/a_o)^n/n! \right\} \frac{\partial^n}{\partial t^n} A(t) \qquad (2.4.3)$$

located at the origin y = 0. It should be noted however that the far field approximations leading to 2.4.2 are not strictly necessary since each term of the series 2.4.1 describes a multipole's field.

This demonstrates how the same acoustic field has been generated by two distinctly different mechanisms, and it is therefore very important that this ambiguity should be considered when interpreting the results from far field source location techniques.

To investigate this further consider the source image calculated from the field of a multipole of order 2^n, whose strength is given by 2.4.3, using equation 2.3.1. First it is necessary to take the Fourier transform of 2.4.3 with respect to time, so that the acoustic field at the fixed frequency 'ω' is defined as

$$\tilde{p}_\omega(\alpha) = (-iKy\sin\alpha)^n A_\omega/n! \cdot \frac{e^{iKR}}{R}$$

where A_ω is the Fourier transform of A(t). Then the source image is given as

$$\tilde{q}_I(z) = \frac{1}{2\pi}\int_{-\infty}^{\infty} (-iKy\sin\alpha)^n \frac{A_\omega}{n!} \cdot \frac{e^{iKR}}{R} W(K\sin\alpha)e^{iKz\sin\alpha} d(K\sin\alpha)$$

which may be evaluated using the properties of Fourier transforms (Churchill (1972) p.471,(3)) to give

$$\tilde{q}_I(z) = \frac{A_\omega e^{iKR}}{n!R}(-y)^n \frac{\partial^n}{\partial z^n} W(z) \qquad (2.4.4)$$

Therefore the source image from a multipole of order 2^n is the nth derivative of the window function W(z); also note how this is a very complete result since the source image from a cluster of multipoles of ascending order, whose strength is given by 2.4.3, is defined as

$$\tilde{q}_I(z) = \frac{A_\omega e^{iKR}}{R} \sum_{n=o}^{\infty} \frac{(-y)^n}{n!} \frac{\partial^n}{\partial z^n} W(z)$$

The series in this equation sums to the window function W(z-y), and the source image represents a monopole located at 'y', from which the source strengths 2.4.3 were derived. Therefore the source image reveals the monopole nature of the source distribution, but conceals its true nature which may consist of a number of interfering higher order sources.

2.5. THE EXTENSION TO "WHITE NOISE" SOURCE DISTRIBUTIONS WITH ARBITARY SPATIAL COHERENCE

The discussion so far has been limited to sources whose fluctuations are known for all time, and therefore have exact representations in the frequency domain. However in practice it is necessary to apply source

location techniques to randomly fluctuating sources, whose Fourier transform with respect to time can only be estimated from a limited record. This estimate has to be used because the source strength in the frequency domain, and thus the far field pressure $\tilde{p}_\omega(\alpha)$, will depend not only on frequency but also on the time of evaluation. Therefore to obtain a meaningful result it is necessary to consider an averaged quantity with non-zero mean. In order to preserve the phase dependence in the far field it is found that the natural quantity to consider is the cross power spectral* density, defined as the averaged cross product between $\tilde{p}_\omega(\alpha)$ at two points in the acoustic far field.

As before the acoustic far field from an almost linear array of sources will be considered on a polar arc of radius 'R' (see Figure 2.1). The cross power spectral density will be taken between a reference point on this arc, defined to be at the angle 'β', as shown in Figure 2.1, and a second point at an angle 'α'. The cross power spectral density is defined as the averaged value of the cross product of the acoustic field variables at these points.

$$\tilde{R}_\beta(\alpha) = Ex\left[\tilde{p}_\omega(\alpha)\,\tilde{p}_\omega^*(\beta)\right] \qquad (2.5.1)$$

The location 'β' is defined as the reference point, at which the phase will be zero. This may be taken as any point on the polar arc. Therefore evaluating the cross power spectral density $\tilde{R}_\beta(\alpha)$ in terms of the source strengths given in 2.2.3, the following relationship is obtained:

$$\tilde{R}_\beta(\alpha) = \frac{1}{R^2}\int_y\int_z Ex\left[\tilde{q}_\omega(y)\,\tilde{q}_\omega^*(z)\right] e^{iKy\sin\alpha - iKz\sin\beta}\,dydz \qquad (2.5.2)$$

Then by defining the average source level as seen at 'β' by the integral over z of the cross power spectral density of the source strengths, $Ex\left[\tilde{q}_\omega(y)\,\tilde{q}_\omega^*(z)\right]$ including the associated phase lag to 'β', i.e.

$$\tilde{Q}_\beta(y) = \frac{1}{R^2}\int_z Ex\left[\tilde{q}_\omega(y)\,\tilde{q}_\omega^*(z)\right] e^{iK(y-z)\sin\beta}\,dz \qquad (2.5.3)$$

it is found that

$$\tilde{R}_\beta(\alpha) = \int_y \tilde{Q}_\beta(y)\, e^{iKy(\sin\alpha - \sin\beta)}\,dy \qquad (2.5.4)$$

*This quantity is sometimes referred to as the cross spectral density.

This defines an equivalent wavenumber spectrum for randomly fluctuating sources, which are typical of the sources of noise associated with aero-engines. As before by taking the inverse Fourier transform of $\tilde{R}_\beta(\alpha)$, as a function of $K(\sin\alpha - \sin\beta)$, the distribution of the source level $\tilde{Q}_\beta(y)$ may be obtained. The same restrictions in terms of the resolution, aliasing and three dimensional effects apply, and the principle of evaluation is identical.

2.6. INTERPRETATION OF THE SOURCE STRENGTH PARAMETER.

The source strength for randomly fluctuating sources has been defined as

$$\tilde{Q}_\beta(y) = \frac{1}{R^2}\int_z Ex\left[\tilde{q}_\omega(y)\,\tilde{q}_\omega^*(z)\right] e^{iK(y-z)\sin\beta}\,dz \qquad (2.6.1)$$

This may be interpreted as the effective source strength as seen by the reference microphone at 'β'. To demonstrate this consider the power spectral density of the acoustic field fluctuations at 'β', defined as

$$P(\beta) = \tilde{R}_\beta(\beta) = Ex\left[\tilde{p}_\omega(\beta)\,\tilde{p}_\omega^*(\beta)\right] \qquad (2.6.2)$$

From equation 2.5.4 it follows that

$$P(\beta) = \int_{-\infty}^{\infty} \tilde{Q}_\beta(y)\,dy \qquad (2.6.3)$$

Thus the power spectral level at 'β' may be defined by the integral of the source strength parameter $\tilde{Q}_\beta(y)$. However from this result it appears that since $P(\beta)$ is entirely real, then only the real part of $\tilde{Q}_\beta(y)$ is significant, its imaginary part being of zero integral scale. This feature can be established by considering 2.6.1 in 2.6.3 and integrating over y and z.

However the interpretation of $\tilde{Q}_\beta(y)$ is not particularly clear. When deriving the pointwise source strength $\tilde{q}_\omega(y)$, its definition was relatively simple, as the complex amplitude of fluctuations at 'y'. The complex nature of this parameter describes the relative phase of the fluctuations at the point 'y'. However in the case of randomly fluctuating sources relative phase is only meaningful if the sources are correlated and $Ex\left[q_\omega(y)q_\omega^*(z)\right] \neq 0$, $y \neq z$. The significance of a source at 'y' depends not only on the magnitude of the fluctuations at that point but also on their interactions with other neighbouring

source fluctuations, and any cancellations which may occur. Since the definition of $\tilde{Q}_\beta(y)$ (see 2.6.1) includes an integral over 'z' relative to the position 'y', including the path length differences to 'β' (given by the $\exp(iK(y-z)\sin\beta)$ term), these cancellations are automatically included. Therefore it appears that $\tilde{Q}_\beta(y)$ is a pertinent definition of the effective source strength, because it identifies the relative significance of each part of the source distribution as seen by the observer at 'β'. However only the real part of this function is significant to the observer since the imaginary part is of zero integral scale, and has no clear physical interpretation. It should be noted, however, that this definition is ambiguous since it does not identify any interference effects. Therefore it is possible to eliminate a section of the measured source distribution and create stronger effective sources due to the lack of destructive interference.

2.7. THE EVALUATION OF COHERENT SOURCE DISTRIBUTIONS

It has been shown that the complex acoustic field at the fixed frequency 'ω', on a polar arc of radius R, is related to a linear distribution of sources by the integral (2.2.3).

$$\tilde{p}_\omega(\alpha) = \frac{e^{iKR}}{R} \int_{-\infty}^{\infty} \tilde{q}_\omega(y)\, e^{-iKy\sin\alpha}\, dy \qquad (2.7.1)$$

However if the sources are randomly fluctuating it is necessary to consider averaged frequency components, and it was argued in section 2.5 that the natural quantity to consider was the cross power spectral density between two points on the polar arc. It was shown how a source strength parameter could be evaluated for sources with arbitary spatial coherence. In this section the special case will be considered where all the sources within the distribution are completely coherent; this means that each source is driven by the same input, so that the source strength parameter may be re-defined as

$$\tilde{q}_\omega(y) = \tilde{Q}(y)\, I(\omega) \qquad (2.7.2)$$

where the amplitude and phase of $\tilde{Q}(y)$ is invariant with time. A typical example of such a distribution might be a vibrating pipe which is driven by a single source, but emits acoustic waves throughout its length. The acoustic emission at any point will then have a fixed amplitude and phase relationship to every other point on the pipe.

This situation may be easily recognised from measurements in the acoustic far field because each point in this field will be completely coherent. To demonstrate this feature consider the C.P.S.D. on the polar arc defined by equations 2.5.1 and 2.5.2, which may be written in terms of 2.7.2 as

$$\tilde{R}_{\beta}(\alpha) = \frac{1}{R^2} \iint_{y\ z} \tilde{Q}(y)\, \tilde{Q}^{*}(z) \cdot Ex\left[|I(\omega)|^2\right] e^{iKy\sin\alpha - iKz\sin\beta}\, dydz \qquad (2.7.3)$$

This may be re-arranged in the simplified form of

$$\tilde{R}_{\beta}(\alpha) = \frac{\tilde{A}(\alpha)\,\tilde{A}^{*}(\beta)}{R^2} Ex\left[|I(\omega)|^2\right] \qquad (2.7.4)$$

where $\tilde{A}(\alpha) = \int_{y} \tilde{Q}(y) e^{iKy\sin\alpha}\, dy$

The P.S.D. at any point α can be defined from this result by letting $\beta = \alpha$, giving

$$P(\alpha) = |\tilde{A}(\alpha)|^2 Ex\left[|I(\omega)|^2\right]/R^2 \qquad (2.7.5)$$

The coherence of this field can be established simply from the definition of coherence

$$\gamma_{\alpha\beta}(\omega) = |\tilde{R}_{\beta}(\alpha)|/\sqrt{P(\alpha)\,P(\beta)}$$

which may be seen from 2.7.4 and 2.7.5 to be unity.

In order to determine the relative amplitude and phase of each point in the distribution, $\tilde{Q}(y)$, it is necessary to measure $\tilde{A}(\alpha)$ and invert the Fourier integral

$$\tilde{A}(\alpha) = \int_{y} \tilde{Q}(y)\, e^{iKy\sin\alpha}\, dy$$

The inversion of this integral has already been fully discussed, and in this section methods of measuring $\tilde{A}(\alpha)$ will be considered.

Since the field is completely coherent, it is unnecessary to measure the variation of the C.P.S.D. on the polar arc. The amplitude variation of $\tilde{A}(\alpha)$ can be determined directly from the P.S.D. defined in equation 2.7.5, suitably normalised to eliminate the constant factor $Ex\left[|I(\omega)|^2\right]/R^2$. Also required is the phase of $\tilde{A}(\alpha)$ and since the field is coherent this may be measured directly by comparing the signals between two points on the polar arc. In many cases this may be the simplest way to take the measurements, but it is also possible to measure $\tilde{A}(\alpha)$ using the C.P.S.D., normalised by the P.S.D. at the

reference angle β . This gives

$$\tilde{R}_{\beta}(\alpha)/_{P(\beta)} = \tilde{A}(\alpha)/\tilde{A}(\beta)$$

By specifying β to be the phase reference point, $\tilde{A}(\beta)$ is real valued and the normalised source strength parameter $\tilde{Q}(y)/A(\beta)$ can be evaluated. This result emphasises the importance of amplitude and phase normalisation inherent in both methods of measurement. Since the source strength definition 2.7.2 is purely relative this normalisation is unavoidable.

2.8. PARTIALLY COHERENT SOURCE DISTRIBUTIONS

2.8.1. Introduction

When sources are randomly fluctuating it is necessary to define a source strength parameter which utilises a time average of their fluctuations. However the averaged strength of a source at any point does not specify its effective radiation since its interference with other sources must be allowed for, and the extent of these interference effects will depend on its coherence with adjacent sources. In section 2.5 a pointwise source strength parameter was defined so that it included the interference effects of all associated sources; however this parameter has certain problems of interpretation and so in this section an alternative source strength parameter will be discussed.

Rather than consider the source distribution as a number of point sources, in this section the distribution will be considered as a number of coherent source regions. A distribution of randomly fluctuating sources may be modelled as the superposition of a number of coherent source regions. Each of the sources within a particular region are defined as having completely coherent fluctuations which are statistically independent of the source fluctuations in another region. Then by allowing these regions to overlap, partial coherence may be obtained between the total fluctuations at any two points. To illustrate this, consider the diagram below which shows two coherent regions of sources.

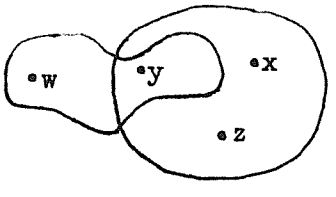

Since all the fluctuations in one region are coherent, the fluctuations at the points 'x' and 'z' will have a fixed amplitude and phase relationship. However the point 'w' is in a completely different region and therefore will be statistically independent of the source fluctuations at either x or z. In the overlapping section of these two regions there exists partial coherence, so the total fluctuations at the point 'y' will be partially coherent with the fluctuations at the points x, z and w.

The advantage of this approach to source strength definition is that all interference effects have been isolated into specific regions. The distribution of sources within a region specifies all the interference effects of sources within that region and will account for all their effective directionality in the acoustic far field. Any number of these independent regions may be superimposed and the acoustic field will include their statistically independent contributions. In this section the source strength parameter will be developed so that it defines the effective strength of each of these independent regions, as if they were an effective point source with its own directionality. This point source will be assumed to lie at the centroid of this region and the source distribution then becomes a distribution of statistically independent point sources. It will then be shown that this source strength definition has certain practical advantages to the application of the Polar Correlation technique.

2.8.2. General Definition of Source Strengths

As before we will start by considering the acoustic field from a linear array of sources, only in this instance the source fluctuations will be defined as a function of the two space variables 'y' and 'z', where 'y' defines the distribution of statistically independent regions and 'z' the distribution of sources within each region. Thus the source strength parameter takes the form $q(y,z,t)$, which specifies the fluctuations at the spatial location $y+z$, associated with the region located at 'y'. By taking the Fourier transform of the fluctuations with respect to time and utilising the wavenumber spectrum principle described in section 2.2, the complex acoustic field at the fixed frequency 'ω' may be defined from equation 2.2.3 as:

$$\tilde{p}_{\omega}(\alpha) = \frac{e}{R}^{iKR} \int_{-\infty}^{\infty}\int \tilde{q}_{\omega}(y,z)\, e^{-iK(y+z)\sin\alpha}\, dydz$$

In this definition $\tilde{p}_\omega(\alpha)$ is the complex acoustic field on a polar arc of radius R which lies in the far field of the source distribution. This result differs from equation 2.2.3 in that a double spatial integral has been used to allow for the definition of source strengths in terms of coherent regions.

However since randomly fluctuating sources are being considered, an averaged quantity must be used and so we are led as before to define the cross power spectral density between fluctuations in the acoustic field. This is defined as

$$\tilde{R}_{\alpha\beta}(\alpha) = Ex\left[\tilde{p}_\omega(\alpha)\ \tilde{p}^*_\omega(\beta)\right]$$

and is related to the source parameter as (2.8.1)

$$\tilde{R}_{\alpha\beta}(\alpha) = \frac{1}{R^2}\int_{-\infty}^{\infty}\int\int\int Ex\left[\tilde{q}_\omega(y_1,z_1)\tilde{q}^*_\omega(y_2,z_2)\right] e^{-iK(y_1+z_1)\sin\alpha + iK(y_2+z_2)\sin\beta}\ dy_1\ dy_1\ dz_2\ dz_2$$

However since source fluctuations associated with the region y_1 are independent of those associated with y_2, the above integrand will only exist when $y_1 = y_2$.

Also the variation of this integrand with z_1, z_2 describes a distribution of completely coherent sources with phase relationships which will not vary with time. The source strength at (y_1,z_1) will have a fixed relationship with the source strength at (y_1,z_2). This may be extracted from the value of $Ex\left[\tilde{q}_\omega(y_1,z_1)\ \tilde{q}^*_\omega(y_1,z_2)\right]$, in terms of a function $\tilde{a}_\omega(y,z)$ which describes the amplitude and phase relationships between different locations in the region 'y'. These amplitude and phase relationships may be conveniently normalised so that

$$\int_{-\infty}^{\infty}\tilde{a}_\omega(y,z)\ dz = 1.0$$

and from this the integrand of 2.8.1 may be defined as

$$Ex\left[\tilde{q}_\omega(y_1,z_1)\tilde{q}^*_\omega(y_2,z_2)\right] = Q_\omega(y_1)\tilde{a}_\omega(y_1,z_1)\ \tilde{a}^*_\omega(y_1,z_2)\,\delta(y_1-y_2) \quad (2.8.2)$$

where the normalising function $Q_\omega(y)$ is

$$Q_\omega(y) = \int_{-\infty}^{\infty}\int Ex\left[\tilde{q}_\omega(y,z_1)\tilde{q}^*_\omega(y,z_2)\right]\ dz_1 dz_2$$

This function $Q_\omega(y)$ defines a source strength parameter which depends on the total strength of the coherent region, and it is real valued

because of the double integral and complex conjugate nature of the integrand.

It is noted that this definition of the integrand of equation 2.8.1, given by 2.8.2, has allowed the separation of the variables y_2, z_1, z_2. Therefore integration with respect to each of these variables may be carried out directly. This is simplified by defining the function which results from the z_1 and z_2 integrations as

$$\tilde{D}_\omega(y,\alpha) = \int_{-\infty}^{\infty} \tilde{a}_\omega(y,z)\, e^{-iKz\sin\alpha}\, dz$$

so that equation 2.8.1 can be written in the form

$$\tilde{R}_\beta(\alpha) = \frac{1}{R^2}\int_{-\infty}^{\infty} Q_\omega(y)\tilde{D}_\omega(y,\alpha)\tilde{D}_\omega^*(y,\beta)e^{-iKy(\sin\alpha-\sin\beta)}dy \qquad (2.8.3)$$

2.8.3. Interpretation of Parameters

The result given in equation 2.8.3 defines a relationship between the cross power spectral density of the far field signals and the source strength parameters $Q_\omega(y)$ and $\tilde{D}_\omega(y,\alpha)$. These parameters may be interpreted quite simply: the function $Q_\omega(y)$ represents the total integrated source strength of all sources within a coherent region whose centroid is specified to lie at 'y', and $\tilde{D}_\omega(y,\alpha)$ represents the directionality of that region. The latter is demonstrated when the power spectral density on the polar arc is considered. This may be obtained by allowing α to equal β in equation 2.8.3 and gives

$$P(\alpha) = \frac{1}{R^2}\int_{-\infty}^{\infty} Q_\omega(y)\,|\tilde{D}(y,\alpha)|^2\, dy \qquad (2.8.4)$$

Thus the overall directionality of each coherent region is specified by $|\tilde{D}(y,\alpha)|^2$, and this accounts for all the interference effects between coherent sources.

2.8.4. Elimination of Directionalities

In order to cast equation 2.8.3 in a form which is more amenable to solution it is necessary to eliminate the dependence of the directionality functions on 'y'. This assumes that the constitution of each coherent region, and consequently their directionalities, are identical. This would appear to be an unjustified assumption and in a later section the implications will be evaluated. However it should be noted that the results from many other source location techniques which have been used on model and full scale jets (Billingsley & Kinns (1976), Grosche

(1973), Laufer et al(1976), Parthasarathy (1974)) have been interpreted assuming no correlation between adjacent sources. This implies that there is no directionality in the acoustic field which is a far grosser assumption than assuming that each coherent region has the same directionality.

Therefore the directionalities $\tilde{D}_\omega(y,\alpha)$ in equations 2.8.3 and 2.8.4 are assumed independent of y and replaced by $\tilde{d}(\alpha)$ giving

$$R_\beta(\alpha) = \frac{\tilde{d}(\alpha)\tilde{d}^*(\beta)}{R^2} \int_{-\infty}^{\infty} Q_\omega(y)\, e^{-iKy(\sin\alpha - \sin\beta)} dy$$

and

$$P(\alpha) = \frac{|\tilde{d}(\alpha)|^2}{R^2} \int_{-\infty}^{\infty} Q_\omega(y)\, dy$$

Then by considering the complex coherence on the polar arc, defined by

$$\tilde{C}_\beta(\alpha) = \tilde{R}_\beta(\alpha) / \sqrt{P(\alpha)\, P(\beta)} \qquad (2.8.5)$$

the following relationship is obtained

$$\tilde{C}_\beta(\alpha) = e^{i\phi(\alpha) - i\phi(\beta)} \int_{-\infty}^{\infty} Q'(y) e^{-iKy(\sin\alpha - \sin\beta)} dy \qquad (2.8.6)$$

where $Q'(y) = Q(y) / \int_{-\infty}^{\infty} Q(y)dy$ defines a source strength parameter normalised to unit area, and $\phi(\alpha)$ defines the phase directionality of $\tilde{d}(\alpha)$.

If it is assumed that $\phi(\alpha) = 0$ then equation 2.8.6 represents a particularly convenient form of the wavenumber spectrum relationship which may be inverted to yield the distribution of the source strength parameter $Q'(y)$. The restrictions of inverting this equation have already been discussed and the distribution $Q'(y)$ may be interpreted as the distribution of effective strengths of coherent regions, normalised to unit area. This is the major result of this section and has some significant advantages over the earlier formulations given in this chapter. First the complex coherence $\tilde{C}_\beta(\alpha)$ is an easier function to measure than the cross power spectral density $\tilde{R}_\beta(\alpha)$ used in earlier formulations. This arises because of the normalisation procedure used in equation 2.8.5, which dispenses with the requirement to calibrate each microphone used to measure the acoustic signals. Secondly the source strength $Q'(y)$ is by definition real valued which means that $\tilde{C}_\beta(\alpha)$ will be symmetrical about $\alpha = \beta$, i.e.

$$\tilde{C}_\beta(\alpha) = \tilde{C}_\beta^*(-\alpha)$$

Therefore only positive values of α-β need be evaluated, which automatically halves the number of measurements required. Finally $Q'(y)$ has a much clearer physical interpretation than the definition of source strength developed in section 2.5.

However this result depends on two significant assumptions. First it is assumed that the directionalities of each coherent region are identical; and secondly it has been assumed that the phase directionality $\phi(\alpha)$ is zero. The first of these assumptions will be evaluated in section 2.9 where it will be shown that it does not result in significant errors, and the second assumption will be discussed in the next sub-section.

2.8.5. The Effect of Phase Directionality

The problem with the phase directionality term $\phi(\alpha)$ is that it cannot be measured using the power spectral density function and so is not eliminated by the normalisation procedure given in equation 2.8.5. To demonstrate its significance consider the features which cause this directionality of phase: it is defined as the phase of the function $\tilde{d}(\alpha)$ given by

$$\tilde{d}(\alpha) = \int_{-\infty}^{\infty} \tilde{a}_\omega(z)\, e^{-iKz\sin\alpha}\, dz$$

where $\tilde{a}_\omega(z)$ describes the distribution of amplitude and phase of sources within a coherent region, and is normalised so that it integrates to unity

$$\int_{-\infty}^{\infty} \tilde{a}_\omega(z)dz = 1.0$$

This specifies the imaginary part of $\tilde{a}_\omega(z)$ as having zero internal scale. Also this function has been defined as having its centroid at $z = 0$. Since the imaginary part is of zero internal scale it is most useful to define this centroidal location in terms of the real part of $\tilde{a}_\omega$ only. Thus the centroid is defined from

$$\int_{-\infty}^{\infty} z c_\omega(z)\, dz = z_c$$

where $\tilde{a}_\omega(z) = c_\omega(z) + id_\omega(z)$

Source distributions with these features have been investigated by Kinns (1976) and it is shown that when KLsinα is small (where L represents the length of the coherent region), the phase $\phi(\alpha)$ is given by

$$\phi(\alpha) = -\frac{K^2 \sin^2\alpha}{2} \int_{-\infty}^{\infty} d_\omega(z)\, z^2 dz - O((KL\sin\alpha)^7)$$

Thus phase directionalities will be of the order $(KL\sin\alpha)^2$, and their magnitude will be dependent on the distribution of the imaginary part of $\tilde{a}_\omega(z)$. In general these phase directionalities will be negligible when coherent regions cannot be resolved, i.e. $KL\sin\alpha \ll 1$; however when the aperture and coherence length scale is large enough then phase errors are likely to be important.

As an example, consider a coherent region which is typical of jet noise having a linear variation of phase with z. Thus the distribution of sources within the coherent region is given by

$$a_\omega(z)\, e^{i\delta z}$$

where $a_\omega(z)$ is real and $a_\omega(o) \neq 0$. Then the phase directionality is given by

$$\phi(\alpha) = -\frac{K^2 \sin^2\alpha}{2} \int_{-\infty}^{\infty} a_\omega(z).\, z^2.\, \sin(\delta z)\, dz$$

This integral will be zero whenever $a_\omega(z)$ is symmetrical about z=o, and in general the phase directionality will depend on the skewness of the distribution of sources within the coherent region

2.8.6 Summary

This section has considered the evaluation of a source distribution which includes randomly fluctuating sources with arbitary coherence. The problem of defining the source strength for this type of source distribution is making the correct allowance for the effects of interference. This section has used an approach which groups source interference effects into complete units, and the strength of each unit is evaluated using the source location technique. The previous definition given in section 2.5 differs from this approach in that the source strengths at two different points are dependent on each other due to their coherence which will result in interference effects.

The definition presented in this section has been shown to have two important practical advantages, providing the assumptions of the theory are reasonable. The first of these advantages is that only one sided transforms are required and the second is that all measurements are normalised. However when dealing with two strongly coherent point sources, separated by a large number of wavelengths this definition is ambiguous since the effective source will be located between the two real sources. In this situation the definition given in section 2.5 will locate the sources correctly, and therefore may be considered more accurate. In conclusion, the choice of source strength definition depends on the possibility of this ambiguity. In the source distributions which are to be considered in this thesis, two strongly coherent point sources separated by a large number of wavelengths are not of major importance. The only case when this effect is likely to occur is on a jet engine when the noise emitted by the inlet is coherent with the noise emitted by the bypass duct or hot core exit at frequencies above 1000 Hz. Therefore the second choice of source strength parameter has been used throughout so that the major practical advantages of one sided transforms and normalised data may be realised.

2.9. NUMERICAL EVALUATION OF APPROXIMATIONS

2.9.1. Far Field Approximations

Throughout this chapter it has been assumed that in the acoustic far field the path length from a source at 'y', on the axis to the measurement point at 'α' on the polar arc (see Figure 2.1) may be approximated by the first two terms in the series:

$$r = R - y\sin\alpha + \frac{y^2}{2R}(1-\sin^2\alpha)$$

(see section 2.2)

In this section the significance of this approximation will be evaluated by considering the errors caused by ignoring the third term in this series. These errors will be calculated by evaluating the source image from a more accurate definition of the acoustic far field which includes the third order path length term. The acoustic far field is defined, using a more accurate form of equation 2.2.3, as

$$\tilde{p}_{\omega}(\alpha) = \frac{e^{iKR}}{R}\int_{-\infty}^{\infty} \tilde{q}_{\omega}(y)\, e^{-iKy\sin\alpha + \frac{iKy^2}{2R}(1-\sin^2\alpha)}\, dy$$

The source image is then obtained by evaluating the inverse Fourier transform of the acoustic far field multiplied by the weighting function $w(K\sin\alpha)$ (see equation 2.3.1)

$$\tilde{q}_I(z) = \frac{1}{2\pi}\int_{-\infty}^{\infty} \tilde{p}_\omega(\alpha)\, w\,(K\sin\alpha)e^{iKz\sin\alpha}\, d(K\sin\alpha)$$

By combining these two definitions it is found that

$$\tilde{q}_I(z) = \frac{e^{iKR}}{2\pi R}\int_{-\infty}^{\infty} \tilde{q}_\omega(y)e^{iKy^2/2R}\int_{-\infty}^{\infty} w\,(K\sin\alpha)e^{-iK(y-z)\sin\alpha - \frac{iKy^2}{2R}\sin^2\alpha}\, dy\, d(K\sin\alpha)$$

This result may be defined in the more convenient form of a convolution between the source distribution and a window function:

$$\tilde{q}_I(z) = \frac{e^{iKR}}{R}\int_{-\infty}^{\infty} \tilde{q}_\omega(y)\; e^{iKy^2/2R} W'(y,y-z)\; dy$$

where

$$W'(y,y-z) = \frac{1}{2\pi}\int_{-\infty}^{\infty}\left\{ w\,(K\sin\alpha)e^{-iKy^2\frac{\sin^2\alpha}{2R}}\right\}\; e^{-iK(y-z)\sin\alpha}\; d(K\sin\alpha)$$

This shows that the effect of the third order path length term on the source image is to modify the window function which operates on the source distribution. Therefore the differences between the modified window and the standard window function define the errors caused by making this path length approximation.

The magnitude of these errors will depend on the phase factor

$$Ky^2\sin^2\alpha/2R$$

This will clearly be worst at the extreme end of the source distribution where $y = Y$ and will also be affected by the aperture angle α_m. In a typical application the aperture is reduced at higher frequencies to avoid aliasing errors while maintaining the same resolution 'l' (see Chapter 3). Thus '$\sin\alpha_m$' is proportional to λ/l and the phase factor ϕ which describes the maximum phase error has the following dependence:

$$\phi = \frac{KY^2\sin^2\alpha_m}{2R} = \pi\,\frac{\lambda}{R}\,\frac{Y^2}{l^2}$$

For a fixed ratio of source length Y to resolution 'l' this factor is dependent on λ/R. Therefore it will be a maximum at low frequencies where large apertures are used.

Typical values of ϕ for some of the tests reported in this thesis are given below

	$\sin\alpha_m$	Y	λ	R	ϕ
RB 211 Jet Engine	0.642	40'	4.5'	100'	4.61
Model Jet ISVR	0.866	24"	10.4"	120"	1.089

In Figures 2.3 - 2.5 the window functions for values of ϕ between 0.392 and 10.17 are presented. These results show that when $\phi > \pi = 3.142$ then significant distortion occurs to the data window. It is noted that the array used on the RB.211 exceeds this limit and it may be shown that distortions will occur at displacements $y > 33'$. However this is not a particularly important part of this distribution (see Figures 6.2 and 6.3) and significant distortion is not apparent.

2.9.2. Three Dimensional Effects

The complex acoustic far field is defined for a three dimensional source distribution $\tilde{q}_\omega(y)$ by equation 2.3.6 as

$$\tilde{p}_\omega(\alpha) = \frac{e^{iKR}}{R} \int_{y_1}\int_{y_2}\int_{y_3} \tilde{q}'_\omega(\bar{y}) e^{-iKy_1\sin\alpha - iKy_2\cos\alpha}\, d\bar{y}$$

It was argued in section 2.3 that if $Ky_2(1-\cos\alpha_m) \ll 1$, then the three dimensional effects could be ignored. In this section the practical limitation of this restriction will be evaluated.

Consider the source image from a three dimensional source distribution, evaluated using equation 2.3.1.

$$\tilde{q}_I(z) = \frac{e^{iKR}}{2\pi R} \int_{-\infty}^{\infty} \int_{y_1}\int_{y_2}\int_{y_3} q'_\omega(\bar{y}) \left\{ w(K\sin\alpha) e^{-iKy_2\cos\alpha} \right\} e^{-iK(y_1-z)\sin\alpha}\, d\bar{y}\, d(K\sin\alpha)$$

Evaluating the integral with respect to $(K\sin\alpha)$ gives the source image as the triple convolution

$$\tilde{q}_I(z) = \frac{e^{iKR}}{R} \int_{y_1}\int_{y_2}\int_{y_3} q'_\omega(y) e^{-iKy_2}\, W(y_2, y_1-z)\, d\bar{y} \qquad (2.9.4)$$

where

$$W(y_2, y_1-z) = \frac{1}{2\pi} \int_{-\infty}^{\infty} \left\{ w(K\sin\alpha) e^{iKy_2(1-\cos\alpha)} \right\} e^{-iK(y_1-z)\sin\alpha}\, d(K\sin\alpha) \qquad (2.9.5)$$

This last equation describes a window function with which sources anywhere in space are convolved. In the case when $W(y_2,y_1-z) \simeq W(o,y_1-z)$, the source image equation 2.9.4 reduces to

$$\tilde{q}_I(z) = \frac{e^{iKR}}{R} \int_{y_1} W(o,y_1-z) \iint_{y_2 y_3} q'_\omega(\bar{y}) e^{-iKy2}\, d\bar{y}$$

The inner integrals of this equation are equivalent to equation 2.3.12 and represent an equivalent on-axis source distribution. Therefore the limits to the on axis approximation can be described by the limits of the approximation that

$$W(y_2,y_1-z) \simeq W(o,y_1-z) \qquad (2.9.6)$$

To evaluate the limits to this approximation it is necessary to consider the integral 2.9.5. Clearly for values of $Ky_2(1-\cos\alpha_m) \ll 1$, the approximation 2.9.6 holds. For values of $Ky_2 \gg 1$ this integral may be evaluated using the principle of stationary phase (Papoulis (1962)). However the region of interest lies between these two limits and so the high wavenumber solution will not be described in detail. However the result for $y_2 \gg y_1-z$ will be quoted as

$$W(y_2,y_1) = \frac{1}{\lambda} \sqrt{\frac{2\pi}{Ky_2}} \int_{-\infty}^{\infty} W(z) \cos\left(\frac{K(y_1-z)^2}{y_2} - \pi/4\right) dz \qquad (2.9.7)$$

(Note: real part only)

where $W(z)$ is the on axis Bartlett window function.

To evaluate these effects when $Ky_2(1-\cos\alpha_m) \simeq 1$ a numerical study was undertaken. The critical parameters are the maximum aperture angle α_m and the non-dimensional off axis displacement y_2/λ. The results of the numerical study are shown in Figures 2.6 - 2.8 giving window functions for source displacements of $y_2/\lambda = 0, 5, 10, 15$, and aperture angles $\alpha_m = 10^\circ, 30^\circ, 60^\circ$.

These results show that for the small aperture angles of 10° there is no significant error for displacements up to 15λ. However for the larger apertures there is a significant error for all displacements. Also note now that at the larger apertures the asymtotic form given by 2.9.7 is apparent. From the results given in Figure 2.6 it would appear that a limit of

$$y_{2/\lambda}\ (1-\cos\alpha_m) < 0.25$$

ensures no off axis displacement error. This also ensures that

$Ky_2(1-\cos\alpha_m) < \pi/2$, which seems a logical limit.

2.9.3. Evaluation of the assumption of Uniform Directionalities.

In section 2.8 it was shown how a source distribution could be modelled by a number of regions of coherent sources. It was then assumed that if the source distribution was dominated by a particular type of coherent region, then all the coherent regions within the distribution could be taken as identical. In this section this assumption will be evaluated.

In order to simplify the analysis the definition of source strength given by equation 2.8.3,

$$Q_\omega(y)\ \tilde{D}(y,\alpha)\ \tilde{D}^*(y,\beta)$$

will be used (where $Q_\omega(y)$ describes the relative level of the coherent region located at y, $\tilde{D}(y,\alpha)$ its far field directionality). Two different regions of coherent sources will be considered, which possess the far field directionalities $\tilde{D}_1(\alpha)$ and $\tilde{D}_2(\alpha)$ and are of relative strengths Q_1 and Q_2. Specifying these two regions a distance '1' apart gives the far field cross power spectral density from 2.8.3 as

$$\tilde{R}_o(\alpha) = \frac{1}{R^2}\left\{ Q_1^2\ \tilde{D}_1(\alpha)D_1^*(o) + Q_2^2\ \tilde{D}_2(\alpha)D_2^*(o)e^{-iKl\sin\alpha} \right\} \qquad (2.9.8)$$

and the power spectral density at 'α' as

$$P(\alpha) = \frac{1}{R^2}\left\{ Q_1^2\ |\tilde{D}_1(\alpha)|^2 + Q_2^2\ |\tilde{D}_2(\alpha)|^2 \right\} \qquad (2.9.9)$$

Also the complex coherence is defined

$$\tilde{C}_o(\alpha) = \tilde{R}_o(\alpha)\ /P^{\frac{1}{2}}(\alpha)\ P^{\frac{1}{2}}(o) \qquad (2.9.10)$$

and is then used to specify a source image defined as

$$q_I(z) = \frac{1}{2\pi}\int_{-\infty}^{\infty}\tilde{C}_o(\alpha)\ w\ (K\sin\alpha)e^{iKz\sin\alpha}\ d(K\sin\alpha) \qquad (2.9.11)$$

Two cases are of interest and will be considered separately:

1) when $Q_1^2|\tilde{D}_1(\alpha)|^2 \gg Q_2^2\ |\tilde{D}_2(\alpha)|^2$ and $\tilde{D}_1(\alpha)$ and $\tilde{D}_2(\alpha)$ are both real valued. In this case $P(\alpha)=\frac{1}{R^2}Q_1{}^2|\tilde{D}_1(\alpha)|^2$ so that from 2.9.9 and 2.9.10

$$\tilde{C}_o(\alpha) \simeq \left\{ 1 + \frac{Q_2^2}{Q_1^2}\ \frac{\tilde{D}_2(\alpha)\ \tilde{D}_2^*(o)}{\tilde{D}_1(\alpha)\ \tilde{D}_1^*(o)}\ e^{-iKl\sin\alpha} \right\}$$

This shows how the effect of the different directionality is localised onto the less significant source. When the source image is calculated using 2.9.11, the most significant source at y=o will be evaluated correctly in its normalised and resolution limited form, while the secondary source has the image:

$$q_I(z) = \frac{1}{2\pi}\left(\frac{Q_2}{Q_1}\right)^2 \int_{-\infty}^{\infty} \left\{\frac{\tilde{D}_2(\alpha)\tilde{D}_2^*(o)}{\tilde{D}_1(\alpha)\tilde{D}_1^*(o)}\right\} w(K\sin\alpha)e^{iK(z-1)\sin\alpha} \, d(K\sin\alpha) \qquad (2.9.12)$$

The differing directionalities therefore modify the weighting function used to calculate the source image, and therefore give a different window function on the secondary source.

A typical example of this effect is given by a jet noise source distribution with the directionality

$$\tilde{D}(\alpha) = (1-M_c\sin\alpha)^{-n}$$

which dominates a tailpipe noise source at the nozzle exit which is omnidirectional. Then

$$\frac{\tilde{D}_2(\alpha)\tilde{D}_2^*(o)}{\tilde{D}_1(\alpha)\tilde{D}_1^*(o)} = (1-M_c\sin\alpha)^n$$

In Figure 2.9 examples are given of the window function imposed on this secondary source for values of n = 1,2,3, with M_c = 0.7. This result shows that very little error is incurred due to this approximation.

2) When the two sources and their associated directionalities are of the same order of magnitude, then the assumption that the power spectral density $P(\alpha)$ is dominated by the field from one of these sources no longer holds.

The complex coherence is given in terms of the sources as

$$\tilde{C}_o(\alpha) = \frac{Q_1^2\tilde{D}_1(\alpha)\tilde{D}_1^*(o)}{P^{\frac{1}{2}}(\alpha)P^{\frac{1}{2}}(o)} + \frac{Q_2^2\tilde{D}_2(\alpha)\tilde{D}_2^*(o)}{P^{\frac{1}{2}}(\alpha)P^{\frac{1}{2}}(o)} e^{iK1\sin\alpha}$$

Considering each term in this relationship separately, and calculating their individual source images gives similar results. Taking the

source at y=o, the source image is given by

$$\frac{1}{2\pi}\int_{-\infty}^{\infty} \frac{e^{i\phi(\alpha)-i\phi(o)}\, w(K\sin\alpha)\, \exp(iKz\sin\alpha)\, d(K\sin\alpha)}{\left\{1+\frac{Q_2^2|\tilde{D}_2(\alpha)|^2}{Q_1^2|\tilde{D}_1(\alpha)|^2}\right\}^{\frac{1}{2}} \left\{1+\frac{Q_2^2|\tilde{D}_2(o)|^2}{Q_1^2|\tilde{D}_1(o)|^2}\right\}^{\frac{1}{2}}}$$

where $\phi(\alpha)$ represents the phase of the source at this location. If this phase is not allowed for it will cause phase distortion in the source image. However in many cases such as jet noise or omnidirectional sources $\phi(\alpha)-\phi(o)$ may be taken as zero and so this term will be overlooked in this evaluation.

Two examples will be considered, first the window associated with an omnidirectional point source which is equally significant as a jet noise source (i.e. $Q_1 = Q_2$) which has the directionality

$$D_2(\alpha) = (1 - M_c\sin\alpha)^{-n}$$

so that the associated window function is given by

$$W(z) = \frac{2^{-\frac{1}{2}}}{2\pi}\int_{-\infty}^{\infty} \left\{1+(1-M_c\sin\alpha)^{-2n}\right\}^{-\frac{1}{2}} w(K\sin\alpha)\, e^{iKz\sin\alpha}\, d(K\sin\alpha)$$

and secondly the window associated with a jet noise source of the same directionality as above, when it is associated with an omnidirectional source of equal significance. This will be given by

$$W(z) = \frac{2^{-\frac{1}{2}}}{2\pi}\int_{-\infty}^{\infty} \left\{1+(1-M_c\sin)^{+2n}\right\}^{-\frac{1}{2}} w(K\sin\alpha)\, e^{iKz\sin\alpha}\, d(K\sin\alpha)$$

The results are shown in Figures 2.10 and 2.11 and demonstrate that very little error is incurred, the correct engineering result always being given.

2.10 CONCLUSION

In this chapter the theoretical basis of the Polar Correlation technique has been described. Starting with a simple model of the source distribution, the principle of the wavenumber spectrum was developed and resolution and aliasing effects were demonstrated. Also the various approximations used in each step of the theory were evaluated using numerical examples.

The ambiguity of the source distribution evaluated from the acoustic far field was discussed and it was shown how the evaluated source image was the equivalent distribution of monopoles which resulted in the measured acoustic far field.

The wavenumber spectrum principle was then extended to the evaluation of randomly fluctuating sources with arbitary spatial coherence. Two approaches to this problem have been considered and two different definitions of the evaluated source strengths are obtained. The first definition of source strength describes a distribution whose value is the effective strength of the source at that point, including any interference effects, as seen by the observer at the reference angle. The second definition, however, groups coherent sources into isolated units and the source strength is defined as the relative strength of these units. In order to evaluate the distribution two assumptions have to be made. First it is assumed that each coherent region has an identical directionality and secondly that each has no phase directionality. It was shown that these assumptions are reasonable for the type of source distributions which will be measured in this thesis, the only exception being on a jet engine when noise from the inlet is strongly coherent with noise from the by-pass duct exit. When these assumptions are reasonable the second definition of source strength provides two major practical advantages: the ability to use one sided transforms and the normalisation of data; neither of these can be realised by using the first definition. Since the majority of source distributions to be evaluated in this thesis may be modelled using the second definition, the significant practical advantages which it offers will be used in the following chapters.

CHAPTER 3: PRACTICAL ASPECTS OF POLAR CORRELATION

3.1. INTRODUCTION

This chapter is intended as a self-contained practical guide to Polar Correlation, which may be read without reference to Chapter 2. It is hoped that it will enable the experimentalist to carry out a source location experiment without the detailed knowledge of the theory which has led to the development of this technique. However in order to undertake a source location experiment, the basic principles of the technique must be understood, and these are described in the next section. In this references will be given to the relevant sections in Chapter 2 so that the detailed theory may be referred to if required.

As with any experiment, the results from the Polar Correlation technique are only meaningful if they are interpreted correctly. It should therefore be remembered that any source location technique, using far field information alone, only evaluates the equivalent distribution of monopoles (see Section 2.4) and the interpretation of the source strength parameter depends on its definition (2.6 and 2.8). In general these techniques should only be applied to source distributions which are virtually omnidirectional over the region of the far field being used for measurements, and they work well in this situation. However when the distribution contains elements which have very strong and markedly different directionalities, and therefore acoustically large correlation regions, the source location results will need careful interpretation.

3.2. THE BASIC PRINCIPLES OF POLAR CORRELATION

To evaluate the distribution of sources along the axis of an aero-engine it is necessary to model the acoustic source distribution. Therefore the aero-engine is considered as a linear array of acoustic monopole sources, and the technique then determines this distribution using a method based on the wavenumber spectrum principle.

To illustrate this principle consider three simple sources A, B and C on a line which represents the axis of the aero-engine (see Fig.3.1). First consider the case when each source is radiating at a fixed frequency so that each source in isolation causes a spherical pattern of waves. At any fixed instant in time these wave fields will have peaks and troughs of pressure amplitude as illustrated on the left

of Figure 3.1. Measurements can then be taken on a polar arc of constant radius, and from these the strength and location of each source can be identified. Taking for example the source at A in isolation: since this lies at the centre of the polar arc, at any fixed instant of time the pressure amplitude on the polar arc will be constant, as illustrated by the top diagram on the right of Fig. 3.1. However the waves from the source at B cross over the polar arc, and so at any fixed instant in time there will be a variation of pressure amplitude around the polar arc. This variation is shown on the right of Fig. 3.1.and is found to be cosinusoidal as a function of the sine of the angle 'α'; similarly for the source at C which lies further downstream from the polar arc centre. In this case the polar arc passes through more peaks and troughs of the wave field and the variation of pressure amplitude as a function of $\sin(\alpha)$ yields a cosine wave of higher frequency.

When all three sources are radiating at the same time the total wave field on the polar arc will be given by the sum of these three cosine waves, illustrated on the bottom right of Figure 3.1. However each cosine wave represents a term in the Fourier series which represents the total wave field. The amplitude of each cosine wave is determined by the strength of the source, and the frequency by the location of the source. It is a relatively simple matter to solve this Fourier series to determine the strength and location of each source.

In the more general case sources are continuously distributed along the axis of the aero-engine, and therefore the Fourier series illustrated here, becomes a Fourier integral. The theoretical background to this form of solution is given in Section 2.2.

However in the case of aero-engines the acoustic sources are randomly fluctuating, which means that the effective source strength at any frequency will vary with time. Therefore it is necessary to consider an averaged source strength. This may be obtained by considering the cross power spectral density on the polar arc. The reasons for choosing this quantity are fully described in Chapter 2, and may be summarised as follows: the pressure amplitude in a harmonic acoustic field at any instant may be defined by $p(t) = A\cos(\omega t+\phi)$

which is sometimes more conveniently described in complex notation as $\tilde{A}\exp(i\omega t)$, where p(t) is given by the real part of this expression. The phase ϕ is included in the complex definition of $\tilde{A} = A\exp(i\phi)$ and describes the relative phase between signals at two different points in the field. When sources are not radiating harmonically it is necessary to consider averaged quantities such as the power spectrum (defined as the expected value of A^2) or the cross power spectrum between two points (defined as the expected value of $\tilde{A}_1 \tilde{A}_2^*$, * denoting complex conjugate). For source location the phase dependence of the acoustic far field is required and so the cross power spectrum is found to be the natural quantity to consider. It is shown in Section 2.5 that the relationship between the cross power spectrum and the source strength as viewed from the angle 'β' in the acoustic far field is given for continuously distributed sources by

$$\tilde{R}_\beta(\alpha) = \int_{-\infty}^{\infty} \tilde{Q}_\beta(y)\, e^{-iKy(\sin\alpha - \sin\beta)}\, dy \qquad (3.2.1)$$

where

$\tilde{R}_\beta(\alpha)$ is the c.p.s.d. between $p(\alpha,t)$ and $p(\beta,t)$

and $\tilde{Q}_\beta(y)$ is the source level as viewed from β.

(see Fig. 2.1 for notation)

This may be recognised as a Fourier integral relationship which may be solved to yield the distribution of source strength $\tilde{Q}_\beta(y)$. Clearly measurements should be taken as a function of $(\sin\alpha - \sin\beta)$, however in the rest of this section β will be taken to be zero for convenience.

It must be remembered that the c.p.s.d. $\tilde{R}_o(\alpha)$ can only be measured in practice at discrete points on the polar arc, and only over a limited range of '$K\sin\alpha$'. This imposes certain restrictions on the evaluated source image which are fully discussed in Section 2.3. In the rest of this section the implications of these restrictions will be discussed.

Solving for the Source Image

In order to solve for the source strength it is necessary to evaluate the inverse Fourier transform:

$$\tilde{Q}_o(y) = \frac{1}{2\pi}\int_{-\infty}^{\infty} \tilde{R}_o(\alpha)\, e^{iKy\sin\alpha}\, d(K\sin\alpha) \qquad (3.2.2)$$

The solution to this integral for measured values of $\tilde{R}_o(\alpha)$ at discrete points over a limited range of 'Ksinα', is an identical procedure to the evaluation of a narrow band power spectral density function from an autocorrelation function (see Fig.3.2). Therefore the physical problems of only having a limited range of measurements at discrete points have exact analogies in each case.

Consider Figure 3.2, and note that the autocorrelation function is only defined over a limited range up to a maximum delay T_{max}. The influence of this maximum delay on the Fourier transform procedure is to define the frequency resolution of the power spectrum. Also the autocorrelation function has only been evaluated at discrete time delays separated by intervals of 'τ'. In the frequency domain this effectively defines an aliasing frequency, which is the maximum frequency component which the power spectrum can possess. Further if the autocorrelation function includes higher frequencies than this aliasing frequency, then the evaluated power spectrum will contain 'aliasing' errors. These concepts are clearly described in Bendat and Piersol (1958), but it is useful to realise that the evaluation of the source distribution obeys the same criteria. First the maximum aperture angle of the measured data defined by 'Ksinα_m', determines the axial resolution of the source image.* Secondly, the interval between measured data points 'KΔ', as shown in Figure 3.2, defines the aliasing length of the source distribution. If the amplitude and phase data contain contributions from sources outside the limits of the aliasing length, then the source image will contain aliasing errors.

One of the discrepancies of this analogy is that the autocorrelation function is real valued, while the cross power spectral density is a complex valued function. The Fourier transform of the autocorrelation function, because it is real valued, yields a symmetrical (even) function of frequency, while the Fourier transform of the complex valued cross power spectral density yields a function which is not necessarily symmetrical about y = 0. The aliasing criteria for the power spectrum therefore applies in principle between $\pm f_{max}$, although the negative frequency has no meaning. However in the case of the source distribution, negative locations -y refer to points forward of the origin, and so the aliasing limits of $\pm L/2$ define the

* A normalising factor of 2π must be included in the definition of the resolution width, as the Fourier transform is with respect to 'Ksinα' rather than $2\pi k$

total aliasing length of the source distribution to be 'L'. This is shown schematically in Figure 3.2.

In conclusion therefore it has been shown that the source distribution may be evaluated from the inverse Fourier transform of measurement taken on a polar arc. The rest of this chapter will discuss the way in which these measurements should be taken.

3.3. THE REQUIREMENT FOR A TWO-SIDED TRANSFORM.

Another application of the power spectrum analogy is to describe the effect of two-sided transforms. It is noted that the autocorrelation function is always symmetrical about the zero time delay $t = 0$, and this ensures that the power spectrum is always a real valued function (i.e. its imaginary part will be zero for all frequencies). This provides a major reduction in data processing since the autocorrelation need only be evaluated for positive time lags, the negative time lags being defined as identical. A similar utilisation may be considered in the evaluation of the far field cross power spectral density; if it can be assumed that the source level $Q_o(y)$ is an entirely real valued quantity and has no imaginary part, then the far field cross power spectral density will be symmetrical about $K\sin\alpha = 0$, therefore only half the measurements need be taken. It may be shown that this assumption is only justified theoretically if all the sources along the axis are effectively uncorrelated, so that their cross power spectral density $Ex\left[\tilde{q}_\omega(y)\ \tilde{q}^*_\omega(z)\right]$ only exists when $y = z$ (see 2.6). In that case it follows that the acoustic far field will be omni-directional, (i.e. the power spectral density on the far field polar arc will be constant). It should be noted that to date all source location measurements on model or full scale jets (Fisher et al(1977), Billingsley and Kinns (1976), Flynn and Kinns (1976), Grosche (1973), Laufer et al (1976)) have been interpreted using this assumption, which is strictly incorrect since jets are not omni-directional acoustic sources. However if the jet is considered as a number of regions of correlation, which may be summed as independent radiators of sound, then the overall directionality in the far field is determined by the summed directionality of each correlated region. Then by making the much less restrictive assumption that each correlated region has the same directionality, the far field may be corrected for this effect so that the field from an equivalent array of uncorrelated sources is

obtained. This field will be symmetrical about $K\sin\alpha = 0$, and so only positive values of $\sin\alpha$ need be considered, halving the number of measurement points required.

However the evaluation of the effective source directionality can only be achieved in terms of its amplitude. A region of correlated sources may possess directionality of both amplitude and phase, but the far field power spectral density will only define the amplitude term. The phase term is unmeasurable since it cannot be differentiated from the phase variation in the field due to the location of the source. Therefore it is necessary to assume that there is no phase directionality associated with the source distribution. It has been demonstrated in section 2.8 that in the case of jet noise this assumption would appear valid. However the type of error which is likely to be caused by ignoring phase directionality is a distortion on the evaluated image similar to those described in terms of signal processing by Papoulis (1962).

To summarise these concepts we will first consider a distribution of sources which are completely uncorrelated and so their distribution gives no far field directionality. The C.P.S.D. in the acoustic far field can be derived from equation 3.2.1 by replacing the source strength $\tilde{Q}_\beta(y)$ by an omnidirectional, real valued distribution $Q(y)$, which defines the mean square level of each source; thus

$$\tilde{R}_\beta(\alpha) = \int_{-\infty}^{\infty} Q(y)\, e^{iKy(\sin\alpha - \sin\beta)}\, dy \qquad (3.3.1)$$

However each of these uncorrelated point sources may be given a directionality $\tilde{D}(\alpha)$ which results from their multipole nature, or equivalently (see section 2.4) a distribution of monopoles about 'y'. If this directionality is the same for each source then equation 3.3.1 may be modified to include this effect as follows:

$$\tilde{R}_\beta(\alpha) = \tilde{D}(\alpha)\, \tilde{D}^*(\beta) \int_{-\infty}^{\infty} Q(y)\, e^{iKy(\sin\alpha - \sin\beta)}\, dy \qquad (3.3.2)$$

The concept put forward in this section is that this second equation may be reduced to the form 3.3.1 by normalising out these directionality factors.

In order to normalise equation 3.3.2 it is necessary to measure the directionalities $\tilde{D}(\alpha)$ and $\tilde{D}(\beta)$. If it can be assumed that these

have zero phase then they can be measured using the power spectral density at α and β. The P.S.D. can be defined from equation 3.3.2 by allowing α to equal β giving:

$$P(\alpha) = \left|\tilde{D}(\alpha)\right|^2 \int_{-\infty}^{\infty} Q(y)\, dy \qquad (3.3.3)$$

Thus by defining the quantity

$$\tilde{C}_{\beta}(\alpha) = \tilde{R}_{\beta}(\alpha) \,/\sqrt{P(\alpha)\, P(\beta)} \qquad (3.3.4)$$

which will be referred to as the complex coherence, it is found from 3.3.2 and 3.3.3 that

$$\tilde{C}_{\beta}(\alpha) = \int_{-\infty}^{\infty} \frac{Q(y)\, e^{ik y(\sin\alpha - \sin\beta)}}{\int_{-\infty}^{\infty} Q(y)\, dy}\, dy \qquad (3.3.5)$$

Therefore by defining $Q'(y)$ as the distribution of source strength normalised to unit area, i.e.

$$Q'(y) = Q(y) \Big/ \int_{-\infty}^{\infty} Q(y)\, dy$$

we obtain from 3.3.5

$$\tilde{C}_{\beta}(\alpha) = \int_{-\infty}^{\infty} Q'(y)\, e^{ik y(\sin\alpha - \sin\beta)}\, dy \qquad (3.3.6)$$

This is a Fourier transform relationship which is identical in form to equation 3.2.1, and methods for inverting this equation to obtain $Q'(y)$ from $\tilde{C}_{\beta}(\alpha)$ are described in section 3.2. However this formulation has two distinct advantages over the form given by 3.2.1, first $\tilde{C}_{\beta}(\alpha)$ is a normalised quantity which greatly simplifies the calibration of the measured signals, and secondly $\tilde{C}_{\beta}(\alpha)$ will be symmetrical about $\sin\alpha - \sin\beta = 0$, as a function of $\sin\alpha - \sin\beta$.

This is a direct result of $Q'(y)$ being defined as a real valued quantity and is of major practical significance since only positive displacements $(\sin\alpha - \sin\beta)$ need be measured.

The detailed theory which has led to this result is described in section 2.8 and some of the approximations which have had to be made

are evaluated numerically in section 2.9 and experimentally in Chapter 5.

This approach not only results in two major practical advantages but also provides a definition of source strength which is easy to interpret. The distribution Q'(y) defines the relative strength of the coherent region associated to the location 'y'. Since this coherent region may be the result of a point multipole or an equivalent distribution of monopoles, resolution within that region is ambiguous and of secondary importance. This approach provides the location of the strongest region of the source distribution which is the prime objective.

3.4. MICROPHONE ARRAY DESIGN*

It has been shown in sections 2.3 and 3.2 that the design of the microphone array determines the resolution and the aliasing length of the source image. Since the number of microphones available for a source location test is inevitably limited, it is important that the microphone array should be designed to satisfy the necessary aliasing and resolution criteria using the minimum number of microphones.

The first requirement of the microphone array is that it should be able to resolve two point sources separated by a distance 'd'. It is shown in 2.3 that these sources are resolved if the angular aperture covered by the microphone array satisfies the condition

$$\sin(\alpha_{max}) \geq \lambda/d$$

where

λ = acoustic wavelength.

In practice it has been found that this criterion is a little optimistic and a better criterion is

$$\sin(\alpha_{max}) \geq 1.5\,\lambda/d \qquad (3.4.1)$$

For an array which includes N microphones equally spaced in '$\sin\alpha$' it follows that $\sin(\alpha_{max}) = (N-1)\Delta$, where Δ is the spacing between the microphones. However the microphone spacing also determines the aliasing length of the source image. This was discussed in section 2.3.and it was shown that to avoid aliasing errors on a source distribution of length 'L', the microphone spacing 'Δ' must satisfy

$$\Delta \leq \lambda/L \qquad (3.4.2)$$

(NOTE: $K = 2\pi/\lambda$ in Fig.3.2)

* β will be taken to be zero in this section

These two criteria depend upon the acoustic wavelength of the source image under consideration, while the requirements for the resolution and aliasing length are determined by the physical dimensions of the source. For example, consider the case of a high by-pass ratio engine for which it is necessary to resolve point sources at the by-pass duct exit and the hot core exit, without aliasing a distant source at the engine inlet. In order to prevent aliasing the microphone array must be designed using equation 3.4.2 for the spacing, with λ taken as the minimum acoustic wavelength which will be considered, and 'L' as the length of the engine*. Thus

$$\Delta = \lambda_{min}/L$$

However, the resolution criterion 3.4.1 must be satisfied using the longest wavelength to be considered in the tests, and 'd' equal to the separation between the by-pass duct and the hot core exit. Thus

$$\sin(\alpha_{max}) = (N-1)\Delta = 1.5. \quad \lambda_{max}/d.$$

Combining these two equations gives the required number of microphones N as

$$N-1 = 1.5 \frac{\lambda_{max}}{\lambda_{min}} \quad \frac{L}{d} \qquad (3.4.3)$$

This result shows how the required number of microphones depends not only on the ratio of the resolution to the aliasing length but also on the ratio of minimum to maximum acoustic wavelengths to be considered. Typically the ratio of L/d for an engine such as the RB.211 is just less than 6, so the required number of microphones is given in this case by

$$N-1 = 8 \left(\lambda_{max}/\lambda_{min} \right)$$

Therefore to cover a frequency range of 500 Hz to 4000 Hz requires 64 microphones, plus a reference microphone.

This number of microphones is often impractical and therefore to reduce it the graded microphone array has been developed. A graded microphone array consists of a number of overlapping sub-arrays, each of which is designed to cover a limited frequency range (see Fig.3.3). By overlapping these sub-arrays the required number of microphones is reduced to a minimum, while still satisfying the criteria given above.

*Note this example assumes no sources downstream of the hot core. In practice these should be included in defining the aliasing length.

If the frequency range in the previous example is separated into the octave bands 500-1000,1000-2000, 2000 - 4000 Hz, then the required number of microphones to cover any of these bands in isolation will be 16. To satisfy the anti-aliasing criteria 3.4.2 in the highest frequency band 2000 - 4000 Hz, the microphone spacing in this sub-array must be $\Delta = \lambda_{min}/L$, and adequate resolution will be provided using 17 microphones at this spacing. However in the middle frequency range 1000 - 2000 Hz, the wavelengths are halved and so a microphone spacing of 2Δ is adequate to prevent aliasing. The resolution criterion is satisfied using 17 microphones at intervals of 2Δ, giving a total aperture of 32Δ. However this array will overlap the higher frequency array in the first half of the arc, and so only 8 additional microphones are required to cover the second half of the arc. Therefore to cover the frequency range of 1000 - 4000 Hz, 25 microphones are required. A similar philosophy may be applied to the lowest frequency range of 500 - 1000 Hz, which may be covered with an additional 8 microphones. Therefore by using a graded microphone array the required number of microphones is only 33, giving a major reduction on the previous estimate.

A general expression for the required number of microphones using a graded array can be given using 3.4.3 with $\lambda_{max}/\lambda_{min} = 2$,

$$N-1 = 3\frac{L}{d} + 1.5\frac{L}{d}(M-1) = 1.5\frac{L}{d}(M+1) \qquad (3.4.4)$$

where M is the number of octaves to be covered.

Although this provides a major reduction in the required number of microphones, it is often found that this number is still unavailable. A further reduction is possible if interest is limited to the octave band centre frequencies only. This allows the array to be designed using the same principle as before, only with $\lambda_{max}/\lambda_{min} = 1$ for each sub-array. To consider the highest frequency in isolation requires only 9 microphones, at a spacing of Δ. To consider 2000 Hz in isolation however requires 9 microphones at a spacing of 2Δ (see Fig.3.3), but by overlapping the arrays only an additional 4 microphones are required. Similarly with 1000 Hz and 500 Hz, so that finally a total of only 21 microphones are necessary. A general formula for the number of microphones in a reduced microphone array is given by

$$N-1 = 1.5\frac{L}{d} + 0.75\frac{L}{d}(M'-1) = 0.75\frac{L}{d}(M'+1) \qquad (3.4.5)$$

where M' is the number of octave band centre frequencies of interest.

In conclusion therefore it has been shown how the very large number of microphones required for an equally spaced microphone array can be reduced significantly using the graded array, without loss of detail in the source image. Further by limiting interest to the octave band centre frequencies, the reduced graded microphone array offers a further reduction in the required number of microphones. This reduced microphone array may be used for frequencies between the octave centre band values, but the resolution criteria 3.4.1 will not be satisfied in these ranges. It should be emphasised that any microphone array cannot be used outside its aliasing limits, since this will create non-correctable errors in the measured source distribution. Although these concepts have been discussed in terms of the Polar Correlation technique, they also apply equally well to any other source location technique which uses a microphone array, for example the Acoustic Telescope, Billingsley & Kinns (1976).

3.5. DATA ACQUISITION AND ANALYSIS

The previous sections of this chapter have described the basic principles of the Polar Correlation technique, and this section will discuss the specifications for data acquisition and analysis.

a) Microphone Layout.

When specifying a Polar Correlation test it is first necessary to ensure that the source distribution is effectively a line source. In general source distributions are three dimensional but they may be modelled by an equivalent acoustic line source providing the data acquired is independent of the distribution of sources across the axis. These effects have been discussed in sections 2.3 and 2.9, and it was illustrated that providing the largest cross axis dimension in the source distribution satisfies the criterion:

$$\frac{z}{\lambda}(1-\cos\alpha_m) < 0.25$$

where z is largest cross axis dimension

λ is the acoustic wavelength

α_m is the maximum aperture angle,

the distribution may be modelled as a line source. This may determine an upper limit to the resolution available in certain circumstances.

Next the polar arc radius must be chosen, and this must be large enough to satisfy the acoustic far field criterion. This has been discussed in section 2.9 and it has been shown that the source furthest from the polar arc centre is most likely to deviate from the far field path length approximation over the microphone array. It is therefore most advantageous to position the polar arc centre in the middle of the source distribution. The far field criterion depends upon the following factors:

i) The polar arc radius in wavelengths R/λ

ii) The maximum source displacement and the maximum aperture of the microphone array. The critical factor is given by

$$\phi = \frac{KY^2 \sin^2 \alpha_m}{2R} = \pi \frac{\lambda}{R} \frac{Y^2}{d^2}$$

where Y is the maximum source displacement and 'd' is the resolution of the array given by $d = \lambda / \sin \alpha_m$. This demonstrates that this type of error is a maximum at low frequencies where λ/R is greatest for a given resolution 'd'. The numerical study in section 2.9 has shown that significant errors will occur when ϕ is greater than $\pi = 3.142$ (see Figure 2.3). Therefore the polar arc radius should be chosen to ensure that ϕ satisfies this criterion at the lowest frequency to be considered. The location of microphones on the polar arc has been discussed in section 3.4 and will not be considered here. However it is important that the microphones should be equidistant from the polar arc centre, since any discrepancy will introduce path length errors. The acceptable limit to this is only a fraction of the smallest wavelength to be considered. This has caused some difficulty in the past and the simplest measurement method used to date has been a piece of piano wire pivoting on the polar arc centre and tensioned by a spring balance. The exact distance of the microphones to the polar arc centre is not critical providing they are all equidistant.

Ideally Polar Correlation tests are done in an anechoic environment. However in many cases it is necessary to use open air test beds, with inherent ground reflection problems. To eliminate these effects ground level microphones should be used, the criterion being that the microphone height should only be a small fraction of the shortest wavelength to be considered.

In certain circumstances it may be convenient to use only a reference microphone and a traversable microphone which is placed at each location on the polar arc in turn. While this is time consuming it does reduce the amount of equipment required. In this case the acoustic emission of each source must remain statistically stationary throughout the test.

b) Recording Standards

It is usually most efficient to record real time signals on magnetic tape for subsequent data analysis. Normal recording standards are usually adequate providing the frequency response of the tape recorder covers the range of interest. In general each microphone signal must be recorded simultaneously with the signal from the reference microphone. Therefore it does not matter whether a two-channel or multi-channel recorder is used providing the acoustic emission from the sources remains statistically stationary throughout the recording time. In many cases multi-channel recording is considerably more efficient and when multi-channel data acquisition computers are used in the subsequent data analysis, considerable speed advantages may be gained. However when only a reference and traversable microphone are available, two-channel recording has to be used and the data acquisition time increases markedly.

Normally about 45-60 seconds provides ample data for subsequent analysis, including time for tape acceleration and computer response time.

c) Calibration.

Apart from the usual pistonphone calibration procedures, which define the gain on each channel, it is imperative that the whole data analysis system is calibrated for phase. This is obtained most efficiently in anechoic surroundings by a loudspeaker test.

A loudspeaker is placed at the polar arc centre (or at a known displacement on the axis) and driven by white noise (or alternatively a tone if reasonable white noise levels cannot be obtained). The loudspeaker diaphragm should face the reference microphone. The complete data acquisition and analysis procedure is carried out on this source and the eventual phase data should be related to the source position by

$$\phi = \frac{2\pi y}{\lambda} \left[\sin(\alpha) - \sin(\beta) \right]$$

at each microphone location

where β is angle of reference microphone

and y is displacement of source from polar arc centre.

The deviations from this give the phase calibration, which should be deducted from subsequent phase measurements.

The advantage of the procedure is that it calibrates the whole system. However in an outdoor test a loudspeaker calibration of this type can introduce errors due to atmospheric effects, wind etc, which are as large as the microphone location errors. Therefore phase calibration of the microphone layout is assumed to be exact, and calibration of the tape recorder and data analysis system can be obtained by recording the same white noise signal on each tape recorder channel. This provides a phase calibration which allows for tape recorder head skew and phase characteristics of filters.

d) Wind and Environmental Data.

Apart from the wind, other environmental data (such as humidity) is not required for Polar Correlation tests. The only reason for which it may be needed is to obtain the level at the reference microphone under normalised conditions for subsequent comparison of source distributions. Source levels are calculated relative to the level at the reference microphone and therefore this is the only level which needs to be calibrated accurately.

However wind effects are very important since they will alter the time of flight of the acoustic signal from the source to each microphone. Wind calibration procedures will be discussed in a later section but for these to be accurate the wind strength and direction must be known.

e) Data Analysis Requirements.

Data analysis is an extremely important topic which will be discussed in detail in Chapter 4. The purpose of this sub-section is merely to outline the requirements.

To calculate the source distribution it is necessary to obtain the complex coherence between each microphone in the sub-array and the reference microphone. The complex coherence is defined as the cross power spectral density normalised by the power spectral density of the two relevant signals, and will be complex in its definition.

$$\underset{\beta}{\tilde{C}}(\alpha) = \frac{Ex\left[p_\omega(\alpha)\ p_\omega^*(\beta)\right]}{\left\{Ex\left[|p_\omega(\alpha)|^2\right].\ Ex\left[|p_\omega(\beta)|^2\right]\right\}^{\frac{1}{2}}}$$

Calculation of this quantity may be obtained using specialised data analysis facilities which are now available in most major centres. Several different systems will be described in Chapter 4.

Because of the random nature of the signals this quantity can at best only be estimated with a certain statistical error. This may be calculated and it will be shown later how it affects the source distribution. The accuracy of these estimates depends upon the B_eT product (where B_e is the effective frequency bandwidth and T is the length of time averaging) used in the data analysis, and as a guide line this should be at least 300 using a microphone array as described in section 3.4. A larger B_eT product is required when a different type of microphone array is used, which requires a linear interpolation procedure to calculate the source distribution. This will be discussed in the next two sections, but the larger time averaging requirement is necessary because the interpolation procedure force fits the estimated data.

3.6. CALCULATION OF SOURCE DISTRIBUTIONS

Historical Note

The Polar Correlation technique was originally developed to evaluate the source distributions in turbulent jets. In the initial studies careful measurements were made of the variation of amplitude (coherence) and phase in the acoustic far field of cold subsonic model air jets in anechoic surroundings. It was found that for this type of source distribution the amplitude function decayed monotonically with increasing angular separation, and the phase was nearly linear. It therefore appeared reasonable to assume that the analytic form of these functions could be approximated by linear interpolation between suitably spaced measured values. The interval between the measurement points was determined by the detailed variation of the amplitude function, and this was found to be most significant at small angular separations; at larger angular separations, the amplitude was found to vary slowly. Therefore measurement points were chosen so that they were closely spaced at the small angles, and the spacing increased at larger angles of separation. This measurement scheme, using linear interpolation, made a good approximation to the analytic form of the amplitude and phase, and therefore very clear detail was obtained on the image source distributions.

However, when this measurement scheme was applied to a high by-pass ratio engine, where several point sources of sound were present, the assumed monotonic decay of the amplitude function and linear variation of phase was not found. This result was not entirely unexpected, and emphasised the necessity for a further investigation into the evaluation of source distributions from measurements.

Linear Interpolation

The purpose of a microphone array is to define the measured data in sufficient detail to obtain the source distribution. Ideally an infinite number of measurement points are required, so that this data is described exactly, and the integrals giving the source distributions may be solved analytically. However, an approximation may be made to the analytic solution if the amplitude and phase varies linearly between measured points, so that unmeasured data may be described by interpolation procedures. This has the advantage that optimum use is made of a limited number of measurement points, describing the resolved source image exactly, without aliases.

An illustration of the type of data for which this method works well is given in Figure 3.4. It is shown that the amplitude and phase are well defined by the measurement points, and the resultant source distribution is given in Figure 3.5.

The problem associated with this method is that the microphone array usually has to be designed before the details of the source are known; it is therefore possible that the results from a specific test may be rendered useless if the microphone array does not describe the data in sufficient detail to define an analytic integral. For example if two point sources are added to the distribution given in Figure 3.5, then the amplitude and phase in the acoustic far field will oscillate rapidly with angular separation, Figure 3.6. It is seen that the microphone array used in the previous example is not sufficient to describe this data, and the resultant source distribution is grossly in error, Figure 3.7. This problem is clearly associated with the more widely spaced microphones which have been placed at larger angles of separation. If these microphones are eliminated from the array, then a more accurate source distribution is obtained at the expense of resolution.

Fourier Series Solution

An alternative method of obtaining the source image is to use a Fourier series solution for the measured data. This requires the data to be measured at equal spacing in '$\sin\alpha$', and defines the source image between fixed alias limits $\pm L$, which are determined by the microphone spacing. Within the limits of aliasing and resolution, the source image is then an exact solution of the measured data, and any errors built in by interpolation procedures are eliminated. The theory of the Fourier series solution is given in Appendix I, where it is shown that the source image is given exactly by

$$Q'(y) = \frac{P(o)}{L} \sum_{m=-M}^{M} W_m(M)\, C_m \exp(-2\pi i m y/L)$$

(A computer programme which evaluates this equation is listed as Computer Programme I)

where $Q'(y)$ is the resolution limited source image; C_m is the complex coherence at microphone location 'm'; $W_m(M)$ is the weighting function (see 2.3), 'L' is the aliasing length, and $2M+1$ is the total number of microphones

In order to compare the two methods of solution, the examples given previously have been solved using a Fourier series on the same number of measurement points equally spaced over the same aperture angle, giving the same resolution. The results are illustrated in Figures 3.5 and 3.8, and it is clear from these that the Fourier series solution is more versatile than linear interpolation, giving the result with quantifable error in both cases.

Perhaps the greatest advantage of the Fourier series solution is that it is exact within easily defined limits. Linear interpolation however is only exact if the amplitude and phase data is compatible with the microphone array.

For these reasons it was decided that the Fourier series solution should be used exclusively and the discussions which follow are described in terms of this method.

3.7. THE EFFECT OF MEASUREMENT ERRORS ON POLAR CORRELATION.

i) Introduction

Any measurement scheme, especially if it uses random noise signals, has associated with it a certain band of measurement errors. To evaluate such a scheme it is important that this error band should

be known, so that the results may be interpreted correctly. The purpose of this investigation was to evaluate the errors associated with Polar Correlation, and to demonstrate both theoretically, and by numerical example, their effect on the source distribution.

The errors which occur in Polar Correlation measurements are of two types; those associated with the positioning of the microphone array, and those associated with the estimation of coherence and phase of the microphone signals. In theory these two types of error may be considered together, since the effect of either will be to cause the measured coherence and phase to differ from its true value. These errors are then transmitted to the source distribution, and it is the amount of distortion produced which gives the criterion for the accuracy required from the measurements.

There are two different methods available for obtaining the source distribution from the measured data. First the linear interpolation method which takes an analytical Fourier integral of the data by interpolating between measured points, and second, the Fourier series solution which uses the measured values as coefficients of a series.

Both these methods will be discussed and the relative efficiency of each will be evaluated. Finally a criterion will be given which defines the accuracy required in the estimation of measured values, and the amount of signal averaging for this to be achieved.

ii) Linear Interpolation

It has been found in practice that the linear interpolation method is not particularly tolerant of measurement errors, and requires consistently good accuracy at all the measurement points. Since the method linearly interpolates between measured values of coherence and phase, any measurement error is transmitted by interpolation so that it affects a significant region about the measured point. However no method of calculating the extent to which such errors are apparent in the source distribution has been found since they critically depend on the shape of the data and how the interpolated points with associated errors fit the true form of the functions. Unfortunately it does not appear possible to evaluate the average statistical errors for a general source distribution. Therefore to develop a criterion

for the required accuracy of the measurements using this method, it is necessary to ensure that the data has been measured extremely accurately, so that errors of measurement do not increase the errors of interpolation. The theory which considers the accuracy of coherence and phase estimators is given by Jenkins & Watt (1968) and shows that phase measurements are considerably less accurate than coherence measurements. It is shown that the variance of a phase estimator is given by

$$\mathrm{Var}[\phi] = \frac{1}{2BT}\left(\frac{1}{|C|^2} - 1\right)$$

where C is the true coherence between the two signals

T is length of time averaging

B is frequency bandwidth.

Therefore at low values of coherence C , a large BT product is required to obtain high accuracy. For instance to ensure that the phase error is less than 10% of 2π in 95% of the measurements the BT product at 10% coherence must be 1111.0. In practice a BT product of 1000 has been used successfully.

iii) Fourier Series Solution

The Fourier series solution for obtaining source distributions from the measured data is much more amenable to evaluating the transmission of error than linear interpolation. This is because the errors may be considered separately from the source distribution and therefore their statistics can be defined. The extent of the source distribution errors can therefore be given in terms of their variance, and this is related to the variance of the measurement errors.

This relationship will be demonstrated in two stages: first, the dependence of the variance of the source distribution errors on the measurement errors and secondly the dependence of the measurement errors on the signal averages. This gives a relationship between the source distribution error and the accuracy of processing the signals.

In principle the Fourier series solution is expected to be more accurate than linear interpolation for a given accuracy of signal processing. This occurs because the Fourier series essentially fits a curve through all the measurement points available and therefore

averages the error associated with each estimated value. However linear interpolation fits a curve to pass through each measurement and therefore does not provide any additional smoothing and therefore transmits more errors.

iv) Transmission of Errors to the Source Distribution

In order to evaluate the manner in which errors of measurement are transmitted to the source distribution, the measured values of complex coherence are defined for each microphone as $\tilde{C}'_m$ (where the subscript 'm' refers to the microphone number). This may be defined as the sum of a true value C_m and an error $\tilde{E}_m$;

$$\tilde{C}'_m = \tilde{C}_m + \tilde{E}_m$$

The errors in the source distribution depend on the way in which the measurement errors $\tilde{E}_m$ are transmitted.

The source distribution may be calculated from these measurements using equation 3.6.1, and will include the transmitted errors $\tilde{\varrho}(y)$

$$Q'(y) + \tilde{\varrho}(y) = \frac{P(o)}{L} \sum_{m=-M}^{M} W_m(M) \left\{ \tilde{C}_m + \tilde{E}_m \right\} e^{-2\pi i m y/L}$$

The errors in the source distribution are therefore directly related to the errors in measurement by the Fourier series

$$\tilde{\varrho}(y) = \frac{P(o)}{L} \sum_{m=-M}^{M} W_m(M)\, \tilde{E}_m\, e^{-2\pi i m y/L}$$

Since only the real part of the source distribution will be considered only the real part of these errors need be evaluated. When $\tilde{\varrho}(y) = \varepsilon(y) + i\mu(y)$ and $\tilde{E}_m = A_m + iBm$ it follows that

$$\varepsilon(y) = \frac{P(o)}{L} \sum_{m=-M}^{M} W_m(M) \left\{ A_m \cos\left(\frac{2\pi m y}{L}\right) + B_m \sin\left(\frac{2\pi m y}{L}\right) \right\}$$

Since A_m and B_m are random variables it is not possible to define $\varepsilon(y)$ exactly. However a measure of the error transmitted to the source distribution is given by the variance of $\varepsilon(y)$ defined as

$$\mathrm{Var}\left[\varepsilon(y)\right] = \frac{1}{L} \int_{-L/2}^{L/2} \varepsilon^2(y)\, dy$$

Using the definition of $\mathcal{E}(y)$, this variance is given by the equation

$$\mathrm{Var}\left[\mathcal{E}(y)\right] = \frac{P^2(o)}{L^3}\int_{-L/2}^{L/2} \sum_{m=-M}^{M} \sum_{n=-M}^{M} W_m(M)W_n(M)$$

$$\times \left\{ A_m A_n \cos\left(\frac{2\pi my}{L}\right) \cos\left(\frac{2\pi ny}{L}\right) \right.$$

$$+ A_m B_n \cos\left(\frac{2\pi my}{L}\right) \sin\left(\frac{2\pi ny}{L}\right)$$

$$+ B_m A_n \sin\left(\frac{2\pi my}{L}\right) \cos\left(\frac{2\pi ny}{L}\right)$$

$$\left. + B_m B_n \sin\left(\frac{2\pi my}{L}\right) \sin\left(\frac{2\pi ny}{L}\right)\right\} dy$$

When this equation is integrated over y the orthogonal properties of the integrands simplify the result considerably (Churchill (1963)), giving

$$\mathrm{Var}\left[\mathcal{E}(y)\right] = \frac{P^2(o)}{L^3} \cdot \frac{L}{2} \sum_{m=-M}^{M} W_m^2(M) \left\{ A_m^2 + B_m^2 \right\}$$

Since $|\tilde{E}_m|^2 = A_m^2 + B_m^2$, this result may be simplified to

$$\mathrm{Var}\left[\mathcal{E}(y)\right] = \frac{P^2(o)}{2L^2} \sum_{m=-M}^{M} W_m^2(M) \, |\tilde{E}_m|^2$$

If the errors $|\tilde{E}_m|^2$ are evenly distributed over all the microphones then this result may be simplified using the expected value of $|\tilde{E}_m|^2$:

$$\sum_{m=-M}^{M} W_m^2(M) \, |\tilde{E}_m|^2 \sim \mathrm{Ex}\left[|\tilde{E}_m|^2\right] \sum_{m=-M}^{M} W_m^2(M)$$

The summation on the right is defined as the inverse of the effective bandwidth of the data window

$$Y_e(M) = \left\{ \sum_{m=-M}^{M} W_m^2(M) \right\}^{-1}$$

so that the variance of the error in the source distribution is defined as

$$\mathrm{Var}\left[\mathcal{E}(y)\right] = \frac{P^2(o)}{2L^2} \frac{\mathrm{Ex}\left[|\tilde{E}_m|^2\right]}{Y_e(M)} \qquad (3.7.1)$$

The effective bandwidth of various types of data window is easily computed, for example

$Y_e(M) = 1/2M$ for a rectangular window

$Y_e(M) = 3/(2M + 1/M) \simeq 3/2M$ for a Bartlett window

The result 3.7.1 defines the variance of the error associated with the source distribution. These will be distributed about the true distribution, and this variance is a measure of the average difference between the measured and true source distribution. It is reasonable to assume that the errors in measurement will be normally distributed with zero mean. This means that the errors in the source distribution will also be normally distributed and over 68% of the curve measured values will lie within one standard deviation (equal to the square root of the variance) of the true values. Therefore the standard deviation is a good measure of the typical error and may be defined as

$$S = \frac{P(o)}{L}\sqrt{\frac{Ex\left[|\tilde{E}_m|^2\right]}{2Y_e(M)}} \qquad (3.7.2)$$

However since $P(o)/L = \int_{-L}^{L} Q(y)dy/L$ is representative of a typical level in the source distribution an effective percentage error is given by

$$\varkappa = \sqrt{\frac{Ex\left[|\tilde{E}_m|^2\right]}{2Y_e(M)}} \times 100\% \qquad (3.7.3)$$

In order to evaluate the permissible percentage error and also to test this theory, a set of numerical examples were considered. The true data from an example of a typical jet engine noise source distribution, which included two point sources and a jet noise region (see Figure 3.9), was calculated. Various sets of errors, generated by random number tables with normal distributions, were added to this data to simulate measurements and these were transformed to give the source distribution inclusive of errors. This could then be compared with the true source distribution calculated from the true data, and the standard deviation of the source distribution error was calculated from the differences. The results are shown in Figures 3.9 - 3.14 for average errors, $Ex\left[|\tilde{E}_m|^2\right]$, between 0.001 and 0.02. Plotting the standard deviation of the source distribution error against $Ex\left[|\tilde{E}_m|^2\right]$

from both theory (equation 3.7.2) and practice demonstrates the accuracy of the theoretical result (see Figure 3.15).

From these results it is also possible to consider a subjectively permissible percentage error in the evaluated source distributions. The typical source level in these examples is P(o)/L = 0.0562 and so Figures 3.9 and 3.10 have a percentage error of less than 10% and are clearly quite acceptable. However Figures 3.11 - 3.13 have a percentage error of 15-20% and are marginally acceptable. Figure 3.14 has an error of 30% and is clearly unacceptable. Therefore it is concluded that the subjectively permissible percentage error level should be set at 10%. In terms of 3.7.3 this gives

$$Ex\left[|\tilde{E}_m|^2\right] \leqslant 2Y_e(M)\left(\frac{\varkappa}{100}\right)^2 = Y_e(M)/50 \qquad (3.7.4)$$

v) The Evaluation of Measurement Errors

The second stage in the evaluation of Polar Correlation measurement errors, is to determine the expected error $|E_m|^2$ in terms of the signal processing parameters. This has been achieved using the method outlined in Jenkins & Watts (1968) and is given in Appendix II. The variance of the errors are shown to depend on: the coherence between the signals from the reference microphone and the microphone in the array, and the B_eT product used in processing the signals. The expected mean square error at each microphone is obtained as

$$Ex\left[|\tilde{E}_m|^2\right] = \frac{1}{2B_eT}\left\{2-3|\tilde{C}_m|^2 + |\tilde{C}_m|^4\right\}$$

$\tilde{C}_m$ = true coherence between signals

T = signal averaging time

B_e = effective bandwidth of spectrum

In order to test this theoretical result an experiment was designed which considered a number of signal pairs covering a range of coherence levels, and were processed using a range of B_eT products. A total of five examples were considered giving results for B_eT products of 48, 98, 248. In each case the bandwidth B_e was kept constant and the averaging time T was adjusted. The procedure for each example was as follows:

1) The two signals were acquired through analog to digital converters on to the ISVR PDP 11/50 computer at a sample rate of 4000 samples per second, the number of samples being defined by the required averaging time.

2) This procedure was repeated ten times using different sections of a signal record from the same test.

3) The co- and quad-spectra, normalised by the power spectra, were calculated for each piece of data.

4) For each of four frequencies the mean measurement C_m was calculated from the ten sets of spectra. This was taken as the true value and enabled the error for each piece of data to be defined.

5) The true value of the coherence $|C_m|$ and the average of the error $|E_m|^2$ was then calculated.

The results of this experiment are given in Figure 3.16 which shows a reasonable agreement between theory and experiment. In general 90% of the points on this graph lie within the worst error given by the theory at zero coherence. This result is considered to be quite acceptable considering the statistical nature of the experiment. In conclusion it seems reasonable to define the expected errors of the measurements to lie within the limits defined by the inequality

$$Ex\left[|E_m|^2\right] \ll \frac{1}{B_eT} \qquad (3.7.5)$$

This result may then be combined with equation 3.7.4 of the previous section to give a criterion for the B_eT product required in signal processing:-

$$B_eT \geqslant \frac{50}{Y_e(M)} \qquad (3.7.6)$$

For example using a microphone array which includes nine microphones and smoothing the source distribution with a Bartlett window requires a B_eT product of at least 300. This offers a considerable improvement on the requirement of the linear interpolation method which experience shows needs a B_eT product of 1000.

vi) Conclusion

The measurement errors of Polar Correlation have been evaluated so that criteria may be defined for the signal processing parameters. A comparison of the two methods used to obtain the source distribution from the measured data has shown that the linear interpolation method is far more critical on the accuracy of signal processing. This occurs because the linear interpolation method force fits each measurement point, while the Fourier series method fits a curve to the distribution of measurement points.

The errors associated with the Fourier series method of solution has been considered in detail and the theory of both the transmission of errors and their relationship with the signal processing parameters has been derived and tested in practice. The major conclusion of this section is that the B_eT product required for a typical source distribution can be demonstrated to be 300. This result depends upon the number of microphones in the array used to measure the far field data and the aliasing length of the source distribution, but in general the value of $B_eT = 300$ provides a suitable guideline for most experiments.

3.8. THE CORRECTION REQUIRED FOR WIND EFFECTS.

A major application of Polar Correlation is to full scale engines on open air test beds. In this environment wind effects are inevitable and must be allowed for since they affect the time of flight of an acoustic signal from source to observer.

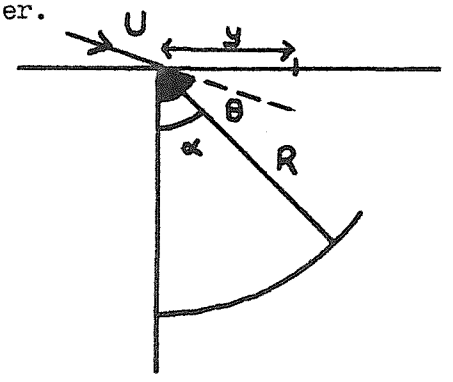

Consider the case when a wind of speed 'U' is blowing across the jet axis, at an angle θ (re. 90° to jet axis). The velocity of the acoustic signal travelling in the direction of the observer at 'α' on the polar arc will be

$$a_o + U\cos(\theta - \alpha) = a_o + U_\alpha$$

Therefore the time taken for the signal to travel from the source at y to the observer will be

$$\tau_m = (R - y\sin\alpha)/(a_o + U_\alpha)$$

However in a stationary medium the time taken will be simply $\tau_s = (R-y\sin\alpha)/a_o$ and so the wind time delay correction is defined by

$$\tau_m - \tau_s = (R-y\sin\alpha)\frac{1}{a_o}\left\{\frac{1}{1+\frac{U_\alpha}{a_o}} - 1\right\}$$

$$= (R-y\sin\alpha)\frac{1}{a_o}\left\{\frac{-M_\alpha}{1+M_\alpha}\right\}$$

where $M_\alpha = U\cos(\theta - \alpha)/a_o$

In the low frequency limit when

$$Ky\sin\alpha\left\{\frac{M_\alpha}{1+M_\alpha}\right\} \ll 1 \qquad (3.8.1)$$

the 'y' dependence of this correction may be ignored without loss of

accuracy, giving the time delay correction as

$$\tau_m - \tau_s = -\frac{R}{a_o}\left\{\frac{M_\alpha}{1+M_\alpha}\right\} \qquad (3.8.2)$$

This correction may be incorporated in the calibration procedures described in section 3.5.

The magnitude of this effect is illustrated by considering an example of a wind blowing directly along the engine axis; then $\theta = 90^\circ$ and

$$M_\alpha = M_W \sin\alpha$$

where M_W is the Mach No. of the wind. In all practical cases $M_W \ll 1$ and so the time delay correction is

$$\tau_m - \tau_s = \left[-RM_W/a_o\right] \sin\alpha$$

The application of this correction is equivalent to shifting the origin of the polar arc a distance RM_W upstream, and so the effect of the wind may be considered as a linear shift of the whole source distribution. For example in a 5 knot wind which blows along the axis, on a test using a polar arc radius of 100 ft, the source distribution will be effectively shifted 0.75 ft downstream due to the wind.

3.9. POLAR CORRELATION IN A NOISY ENVIRONMENT.

In this section the evaluation of source distributions in a noisy environment will be discussed. The theory of the Polar Correlation technique implicitly assumes that the only sources of noise present are those close to the jet axis. The presence of other noise sources, well away from this region, must induce some error even if their levels are negligible compared with the major source region. For example it will be shown that a buried source which is 10 dB below the level of other sources within a defined source region, can be determined using this technique. Therefore the effect of having a low level source outside the region must be important, since it will apparently alter the measured source distribution. The "cleanliness" of the background environment is therefore an important parameter in source location work, and the necessary criteria must be developed before results can be interpreted correctly.

To consider this problem, the overall signal at the microphone 'm' will be defined as $P'_m(t)$, which may be broken down into three components:-

1) the required signal from the source distribution $P_m(t)$

2) the signal from the background sources $Z_m(t)$, which is correlated across the array

3) the signal from background noise $X_m(t)$, which is uncorrelated across the array (e.g. turbulence across face of the microphone)

Thus the signal at each microphone is given by:

$$P'_m(t) = P_m(t) + Z_m(t) + X_m(t)$$

Since each of these three components are uncorrelated with each other, the spectral level of the overall signal is the linear sum of each component

$$P'_m(\omega) = P_m(\omega) + Z_m(\omega) + X_m(\omega)$$

where $P'_m(\omega)$, $P_m(\omega)$, $Z_m(\omega)$ and $X_m(\omega)$ are the power spectral levels of $P'_m(t)$, $P_m(t)$, $Z_m(t)$ and $X_m(t)$ respectively. Then providing the two background noise components are at least 10 dB below the signal from the source distribution:

$$P'_m(\omega) \simeq P_m(\omega)$$

However in Polar Correlation it is necessary to evaluate the cross power spectral level between microphone zero and microphone 'm'. This will eliminate the $X_m(t)$ component which is uncorrelated across the array and gives

$$\tilde{R}'_m(\omega) = \tilde{R}_m(\omega) + \tilde{U}_m(\omega)$$

where R'_m is the c.p.s.d. of $P'_m(t)$ and $P'_o(t)$

R_m is the c.p.s.d. of $P_m(t)$ and $P_o(t)$

U_m is the c.p.s.d. of $Z_m(t)$ and $Z_o(t)$

This quantity is then normalised by the overall power spectral levels to give the complex coherence as

$$\tilde{C}'_m = \tilde{C}_m + \tilde{E}_m \quad \text{where } \tilde{E}_m = \tilde{U}_m / \sqrt{P_o P_m} \qquad (3.9.1)$$

(note: the frequency dependence has been dropped for convenience)

This result shows that the measured coherence $\tilde{C}'_m$ may be considered as the sum of the two components $\tilde{C}_m$ and $\tilde{E}_m$. The first term, $\tilde{C}_m$, is the result of the signal from the source distribution which is being investigated, while $\tilde{E}_m$ represents the contribution from the background

noise sources. This is an unwanted component and so will be defined as measurement error. The transmission of measurement errors and their effect on the source image were discussed in section 3.6(iv) where it was shown that their contribution to the source image at the location 'y' was given by:

$$\tilde{\rho}(y) = \frac{Po}{L} \sum_{m=-M}^{M} W_m(M)\, \tilde{E}_m\, e^{-2\pi i m y/L} \qquad (3.9.2)$$

The difference between this and the previous analysis is that in this case each of the error terms $\tilde{E}_m$ will be correlated across the array and will combine to give an image of the background noise sources. This may be a very distorted image since the background sources may not satisfy either the aliasing or the far field conditions. It is therefore important to establish the maximum permissible background source level which does not cause significant distortion to the required source image.

To establish this criterion, consider the [illegible]n error on the source image, which may be approximated as

$$|\tilde{\rho}(y)| \sim \left\{ \frac{1}{L} \int_{-L/2}^{L/2} |\rho(y')|^2\, dy' \right\}^{\frac{1}{2}}$$

However using Parsavals theorem and 3.9.2 enables this to be written in terms of the errors $\tilde{E}_m$

$$|\tilde{\rho}(y)| \sim \frac{Po}{L} \left\{ \sum_{m=-M}^{M} W_m^2(M)\, |\tilde{E}_m|^2 \right\}^{\frac{1}{2}}$$

However since $\tilde{E}_m$ will be less than some maximum error E, we may use the inequality to extract the $|\tilde{E}_m|^2$ from under the summation and define

$$|\tilde{\rho}(y)| \sim \frac{Po.E.}{L}\, Y_e^{\frac{1}{2}}(M)$$

where

$$Y_e(M) = \left\{ \sum_{m=-M}^{m=M} W_m^2(M) \right\}^{-1}$$

and is defined as the effective bandwidth of the data window, as discussed in section 3.6.

It has already been shown that a typical level in the source distribution is given by Po/L and so to ensure that the error $\tilde{\rho}(y)$ is

very much less than this, requires

$$E \ll Y_e(M)^{\frac{1}{2}} \qquad (3.9.3)$$

Finally to estimate the value of E we will use equation 3.9.1 to give

$$E \sim |\tilde{E}_m| = \frac{|\tilde{U}_m|}{P_o P_m} \leqslant \sqrt{\frac{Z_m Z_o}{P_m P_o}} \simeq \frac{Z_o}{P_o}$$

where Z_o, P_o are the power spectral levels of each source distribution at the reference microphone. This gives the criterion for the background noise level as

$$\frac{Z_o}{P_o} \ll Y_e(M)^{\frac{1}{2}} \qquad (3.9.4)$$

In a typical example where data has been analysed using a Bartlett window and an array with nine microphones has been used, $Y_e(M) = 0.1666$ and so Z_o/P_o should be very much less than 0.4082. A suitable ratio would be 0.04082 which is equivalent to the unwanted sources being 14 dB below the level of the required source distribution.

3.10. CONCLUSION.

The purpose of this chapter is to provide a detailed description of the Polar Correlation technique for the experimentalist. Since a large number of points have been covered, this section will summarise the more important aspects of the technique.

1) In section 3.2 it was shown how the technique utilises a particular relationship between a one dimensional source distribution and its acoustic far field. It was shown how this is a Fourier integral relationship which may be inverted to give the distribution of source strength from acoustic measurements in the far field.

2) It was also shown in section 3.2 that the measured source distribution was a resolution limited image of the true source distribution, and also how the length of the distribution restricted the interval between measurement locations. In general sources which are closer than $d = \lambda/\sin\alpha_m$ cannot be resolved and source distributions of length L require far field measurements at intervals of $\Delta = \lambda/L$ on the polar arc of radius R (see Figure 3.2).

3) In section 3.3 it was demonstrated that by modelling the source distribution as an equivalent array of statistically independent multi-

poles with uniform directionalities, then only a one sided microphone array need be used in the far field. This model requires the evaluation of the "complex coherence" between the reference microphone and the others in the array (see equation 3.3.3), and from these the source distribution may be calculated.

4) The optimum design of microphone arrays was described in section 3.3. The minimum number of microphones required to consider the source distribution at M octave centre band frequencies is given by N where

$$N-1 = 0.75 \frac{L}{d} (M+1)$$

5) A description of the experimental procedure and data analysis was given in section 3.5. This included criteria for the equivalent line source and the polar arc radius. A description of recording standards, calibration procedures, wind measurements, and data analysis was also given.

6) The method for calculating the source distribution was described in section 3.6.

7) A detailed analysis of the manner in which measurement errors affect the calculated source distribution was given in section 3.7. This concluded that a B_eT product of 300 should be used in order to limit the errors associated with spectral estimation to an acceptable level.

8) The correction for wind effects on the measured source distribution is described in section 3.8. This does not include the effect of the wind on the source mechanism.

9) In section 3.9 the affect of unassociated background noise on the measurements was considered. This analysis demonstrated that these sources should have a level which is 14 dB below the level of signals from the source distribution to be measured, at all locations on the microphone array.

CHAPTER 4: DATA ANALYSIS SYSTEMS FOR POLAR CORRELATION

4.1. INTRODUCTION

In order to obtain source distributions using the Polar Correlation technique, it is necessary to measure the complex coherence* between the signals at the reference microphone and each of the other microphones in the array. The resultant values are then analysed with respect to their spatial location to calculate the source distribution. This chapter will discuss the various methods which may be used to measure the complex coherence from the microphone signals.

Since the signals are in general fluctuating randomly, it is only possible to estimate their complex coherence. The accuracy of these estimates depends upon two factors: the effective smoothing of the spectrum by finite frequency resolution and secondly the amount of time averaging used in estimating the spectrum. These factors may be quantified into a single parameter using the B_eT product, where B_e refers to the effective bandwidth of frequency resolution, and T is the length of the sample in time. (Jenkins and Watts (1968)). In most spectral applications a B_eT product of 50 is found to be sufficient. However for Polar Correlation the error analysis given in Section 3.7 demonstrated that the B_eT product should be at least 300, and sometimes greater. This requirement for very high accuracy has presented a major problem in developing efficient data analysis systems, and represents a major part of this project.

There are several different methods which may be used to calculate the complex coherence using either analog or digital facilities, or a combination of both. Each of these has been investigated, developed and used to calculate source distributions. These will be fully described and their relative merits discussed.

Since the project requires such a large amount of data analysis, the ultimate requirement must be for a dedicated digital computer, since this will give the fastest and most versatile method of analysis. Such systems have been developed and will be discussed in Sections 4.6 and 4.7. These machines have the capability of carrying out the Polar Correlation analysis very much faster than can be done using an analog machine, and therefore have major advantages for large data analysis projects.

*Defined for the purpose of this thesis as the C.P.S.D. normalised by the P.S.D. from each signal.

4.2. DATA ANALYSIS REQUIREMENTS

The data analysis requirement for Polar Correlation is the calculation of the complex coherence between the reference microphone and each of the other microphones in the array. Once these values have been obtained for each frequency of interest the subsequent evaluation of the source distribution is relatively simple.

In order to calculate the complex coherence it is first necessary to obtain the cross power spectral density between the two signals at the frequency of interest, and also their power spectral densities. The complex coherence may then be defined as

$$\tilde{C}_{xy}(\omega) = \tilde{G}_{xy}(\omega) \Big/ \left\{ P_x(\omega)\, P_y(\omega) \right\}^{\frac{1}{2}} \qquad 4.2.1.$$

Where $\tilde{G}_{xy}(\omega)$ is the c.p.s.d. at freq. 'ω'

$P_x(\omega)$, $P_y(\omega)$ are the p.s.d's at freq. 'ω'.

Therefore a method is required which calculates $\tilde{G}_{xy}(\omega)$, $P_x(\omega)$ and $P_y(\omega)$ to the required accuracy. However by definition:

$$P_x(\omega) = \tilde{G}_{xx}(\omega), \quad P_y(\omega) = \tilde{G}_{yy}(\omega)$$

and so the requirement is simplified to a method which calculates the cross power spectral density $\tilde{G}_{xy}(\omega)$. This may then also be used to calculate $P_x(\omega)$ and $P_y(\omega)$, and the complex coherence computed using equation 4.2.1.

In order to calculate a source distribution it is necessary to calculate three c.p.s.d's for each signal pair (equal to the number of microphones in the array). For an array of 20 microphones this means the calculation of 60 c.p.s.d's, and therefore any small improvement to the c.p.s.d. algorithm will be worthwhile. Various different algorithms will be described in the next section, and the relative advantages of each will be discussed.

The definition used in chapters two and three for the c.p.s.d. $\tilde{G}_{xy}(\omega)$ (see section 2.5) is

$$\tilde{G}_{xy}(\omega) = Ex\left[\tilde{X}(\omega)\ \ \tilde{Y}(\omega)^{*} \right] \dagger \qquad 4.2.2.$$

† Note: this definition is more usually referred to the two sided cross spectral density since it exists for both +ve and -ve frequencies. Bendat and Piersol (1958) p.82. Since the negative frequencies have no physical meaning and $G_{xy}(\omega) = G^{*}_{xy}(-\omega)$, only +ve frequencies will be considered.

Where $\tilde{X}(\omega)$, $\tilde{Y}(\omega)$ are the instantaneous (resolution limited) frequency components of the signals X(t) and Y(t). The frequency component $\tilde{X}(\omega)$ may be defined as

$$\tilde{X}(\omega) = \int_{t_o-T_B}^{t_o+T_B} X(t)\, W(t-t_o)\, e^{i\omega(t-t_o)} dt \qquad 4.2.3.$$

and will depend upon the time of evaluation 't_o'. The function W(t) is a weighting function which defines a spectral window and is zero when $t > T_B$. Putting $t' = t-t_o$ enables a sample value of $\tilde{X}(\omega)$ to be defined as

$$\tilde{X}_K(\omega) = \int_{-\infty}^{\infty} X(t' + t_K)\, W(t')\, e^{i\omega t'} dt' \qquad 4.2.4.$$

When X(t) is a random process with zero mean, then the sample frequency components will be randomly distributed, also with zero mean, i.e.

$$Ex\left[\tilde{X}_K(\omega)\right] = \int_{-\infty}^{\infty} Ex\left[X(t'+t_K)\right]\, W(t')\, e^{i\omega t'} dt' = 0$$

However the c.p.s.d. is not expected to be zero since

$$Ex\left[\tilde{X}_K(\omega)\tilde{Y}_K^*(\omega)\right] = \iint_{-\infty}^{\infty} Ex\left[X(t+t_K)Y(t'+t_K)\right]\, W(t)W(t')\, e^{i\omega(t-t')} dt dt' \qquad 4.2.5.$$

and $Ex\left[X(t+t_K)Y(t'+t_K)\right]$ is the cross correlation between the two signals and will be non-zero over a range of values $\tau = t-t'$.

In order to evaluate the c.p.s.d. it is necessary to compute the sample frequency components given by 4.2.4 or alternatively the Fourier transform of the cross correlation coefficient, (see 4.2.5). Different methods of doing this will be described in the next section.

4.3. DATA ANALYSIS TECHNIQUES

a) Analog, using narrow band cross correlation.

Perhaps the simplest technique of obtaining the cross power spectral density between two signals X(t) and Y(t), is to cross correlate the output from two identical narrow band filters.

The output from two identical narrow band filters is given by

$$f_x(t) = x(\omega,t)\cos\left(\omega t + \phi_x(\omega,t)\right)$$
$$f_y(t) = y(\omega,t)\cos\left(\omega t + \phi_y(\omega,t)\right)$$

Note $x(\omega,t) = |X_t(\omega)| + |X_t(-\omega)| = 2|X_t(\omega)|$

This additional factor of 2 is eliminated by normalisation in the complex coherence.

where $x(\omega,t)\cos(\phi_x(\omega,t))$ and $y(\omega,t)\cos(\phi_y(\omega,t))$ represent slowly varying components of the signals X(t) and Y(t) at the frequency 'ω'. The rate of change of these modulating components will depend upon the bandwidth of the filters, and for a narrow band filter of width $\Delta\omega$ the highest frequency component of the modulated signal will be very much less than 'ω', when $\omega \gg \Delta\omega$. The cross power spectral density between these two signals may be defined by

$$Ex\left[x(\omega,t)\, y(\omega,t)\, \exp\left(i\phi_x(\omega,t) - i\phi_y(\omega,t)\right)\right]$$

and this may be obtained in terms of amplitude and phase by cross correlating the outputs of the filters.

The principle of operation of this method is shown in diagramatic form in Fig. 4.1. It should be noted that this method requires a cross correlation with the appropriate signal averaging time for each c.p.s.d. at each frequency required. It has already been pointed out that to calculate a source distribution 3 c.p.s.d's are required per microphone, and about ten microphones will be used in a sub array. Therefore to calculate the source distribution at a single frequency would require 30 cross correlations. Practice has shown that this takes about a quarter of a day to complete.

The major disadvantages of this method are that only one frequency can be computed at a time, and the operator has to work the correlator throughout the analysis. Usually the source distributions from a particular test are required at several different frequencies, and this method requires a large amount of time. This has led to the development of techniques which analyse the c.p.s.d's over the complete spectrum in a single run, which gives a considerable reduction in operating time. These will be discussed in the next section.

The only advantage of this technique is that the operator is in control of the data at all stages, therefore snags may be easily traced. This proved to be very useful in the development stages of the technique.

b) Analog/Digital: giving cross power spectra from overall cross correlations

It is shown in section 4.2 and also in Bendat and Piersol (1958) that the cross power spectrum, giving values of the cross power spectral density between 0 and ω_m, may be calculated from the Fourier transform of the overall cross correlation between the two signals X(t) and Y(t).

This method is shown diagramatically in Fig. 4.2. and may be outlined as follows. The two signals are passed through anti aliasing

filters (with cut off at ω_m) and cross correlated using the analog correlator for both +ve and -ve time delays. These cross correlations are transferred using some alternative storage medium such as paper tape, into a digital computer which takes the fast Fourier transform of the cross correlations as a function of time delay. This yields the cross power spectrum. This algorithm may be improved for power spectral levels since the overall cross correlation of the same signal (see section 4.2) is defined as the auto-correlation which is symmetrical for both positive and negative time delays. Therefore only positive time delays need be evaluated for power spectra, halving the correlation time. To calculate the cross spectrum and two power spectrums therefore requires four correlations for each pair of signals. For a test which used 20 microphones a total of 80 correlations are required, which may be achieved in approximately half a day.

The advantage of this method over the analog method is that the whole spectrum is calculated giving results for all the frequencies of interest for only a doubling of time. In the long run it is therefore approximately twice as fast. Its advantage over completely digital systems described in c), is that it is only partially computer orientated and is therefore more reliable and requires less sophisticated equipment.

c) Digital: Calculation of cross power spectra using F.F.T. routines

The most sophisticated method of calculating the cross power spectrum is to use a digital computer. In this method the two signals are passed through anti-aliasing filters and into analog to digital converters which are linked to the computer. The signals, which are then in digital form, may be operated on entirely by the computer.

The algorithm which computes the cross power spectrum may be described as follows: the two signals in digitised form are split into blocks, equivalent in time to $2T_B$ (see equation 4.2.3). The Fourier transform of each of these blocks is calculated giving samples $X_K(\omega)$ and $Y_K(\omega)$ of the frequency components of each signal. Averaging over a number of blocks as indicated by equation 4.2.2 yields the cross power spectrum between 0 and ω_m, where ω_m is the aliasing frequency (this is determined by the sampling rate of the analog to digital converters).

The advantage of this method is its speed and also that it requires the minimum of operator intervention. The operator is only required to feed the signals to the A/D converters, and this part of the algorithm can be completed for a test using 20 microphones in less than an hour and a half. The rest of the algorithm may be completed at the computer's convenience and does not require the operator to intervene.

4.4. NARROW BAND CROSS CORRELATION

In this section the method and settings required for computing the cross power spectral density using narrow band cross correlation will be described.

The layout of the equipment is shown in Fig. 4.4. The two signals which are to be analysed are taken from the tape deck, and are passed through a switch into two identical B & K Type 2113 8% filters. The purpose of the switch is to enable easy calculation of the power spectral levels of each signal by allowing either signal A or signal B to be passed to both outputs. In either of these modes the same signal passes through the filters and is cross correlated by the correlator giving the power spectral level at the peak nearest zero time delay. (If the filters are phase matched this peak will occur at zero time delay). Alternatively the switch may be set so that signals A and B pass straight through and the cross spectral level is calculated.

The two filters are tuned to the frequency of interest, and RMS Fast time averaging and maximum frequency rejection are used. The frequency rejection may sometimes be reduced since this will effectively damp the cross correlation curve either side of the major peak, enabling this peak to be identified more easily.

The correlator is set up in cross correlation mode with either Channel A delayed or Channel B delayed, depending on the location of the major peak in the curve. This curve takes the form of a damped cosine wave given by:

$$Ex\left[x(\omega,t)\ y(\omega,t)\right]\cos\left(\omega\tau + Ex\left[\phi_y(\omega,t) - \phi_x(\omega,t)\right] + \theta_A - \theta_B\right) \times A\left(\tau + (\phi_y - \phi_x + \theta_A - \theta_B)/\omega\right)$$

where $Ex\left[x(\omega,t)\ y(\omega,t)\right]$
is the amplitude of the c.p.s.d. at frequency 'ω'.
$Ex\left[\phi_y(\omega,t) - \phi_x(\omega,t)\right]$
is the phase of the c.p.s.d. at frequency 'ω'
θ_A, θ_B are the phase shifts in the filters.
$A(\tau)$ is the damping provided by the filters of finite bandwidth. $(A(o) = 1.0)$

The major peak of this curve occurs when

$$\tau_m = [Ex[\phi_y(\omega,t) - \phi_x(\omega,t)] + \theta_A - \theta_B]/\omega$$

and its amplitude gives the amplitude of the c.p.s.d. at frequency 'ω'. The phase mis-match of the filters ($\theta_A - \theta_B$) may be calculated by passing the same signal into each filter, enabling the phase of the c.p.s.d to be calculated from the time delay of the major peak, i.e.

$$Ex[\phi_y(\omega,t) - \phi_x(\omega,t)] = \omega\tau_m - (\theta_A - \theta_B)$$

The cross power spectral density and power spectral densities are computed for each signal pair and the complex coherence computed using equation 4.2.1. This procedure is repeated for each microphone and each frequency of interest, to enable the source distributions to be calculated for a particular test.

In order to ensure that these values are estimated with sufficient accuracy it is necessary to use the correct settings for the time scale and time averaging. The time scale switch should be set to approximately $(2\pi/\omega)$ x 3/100, so that approximately 3 periods of the cosine wave appear on the correlator screen. The time averaging in the summation mode is defined by the number of updatings to each time delay value, which is given by the number of samples with value N, divided by the total number of time delays (= 100). An effective BeT product of 300 requires an average of 300 samples and so N is chosen such that

$$N > 300 \times 100 = 30 \times 10^3$$

This is satisfied by the setting N = 32 x 1024.

4.5. OVERALL CROSS CORRELATION

One method for computing the cross power spectrum for all frequencies between 0 and ω_m, is to calculate the Fourier transform of the overall cross correlation between the two signals. A method for calculating these levels will be described in this section.

The layout of equipment is shown in Fig. 4.5. The signals from the tape recorder are passed through two low pass anti-aliasing filters set to the maximum frequency of interest 'ω_m'. If the tape recorder output includes a significant amount of background noise at low frequencies (e.g. 50 Hz components from mains supplies), a high pass filter at 200 Hz may also be necessary. The output from the filters are then cross correlated on a Hewlett Packard correlator for both positive and negative time delays; these are output on to a paper tape interface so that they may be transferred to a digital computer.

The time scale on the correlator should be chosen to prevent aliasing, i.e.

$$\Delta t < 2\pi / 2.5\,\omega_m$$

The time averaging should be set to the summation mode, and the length of time averaging is defined by the number of samples N and the time scale Δt, i.e.

$$T = N\Delta t$$

To calculate a B_eT product the bandwidth can be defined by $B_e = 1/100\ \Delta t$ giving the B_eT product as

$$B_eT = N\,\Delta t / 100\,\Delta t = N/100$$

For a B_eT product of 300, N should be set to 32 x 1024.

The output from the correlator gives two arrays A_n and B_n (n = 1, 100) which define the cross correlation for the two signals at intervals Δt.

$$A_n = R_{xy}\,((n-1)\,\Delta t)$$
$$B_n = R_{xy}\,(-(n-1)\,\Delta t)$$

where $R_{xy}(t)$ is the overall cross correlation of the two signals.

These arrays may now be weighted using a spectral window function (see Jenkins and Watts); however in the system used in this project no weighting was used. The cross power spectrum was then calculated using an FFT routine by solving the equation

$$C_K + iD_K = \Delta t \left\{ A_1 + \sum_{n=1}^{99} A_{n+1} \exp \frac{i\pi Kn}{128} + B_{n+1} \exp \frac{-i\pi Kn}{128} \right\}$$

In order to interpret this equation it may be re-written in terms of the overall cross correlation $R_{xy}(\tau)$ as

$$C_K + iD_K = \Delta t \sum_{n=-99}^{99} R_{xy}(n\Delta t) \exp \frac{i\pi Kn}{128}$$

If the variable ω_k is defined as

$$\omega_k = K \frac{\pi}{128.\,\Delta t}$$

then the dependence of the exponential function above on K may be redefined as

$$\frac{(i\pi Kn)}{128} = i\omega_K\,\Delta t n$$

giving $C_K + iD_K = \Delta t \sum_{n=-99}^{99} R_{xy}(n\Delta t) \exp(i\omega_K \Delta t.n.)$

This is a series approximation to the Fourier integral which defines the c.p.s.d. from the cross correlation function, and therefore C_K and D_K represent the real and imaginary parts of the c.p.s.d. at frequencies $\omega_K = K\pi/128\,\Delta t$.

A similar algorithm may be used to compute the power spectral density using only the data for positive time lags, and placing $B_n = A_n$. Then it is a simple matter to compute the complex coherence over the whole frequency range. Once the complex coherence spectra have been computed for each microphone pair, the data is then re-arranged to give the complex coherence for each microphone at a fixed frequency. This data may then be used to calculate the source distributions.

4.6. DIGITAL COMPUTER METHODS (1): PROGRAMMES ON THE PDP 11/50 at ISVR

Due to the large amount of operator time required to run the analog facilities described in the previous two sections, a considerable amount of effort has been spent on developing digital computer routines for Polar Correlation analysis. The result of this development work is a relatively simple suite of programmes using standard routines on the PDP 11/50 at ISVR. The principle of this programme suite is shown in Fig. 4.6 and in this section each stage of the analysis will be outlined.

Acquisition of data

The first stage of the analysis is to acquire the signals from each microphone pair through the A/D converters on to file. This is achieved by running the JOB GATHER, which is listed as Computer Programme II, and requires the following specifications.

1) Sample Rate: this should be chosen as 2.5 times the maximum frequency of interest.
2) No. of Samples: specifies the number of samples to be acquired on each channel and should be chosen to give 600 degrees of freedom in c.p.s.d. analysis. See notes below.
3) Start File No; and Stop File No: The programme works in a loop which acquires the signals from each microphone pair* sequentially. The Start File No. specifies the first microphone pair to be acquired and the Stop File No. the last. Once the data has been accepted (see later note) it will be protected on file; therefore if the running of the programme is interrupted for any reason it may be re-run,

*i.e. The reference microphone and each of the others in the array.

starting with the microphone pair which follow the last successful acquisition. The data from any microphone pair may be re-acquired and this will over write the original file.

4) Series No: (1-4). This allows the data from more than one test to be stored on file before analysis. It is important that data is analysed using CHURN soon after acquisition since the raw data uses a large amount of disk space.

The signals are then acquired using a standard procedure (see DAC notes); the signals from each microphone pair are passed through anti-aliasing filters set to the maximum frequency of interest, (and also High Pass filters set to 200 Hz if there is noticeable mains interference at 50 Hz) and into the back of a terminal, which is connected to the A/D converters. Once the computer has simultaneously acquired the signals in digital form, the statistics of each signal are calculated and written on the screen. These indicate to the operator whether the "acquire" has been successful, and for Gaussian signals should have the following values:

Mean: should be very small $\ll$ S. Dev.

Standard Deviation: this is the RMS level and should lie in the range 0.25 - 2.5

Skewness: should be very small

Kurtosis: should be $\sim$ 3.0

Any discrepancies from these values indicates that the signal should be re-acquired unless the signals are clearly non Gaussian, and the operator has the option of doing this before the data is stored on file permanently. If the standard deviation is too large the signal will be clipped and therefore should be re-acquired with less gain.

Computation of Complex Coherence

Once data acquisition is complete, the signals from each microphone pair are stored on disk file in digital form, and their complex coherences may be computed using the JOB CHURN. This is listed as Computer Programme III and requires the following specifications:

1) Start File No. and Stop File No: These have the same meanings as in the JOB GATHER. If the programme is interrupted for any reason, it may be restarted at the microphone number being analysed when the interruption

occurred. Any microphone pair may be re-analysed using new input data, and the new data will overwrite the old data. (This does not apply to microphone pair 1, see below). The input data for each microphone pair (i.e. the digitised microphone signals) are "killed" as soon as they have been analysed.

2) Test No: This should be a 4-figure number which identifies the test. It is used by the computer to name the file in which the output data is stored. This file is created when microphone pair 1 is analysed, and cannot be re-created at any time, unless it has been eliminated by a deliberate "kill" procedure (see DAC notes).

3) Series No: This should be the same as used in JOB GATHER.

4) Resolution: This specifies the frequency resolution which will be used to compute the spectra. Any value may be specified but the computer only uses values which are defined by

$$\text{Resolution} = (\text{Sample Rate}) / 2^n$$

$$\text{Where} \qquad 8 \ll 2^n \ll 1024$$

Specified values will be rounded down. The resolution and the number of samples determine the accuracy of the computed spectra. As was indicated in Section 4.3, the algorithm which computes the c.p.s.d. splits the signals into blocks. Each of these blocks contains TL sequential samples, where TL is a power of two defined by

$$TL = 2^n = (\text{Sample Rate}) / (\text{Resolution})$$

$$8 \ll TL \ll 1024$$

The number of blocks into which the signal is split is equal to the B_eT product (or half the number of statistical degrees of freedom). The algorithm used on this machine overlays blocks of data so that (2N-1) blocks may be obtained from a signal length NS = N x TL. Therefore the number of samples NS, and the resolution should be chosen so that sufficient accuracy is obtained, i.e. a B_eT product of 300 or more.

$$\left(\frac{2NS}{TL} - 1\right) > 300$$

A method of choosing these values is as follows:

a) Choose the resolution as the third octave bandwidth at the lowest frequency of interest.

b) Calculate the transform length TL, using a) and the sample rate.

c) Calculate the number of samples required to ensure that 300 blocks of data are analysed.

Once these parameters have been specified the programme runs automatically in a loop, analysing each microphone pair in turn. First the c.p.s.d. and the two p.s.d's are calculated over the whole frequency range using standard routines. From these the complex coherence spectrum is obtained (again using standard routines); these spectra are stored for reference in files named 11-14 as follows:

11 - P.S.D's of reference microphone stored sequentially

12 - P.S.D's of each microphone in sub array stored sequentially

13 - c.p.s.d's stored sequentially

14 - complex coherences stored sequentially.

Finally the complex coherence spectra are re-arranged in a special programme XCOLEC, listed as Computer Programme IV. The output from this programme is the file whose name is the test number. The manner in which the data is stored in this file is as follows: The files on this machine are split into blocks containing 128 samples. The data is re-arranged so that each block contains the data for a particular frequency component, i.e. the nth block will contain data for the frequency n x RES. Values computed for each microphone pair are stored sequentially in each block.

To analyse a complete test using this programme may take several hours, depending on the time sharing requirements of the system. However the running of the programme requires no operator intervention, and so this time is not an important factor in the efficiency of the system.

Calibration of System

Before these results may be used they must be corrected for time delay errors in the system (see section 3.5.c). These may be obtained from analysing a loud speaker or white noise test with no corrections. In order to calibrate these errors out of all subsequent tests the time delay errors (in microseconds) are specified in a file called "Tape",

created by the JOB FIDDLE. This is listed as computer Programme V and requires the following specifications:

1) The number of microphone pairs used in the test.

2) Whether the calibration of each microphone is identical

Answer: for YES

for NO

3) The time delay calibrations between the reference microphone and the other microphone in each microphone pair, in micro-seconds.

The recommended procedure for obtaining these time delay calibrations is to analyse a loud speaker test (see section 3.5.c) using this system and to set the calibration file "Tape" to zero for each location. Then from the results at several frequencies a mean time delay calibration may be obtained from the evaluated phases for each microphone pair. For instance the mean time delay, calibration for the nth microphone pair 'τ_n' may be calculated from

$$\tau_n = \frac{1}{8\pi}\left\{\frac{\phi_n(f_1)}{f_1} + \frac{\phi_n(f_2)}{f_2} + \frac{\phi_n(f_3)}{f_3} + \frac{\phi_n(f_4)}{f_4}\right\}$$

where the frequencies f_1 to f_4 cover the frequency range of interest. The file "Tape" should then be re-calibrated using the values τ_n.

Evaluation of Results

Finally the calibrated complex coherences may be obtained as a listing at a specified frequency using the JOB RESULT, which is listed as Computer Programme VI. This requires the following specifications:

1) Test Number: As defined in CHURN.

2) Frequency of data to be listed.

3) Frequency resolution used by CHURN in calculating spectra.

The programme then lists the complex coherences as amplitude and phase (note: not real and imaginary parts as indicated by DAC routine SCREEN) for each microphone pair. This data may then be used as an input to Computer Programme I which calculates the source distribution, and operates on the main University ICL 1907 computer.

In conclusion this suite of programmes provides an automated data analysis system which is very much more efficient than either of the analog methods described earlier. Operator intervention has been kept to a minimum and is only required at the data acquisition stage. Providing the facility is fully operational a complete test may be easily analysed in half a days effort.

4.7. DIGITAL COMPUTER METHODS (2). PROGRAMMES ON THE ALPHA (CAI LSI-2) MINI-COMPUTER

In order to provide the sponsors of this project, Rolls Royce Ltd (DED), with an in-house data analysis facility for Polar Correlation, a set of programmes were developed for an Alpha (CAI LSI-2) Mini-computer. This machine has previously been used to develop the Acoustic Telescope (Billingsley and Kinns (1976)), and with the additional programmes for Polar Correlation it was planned that this machine should provide a complete source location analysis facility.

The Alpha computer is a mini-computer which has 8-bit precision and may be programmed in Fortran II. It has a core of 32K and is attached to two "floppy" disks each of which can hold 0.3M bytes. One of the major problems with this computer is designing programmes to run within these storage limitations. All programmes are stored on one disk, and the other disk is used entirely for data files. The disk space may be increased ad infinitum by the use of back up data disks, and this was found necessary for large data analysis projects; however this does require very good file initialisation to ensure all the data subsequently required is available. Interaction with the computer is via a Tektronix teletype terminal (with video screen) and there is also a 'Diabalo' printer available. Data signals may be acquired through a 16 channel, parallel A/D converters, with a maximum sample rate of 320K samples/sec (total).

One of the features of this machine is that any programme on core (i.e. in command status) may ~~overwrite itself with~~ be over written by any other programme on file. This enables command status to be transferred from one programme to another. The transfer of assigned variables is also possible since the "common" block areas in core remain the same for each programme, and so any assigned variable in this area retains its value when the new programme is over written. Therefore a very long analysis may be broken down into several programmes, thus releasing a considerable area of core, and command status may be transferred to each programme as required.

The layout of the programmes on this computer is illustrated in Fig.4.7. The analysis is started by running the programme POCO, from this the operator may choose any of the options indicated in Fig. 4.7. Each of these options and the details of the programmes involved will now be described.

Calibration of Store

Before any analysis may be undertaken the common block area of the core must be calibrated, assigning values to each of the variables which will be needed in the analysis. This may be undertaken by either initialising the store with new values, typed in by the operator, or by reading these values from a disk file. Each data file includes in its first segment all the values stored in the common block when it is created, and these values may be recalled by reading the file in this area. The lower area of the common block may be referred to by the array IGUF (300) and this is read from file by the subroutine RBDISK, which is included in most programmes. (See XOPOCO, computer programme A1). Once the file has been read control is transferred to the programme CALI. Alternatively if the operator chooses to type in the new calibration control is transferred immediately to CALI.

The programme CALI asks initially if this is a new set up, which requires the operator to type in the calibration. This requires the definition of:

1) Test Number, Tape Number and a Test description (i.e. Place, date, nature of test up to 46 characters)
2) Wind Speed Data: wind speed (m/sec), wind direction re-axis, polar arc radius
3) Microphone array calibration: number of microphones used, number of sub-arrays(see section 3.4), angle of reference microphone to jet-axis, the number of microphones in each sub-array, and their separation in sin(x). Also required is the microphone identification number at each location in each sub-array.
4) Time Delay Calibration: The time delay calibration for each microphone in microseconds.
5) Data Analysis Constants: Maximum frequency required, frequency bandwidth, and the number of degrees of freedom (= 2 B_eT) required in calculation of spectra.
6) Input Data Definition: Number of channels to be acquired and the microphone identification numbers for each channel.

Once this data has been typed in or read from file, it is presented on the screen. Any mistakes may be identified and altered, and when it is correct control may be transferred back to the option area of the programme POCO.

Acquisition of Data on to Disc

When this option is chosen, it is assumed that the common block area has been calibrated (otherwise failure will occur) and control is transferred to the programme PLOG (see computer programme A3).

The first step in this programme is to open the data file using the subroutine FILEOP. This requires the definition of a 3 character test name which will be used to name the file which is to be written. Also required is the "Take" number (n.b. there may be several takes to one test, necessitating the definition of several different files) and the disk handler number which contains the disk on which the file will be written. Next the common block area is written to this file, and it is this data which will subsequently be used in all the analysis on this data.

The data is then acquired using standard data logging procedures available on this system. The signals from each channel may be viewed in real time on the video screen, and data logging starts by pressing the space bar. When data logging starts each channel will be acquired almost simultaneously (i.e. when more than two channels are acquired there will be a skew of six microseconds between each block of two channels). The programme reads a total of 16K words (32K bytes) from the A/D converters on to core, and then writes these to the open file. This procedure is repeated until the number of samples required has been logged.

This procedure is repeated using different "take" numbers until the data from all the microphones of the test is on file. After each take, control is transferred to the option area of POCO, and the common block area must be up dated to define the microphone identification numbers in the next take. It should be noted that the reference microphone must be included on channel 1 of each take, with a maximum of 7 others.

Once these data files have been created they may be analysed to compute the complex coherence between each microphone and the reference microphone.

Analysis of Data to give Complex Coherences

Taking the data analysis option in POCO, transfers control to the programme PANA (see computer programme A4). To run this analysis it is necessary to define the Test name which defines the data files and the number of takes which have been used to place this data on file.

The programme then analyses each file in turn, computing the complex coherences and spectral information between channel one and the other channels on file, writing the results on to a new file. (There will be a results file for each input file)

The analysis on each file may be described as follows (see Figure 4.8):

1) The file is opened and the common block read, using sub-routines ANFILE and RBDISK

2) 16K data samples are read from the file into core (IBUF array)

3) The CPSD (real and imaginary) of each channel re channel 1 and PSD of each channel, is computed as a running average.

4) Another 16K samples are read and 3) is repeated until the file is exhausted.

5) The complex coherence spectra for each channel are computed.

6) The complex coherences and p.s.d's are written to an output file.

The major part of this programme is to compute the c.p.s.d. and p.s.d's for each channel re channel 1. This part of the programme is illustrated in Figure 4.9. The principle on which this algorithm was based is described by Welch (1967) and its application to multi-channel analysis was developed specially for this programme.

The 16K data block which is read from file contains 16K/N data samples simultaneously acquired on N different channels, channel 1 being the reference channel. These values are stored in the data array IBUF with two samples contained in each word. The arrangement of data within this array is illustrated by the diagram below:

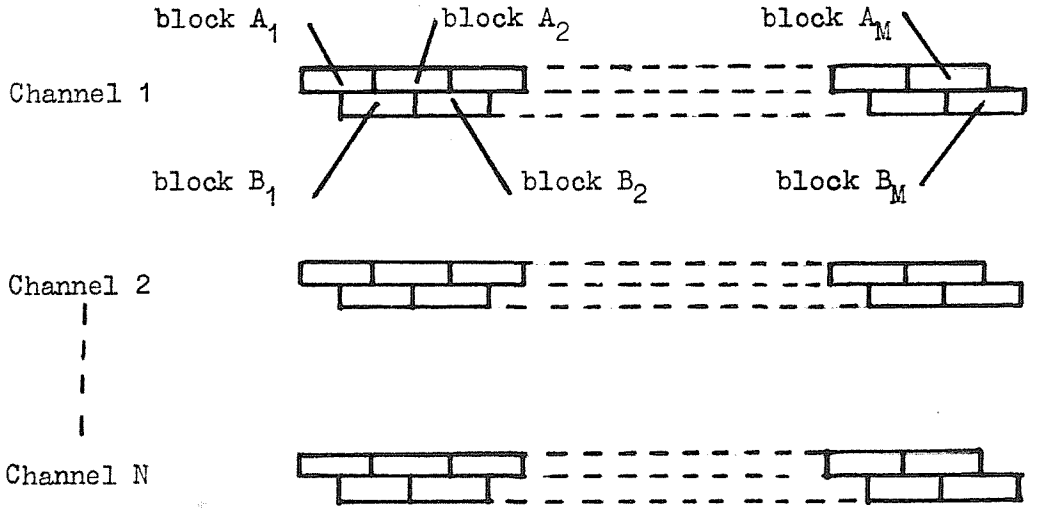

The data record on each channel is split into blocks containing "ITL" data samples. "ITL" defines the transform length and must be a power of 2. It essentially specifies the frequency resolution of the spectra and is calculated in the calibration programme. Each channel has a set of A_m and B_m blocks which are overlapping as illustrated above. By defining the location of the first sample in each block the data in each block may be extracted from the array IBUF using the sub-routine FISH. The principle of the algorithm is to extract the data in blocks A_m and B_m in turn, calculate their Fourier coefficients, cross multiply these with the reference channel and themselves giving instantaneous CPSD's and PSD's, and adding the results to update arrays. When all the blocks have been analysed the updated arrays will contain the averaged CPSD's and PSD's.

The instantaneous CPSD's and PSD's are calculated using a special algorithm which minimises the number of Fourier transforms which have to be calculated. This algorithm utilises some of the special properties of Fast Fourier transforms which are described by Cooley et al (1969). To describe the principle of this method the data in any block A_m of Channel 1 will be referred to as the record c_n when $1 \leqslant n \leqslant ITL$ and the data in block B_m of Channel 1 as d_n. The Fast Fourier transforms of the data records c_n and d_n are C_n and D_n, which are complex valued records of length ITL which have the following properties because c_n and d_n are real

$$C_n = C^*_{ITL-n} \qquad D_n = D^*_{ITL-n}$$

Similarly the data in blocks A_m and B_m of another channel may be referred to as a_n and b_n and have Fourier transforms A_n and B_n with the same properties. Ultimately to calculate the CPSD between these two channels it is necessary to calculate the sum

$$A_n C^*_n + B_n D^*_n$$

This requires 4 Fourier transforms; however by calculating the two Fourier transforms

$$c_n + id_n \xrightarrow[F.T.]{} C_n + iD_n = X_n$$

and

$$a_n + ib_n \xrightarrow[F.T.]{} A_n + iB_n = Y_n$$

it is found that

$$Y_n X^*_n = A_n C^*_n + B_n D^*_n + i\left\{ B_n C^*_n - A_n D^*_n \right\}$$

and using the properties described above

$$Y^{*}_{ITL-n}X_{ITL-n} = (A_n - iB_n)\,(C^{*}_n + iD^{*}_n)$$

$$= A_nC^{*}_n + B_nD^{*}_n - i\left\{B_nC^{*}_n - A_nD^{*}_n\right\}$$

Thus

$$A_nC^{*}_n + B_nD^{*}_n = \tfrac{1}{2}\left\{Y_nX^{*}_n + Y^{*}_{ITL-n}X_{ITL-n}\right\}$$

which requires 2 rather than 4 Fourier transforms. The complex multiplication, addition and updating of CPSD arrays is performed by subroutine CMULAD.

Once the CPSD's and PSD's have been calculated the complex coherences are evaluated and written away to file, with the PSD's for future reference. Each of these files also includes the calibration data stored in the common block.

Calculation of the Source Distribution

The next option available in this programme suite is to calculate the source distribution from the complex coherences. In this calculation it is assumed that the far field is almost omnidirectional over the array.

When the source distribution option is chosen in POCO, control is transferred to label 400 in the same programme. The first step in this analysis which is outlined in figure 4.10, is to read the input data from file. This requires the definition of the test name used to identify files, and the number of files (or takes) which contain the data for the whole array. Next the operator must specify the frequency of interest and the upstream and downstream limits to the source distribution which is to be calculated. From this information and the data which describes the microphone spacings the programme then computes the sub-array which provides the aliasing length to fit the limits of the source distribution required. The programme then extracts the data for the correct sub-array locations from the files which hold the data. This is then corrected for time delay errors and weighted with a Bartlett window function. The Fourier transform of this data is then taken using the principle described in Appendix I. Finally the data is re-arranged in a suitable format for the plotting routines. This requires the definition of 128 equally spaced values along the axis between the upstream and downstream limits specified. Since the output from the Fourier transform contains a source distribution which is defined at 128 equally spaced points between zero and the aliasing

length 'L', it is necessary to use a linear interpolation procedure to evaluate the source level at the required points. It should be noted that the output from the transform is periodic, with period 'L', and is only defined for positive locations. Therefore if a negative location, 'x' say, is to be evaluated it must be calculated using the location 'L-x' in the transform output. Once the file which may be used for plotting is defined, containing source levels between the specified upstream and downstream limits, control is returned to the option array of POCO.

Plotting Results

If the Screen Plot or Hard Copy options are chosen in the option area, control is transferred to label 500 or 600 in POCO. Both options give the same output, either to the screen or to the printer, the only difference being that the hard copy output also prints the numerical values of the source distribution.

When either of these options is chosen the data for the source distribution which has just been calculated is presented. First the input data is presented, including specification of the microphone number, its displacement in $\sin\alpha$, its coherence and phase at the frequency specified, and also its PSD in dB.

Next the source distribution is plotted between the upstream and downstream limits specified.

Finally if the hard copy option is chosen the numerical values of the source distribution at each location are written out on the printer. Also included in this is the integrated level, between the upstream limit and each location. This enables the area under any portion of the source distribution to be calculated so that the relative strengths of different sources may be determined.

Plotting Spectra

This is an additional feature of this programme suite which presents the coherence (amplitude) and power spectra for any microphone in the array. If this option is chosen control is transferred to the programme SPECTRA (see computer programme A5). The operator then specifies the test number, take number, and microphone of interest and the two spectra are plotted as a function of frequency on the screen. This provides a useful extra facility to the programme suite since it enables the standard acoustic test data to be available as well as the source location data.

Conclusion

In this section a complete in house facility for source location and narrow band data analysis has been described. However since this programme suite was developed near to the end of this project, it is considered that it has not yet reached its ultimate development, and it is hoped that in the future it will be improved so that a more ergonomic system is available for both programmer and user.

CHAPTER 5: EXPERIMENTAL RESULTS (1) : MODEL TESTS

5.1. INTRODUCTION

This chapter will describe the results from a number of tests on model air jets. The purpose of these experiments was twofold: first to evaluate the technique and secondly to determine the distribution of acoustic sources in clean jets. All the tests described in this chapter were taken in anechoic surroundings and the model air jets used were representative of pure jet mixing noise which is not contaminated by the extra sources which occur on full scale jet engines. Therefore these tests have been carried out under very much more controlled conditions than would ever be expected in an outdoor test on a full scale engine, and so the results are expected to be considerably more consistent.

The first detailed study of model jet mixing noise using the Polar Correlation technique of source location was carried out by Harper-Bourne, and is reported by Fisher, Harper-Bourne and Glegg (1977). Those results not only demonstrated the feasibility of the technique, but also demonstrated the features of cold jet mixing noise. Similar results were also obtained by Grosche (1974), Laufer (1976), Glegg (1975) who used acoustic mirrors focussed on to the jet. However the original tests taken by Harper-Bourne were restricted by the design of the rig to either positive measurements of $(\sin\alpha - \sin\beta)$ with $\beta = 0$ or negative measurements of $(\sin\alpha - \sin\beta)$ with $\beta = 45^{\circ}$. Since these measurements agreed it was argued that the measurements about any reference angle 'β' would be symmetrical, and so only positive or negative displacements need be considered. This was further justified by the theoretical work outlined in section 2.8, but it was felt that more tests were required to fully justify this result. Therefore some tests were undertaken which evaluate the measurements for both positive and negative displacements of $(\sin\alpha - \sin\beta)$ with $\beta = 0$. These tests are reported in section 5.2 of this chapter.

All the results mentioned above were obtained using model jets at ambient temperature. However the jets of full scale engines are inevitably 'hot', in that their stagnation temperature will be above ambient temperature. The theoretical work of Morfey (1973) suggests that hot jets have a different noise generation process than cold

jets, and therefore are liable to have a different distribution of jet noise sources. In section 5.3 of this chapter the results of some tests on hot and cold jet noise, with and without a by-pass flow are described, and these demonstrate the differences between the two mechanisms involved. These tests were undertaken in the large anechoic room at N.G.T.E. using the hot jet noise facility, and were analysed in ISVR.

5.2. AN INVESTIGATION INTO THE NOISE FROM COLD JETS.

The purpose of these tests was to consider in detail the noise from a 1" model air jet at ambient temperature, and to evaluate differences in the source location measurements from the forward and rear arcs. These have been predicted from theoretical arguments in section 2.8, and the results of these tests will be used for a detailed comparison with this theory. Two subsonic jet velocities of U_J/a_o = 0.4 and 0.8 were considered, and the nozzle used was a one inch diameter parallel nozzle, which had previously been used in Polar Correlation tests by Harper-Bourne.

Test Facility

The rig used for these tests was a horizontal model air jet in the anechoic room at ISVR (see Figure 5.1). The established jet noise facility in the ISVR anechoic room is situated in the roof and the model jet exhausts vertically downwards (Lush (1971)). Unfortunately this means that forward arc measurements cannot be taken, and so a horizontal jet rig was developed with access both in front and behind the jet. This rig was designed and built for some jet noise shielding experiments and it was fortunate that the source location measurements presented here could be taken during the same period.

The jet was connected to the air supply in the roof by a 3" diameter flexible pipe and it then passed through a stainless steel tube, before being exhausted by a 1" diameter nozzle (see Figure 5.1). The microphone could be traversed through both forward and rear arcs on a 10' radius and every effort was made to minimise reflections using sound absorbent foam.

Data Collection and Analysis

The microphone array used in these tests was designed according to the principles laid down in section 3.5. Each sub-array included

ten microphones plus a reference microphone, and the designed aliasing length was chosen as 30 inches (equivalent to 30 nozzle diameters). This led to the choices of microphone spacing 'Δ' given in the table below for each maximum frequency:

Δ	max. frequency
0.0208	21.6 kHz
0.0416	10.8 kHz
0.0832	5.4 kHz

These maximum frequencies correspond to Strouhal numbers of 2.0, 1.0, 0.5 for U_J/a_o = 0.8 and 4.0, 2.0, 1.0 for U_J/a_o = 0.4.

The microphones used were $\frac{1}{2}$" B & K Type 4134 and were traversed as described above. The signals were passed through two identical B & K Type 2103 microphone amplifiers, and recorded on a Ferrograph Seven two channel tape recorder. The spectra of the signals were taken from the microphone amplifiers at locations of $\sin\alpha$ = 0.0, $\pm$ 0.208, $\pm$ 0.416, $\pm$ 0.833.

The time delay calibration between channels was evaluated from the signals at zero microphone separation and was found to be 39μsec. Data analysis was carried out using the suite of programmes on the ISVR PDP 11/50.

Discussion of Results

a) The Symmetry of Source Location Measurements

It was argued in section 2.8 that providing the source distribution was dominated by a particular type of coherence region, and the correct amplitude and phase normalisation was used, then the complex coherence $\tilde{C}_\beta(\sin\alpha)$ would be symmetrical about $(\sin\alpha - \sin\beta) = 0$. In order to evaluate whether this is the case, the source distributions from either positive or negative displacements of $\sin\alpha$ ($\beta = 0$) were calculated and are compared in Figures 5.2 - 5.9, for frequencies of 1293 Hz to 10775 Hz and speeds U_J/a_o = 0.4 and 0.8. If $\tilde{C}_\beta(\sin\alpha)$ is symmetrical then the source distributions should be the same within the limitations of the measurements.

The results show that in general there is good agreement between forward and rear arc measurements (i.e. positive and negative locations of $\sin\alpha$), especially at the higher frequencies, of 5603 Hz and 10775 Hz. The largest discrepancies are apparent at the lower frequencies of 1293 Hz and 2586 Hz. The main feature is a shift in the location

of the peak in the distribution, which in the worst case is 3.2 nozzle diameters (Figure 5.6). However this is equivalent to a shift of 0.3 wavelengths, and therefore might be explained by errors caused by measurement procedures. The differences in level which occur, especially at the higher speed, are not considered to be of major practical significance. The distributions from either positive or negative arcs will integrate to the same value over an aliasing length, due to the normalisation used in the Fourier transform routine (see Appendix I). Therefore discrepancies in peak level are due to small but distributed differences in the low level tails of the distribution. In the lower frequencies the aliasing lengths are very long and the low level tails are not shown. It is considered that the 10% errors in peak level are within the margin of measurement errors considered in section 3.7.

b) General Features of the Source Distributions

In general the source distributions are single peaked and are significant over about 25 nozzle diameters. The peak moves closer to the nozzle at higher Strouhal numbers and the source distribution also becomes more compact, although this may be a feature of the resolution. A detailed comparison with the results of Harper Bourne given by Fisher, Harper Bourne, and Glegg (1977), Figure 8, shows very good agreement for all Strouhal numbers (Note $U_J/a_o = 0.8$ only). This is not unexpected since the same nozzle was used in both tests.

However at the higher frequencies it would appear that the rig is reflecting sound and acting as an additional source (see Figures 5.5 and 5.9). This explains the high level in the tails of the distribution, which unlike the results at lower frequencies do not decay. These reflections will have been caused by the structure upstream of the nozzle and the results in Figures 5.5 and 5.9 demonstrate an unexpectedly high level in this region. Also the high level downstream of the jet is explained as an alias of this upstream reflection. However the effective source levels caused by the reflections are very much lower than the jet noise source, and in most applications will not be significant.

c) A Model for Jet Noise Source Distributions

It has been found useful for modelling purposes to develop an analytical fit to the jet noise source distributions of the type presented in this chapter. The curve chosen to fit the source dis-

tributions is given by

$$q(y) = (y/\lambda)^{n-1} \exp(-2\pi p(y/\lambda)) \qquad y \geq 0, \; n \geq 1 \qquad (5.2.1)$$

The complex coherence data from a distribution of this type is given by the Fourier transform of this curve with respect to 'Ksinα'; this is given by Churchill (1972) p.471 as

$$\tilde{C}_o(\sin\alpha) = \left[\frac{p}{p - i\sin\alpha}\right]^n$$

Therefore the phase of the coherence data is given by

$$\phi(\alpha) = +n\tan^{-1}(\sin\alpha/p)$$

To evaluate n and p consider the limits

$$\frac{\sin\alpha}{p} \to \infty \qquad \text{where } \phi(\alpha) \sim + n\pi/2$$

and $$\frac{\sin\alpha}{p} \to 0 \qquad \text{where } \phi(\alpha) \sim n\sin\alpha/p$$

Therefore values of 'n' and 'p' may be obtained from the asymtotic values of the phase of the complex coherence.

From the phase measurements obtained in this test the following values of 'n' and 'p' were obtained.

U_J/a_o	Strouhal No.	'n'	'p'
0.4	0.24	2	0.4622
0.4	0.48	2	0.2971
0.4	0.96	3	0.2836
0.4	1.92	5	0.325
0.8	0.12	3	0.39
0.8	0.24	3	0.254
0.8	0.48	4	0.208
0.8	0.96	7	0.364

To demonstrate the type of result obtained the calculated source distribution at $U_J/a_o = 0.8$, Strouhal Number = 0.48 is presented in Fig. 5.10. Also shown is the source image at this condition evaluated from the measured data. Good agreement has been obtained and the only discrepancies are due to the effects of resolution on the measured data.

5.3. RESULTS FROM THE NOISE TEST FACILITY AT N.G.T.E.

Introduction

An investigation into fundamental jet mixing noise using source location was undertaken in the large anechoic room (N.T.F.) at N.G.T.E. (Pyestock). The purpose of this test was to obtain the

source distributions for hot and cold jet mixing noise, with and without a by-pass flow, in order to evaluate the differences which may be associated with the different types of source mechanisms involved.

The test programme, giving the jet conditions considered, is laid out in the table below:

Test No.	Test Point (NGTE)	Primary Jet Velocity m/sec	Secondary Jet Velocity m/sec	Primary Jet.Temp.
5100	98	314	0	308°K
5200	101	530	0	880°K
5300	102	307	0	880°K
5400	103	307	60	880°K

Primary jet nozzle diameter = 0.0864 m.
Secondary jet nozzle diameter = 0.482 m.
Area ratio = 30/1

It was planned to use these conditions to consider the source distributions at three different Strouhal Numbers: 0.3, 1.0, 2.0; which cover the whole of the frequency range of interest, and from this the overall features of the jet noise source distribution were to be evaluated. Clearly this is not a fully comprehensive study of jet noise source distributions, since this would require the evaluation of a larger range of conditions. However it should provide sufficient data to highlight the significant features of hot and cold jet source distributions.

Data Acquisition

The data was collected using a fixed reference microphone at 90° to the jet axis and a traversable microphone on a boom which could be rotated from 90° to 45° (re-jet axis). The angular separations used between these two microphones are given in Table 5.1.

The polar arc centre about which the traversable microphone was pivoted did not lie on the jet axis, and therefore the data had to be corrected for this displacement. The correction was obtained in the form of a set of time delays which define the difference in sound

propagation time to the reference and traversable microphones at each angular separation, for a source at the nozzle exit (e.g. if the traversable boom was centred at the nozzle then this difference would be zero; however since the centre is misplaced from the nozzle, there will be a difference in the path length to each microphone which must be allowed for).

These corrections were obtained using a loudspeaker as a point source, emitting white noise, located at 8" and 40" downstream of the nozzle on the jet axis. The time delay of the peak in the cross correlation curves between the signals of the two microphones are given in Table 5.1 and are illustrated in Figure 5.11, as a function of angular separation. From these results the time delay correction can be calculated using

$$\tau(\alpha)_{\text{correction}} = \tau(\alpha) - y\sin\alpha/a_o$$

where y = location of loudspeaker

a_o = speed of sound

α = angular separation

These corrections are also given in Table 5.1 and plotted in Figure 5.12.

The spectra for each test condition were obtained using the standard facilities at N.G.T.E. These are given in Figure 5.13 for a microphone at 92° to the jet axis. It is assumed that these will only show very small differences from the spectra at the reference microphone at 90°. Further details of the spectra at different angles and jet conditions are given in detail by Way (1977).

All the microphones used in this test were $\frac{1}{2}$" B & K, and the G.R. integration time for $\frac{1}{3}$ octave analysis was 4 seconds. The source location data was recorded on a Ferrograph Seven two channel tape recorder at 15 ips, provided by ISVR. All other equipment was provided by N.G.T.E. and is described by Martlew et al (1976).

Data Analysis

It was originally planned to process this data using the Analog/Digital method described in section 4.5. This takes the overall cross and auto correlations between the signals and interfaces them to a digital computer, which calculates the complex coherence spectra. However the spectra obtained using this method were particularly jagged and the data was badly contaminated by statistical errors which were transmitted to the source distribution. These errors were attributed to an insufficient averaging time being used in the processing of the correlation curves. An equivalent B_eT product of 82 was used to obtain these results, and this was clearly insufficient. This prompted an investigation into the statistical errors of Polar Correlation, which is reported in section 3.7, and demonstrates the requirement for a B_eT product of at least 300.

Another problem of processing this data using overall cross correlations occurred because the polar arc centre was misplaced. This resulted in the peak of the cross correlation moving out of the correlator "window" at large angular separations, and this effectively reduced the resolution at low frequencies. Rather than re-write the programmes for this method it was decided to re-process the data using the Analog method described in section 4.4, which is amenable to handling this problem, and gave complex coherence data at the required frequencies to the required accuracy.

Calculation of Source Distributions

The microphone array which was used in this experiment was designed before the work on optimum microphone arrays (section 3.4) was complete. Therefore the microphone separations were chosen at convenient angular displacements 'α', and it was intended to analyse this data using the linear interpolation procedure described in section 3.6. For this type of data, which includes continuously distributed sources, this method is as accurate as the Fourier series method described in section 3.6, since the interpolation procedure does not induce additional errors providing the data is sufficiently accurate, (i.e. a suitable time average has been used). However since statistical errors had been shown to be a problem, it was decided in retrospect to adhere to the principle of the Fourier series solution as

closely as possible. Therefore a method was used which is available as an option in Computer Programme I; in this method the optimum spacing in '$\sin\alpha$' is chosen according to the principles laid out in section 3.4, and the values of the complex coherences at these points is estimated from the measured data using linear interpolation of amplitude and phase. Thus the data from an equivalent array at equal intervals of '$\sin\alpha$' ($=\Delta$) is obtained, and this is used to calculate the source distribution according to the principles given in Appendix I. The calculation procedure is given in Computer Programme I, and a Bartlett window function was used.

Discussion of Results.

a) Source Distributions from Hot Jets.

The source distributions from jets at the temperature of 880°K are given for two jet velocities and a range of Strouhal numbers in Figures 5.14 and 5.15. Although each curve in these distributions has been obtained with different resolution, the following features are apparent.

1) The peak location moves towards the nozzle at the higher Strouhal numbers.

2) For a given Strouhal number the peak location is farther downstream in the higher velocity jet.

3) The jet is apparently more compact at the lower speed.

Of all the source distributions shown in this chapter the result at 6161 Hz in Figure 5.15 is exceptional in that it has a large negative loop close to the nozzle. This is probably an error since the source level must always be greater than zero. It is conjectured that this negative loop is the result of statistical measurement errors on the source distribution, which have been amplified by the linear interpolation calculation procedure.

b) Comparison of Source Distributions from Hot and Cold Jets.

In order to demonstrate the effect of jet temperature on the source distribution, the results for Strouhal numbers of 0.3, 1.0, and 2.0 (based on the primary jet conditions) are plotted in Figures 5.16 - 5.18. In these results the primary jet velocity remains constant at 307 m/s. The results appear to be consistent throughout the frequency range, and for the cold jet (upper curve in each case) agree with the results given in section 5.2, although the peak locations are about one diameter further downstream.

However when the jet is heated to a temperature of 880°K the source levels are reduced, and the distribution is more compact with a peak location closer to the nozzle. To explain this result consider the theory given by Morfey (1973) for heated jets. This suggests that there are two mechanisms involved in the generation of noise from hot and cold jets. In the cold jet the major noise sources are the fluctuating Reynolds stresses, which have a quadrapole nature, and scale on the eighth power of the velocity. (These were first described by Lighthill (1952)). However when the jet is heated Morfey suggests that these Reynolds stress sources will be reduced in level by a factor of $30 \log_{10} (T_{ambient}/T_{source})$ which in this case will be 10 dB. This would reduce the peak level in the source distribution by a factor of 10, which is well below the measured result. Therefore the source distribution appears to be dominated by an alternative noise source, suggested by Morfey to be caused by convected flow inhomogeneities. These are dipole in nature and scale on the sixth power of the jet velocity. The source location results suggest that these have a different distribution within the jet from the Reynold stress sources, peaking closer to the nozzle and decaying more rapidly.

The source distributions for the hot jet with a secondary flow are given by the lowest curve in Figures 5.16 - 5.18. These appear to have the same distribution as the hot jet, but merely to be of a lower level. Since the jet is dominated by dipole type sources the attenuation given by the secondary flow is expected to be proportional to the sixth power of the relative velocity between the two flows (i.e. $(V_{rel}/V_p)^6$). In this case the peak level would be expected to be reduced by a factor of 0.271 ($\equiv$ 5.66 dB). Measurements of this factor for the Strouhal numbers 0.3, 1.0, 2.0, are respectively 0.28, 0.325, 0.321, and the discrepancies between these and the predicted result are probably within experimental error (i.e. the differences are less than 0.7 dB).

It therefore appears that these results are consistent with the theory and that the noise sources in hot jets are less distributed than those in cold jets.

CHAPTER 6: EXPERIMENTAL RESULTS (2): ENGINE TESTS

6.1. INTRODUCTION

One of the major applications of source location techniques is to full scale jet engines which include several different sources of noise. A typical jet engine will produce noise from several different locations, for instance the engine inlet, the hot core exit and the jet flow behind the engine; therefore the noise control engineer requires information on the relative significance of each of these sources, and this can be provided to a certain extent by source location methods. In this chapter the application of the Polar Correlation technique to full scale engines will be described and a complete set of results will be given.

The measurements described in this chapter were undertaken to evaluate the Polar Correlation technique as a source location method for full scale engines. The criterion by which such a technique must be judged is whether it can provide a significant amount of useful information, which cannot be obtained more easily using other techniques. It is hoped that these results will demonstrate that this objective has been achieved.

This chapter describes the results of a test on the Rolls Royce R.B.211 Quiet Engine Demonstrator. This engine possesses a number of sources of noise which are of equal significance and therefore it is of great practical importance to distinguish their relative levels. Previous attempts to determine this information have relied on prediction techniques and engine testing methods which use acoustic liners to effectively eliminate a particular source. Such methods involve a considerable amount of trial and error, and consequently are very expensive due to the large amount of engine testing required. Source location however can yield the same information more accurately in a single test, providing the quality of the data is sufficiently high. The purpose of these tests was to determine the standard of data which could be obtained on the R.B.211.

This test was undertaken quite early on in this project and provided a great deal of information about the technique which has led to improved methods of measurement and interpretation. The microphone array used in these tests was designed for the linear interpolation procedure which has subsequently been superseded. The results shown

here however have not been re-analysed using an equivalent array of microphones, based on the principles described in chapter 3, but rely on the original linear interpolation method, and therefore in many cases they do not satisfy the aliasing criterion for the engine. Consequently the results given here occasionally include dramatic oscillations which are the result of aliasing errors. By re-analysing the results with an equivalent array of microphones the aliasing errors may be eliminated at the expense of resolution, and the degree of improvement which can be obtained will be demonstrated.

Before analysing source location data on an engine it is necessary to decide on the source strength parameter which should be evaluated. In Chapter 2 it was shown that there are two different definitions of this source strength parameter, and the choice between them depends on the type of sources within the distribution. If the distribution includes coherent regions of sources, which are effectively identical throughout the distribution, then it was argued that a normalised source strength parameter should be evaluated which gives the effective strength of each coherent region. This definition has the major practical advantages that only a one-sided microphone array is required, and the gain on each channel is corrected by normalisation in data analysis. It has also been shown that even when sources have quite different directionalities, the error associated with assuming them identical is not grossly misleading. Alternatively a source strength parameter may be chosen which is defined as the total contribution to the field at the reference microphone from the sources which interact with a source at a particular location. To evaluate this parameter a two-sided microphone array is required, unless each source is independent.

In general, experience has shown that the first of these two definitions is preferable because of the major practical advantages involved. The only occasion when it has been shown to give misleading results is when sources from the inlet of the engine and the nozzle exit are highly correlated.* These sources are 20 ft apart and this condition only occurs at blade passing frequencies where the wavelength is about 1 ft. In this situation the assumptions which are associated

*Private communication from Rolls-Royce (D.E.D.)

with the former definition no longer apply, especially when there exist jet noise sources and other effectively omnidirectional sources. However away from blade passing frequencies the assumptions required appear to be valid.

6.2. SOURCE LOCATION ON THE R.B.211 Q.E.D.

Introduction

This section presents the results of source location measurements on the R.B.211 Q.E.D. test facility at Hucknall. These tests were undertaken to evaluate the Polar Correlation technique as a method of identifying the sources of noise on the engine. Therefore this report will concentrate on the quality and evaluation of the data, leaving a comparison of the results with the Rolls Royce Noise Department (D.E.D.) prediction schemes to be reported on elsewhere.

Previously the evaluation of the various sources of engine noise has been achieved from far field spectra and prediction schemes. However this method requires a great deal of experience with the engine and the necessity for a more deterministic method of source identification is apparent. The Polar Correlation technique has been developed for this purpose and provides a distribution of source strength intensity along the axis of the engine. Therefore it is possible to measure the relative contribution of each engine noise component (i.e. jet, tailpipe, by-pass duct exit, etc.) to the far field noise spectrum.

The Measurement Scheme

These tests were carried out by Rolls Royce D.E.D. on the Q.E.D. test facility at Hucknall and the data was analysed using the suite of programmes on the P.D.P. 11/50 computer in ISVR (see Chapter 4). In these tests the microphones were located on a polar arc of radius 100 ft, centred on the hot nozzle exit, with the reference microphone at 90° to the engine axis. The location of each microphone is given in Table 6.1. The tests were carried out on a single run of the engine using the standard procedure for the Q.E.D., which includes running the engine at five different conditions between 60% and 90% N_L (where N_L is the maximum operational fan shaft speed). The signals were recorded on a 14 Channel Ampex FR 1300 tape recorder in two different blocks. Block A included microphones 1-12 and Block B included microphones 1, 2 and 13-22. The wind speeds throughout the tests were very low (2-3 knots) and therefore have been ignored.

Source Distributions

Source distributions have been obtained over a range of frequencies and engine speeds for two different builds of the R.B.211 on the Q.E.D. test facility at Hucknall. The engine builds considered were:-

1) ISVR 1; Build 154: incorporating a lined nose cone, production standard intake and by-pass duct liners; unlined hot stream.

2) ISVR 2; Build 155: as above with the exception of the hot stream where two bulk absorber tailpipes were incorporated, extending the hot nozzle 5 ft downstream.

The graphical representations of the source distributions which follow are plotted to a free scaling peak level and the area beneath each curve is equal to the level at the reference microphone (see for example Fig. 6.2). The y-scale therefore represents the noise source intensity per unit length relative to the peak level, and the scaled area beneath each section of the curve represents the proportion of the intensity measured at the reference microphone from that part of the source (note: all scales are linear). The x-scale gives the location along the axis of the engine, and each unit is 10 ft as standard. The size of the engine to this scale is given in Fig.6.1, and the relative location of each component is shown; the origin of all graphs lies at the unlined hot nozzle exit.

All the results have been computed using the linear interpolation procedure described in Chapter 3. In this procedure all the microphones in the array are used, regardless of spacing, and spatial aliases in the source image are artificially suppressed. This however leads to gross errors at the higher frequencies where the source distribution spans a large number of acoustic wavelengths. This problem is partially overcome by eliminating the more widely spaced microphones from the array, and since this also reduces the aperture, the resolution is reduced. However in some cases this remedy was insufficient to completely eliminate these effects and by re-analysing the results as suggested in Chapter 3, a much clearer source image was obtained.

The source images will be presented for the engine speeds of 60% and 90% N_L, over a range of frequencies. The source distributions at 75% N_L have also been evaluated but will not be shown; however information from these results will be used in the evaluation of the source breakdowns, which summarise the results.

Results at 250 Hz

The source distributions at this frequency for both builds at 60% and 90% N_L are shown in Figs. 6.2 and 6.3. It is clear that for both builds there is an important tailpipe noise source at the hot nozzle exit, and that the level of jet noise increases with speed relative to this source. More detail will be given on the relative levels of the jet, engine and tailpipe noise in the next section, but it is interesting to note that the bulk absorber tailpipe extension attenuates this source and moves it 5 ft downstream as expected. Apart from this effect, the result at 60% N_L (Fig.6.2) shows the noise from the jet and engine to be of the same level for both builds. However at 90% N_L the two builds do not show such good agreement. In the case of the unlined hot stream (Fig.6.3) there is a significant source 15 ft upstream of the hot nozzle; this appears to come from the engine front flange on the fan casing, but its cause has not yet been identified. This source also appears at the same condition with the bulk absorber tailpipe, but is of a much lower level relative to the jet noise. This is the only result where a discrepancy of this nature has been found between the source distributions of the two different builds. It should be noted that in the ISVR 1 (unlined) test the engine was running at 89.9% N_L whereas in the ISVR 2 (bulk absorber) test the engine was running at 88.4% N_L. Therefore if the source upstream of the nozzle exit is associated with a buzz saw tone of the fan, then this change of speed could account for the discrepancy of levels between these two tests. There is also a discrepancy of jet noise levels which is greater than might be expected from this speed difference alone, and this effect will be discussed in more detail later.

Results at 500 Hz

The results at 500 Hz are expected to be dominated by tailpipe noise, since this is the peak frequency on the spectrum for this source. The source distributions (Fig. 6.4 and 6.5) demonstrate that this is the case although the bulk absorber tailpipe provides an attenuation of about 70% in level, which is equivalent to 5 dB. It is also possible to identify relatively small sources on the engine at the inlet and by-pass duct, which are consistent in level on both builds. Also it should be noted that the result at 60% N_L for the ISVR 1 (unlined) test has a relatively large negative loop downstream of the tailpipe source.

This is the type of error which is often caused by the linear interpolation procedure, and this will be demonstrated in more detail at the end of this section. It is this type of result which has led to the development of the analysis procedures described in Chapter 3, which do not rely on linear interpolation.

Results at 1000 Hz

At this frequency the source distributions were all found to be well distributed on a wavelength scale and it was therefore necessary to reduce the aperture angle of the microphone array to avoid aliasing problems. This has reduced the resolution from 3.5 ft at 500 Hz to 6.5 ft at 1000 Hz where only a 10^{o} aperture was used.

The results of the ISVR 1 (unlined) test (Fig 6.6 and 6.7) are dominated by a tailpipe noise source but some significant sources also appear on the engine. At both speeds there are three sources on the engine which are consistently located in the same positions. The first source 20 ft upstream of the origin lines up with the engine intake; the second source 10 ft upstream of the origin lines up with the air cooled oil cooler outlet; and the third source 5 ft upstream of the origin lines up with the by-pass duct exit. It is therefore possible from these results not only to define a level of engine noise, but also to indicate that part of the engine from which it is emanating.

The results for the ISVR 2 (bulk absorber) test show that the bulk absorber has reduced the tailpipe noise so that it is no longer the dominant source (Figs. 6.6 and 6.7). At 60% N_L the dominant source is clearly the by pass duct, while at 90% N_L there are two important engine noise sources of approximately equal strength; the first located at the engine intake and the second at the by-pass duct exit. At this higher speed the agreement between the levels of noise sources on the two different builds is not good. In the case of the ISVR 2 (bulk absorber) test there is unexpectedly more intake noise and less by-pass exit and jet noise. The only explanation of this discrepancy is the difference in engine speed mentioned earlier.

High Frequency Results.

In order to evaluate broadband fan noise, the source distributions at 1.5 times blade passing frequency were evaluated. Since aliasing effects were important at these frequencies only microphones spaced at 1^{o} intervals were used. The results for 60% N_L (2250 Hz) and 90% N_L

(3380 Hz) are given in Figs. 6.8 and 6.9 for the ISVR 2 (bulk absorber) test. It is clear that the major noise source is the by-pass duct exit, and that the other noise sources such as the jet, air cooled oil cooler, and inlet are correctly located but of secondary importance.

Suppression of Spatial Aliases

One of the problems with the results from this series of tests was the spatial aliasing effect. This is described in Chapters 2 and 3 and occurs because two adjacent microphones cannot differentiate between the acoustic waves from two sources spaced well apart on the jet axis. This is very similar to the aliasing effects which can occur in the analysis of digitised signal analysis. The solution to this problem is to eliminate the more widely spaced microphones in the array, so that the aliasing phenomenon does not occur.

A typical example of this effect is shown in Figure 6.10 which gives the source image computed using the complete microphone array for the ISVR 2 (bulk absorber) test at 75% N_L and 500 Hz. The effect of spatial aliasing causes the oscillations of source level downstream of the origin. This effect is suppressed by eliminating the most widely spaced microphones from the array, and the corrected result is shown in Fig. 6.11. This demonstrates a considerable improvement although the resolution is much broader since the aperture has been reduced. In this case the most widely spaced microphones are at 2.5° intervals compared with 5° used in the original analysis. A further reduction of maximum microphone spacing is shown in Fig. 6.12, where only 1° intervals have been used. In this case the resolution has been reduced significantly and very little detail is obtained on the source image. In this figure the result for the ISVR 1 (unlined) test is also shown, and this demonstrates the good agreement obtained between the levels of jet and engine noise, the ripples on the curve being associated with the side lobes of the window function.

The significance of this effect led to the investigation on microphone array design described in Chapter 3. As a result of this investigation it was shown that an alternative method for computing the source image was preferable. The method used in these tests effectively linearly interpolates between measurements at each microphone, and obtains the source image from the evaluation of a Fourier integral on

these interpolated values. It has been shown that this results in errors due to the interpolation procedure which force fits a curve through measured values. An alternative method has been developed which fits a Fourier series to the measured values and evaluates the source distribution from this series. This has the advantage that it is more accurate, since the curve is not forced directly through the measurements, and it also has a very precisely defined aliasing length, which can be specified from the wavelength and the microphone spacing. In many of the source distributions presented in this chapter, this Fourier series aliasing limit has been exceeded, but because most of the results are dominated by a single source close to the origin and linear interpolation has been used, the errors are relatively insignificant; aliasing effects are only apparent when sources are evenly distributed over a large number of acoustic wavelengths. It is therefore to a certain extent fortuitous that these results are not completely corrupted by aliasing effects, and it is recommended that for future tests a Fourier series approach is adopted, with a correctly designed microphone array.

Source Breakdowns

In the last section the measured source distributions were presented, demonstrating the qualitative features of this data. However for practical purposes it is necessary to have a more quantitative set of results giving the total noise level from each component at the reference microphone. This may be obtained from the source distributions by integrating the area under the curve associated with each component.

It was noted earlier that the total area under each source distribution has been scaled on the measured level at the reference microphone, and therefore it is possible to define an absolute level for each source component by determining the fraction of the total area of the curve to which it contributes.

Integration Routine

In order to develop a fast and consistent method of integration, a routine on the P.D.P. 1150 computer in ISVR has been utilised. This routine gives a trapezoidal integration between each point on the curve and presents the result in the form of an accumulative plot. For example in Fig.6.13 the integrated curve of a normalised Bartlett window is given, firstly note that well upstream of the origin the area is

negligible, but downstream of the origin the area has integrated to unity. Also the area beneath the main lobe of the window function may be determined by using the construction shown in Fig.6.13, i.e. the main lobe of the window lies between $\pm \lambda/\sin\alpha_m$ (where λ = acoustic wavelength and α_m is the aperture angle), therefore the difference between the y-scale values at these two points yields the area of the main lobe as a fraction of the total.

It is possible to use this result when breaking down the integrated source distribution, since the tailpipe noise source which separates the engine noise from the jet noise is effectively a point source (see Fig.6.2). Since 90% of the area contributed by this point source lies within $\pm \lambda/\sin\alpha_m$ of its peak (Fig.6.13) a level of tailpipe (or core) noise may be defined. Everything upstream of this may be attributed to the engine and everything downstream to the jet. The engine noise may also be broken down into its various components by using the same method.

Source Levels

The source levels of each engine component as measured is given in Table 6.2. This report will concentrate on reviewing the consistency of this data between the two builds, a more detailed comparison with predicted levels has been undertaken by Rolls-Royce staff and will be reported elsewhere.

Since the only difference between the two builds ISVR.1 and ISVR.2 was the bulk absorber tailpipe the levels of jet and engine noise were expected to be the same in both cases. From Fig. 6.14 it is seen that this comparison is better for engine noise than it is for jet noise. Apart from the result at 250 Hz; 90% N_L the engine noise levels agree with a maximum discrepancy of 2.2 dB and an average error of 0.5 dB. The result at 250 Hz; 90% N_L was first noted in the previous section where the comparison of the source distributions (Fig.6.3) showed poor agreement. The lower level of the source at the engine front flange on the fan casing is clearly reflected by the lower measured level of engine noise (Fig. 6.14). If this source is associated with buzz saw noise then it is expected that its level at this frequency will be very dependent on engine speed. Therefore the engine speed discrepancy (89.9% N_L and 88.4% N_L) between these two tests may explain this result.

The discrepancies in the jet noise levels were originally excused by experimental error, buried sources, and engine speed discrepancies. However two points of interest prompted a further look at the data; firstly it was noted that the jet noise with the bulk absorber tailpipe was always less than for the unlined case (Fig. 6.14) and secondly the discrepancies were notably worse than those of the engine noise. If such discrepancies were a result of experimental errors then they should be scattered randomly; however a consistent trend of data was found and this will be discussed in the next section.

From these measured levels it is also possible to define the attenuation given by the bulk absorber. This is shown in Fig. 6.15 and appears reasonably consistent with speed apart from at the highest frequency. Even here, of course, it is conceivable that the increased flow speed has decreased the linear attenuation at this highest frequency.

Collapse of Jet Noise Levels

Initially it was assumed that the bulk absorber tailpipe would not affect the level of jet noise. However the results showed discrepancies which were much larger than expected (i.e. more than 2 dB in 50% of the results) and it appeared that the bulk absorber always attenuated the jet noise. In order to determine whether this effect was consistent the measured levels of jet noise were plotted against engine condition for each frequency (Fig. 6.16). This demonstrated that the levels for each engine build and frequency were proportional to engine speed with very little scatter. It also appears from this graph that the bulk absorber is attenuating the jet noise at high frequencies and low speeds. This attenuation is plotted in Fig. 6.17 using values for a particular engine condition obtained from Fig. 6.16. It appears that at 60% and 75% N_L the attenuation is proportional to frequency, while at 90% N_L there is no attenuation apart from at 250 Hz.

This collapse of data suggests that there is some mechanism behind the bulk absorber attenuation of jet noise. One possible explanation which must be dismissed is that the apparent jet noise may be severely contaminated in data analysis by leakage from the window function side lobes of the tailpipe noise source. However consideration of this possibility shows that the apparent attenuations are at

least an order of magnitude too large. Frequently they are of the same order as the attenuation of the tailpipe source itself, a situation which would require the "apparent jet noise" to be at least 13 dB below the tailpipe noise; as Fig. 6.14 shows this is not the case.

Without further tests it is only possible to speculate on these results. However three possibilities exist:

1) The pressure losses in the bulk absorber tailpipe extensions are causing a reduction in jet exit velocity. However this does not account for the frequency and velocity dependence shown in Fig. 6.17.

2) Energy from the tailpipe source may be refracted and scattered so that it appears to come from the mixing region. However some doubt exists about this explanation because at 60% N_L the attenuation is very comparable to that of the core noise. This suggests that the actual jet noise is very much lower than inferred from these results and therefore very much lower than predicted.

3) There is also the possibility that the jet noise is being driven acoustically by sources upstream of the hot nozzle exit.

Conclusion

The results presented in this chapter demonstrate the quality of source location data which may be obtained using the Polar Correlation technique on full scale engines. In general the results are consistent and the levels of the major noise sources on the engine have been defined (Fig. 6.14). This type of data is clearly useful in the development of engine silencers, especially since most of the sources are of about the same level. The information on Fig. 6.14 shows immediately where significant noise reductions may be made, without requiring further engine tests.

These results have also demonstrated the effectiveness of the bulk absorber tailpipe in reducing tailpipe (or core) noise. It also appears to have attenuated the jet noise, and this effect perhaps warrants further investigation. It is noteworthy that this type of data could only be obtained using a source location technique.

The results at high frequencies, which were undertaken to investigate broadband fan noise, confirmed the view that this was propagating from the by-pass duct. This would suggest that previous attempts to reduce this noise have been unsuccessful because duct liners were ineffective rather than a mislocation of the source.

Perhaps the major conclusion from this data is that tailpipe noise is an important contributor over a wide range of the spectrum. An obvious extension of this work is to use this technique to obtain a more complete understanding of the extent and effects of tailpipe noise. A better understanding of this source, on different engines, could help to explain the problems associated with in flight jet noise, where it may be especially important.

CHAPTER 7: CONCLUSION

The objective of this project has been to develop a technique which evaluates the relative strengths of noise sources on jet engines. At the outset the technique, known as Polar Correlation, had been shown to work in practice, and the purpose of this project was to refine it into a method suitable for general application.

In this thesis each aspect of this technique has been covered, starting with its theoretical background and concluding with its application to jet engines. Also included in this work has been discussion of the practical application of the technique, the development of data analysis systems, and experimental results on a number of different rigs. This covers a wide range of topics and it is hoped that this chapter will provide an overall review of this work.

Theoretical Work

In the discussion of the theoretical background to the technique, the limitations to the types of source distribution which may be considered was demonstrated. It was shown that in principle the technique can only evaluate a source distribution which is realistically modelled as a linear array of effectively monopole sources, and that the source image obtained is limited by resolution which depends on the maximum aperture of the far field microphone array used by the technique. Also described was the aliasing effect which is similar to the aliasing effects found in signal analysis. This required the spacing between the microphones in the far field array to be small enough to ensure that the path length difference from any source to adjacent microphones is less than an acoustic wavelength. This effect is dependent upon the total length of the source distribution while the required resolution is determined by the most closely spaced sources. Therefore the relationships between these parameters and the microphone array layout may be used for design purposes. A method for arranging the minimum number of microphones in order to provide the most information about a source distribution is described in Chapter 3.

When an acoustic source is fluctuating randomly, as is always the case with jet noise sources, its effective strength at any particular frequency and consequently its interaction with neighbouring sources, varies with the time of evaluation. Therefore the definition

of a pertinent source strength parameter presents a major problem. Two definitions have been discussed and the relative merits of each have been highlighted. The first of these definitions describes the source strength as the mean square average of the fluctuations within a narrow frequency band, at a particular point in the source distribution, including the averaged interference effects of the source at that point with neighbouring sources, as would be observed at the reference microphone. While this would appear to be a very useful description of the source strength for the observer at the reference location, it has the practical disadvantages that a two sided microphone array must be used, and that each channel must be calibrated for intensity. For large source location tasks, these problems are very significant. Therefore an alternative source strength parameter has been proposed which overcomes these problems under certain assumptions. In this definition the source interaction effects are grouped into coherent regions and the relative intensity of each coherent region is evaluated. This definition offers the major practical advantages that no intensity calibration of the microphone array is required and that measurements are symmetrical about the reference point so that only half the microphone array is required. However it also depends on two major assumptions: first it is assumed that the interactions between coherent sources within any region are identical and so the far field directionality from each region throughout the distribution is invariant, and secondly it is assumed that there is no significant phase directionality from a coherent region. The errors associated with these assumptions have been evaluated numerically and it appears that in most practical cases there is no significant misrepresentation in the source image.

In the theory of the Polar Correlation technique there are a number of assumptions which strictly cannot be adhered to in practice. For instance, theoretically the source distribution is assumed to be a line source, while in practice it will always have finite dimensions in three directions. However within certain limitations the assumptions of the theory are quite acceptable and these limitations have been evaluated in a numerical study. These results demonstrated that finite three dimensional effects were not a severe restriction in the

practical applications considered. Another theoretical assumption considered was the acoustic far field approximation. This requires that the length of the source distribution should be short compared with the polar arc radius on which the microphone array lies. The results of a numerical investigation into this approximation have shown that this is a low frequency effect and is liable to cause significant errors to the source images at the extreme ends of the distribution when high resolution is used with a large aliasing length. The compromises which may be used to ensure that there is no error are outlined in Chapter 2. A further cause of error which occurs in practice on outdoor tests is the effect of atmospheric wind on signal propagation. However providing its strength and direction are known at the time of the test, then corrections may be applied which eliminate this effect. Finally the background noise criterion for Polar Correlation was evaluated theoretically, and it was shown that unwanted sources should be at least 14 dB below the level produced by the source distribution.

Data Analysis

One of the major features of this project has been the development of signal processing systems for Polar Correlation. Since this technique is very dependent on signal processing, the development of highly efficient routines has been of major practical importance. In order to evaluate the source distribution it is necessary to compute the "complex coherence" between the signals from the reference microphone and each of the others in the array. The "complex coherence" is a quantity which has been defined for the purpose of this work, and is calculated by normalising the cross power spectral density between two signals by the square root of their respective power spectral densities. Once this quantity has been evaluated, a Fourier transform routine yields the source distribution from the measurements. However the complex coherence between two signals which are fluctuating randomly can only be estimated with an accuracy which depends on the amount of averaging used in processing the signals. Consequently the source image which is computed from these measurements can only be an estimate of the true source image, and the factors which affect the accuracy of this estimate have been evaluated. In order to obtain an acceptable error bound on the evaluated source it has been shown that the

microphone signals should be averaged using a B_eT product of 300. This is approximately 6 times greater than the amount of averaging customarily used in power spectral density estimation and is necessary because a number of estimates are being used to compute the source image. An interesting feature of this analysis is that the window function imposed on the source image provides a certain amount of smoothing and therefore error variance reduction, in the same manner as a window function smooths a power spectrum.

The high degree of accuracy required in signal processing inevitably results in a large amount of data processing, and a number of different systems have been evaluated in order to obtain a highly efficient technique. Methods which use analog, analog/digital, and digital processing have all been used to process data, and while each method has advantages in certain circumstances, the ultimate requirement is for a dedicated high speed digital computer system. Such a system has been developed on the CAI LSI-2 mini-computer and this provides the best tool for large data processing projects. One of the major advantages of this system is that it is self-contained. Each of the three other systems developed require the interfacing of various facilities, while the programme suite on the CAI LSI-2 handles the complete data processing task from the microphone signal input to the evaluated source image. It also provides additional acoustic data such as the power spectral density of each microphone signal on the polar arc, which is normally obtained in standard acoustic tests. This system is now being used by Rolls Royce (D.E.D.) as a jet noise source evaluation facility.

Experimental Results

The experiments described in this thesis were primarily designed to evaluate the practical application of Polar Correlation. However there has also been a certain success in demonstrating the features of jet noise sources. For instance the experimental tests on the hot jet noise facility at NGTE (Pyestock) demonstrated that the source distributions from hot jets were more compact and peaked closer to the nozzle than in a "cold" jet at the same velocity and Strouhal number. Also the effect of a by-pass flow on hot jet noise was demonstrated as reducing the rate of mixing, and apparently not altering the noise

generation process. These results agree in principle with the theory of hot jet noise given by Morfey's (1973) extension to Lighthill's (1952) original model.

Some tests on an unheated model air jet in the anechoic room at ISVR were also described in Chapter 5. These tests were designed to investigate various assumptions associated with the technique. The results have helped to justify some of the theoretical concepts presented in Chapter 2; for instance there has always been a certain amount of debate as to whether a one-sided microphone array is sufficient to describe the source image. In theory this debate hinges on the assumptions made about the nature of the source strength parameter, while in practice it depends on whether measurements made in the forward and rear arcs only, give the same source image. The results of this test have shown that for the unheated jet considered, a one-sided microphone array was sufficient, and this goes some way to justify the one-sided microphone array. This has important practical implications since it means that the number of microphones and the amount of data processing is halved.

The ultimate justification for a technique of this nature must be its ability to provide information about full scale jet engine noise sources. To demonstrate this, the tests on the RB.211 Q.E.D. were undertaken and the results are described in Chapter 6. A high by-pass ratio engine of this type has a number of noise sources which in many cases are of equal significance, and in order to control the overall noise output, it is important to know the relative levels of each source. When this information is available it is possible to specify the areas where significant noise reductions can be made, and this is of major practical importance in any noise control programme. As a result of the tests on the RB.211 Q.E.D. it has been possible to measure a source breakdown which is given in the form of a bar chart in Fig.6.14. This chart shows immediately where there is a single dominant source and where there are two sources of approximately equal magnitude. This enables noise reduction techniques to be concentrated on the correct areas, where significant attenuation can be achieved.

APPENDIX I

A Fourier Series Solution for the Source Image

In section 3.3 it is shown that the complex coherence between signals in the acoustic far field are related to the source distribution $Q_o(y)$ by

$$\tilde{C}_o(\alpha) = \frac{1}{P(o)} \int_{-\infty}^{\infty} Q_o(y)\, e^{iky\sin\alpha}\, dy \qquad (A1)$$

where

$C_o(\alpha)$ is the complex coherence between the reference microphone and the microphone at 'α'.

$P(o)$ is the P.S.D. at the reference microphone

If the source distribution $Q_o(y)$ is zero everywhere when $|y| \geq L/2$, then it is possible to define a periodic function $F(y)$, which has a fundamental period of L, and is equal to $Q_o(y)$ when $|y| < L/2$.

$$F(y) = Q_o(y) \quad |y| < L/2 \qquad (A2)$$

The periodic function $F(y)$ can be represented by a Fourier series of the type

$$F(y) = \sum_{m=-\infty}^{\infty} r_m \exp(-2\pi imy/L) \qquad (A3)$$

for which the Fourier coefficients r_m are defined by

$$r_m = \frac{1}{L} \int_{-L/2}^{L/2} F(y) \exp(2\pi imy/L)\, dy \qquad (A4)$$

Within the limits of this integral, $F(y)$ may be replaced by $Q_o(y)$, and since $Q_o(y) = 0$ when $|y| > L/2$, the integral may be written:

$$r_m = \frac{1}{L} \int_{-\infty}^{\infty} Q_o(y) \exp(2\pi imy/L)\, dy \qquad (A5)$$

Comparing this result with (A1) defines the Fourier coefficients as

$$r_m = \frac{P(o)}{L} \cdot \tilde{C}_o(m\Delta) \qquad (A6)$$

where $m\Delta = \sin\alpha = m\lambda/L$

and $\Delta = \lambda/L$

Therefore using this with the definitions (A3) and (A2) defines the source distribution over the range $|y| < L/2$ as

$$Q_o(y) = \frac{P(o)}{L} \sum_{m=-\infty}^{\infty} C_o(m\Delta) \exp(-2\pi imy/L) \qquad (A7)$$

The source distribution is therefore defined by an infinite series with coefficients $C_o(m\Delta)$. To determine these coefficients it is necessary to measure the complex coherence at equal increments in '$\sin\alpha$', defined by $\Delta = \lambda/L$. It must be remembered that this analysis is only correct if the sample interval, Δ, is sufficiently small to ensure that the source strength is zero outside the bounds $|y| < L/2$ where $L = \lambda/\Delta$. This condition defines the fundamental aliasing length of the sampling array.

To solve the series (A7) requires an infinite number of coefficients to be measured; this is physically impossible since the data may only be measured up to a finite aperture angle α_m, such that $m\Delta < \sin\alpha_m$. This requires a source image equation to be defined, which only includes M terms of the series where $M = \sin\alpha_m/\Delta$. To obtain this source image equation each term in the series is weighted by a window function $W_m(M)$; this function has the properties:

$$W_m(M) = W_{-m}(M)$$

$$W_m(M) = 0 \quad |m| > M$$

$$W_o(M) = 1.0$$

A source image is then defined by

$$Q_I(y) = \frac{P(o)}{L} \sum_{m=-M}^{M} W_m(M)\, \tilde{C}_o(m\Delta) \exp(-2\pi imy/L) \qquad (A8)$$

where $|y| < L/2$

In order to relate the source image to the actual source distribution, substitute (A5) into (A8) giving

$$Q_I(y) = \frac{1}{L}\int_{-\infty}^{\infty} Q_o(z).\sum_{m=-M}^{M} W_m(M)\ \exp(2\pi i m(\frac{y-z}{L}))dz \qquad (A9)$$

where $|y| < L/2$

The Fourier series defines the window function

$$L.W(y) = \sum_{m=-M}^{M} W_m(M)\ \exp(2\pi imy/L)$$

so that the source image $Q_I(y)$ is described by a convolution integral:

$$Q_I(y) = \int_{-\infty}^{\infty} Q_o(z)\ W(y-z)\ dz$$

where $|y| < L/2$

This defines the source image as a resolution limited image of the actual source distribution. Various types of window function may be used, providing they have the correct bounding values, and this is discussed in section 2.3.

The Area under the Source Image Curve

To determine the area under the source image curve consider the integral of equation (A8),

$$\int_{-L/2}^{L/2} Q_I(y)dy = \frac{P(o)}{L}\sum_{m=-M}^{M} W_m(M)\ \tilde{C}_o\ (m\Delta)\int_{-L/2}^{L/2} \exp(2\pi\frac{imy}{L})dy$$

The integral on the RHS of this equation is given by

$$\int_{-L/2}^{L/2} \exp(2\pi\frac{imy}{L})\ dy = \begin{cases} L & m = 0 \\ 0 & m \neq 0 \end{cases}$$

Therefore

$$\int_{-L/2}^{L/2} Q_I(y)dy = P(o)\ W_o(M)\ \tilde{C}_o(o)$$

Since $W_o(M)$ and $C_o(o)$ are unity, the area under the source image curve is equal to the level at the reference microphone.

Solution by Fast Fourier Transform Routines

The source image equation (A8) may be solved at discrete points $y = nL/2N$ by an FFT routine in the form

$$Q_I\left(\frac{nL}{2N}\right) = \frac{P(o)}{L} \sum_{m=-N}^{N} W_m(M)\, \tilde{C}_o(m\Delta)\, \exp\left(-i\pi \frac{mn}{N}\right) \qquad (A10)$$

where $|n| < N$

It is convenient to normalise the source image computed in this way, to unit area. The normalised curve is given by

$$Q_N(n) = \frac{Q_I(nL/2N)}{P(o)}$$

which in terms of the Fourier series is

$$Q_N(n) = \frac{1}{L} \sum_{m=-N}^{N} W_m(M)\, \tilde{C}_o(m\Delta)\, \exp\left(-i\pi \frac{mn}{N}\right) \qquad (A11)$$

This series may be solved for $N=2^k$ output points using an FFT routine. It should be noted that the number of output points, N, may be greater than the number of input points, M, depending on the detail required.

The area beneath the curve defined by (A11) is calculated as

$$\sum_{n=-N}^{N} Q_N(n)\, \frac{L}{2N+1} = \frac{1}{2N+1} \sum_{n=-N}^{N} \sum_{m=-M}^{M} W_m(M)\, \tilde{C}_o(m\Delta)\, \exp\left(-i\pi \frac{mn}{N}\right)$$

The summation over N only yields a result when $m = 0$, and so this gives

$$\sum_{n=-N}^{N} Q_N(n)\, \frac{L}{2N+1} = W_o(M)\, \tilde{C}_o(o) = 1.0$$

APPENDIX II

Estimation of the Expected Value of $|\tilde{E}_m|^2$

To estimate the expected value Ex E_m^2 the method outlined in Jenkins & Watts (Sec. 9.22) will be used. The measured coherence and phase C'_m will be defined in terms of the estimated cross and power spectra as:

$$C'_m(\omega) = \frac{\hat{L}_m(\omega) + i\hat{Q}_m(\omega)}{\sqrt{\hat{P}_1(\omega)\,\hat{P}_m(\omega)}} \qquad (B1)$$

Where $\hat{L}_m(\omega)$, $\hat{Q}_m(\omega)$ are estimates of the co- and quad spectra and $\hat{P}_1(\omega)$, $\hat{P}_m(\omega)$ are estimates of the power spectra at the reference and mth microphone. For convenience the frequency dependence will now be dropped. Any function, as C'_m, which depends on a number of statistical estimates X_1, X_2 ..... X_N, may be expanded in the form of a Taylors series:-

$$g(X_1,X_2.....X_N) \simeq g(a_1,a_2....a_N) + \sum_{n=1}^{N} \left(\frac{\partial g}{\partial X_n}\right)_a (X_n-a_n) \qquad (B2)$$

where a_1, a_2 .... a_N are the expected values of X_1, X_2 .... X_N. Defining the measured values in the form

$$C'_m = f(\hat{L}_m, \hat{P}_1, \hat{P}_m) + ig(\hat{Q}_m, \hat{P}_1, \hat{P}_m) \qquad (B3)$$

and then expanding C'_m in the form of the series above allows the errors associated with C'_m to be defined by

$$\tilde{E}_m = \sum_{n=1}^{3} \left(\frac{\partial f}{\partial X_n}\right)_a (X_n-a_n) + i\sum_{n=1}^{3} \left(\frac{\partial g}{\partial Y_n}\right)_b (Y_n-b_n) \qquad (B4)$$

where X_n and Y_n have been substituted for the appropriate estimates in (B3). The modulus of the errors is then given by

$$|\tilde{E}_m|^2 = \sum_{n=1}^{3}\sum_{m=1}^{3} \left(\frac{\partial f}{\partial X_n}\right)\left(\frac{\partial f}{\partial X_m}\right)(X_n-a_n)(X_m-a_m) + \left(\frac{\partial g}{\partial Y_n}\right)\left(\frac{\partial g}{\partial Y_m}\right)(Y_n-a_n)(Y_m-a_m) \qquad (B5)$$

In order to define the expected value of $|\tilde{E}_m|^2$, it is noted that

$$Ex\left[X_n\right] = a_n$$

so that

$$Ex\left[(X_n-a_n)(X_m-a_m)\right] = COV\ (X_n,\ X_m)$$

using this in B5 gives

$$Ex\,|\tilde{E}_m|^2 = \sum_{n=1}^{3}\sum_{m=1}^{3}\left(\frac{\partial f}{\partial X_n}\right)\left(\frac{\partial f}{\partial X_m}\right) COV\ (X_n,X_m) + \left(\frac{\partial g}{\partial Y_n}\right)\left(\frac{\partial g}{\partial Y_m}\right) COV\ (Y_n,Y_m) \qquad (B6)$$

These covariances may be obtained from the covariance matrix in Jenkins & Watts (sec. 9.1.3), and the eighteen terms in this series are defined as follows:

$$\left(\frac{\partial f}{\partial X_1}\right)^2 COV(X_1,X_1) = \frac{1}{P_1P_m}\cdot\frac{1}{BT}\cdot\frac{1}{2}\left\{P_1P_m + L^2 - Q^2\right\}$$

$$\left(\frac{\partial f}{\partial X_1}\right)\left(\frac{\partial f}{\partial X_2}\right) COV(X_1,X_2) = \frac{-L}{2P_1P_m}\cdot\frac{1}{P_1}\cdot\frac{1}{BT}\left\{LP_1\right\}\ \times 2.$$

$$\left(\frac{\partial f}{\partial X_1}\right)\left(\frac{\partial f}{\partial X_3}\right) COV(X_1,X_3) = \frac{-L}{2P_1P_m}\cdot\frac{1}{P_m}\cdot\frac{1}{BT}\left\{LP_m\right\}\ \times 2.$$

$$\left(\frac{\partial f}{\partial X_2}\right)^2 COV(X_2,X_2) = \frac{L^2}{4P_1P_m}\cdot\frac{1}{(P_1)^2}\cdot\frac{1}{BT}\left\{P_1^2\right\}$$

$$\left(\frac{\partial f}{\partial X_2}\right)\cdot\left(\frac{\partial f}{\partial X_3}\right) COV(X_2,X_3) = \frac{L^2}{4P_1P_m}\cdot\frac{1}{P_1P_m}\cdot\frac{1}{BT}\cdot\left\{L^2+Q^2\right\}\ \times 2$$

$$\left(\frac{\partial f}{\partial X_3}\right)^2 COV(X_3,X_3) = \frac{L^2}{4P_1P_m}\cdot\frac{1}{(P_m)^2}\cdot\frac{1}{BT}\cdot\left\{P_m^2\right\}$$

A similar set of equations may be defined for $g\ (Q,\ P_1,\ P_m)$ with Q substituted for L above. Summing this set of equations gives

$$\frac{1}{P_1P_m}\cdot\frac{1}{2BT}\cdot\left\{P_1P_m + L^2 - Q^2 - 2L^2 - 2L^2 + \frac{L^2}{2} + \frac{L^2(L^2+Q^2)}{P_1P_m} + \frac{L^2}{2}\right\}$$

$$= \frac{1}{P_1P_m}\cdot\frac{1}{2BT}\left\{P_1P_m - 2L^2 - Q^2 + \frac{L^2(L^2+Q^2)}{P_1P_m}\right\}$$

Adding this to an identical equation with Q replacing L and vice versa gives $Ex\left[|E_m|^2\right]$

$$Ex\left[|E_m|^2\right] = \frac{1}{P_1 P_m} \cdot \frac{1}{2BT} \cdot \left\{ 2P_1 P_m - 3\left[L^2+Q^2\right] + \frac{(L^2+Q^2)^2}{P_1 P_m} \right\}$$

Noting that $(L^2 + Q^2)/P_1 P_m = |C_m|^2$ allows this equation to be simplified to

$$Ex\left[|E_m|^2\right] = \frac{1}{2BT} \left\{ 2-3|C_m|^2 + |C_m|^4 \right\} \qquad (B7)$$

The largest expected value of $|E_m|^2$ is therefore defined at $|C_m| = 0$ so that

$$Ex\left[|E_m|^2\right] \leqslant \frac{1}{BT} \qquad (B8)$$

References

AOKI, Y., 1970, IEEE Transactions on Audio and Electroacoustics, AU-18, No.3, 258

BEASLEY, J.A. 1977, RAE Tech. Report 77038

BENDAT, J.S. & PIERSOL, A.G. 1958, "Measurement and Analysis of Random Data", Wiley.

BILLINGSLEY, J. & KINNS, R., 1976, J. Sound Vib., 48, 485

BISHOP, K.A., FFOWCS-WILLIAMS, J.E., & SMITH, W., 1971. J. Fluid Mech., 50 (1), 21

BLACKMAN, R.B. & TUKEY, J.W., 1958, "The Measurement of Power Spectra", Dover

BROWN & REYNOULDS, 1959, J. Acoust. Soc. Am., 31, 1638

CHU, W.T., LAUFER, J. & KAO, K., 1972, International Conference on Noise Control, Washington D.C., Oct.1972, 472

CHURCHILL, R.V., 1963, "Fourier Series and Boundary Value Problems", McGraw Hill, Inc, N.Y.

CHURCHILL, R.V., 1972, "Operational Mathematics", McGraw Hill, Inc, N.Y.

COOLEY, J.W., LEWIS, P.A.W., & WELCH, P.D., 1969, Conf. on Applications and Methods of Random Data Analysis, ISVR, University of Southampton, July 1969

DAMMS, S.M., 1977, RAE Tech. Report 77032

DAVIDS, THURSTON & MUESER, 1952, J. Acoust. Soc. Am., 24, 50

DYER, I, 1959, J. Acoust. Soc. Am., 31 (7), 1016

EL-SUM, H.M.A., 1969, "Acoustic Holography", Vol.I, Eds: A.F.Metherell, H.M.A. El-Sum, L.Larmore, Plenum Press N.Y.

FFOWCS-WILLIAMS, 1973, Agard CP 131 Tech. Evaluation Report

FFOWCS-WILLIAMS, 1974, Invited Lecture, 8th I.C.A., London

FISHER, M.J., HARPER BOURNE, M., & GLEGG, S., 1977. J. Sound Vib. 51 (1), 23

FLYNN, O.E., & KINNS, R., 1976, J.Sound Vib. 46 (1), 137

GLEGG, S., 1975, M.Sc Dissertation, University of Southampton

GREENE, D.C., 1969, J. Acoust. Soc. Am. 46, 44

GROSCHE, F.-R., 1968, DLR-FB 68-46, 1

GROSCHE, F.-R., 1973, Agard CP 131, 4. Conference on Noise Mechanisms.

HAHN, W.R., 1975, J. Acoust. Soc. Am. 58, 201

JENKINS, G.M. & WATTS, D.G., 1968, "Spectral Analysis and its Applications", Holden Day, San Francisco

KEMPTON, A.J., 1976, J. Sound Vib. 48 (4), 485

KINNS, R., 1976, J. Sound Vib. 44 (2), 275

LAUFER, J., SCHLINKER, R. & KAPLAN, R.E., 1976, AIAA Jnl. 14, 489

LIGHTHILL, M.J., 1952, Proc. Roy. Soc. A221, 564

LUSH P.A., 1971, J. Fluid Mech. 46, 477

MacDONALD, V.H., & SHULTHESIS, P.M., 1968, J. Acoust. Soc. Am., 46, 37

MAESTRELLO, L., & McDAVID, E., 1971, AIAA Jnl., 9 (6), 1058

MAESTRELLO, L., & LIU, C.-H., 1976, AIAA 3rd Aero-Acoustics Conference, AIAA 76-543

MARTLEW, D.L., HAWKINS, J.M., BROOKING, R.L., & KENNEDY, A.S., 1976, Jnl. Roy. Aero. Soc. Jan.1976

MORFEY, C.L., 1973, J. Sound Vib. 31 (4), 391

MUELLER, R.K., 1971, Proc. IEEE, 59 (9), 1319

PAPOULIS, 1962, "The Fourier Integral and its Application", McGraw-Hill, N.Y.

PARTHASARATHY, S.P., 1974, AIAA Jnl. 12 (5), 583

POTTER, R. & JONES, 1967, "An Experiment to locate the acoustic sources in a high speed jet exhaust stream". Wyle Laboratory Report

SASAKI, K., SATO, T., NAKAMURA, Y., 1977, IEEE SU-24 (3), 193

SIDDON, T.E., 1973, Agard CP-131, Conference on Noise Mechanisms

UHEA, S., FUJINAMI M., UMEZAWA, K., & TSUTIUCHI, J., 1975, Appl. Optics 14 (7), 1478

VAN BUREN, 1973, J. Acoust. Soc. Am. 53, 192

WATSON, E.E., 1973, J. Acoust. Soc. Am. 54. 685

WAY, D.J., 1977, AIAA 4th Aero-Acoustics Conference AIAA 77-1305

WELCH, 1967, IEEE Trans. AU-15, 70

YADLEY, P.D., 1974, Ph.D. Thesis, University of Southampton.

Acknowledgements

The work presented in this thesis could not have been completed without the help of many others. In particular I would like to thank:

Dr M.J. Fisher, who supervised this project, and who was undoubtedly the driving force behind the work which was undertaken. I greatly appreciate his dedication, help and continual advice and encouragement which made the difference between the success and failure of the results which have been obtained.

Mr M.Harper Bourne, who originally developed the principle of Polar Correlation, was responsible for the collection of data at NGTE, made a trip to Derby to supervise the tests on the RB.211 engine.

Brian Edwards, who helped with the tests in the anechoic room at ISVR, and provided Figs.1.1 & 5.1. Without the help of such a good experimentalist these tests would not have been completed.

Mrs M.Davies, who analysed data from the test at NGTE on the Hewlett Packard correlator and provided assistance on many of the other results.

Members of the Data Analysis centre at ISVR who helped with the development of computer programmes on the PDP 11/50.

Dr J. Billingsley of Portsmouth Polytechnic, who provided facilities and helped with the development of the programmes on the CAI.LSI, Alpha computer.

This project was sponsored by Rolls Royce Ltd and I would like to acknowledge my appreciation of their support. There are a number of members of Rolls Royce staff who helped considerably with this work. In particular I would like to thank Mr J. Hill, Dr B. Lowrie, Dr M. McCormick, Mr A. Syed, Mr J.Brown, and all the other members of the Rolls Royce Noise Department who were involved with this work.

I would also like to thank the members of staff at NGTE for their help in carrying out the tests in the N.T.F.

Finally I would thank my present employers Westland Helicopters Ltd for the time they have made available for the completion of this thesis.

TABLE 5.1: MICROPHONE LOCATIONS FOR N.G.T.E. TEST AND RESULTS OF LOUDSPEAKER CALIBRATION TESTS.

Angular Separations degrees	L/S 8" from Nozzle		L/S 40" from Nozzle	
	Measured Time Delay μsec	Calculated Correction Factor μsec	Measured Time Delay μsec	Calculated Correction Factor μsec
0	15	15	15	15
0.5	50	45	65	34
1	92	82	145	83
1.5	125	110	198	105
2	172	151	262	138
2.5	205	179	328	173
3	240	209	380	194
4	315	274	505	257
5	395	343	640	330
6	485	423	785	413
7	570	498	899	466
8	645	563	1016	521
9	730	637	1132	576
10	815	712	1265	648
12	982	859	1548	809
14	1132	989	1832	972
16	1332	1169	2131	1151
18	1499	1316	2381	1282
20	1682	1479	2681	1465
22	1865	1643	2950	1618
25	2131	1880	3400	1897
30	2597	2300	4100	2322
35	3100	2760	4850	2811
40	3600	3219	5550	3265
45	4100	3681	6300	3786

LOCATIONS OF MICROPHONES USED IN RB.211 TEST TABLE 6.1

The mircophones were laid out in a polar array with a radius of 100 ft; the angular locations of each microphone are given below.

Microphone No.	Angle to Reference (degrees)	Angle to Intake (degrees)
1 (Ref.)	0	90
2	0.5	90.5
3	1.0	91
4	1.5	91.5
5	2.0	92
6	2.5	92.5
7	3	93
8	4	94
9	5	95
10	6	96
11	7	97
12	8	98
13	9	99
14	10	100
15	12.5	102.5
16	15	105
17	17.5	107.5
18	20	110
19	25	115
20	30	120
21	35	125
22	40	130

NOISE LEVELS OF ENGINE COMPONENTS — TABLE 6.2

250 Hz (32 Hz Bandwidth) — Breakdown of engine noise

Condition	Build	Total	Jet	Core	Engine	By-Pass	Inlet	O/C etc
60%	ISVR 1	88.5dB	82.5	85.7	82.2			
	ISVR 2	88.5dB	81.3	85.4	83			
75%	ISVR 1	96 dB	91.2	92.5	89.7			
	ISVR 2	95 dB	90.7	91.5	87.5			
90%	ISVR 1	103.6dB	101	97.9	96.1			
	ISVR 2	101 dB	98.2	96.6	91.2			

500 Hz (32 Hz Bandwidth)

Condition	Build	Total	Jet	Core	Engine	By-Pass	Inlet	O/C etc
60%	ISVR 1	90 dB	80.8	88.2	83	80.7	-	79.2
	ISVR 2	87 dB	77.5	82.8	83.6	79.8	73.5	80.5
75%	ISVR 1	96.6dB	89.4	93.9	91	89.0	-	86.4
	ISVR 2	94.5dB	88	88.6	91.5	87.8	85.6	86.3
90%	ISVR 1	101.6dB	97.7	97.7	94.2	92.5	89.5	-
	ISVR 2	100.5dB	97.6	93.9	94.7	93.5	88.5	-

1000 Hz (32 Hz Bandwidth)

Condition	Build	Total	Jet	Core	Engine	By-Pass	Inlet	O/C etc
60%	ISVR 1	87.6dB	80.2	84.1	83.3	80.5	75.6	78.2
	ISVR 2	86 dB	74	77.7	85	82.3	76.5	80
75%	ISVR 1	94.8dB	89.2	90.5	90.4	86.8	82.8	86.2
	ISVR 2	92.5dB	84.8	84.5	90.7	87.4	85.6	86.3
90%	ISVR 1	100.8dB	96.9	95.8	95.3	92.9	88.9	88.1
	ISVR 2	100 dB	95.7	91.2	97	93.6	84.3	-

Pages 133 is missing from this Thesis

Computer Programme I

This programme is used to calculate the source image from the values of complex coherence measured in a Polar Correlation test. The basis of this programme is described in Appendix I.

```
      MASTER SELLC
      DIMENSION XT(500),XT(64),Z1(128),Z2(128),Z3(128),X(110),A(110)
      DIMENSION HX(111),HY(110),B(110),AP(5,110)
C*****************************************************************
C
C          POLAR CORRELATION SOURCE IMAGE PROGRAM
C
C*****************************************************************
C
C       THIS PROGRAM CALCULATES THE SOURCE IMAGE FOR THE POLAR
C       CORRELATION TECHNIQUE, THE BASIC DATA INPUT IS THE C,P,S,O,
C       (OR COMPLEX COHERENCE) IN AMPLITUDE AND PHASE AT A FIXED
C       FREQUENCY BETWEEN A REFERENCE MICROPHONE AT 'BETA' AND A
C       MOVING MICROPHONE AT 'ALPHA' (ANGLES RE YO DEGREES TO AXIS)
C
C       IDEALLY MEASUREMENTS ARE TAKEN AT EQUAL INTERVALS 'DEL' IN
C       TERMS OF THE VARIABLE  (SIN(ALPHA)-SIN(BETA)), HOWEVER IF
C       THE DATA HAS BEEN MEASURED AT ARBITARY ANGLES, AN INTERPOLATION
C       ROUTINE IS PROVIDED WHICH ESTIMATES THE DATA AT THE REQUIRED
C       LOCATIONS (WHICH MUST BE SPECIFIED).
C       CARE MUST BE TAKEN NOT TO ALIAS THE SOURCE IMAGE USING THIS
C       METHOD; THE TRUE ALIASING LENGTH WILL DEPEND ON THE WIDEST
C       MICROPHONE SEPARATION IN THE ACTUAL ARRAY USED.
C
C       THIS PROGRAM CAN ALSO BE USED TO SIMULATE SOURCE IMAGES,
C       A SOURCE DISTRIBUTION INCLUDING POINT SOURCES AT ARBITARY
C       LOCATIONS AND DISTRIBUTED SOURCES MAY BE SPECIFIED AT A FIXED
C       FREQUENCY, AND THE POLAR CORRELATION SOURCE IMAGE IS THEN
C       COMPUTED.
C
C       THE INPUTS ARE INDICATED IN THE LISTING AND REPEATED CALCULATIONS
C       MAY BE UNDERTAKEN USING DO LOOP 110.
C
C*****************************************************************
C
C       *****INPUT DATA  ******
C       NUMBER OF SOURCE DISTRIBUTIONS TO BE ANALYSED
C
C       LAA= 0  FOR TEST DATA
C            1  FOR COMPUTED DATA(SEE SOURCE FOR INPUTS)
C            2  FOR TEST DATA AT ARBITARY ANGLES( INPUT ANGLES IN REHASH)
C       L1= NO OF INCHES TO BE PRESENTED  (+VE)
C       L2= NO OF INCHES TO BE PRESENTED  (+VE)
C        LCAL= CALCOMP PLOTTER MARKER& 1 FOR PLOT
C       RC=INTERVAL BETWEEN PLOTTED POINTS IN INCHES
C*****************************************************************
      READ(2,15)JS,LAA,L1,L2,LCAL,RC
15    FORMAT(5I5,F10.3)
C*****************************************************************
      IF(LCAL.NE.1)GO TO 151
      CALL PLOTS(0,0,1)
      CALL JNAME
      CALL PLOT(0.0,0.0,3,-3)
      AMAX=0.0
      AMIN=0.0
151   DO 110 J1=1,JS
C       ITEST=TEST NUMBER
C       DEL=SAMPLE INTERVAL
C       NSAMPLE=NUMBER OF MEASUREMENT POINTS
C       LABINDEX FUNCTION MARKER
C       PT=LEVEL AT REF MICROPHONE IN DB
C       FREQ=FREQUENCY
C*****************************************************************
      READ(2,10)ITEST,DEL,NSAL,FREQ,PT
10    FORMAT(I5,F10.0,2I5,2F10.0)
C*****************************************************************
      IF(LAA.NE.1)GO TO 120
      CALL SOURCE(XX,FREQ,DEL,X1,X2)
      GO TO 121
120   DO 100 I=2,NS
C       A1( I)=THE AMPLITUDE
C       X2( I)=PHASE
C       I=MICROPHONE NUMBER
C*****************************************************************
      READ(2,11)I,X1(I),X2(I)
11    FORMAT(I5,2F10.0)
C*****************************************************************
100   CONTINUE
      IF(LAA.EQ.2)CALL REHASH(X1,X2,NS,DEL)
```

```
C      ******* PLOT INPUT DATA  *******

121    NA=19
       X1(1)=1.0
       NJ=0
       WRITE(6,19) ITEST,FREQ
114    NJ=NJ+1
       T1=1.0
       DO 113 N=1,NA
       A(I)=A1(N)
       X(I)=(I-1)*DEL
       IF(I2U.EQ.1)WRITE(6,25)I,X(N),X1(N),X2(N)
25     FORMAT(20X,I3,3(E10.4,F11.5))
       IF(I2U.EQ.2)A(I)=X2(N)
       I=INT(A(N))
       IF(T.GT.T1)T1=T
113    CONTINUE
       IF(T1.EQ.0.0)GO TO 115
C      WRITE(6,16)
C      CALL LPPLOT(X,A,NA,0.3,1.0,100.35,NX,NY)
       IF(I2U.NE.2)GO TO 114

C      ****  SET ARRAYS TO ZERO

115    DO 101 I=1,I2U
       Z1(I)=0.0
       Z2(I)=0.0
       Z3(I)=0.0
101    CONTINUE

C      ******  DATA TRANSFORM SECTION  *****

       F=2.*DEL*SQRT(12.0)
       Z1(1)=F*0.5
       SN=IS-1

       DO 103 I=2,IS
       IF(L.EQ.1)X1(I)=X1(1)*(1-(N-1)/SN)
       Z1(I)=X1(N)*COS(X2(I))*F
       Z2(I)=X1(N)*SIN(X2(I))*F
103    CONTINUE

       IP=128
       II=1
       CALL CUBASP(Z1,Z2,IP,,TRUE,,N9,Z3)



C      *****PLOTTER  SECTION  ******
C      *****DEFINE PLOTTER CONSTANTS  ****
C      LT= TOTAL NO. OF INCHES TO BE PRESENTED
C      X( )=X-SCALE ARRAY
C      X0=ORIGIN OF X-SCALE
C      Y0=ORIGIN OF Y-SCALE
C      NL=NO. OF LINES

       LT=1.1*L2
       NL=15
       X0=1.0
       Y0=1.0

C      ****  DEFINE X-SCALE  ******

       NP=LT/RC
       DP=4L2/RC
       IF(NP.GT.110)NP=110
       DO 104 I=1,NP
       X(I)=(I-NP2)*RC
104    CONTINUE

C      ****    DEFINE DATA FOR PLOTTING   ******

       ANDA=T1500.0/FREQ
       RES=ANDA/((NS-1)*DEL)
       ALIAS=ANDA/DEL

       CALL RETRR(Z1,A,128,NP,NP2,RC,ALIAS)

C      ******PLOT RESULTS   ******

       WRITE(6,12)ITEST,FREQ
       WRITE(6,15)IS,RES
       WRITE(6,17)ALIAS
       IF(L.EQ.1)WRITE(6,14)

       CALL LPPLOT(X,A,NP,X0,Y0,NP,NL,NX,NY)

C      *******  INTEGRATION SECTION  ******

       SUMC=A(1)
       CALL RETRR(Z1,A,128,NP,NP2,RC,ALIAS)
       CALL INTEG(A,SUM,NP,)

C      ****    WRITE OUT RESULTS IN DETAIL  ******
```

```
                WRITE(6,12)ITEST,FREQ
                WRITE(6,20)
                DO 150 I=1,NP
                X(I)=(I-NP/2)*RC
                A(I)=A(I)**2,*(P1/10.0)
                Z2(I)=X(I)/RE
                WRITE(6,21)X(I),Z2(I),Z3(I),A(I)

                IF(A(I).GT.AMAX)AMAX=A(I)
                IF(A(I).LT.AMIN)AMIN=A(I)

        150     CONTINUE

                IF(LOAL.EQ.1)CALL CALCU(A,AP,AMAX,AMIN,NP,X)

        110     CONTINUE
                IF(LOAL.EQ.1)CALL PLOT(1,0.0,0.999)

        12      FORMAT(1H1,///,2X,'TEST NO. =',I6,10X,'FREQUENCY=',F6.1)
        13      FORMAT(///,24X,'NO. OF MEASUREMENT POINTS=',I2,12X,'RESOLUTION
               CIN INCHES=',F7.4)
        14      FORMAT(///,24X,'BARTLETT WINDOW USED',///)
        17      FORMAT(/,24X,'ALIASING LENGTH=',F8.4)
        18      FORMAT(1H1)
        19      FORMAT (1H1,24X,'INPUT DATA',10X,'TEST NO. =',I5,10X,'FREQ=',F7.1,
               1'MHZ'//35X,'ANGLE',13X,'AMPLITUDE',12X,'PHASE')
        20      FORMAT(///,31X,'LOCATION',17X,'LOCATION',16X,'INTEGRATED',13X,
               1'MEASURED',/,34X,'IN INS ',11X,'IN LAMBDA/SIN(ALPHA)',12X,'LEVELS'
               2,19X,'LEVELS'////)
        21      FORMAT(31X,F8.4,10X,F9.4)
        110     STOP
                END
```

END OF SEGMENT, LENGTH 380, NAME SELEC

```
                FUNCTION PHASE(Z1)
                COMPLEX Z1
                PIE=4.0*ATAN(1.0)
                R=REAL(Z1)
                AI=AIMAG(Z1)
                P=PIE/2.0
                IF(R.NE.0.0)P=ATAN(AI/R)
                IF(R.LT.0.0)P=P+PIE
                PHASE=P
                RETURN
                END
```

END OF SEGMENT, LENGTH 39, NAME PHASE

```
0241                  COMPLEX FUNCTION DIST(Z,N1,P1,A,P2,N2)
0242                  DIMENSION P1(10),N1(10),P2(10),N2(10)
0243                  COMPLEX ZS
0244                  N1=N1(J)
0245                  GO TO(1,2,3,4,5),NJ
0246            C     POINT SOURCE AT ZERO
0247            1     DIST=CMPLX(1.0,0.0)
0248                  RETURN
0249
0250            C           CONTINUOUS SOURCE DIST,       EXP(-P*Y)*(Y**N1)/N1!
0251            2     ZS=CMPLX(P1(J),-A)
0252                  NJ=-(N1(J)+1)
0253                  DIST=ZS**NJ
0254                  RETURN
0255
0256            C      POINT SOURCE WITH 1 ST ORDER ERROR P1=1/C*(2PIE*DEL/LAMBDA)**2
0257
0258            3     X=1*A*P1(J)
0259                  DIST=CMPLX(COS(X),0.0)
0260                  RETURN
0261
0262            C      POINT SOURCE DISPLACED FROM AXIS BY P1 WAVELENGTHS,FREQ=13.5 KHZ
0263
0264            4     SI=A/0.285
0265                  CO=SQRT(1-SI**2)
0266                  X=0.285*P1(J)*C
0267                  DIST=CMPLX(COS(X),0.0)
0268                  RETURN
0269
0270            C      SECONDARY SOURCE OF LEVEL P1 RE JET NOISE
0271            C      WITH DIRECTIVALITY  (1-B2*SIN(A))**-N1
0272            C      FREQ=13.5KHZ
0273            C      (NOTE I N1=0 GIVES WINDOW ON JET NOISE)
0274
0275            5     N=N1(J)*2.0
0276                  X=(1-P2(J)*A/0.285)**(-N)
0277                  DIRN=1/SQRT(1-X/P1(J))
0278                  DIST=CMPLX(DIRN,0.0)
0279                  RETURN
0280
0281                  END
```

END OF SEGMENT, LENGTH 181, NAME DIST

```
0282                  SUBROUTINE ITEG(A,B,NP,D)
0283                  DIMENSION A(110),B(110)
0284                  B(1)=0.0
0285                  DO 300 I=2,NP
0286                  B(I)=B(I-1)+(A(I)+A(N-1))/2.0*D
0287            300   CONTINUE
0288                  RETURN
0289                  END
```

END OF SEGMENT, LENGTH 70, NAME ITEG

```
0294                  SUBROUTINE SOURCE(JV,FREQ,DEL,AMP,PH)
0295                  DIMENSION NT(10),J1(10),P1(10),P2(10),X(10),Y(10),AMP(100),PH(100)
0296                  DIMENSION TITLE(10)
0297                  COMPLEX Z(100,10),Z1,ZY,CIST
0298
0299            C     SET ARRAYS TO ZERO
0300                  DO 1100 I=1,100
0301                  DO 1100 J=1,10
0302            1100  Z(I,J)=CMPLX(0.,0.)
0303
0304            C     DEFINE SOURCE DISTRIBUTION PARAMETERS
0305
0306            C      NS= #, OF SOURCE DISTRIBUTIONS  <10
0307            C      NT(J)= SOURCE TYPE INDICATOR   <5
0308            C       1= POINT SOURCE
0309            C       2= CONTINUOUS SOURCE DIST.   P1*EXP(-P2*Y)*(Y**N1)/N1!
0310            C       3= 1 ST ORDER ERROR FOR SOURCE AT Y
0311            C            P1= (LAMDA/2)*Y*Y/(4.*PIE)
0312            C      P1(J),P2(J),=REAL CONSTANTS FOR SOURCE  J
0313            C      N1(J)=INTEGER CONSTANT FOR SOURCE J
0314            C      P2(1)= WT PRODUCT
0315            C      Q(J)= SOURCE STRENGTH
0316            C      Y(J)= SOURCE LOCATION
0317
0318            C     DEFINE OUTPUT PARAMETERS
0319            C      NV=NO. OF VALUES REQUIRED
0320            C      FREQ=FREQUENCY OF DATA
0321
0322            C     WRITE TITLES TO OUTPUT
0323            C*************************************************
0324                  READ(2,52)(TITLE(I),I=1,10)
0325            52    FORMAT(10A8)
0326            C*************************************************
0327                  WRITE(6,51)(TITLE(I),I=1,10)
0328            C*************************************************
0329                  READ(2,30)NS
0330            30    FORMAT(I5)
0331            C*************************************************
0332
0333                  DO 1101 J=1,NS
0334            C*************************************************
0335                  READ(2,31)NT(J),N1(J),P1(J),P2(J),X(J),Y(J)
0336            31    FORMAT(2I5,4F10.0)
0337            C*************************************************
0338
0339            1101  WRITE(6,54)J,NT(J),N1(J),P1(J),P2(J),X(J),Y(J)
0340                  DO 1102 I=1,NV



0341                  AM=DEL*(I-1)
0342                  A=6.283*AM*FREQ/13500.0
0343                  AG=SIN(A/4)**2
0344                  Z1=CMPLX(0.,0.)
0345                  DO 1103 J=1,NS
0346                  A1=A*Y(J)
0347                  ZY=CMPLX(COS(A1),SIN(A1))
0348                  Z(I,J)=CIST(NT,N1,P1,P2,J,A)*Q(J)*ZY
0349                  Z1=Z1+Z(I,J)
0350            1103  CONTINUE
0351                  IF(I.EQ.1)AMP1=CABS(Z1)
0352                  AMP(I)=CABS(Z1)
0353                  PH(I)=PHASE(Z1)
0354                  AMP(I)=AMP(I)/AMP1
0355            1102  CONTINUE
0356                  RETURN
0357            51    FORMAT(1H1///24X,10A8)
0358            54    FORMAT(///,40X,'INPUT FOR SOURCE NUMBER  ',I2,///,34X,'SOURCE TYPE=
0359                 C,I7,/,33X,'N1=',I5,10X,'P1=',F10.4,10X,'P2=',F10.4,//,27X,'SOURCE ST
0360                 CRENGTH=',F10.4,/,'SOURCE LOCATION=',F10.4,'(FT)')
0361                  END
```

END OF SEGMENT, LENGTH 707 NAME SOURCE

```
0376
0397                  SUBROUTINE REARR(A,B,IT,NP,NP2,RC,ALIAS)
0398                  DIMENSION A(143),B(110)
0399                  IF(IP.GT.110)IP=110
0396
0395            C     NP=NO. OF OUTPUT POINTS
0394            C     IT=NO. OF INPUT POINTS
0393            C     RC=INTERVAL BETWEEN O/P POINTS
0392            C     ALIAS=LENGTH OF I/P
0391            C     NP2=NO. OF NEGATIVE O/P POINTS
0390            C     RI=INTERVAL BETWEEN I/P POINTS
0389
0387            C     CALCULATE +VE RESULTS
0386
0385                  IP1=IP+1
0384                  RI=ALIAS/FLOAT(IT)
0383                  DIF=RC/RI
0382                  B(1)=A(1)
0381
0380                  DO 200 I=1,IP1
0379                  I=I+DIF
0378                  D=I*RC-I+RI
0377                  I1=I+1
0376                  I2=I1+1
0375                  IF(I1.GT.128)I1=I1=128
0374                  IF(I2.GT.128)I2=I2=128
0373                  B(I+1)=A(I1)+(A(I2)-A(I1))*D/RI
0372            200   CONTINUE
0371
0370            C     CALCULATE -VE RESULTS
0369
0368                  DO 201 I=2,NP+1
0367                  I=(I-1)+DIF
0366                  D=(I-1)*RC-I+RI
0365                  I1=129-I
0364                  I2=I1-1
0363                  IF(I1.GT.128)I1=1
0362                  IF(I1.LT.1)I1=I1+128
0361                  IF(I2.LT.1)I2=I2+128
0360
0359                  B(I+2*NP+1)=A(I1)+(A(I2)-A(I1))*D/RI
0358            201   CONTINUE
0357                  RETURN
0356                  END
```

END OF SEGMENT, LENGTH 235, NAME REARR

```
0404                SUBROUTINE REHASH(X1,X2,NS,DEL)
0405                DIMENSION X1(400),X2(400),Z1(512),Z2(512),ANG(60)
0406          C      THIS SUBROUTINE MODIFIES THE DATA IN X1,X2, USING LINEAR
0407          C      INTERPOLATION OF AMPLITUDE AND PHASE, SO THAT EACH MEASUREMENT
0408          C      EFFECTIVELY LIES AT EQUAL INTERVALS 'DEL', ORIGINAL MEASUREMENT
0409          C      ANGLES ARE GIVEN IN 'ANG'.
0410
0411
0412          C      ***   READ MEASUREMENT ANGLES:  ANG(1)=REFERENCE   *****
0413          C**************************************************
0414                READ(5,40)(ANG(I),I=1,NS)
0415          40    FORMAT(10F10.0)
0416          C**************************************************
0417
0418
0419          C      ***   ELIMINATE 2*PIE PHASE JUMPS IN X2
0420
0421                X1(1)=X1(1)
0422                X2(1)=X2(1)
0423                DO 503 N=4,NS
0424                G1=(X2(I-2)-X2(I-3))/(ANG(N-2)-ANG(N-3))
0425                G2=(X2(I-1)-X2(I-2))/(ANG(N-1)-ANG(N-2))
0426                G=(G1+G2)/2.0
0427                Z=X2(I-1)+G*(ANG(N)-ANG(N-1))
0428
0429          504   I=1
0430                IF(X2(N).GT.Z)I=-1
0431                T=ABS(Z-X2(I))
0432                T1=ABS(Z-X2(N)+I*6.283)
0433                IF(T.LT.T1)GO TO 503
0434                X2(I)=X2(N)+I*6.283
0435                GO TO 504
0436          503   CONTINUE
0437
0438
0439          C      ***  INTERPOLATE RESULTS INTO QUANTISED CONTINUOUS ARRAYS
0440          C             AT INTERVALS OF 1/NQUANT;  NQUANT=512
0441
0442                NQUANT=512
0443                CALL INTERP(ANG,X1,X2,Z1,Z2,NQUANT,NS,SAM)
0444
0445          C      ***   READ D OFF VALUES IN Z1,Z2, AT EQUAL INTERVALS 'DEL'
0446
0447                RN=NQUANT*DEL/SAM
0448                RN=1+(1/RN)
0449                INT=SAM/RN
0450                NS=RNN1
```

```
0451                QUANT=NQUANT
0452                DEL=INT/QUANT
0453                DO 502 N=1,NS
0454                X1(I)=Z1(1+(N-1)*INT)
0455                X2(I)=Z2(1+(N-1)*INT)
0456          502   CONTINUE
0457
0458                RETURN
0459                END
```

END OF SEGMENT, LENGTH 299, NAME REHASH

```
0489                SUBROUTINE INTERP(A1,A2,X1,X2,Y1,Y2,SA1)
0490
0491          C      DEFINE NUMBER OF O/P POINTS IN APERTURE
0492                SA1=SIN(A(NA//57.3)-SIN(A(1)/57.3))*4
0493
0494          C      *** LINEARLY INTERPOLATE BETWEEN VALUES
0495
0496                N=1
0497                NA1=NA-1
0498
0499                DO 300 I=1,NA1
0500
0501                I1=1+SIN(A(I)/57.3)+1
0502                I2=1+SIN(A(I+1)/57.3)+1
0503
0504                ID=I2-I1
0505                D1=ID
0506
0507                DIF1=A1(I+1)-A1(I)
0508                DIF2=A2(I+1)-A2(I)
0509
0510                DO 300 J=1,ID
0511
0512                N=N+1
0513                D2=J-1
0514                GRAD=D2/D1
0515                Y1(I)=X1(I)+DIF1*GRAD
0516                Y2(I)=X2(I)+DIF2*GRAD
0517
0518          300   CONTINUE
0519
0520
0521          C      ***   ZERO REST OF ARRAY   ***
0522
0523                N=I+1
0524                DO 301 I=N,514
0525                Y1(I)=0.0
0526                Y2(I)=0.0
0527          301   CONTINUE
0528
0529                RETURN
0530                END
```

END OF SEGMENT, LENGTH 209, NAME INTERP

```
0531                SUBROUTINE CALCJ(A,AP,AMAX,AMIN,NP,X)
0532                DIMENSION A(110),X(110),AP(5,110)
0533
0534          C*******************************************************
0535                READ(3,2002)NJV,NTOT
0536          2002  FORMAT(2I5)
0537          C*******************************************************
0538
0539                DO 2004 I=1,NP
0540          2004  AP(JDV,I)=A(I)
0541
0542                IF(JDV.NE.NTOT)RETURN
0543
0544                FV=AMAX
0545                DV=0.1
0546                CALL SGPLOT(AP,X,FV,DV,NP,NTOT)
0547                AMAX=0.0
0548                AMIN=0.0
0549                RETURN
0550                END
```

END OF SEGMENT, LENGTH 91, NAME CALCJ

```
0541
0542                    SUBROUTINE SGPLOT(AP,A,FV,DV,NP,NTOT)
0543                    DIMENSION A(1300),X(110),AP(9,114)
0544
0545                    CALL PLOT(20.,0.,1,0,-3)
0546                    CALL SCALE(X,10.,0,NP,1)
0547                    CALL AXIS(0.,0.0,0,'OBJECT AXIS',-8,10.0,0.0,0.0,X(NP+1),X(NP+2))
0548
0549                    XO=(NP+1)/X(NP+2)
0550                    XO=-XO
0551                    A(1)=FV
0552                    FV=1.0
0553
0554                    CALL AXIS(XO,0.,1H ,1,10.0,90.0,FV,DV)
0555                    A(2)=FV
0556                    A(3)=DV
0557                    DO 2000 N=1,NTOT
0558                    N1=1
0559                    IF(I.EQ.1)N1=0
0560                    DO 2001 I=1,NP
0561            2001    A(I)=AP(N,I)/A(1)X
0562            2000    CALL LINE(X,A(NP,1,,1,+1)
0563                    RETURN
0564                    END

END OF SEGMENT, LENGTH   167, NAME  SGPLOT
```

```
 0565                   FINISH

END OF COMPILATION -  NO ERRORS

$/C SUBFILE;              34 BUCKETS USED
COOR3;  #XFAT(DEL ;*FI #APCK
COOR3;  JOB REQUEST  1100# WORDS
COOR3;  JOB REQUEST  1100# WORDS


CONSOLIDATED BY APCK 120   DATE      20/09/77   TIME 18/44/36

ICLROUTINAM  (0)    REMARED  ICLA=DEFAULT(0)

BRUGHAM A365
COMPACT DATA (1541)
COMPACT BRUGHAM (OBJ#)
COOR3;  JOB REQUEST  2235) WORDS
COMP              22844


                SEG     SELEC
                SEG     PLOTS
                SEG     INAME
                SEG     PLOT
                SEG     SYMBOL
                SEG     REMARK
                SEG     AXIS
                SEG     SYMBF
                SEG     CURV
                SEG     SYM
                SEG     CONNAME
                SEG     SCARR
                SEG     LGPLOT
                SEG     INTEG
                SEG     CALCU
                SEG     MINMAX
                SEG     STAT
                SEG     REAL
                SEG     MINAD
                SEG     DIST
                SEG     COPLA
                SEG     ANIM
                SEG     CURV
```

Computer Programmes II - VI

These programmes form part of a suite which may be used on the ISVR PDP 11/50 DAX/11 system. Their operation is described in Chapter 4.

Computer Programme II

********** LISTING OF GATHER **********

```
/READ('SAMPLE RATE',SR)
/READ('NO OF SAMPLES',SN)
/READ('START FILE NO',N1)
/READ('STOP FILE NO',N2)
/READ('SERIES NO',NL)
DO 100 N=N1,N2
/WRITE('MIC NO',N)
I1=((2*NL-1)*100)+N
I2=I1+100
101/KILL(1,2,I1,I2)
/ACQUIR(SR,SN,2,1,"FIDO")
/CONV(1,I1,4,SN)
/CONV(2,I2,4,SN)
/STAT(I1)
/STAT(I2)
/READ('ANSWER 1;OKAY 2;RETAKE',M)
IF(M.EQ.2)GO TO101
100 CONTINUE
END
```

Computer Programme III

********** LISTING OF CHURN **********

```
/READ('START MIC NO',N1)
/READ('STOP MIC NO',N2)
/READ('TEST NO',NAME)
/READ('SERIES NO',NL)
/READ('RESOLUTION',RES)
DO 100 N=N1,N2
/WRITE('MIC NO',N)
I1=((2*NL-1)*100)+N
I2=100+I1
/KILL(1,2,3,4,5,6,7,16,17,18,19)
/CSD(I2,I1,3,RES,2)
/PSD(I1,1,RES,2)
/PSD(I2,2,RES,2)
/ARITH(1,5,3,2)
/FUNC(5,6,4)
/ARITH(3,7,4,6)
/MOPH(7,4,-1)
DO 101 K=11,14
K1=K+5
K2=K-10
IF(N.EQ.1)GO TO 102
/ARITH(K,K1,7,1)
/KILL(K)
/MERGE(K,2,0,K1,K2)
GO TO 101
102/KILL(K)
/ARITH(K2,K,7,1)
101CONTINUE
/KILL(1,2,3,5,6,7,8,9,16,17,18,19)
/XCOLEC(N,4,NAME)
/KILL(I1,I2,4)
100 CONTINUE
END
```

Compter Programme IV

```
********  XCOLEC FTN  *******

      DIMENSION A(300),B(300),CB(128),CUF(256)
      DIMENSION BCB(128),IRCB(32)
      EQUIVALENCE(BCB(33),IRCB(1))
      CALL TYPE('&COLECT  DATA')
      M=0
      CALL ASKI(N,'&MIC NO=')
      CALL ASKN(B,'&INPUT FILE NAME=')
      CALL INPUT(B,CB,L3)
      CALL ASKN(A,'&OUTPUT FILE=')
      IF(N EQ 1)GO TO 4
      CALL INPUT(A,BCB,L5,0)
    GO TO 3
4    CALL OUTPUT(A)
3     F=100
      L1=1
      ASSIGN 110 TO L3
1       F=F+CB(4)
      P=(F-CB(3))/CB(4)
      NP1=P
      P2=P-NP1
      IF(P2.GT.0.5)NP1=NP1+1
      NP=2*(NP1)
      L1=L1+1
      CALL INS(B,NP,0)
      CALL IN(B,AMP)
      CALL IN(B,PH)
      IF(N.NE.1)CALL INBLK(A,CUF,L1)
      N2=2*N-1
      CUF(N2)=AMP
      CUF(N2+1)=PH
      CALL OUTBLK(A,CUF,L1)
      GO TO 1
110     CONTINUE
      IRCB(1)=7
      BCB(2)=1.0
      BCB(4)=1.0
      CALL OUTEND(A,BCB,128)
      CALL INEND(B)
200     END
```

Computer Progamme V

```
********** LISTING OF FIDDLE **********

100/READ('NO OF MICS=',N)
/KILL("TAPE",1,2,3)
/GEN(1,1)
/ALTER(1,2,1,N)
/CONV(2,3,2)
/CONV(3,"TAPE",1)
/DISPLY("TAPE",30,"TAPE",1030,"DATA",10033,1.58,0)
/READ('ANSWER 1;OKAY 2;RUBBISH',M)
IF(M.EQ.2)GO TO 100
/KILL(1,2,3)
 END
```

Computer Programme VI

```
********** LISTING OF RESULT **********

/READ('&TEST NUMBER',NR)
/READ('&FREQUENCY',F)
/READ('&FREQ RESOLUTION',RES)
/KILL(1,2,3)
I=(100+RES)/RES+0.5
MR=(2*F/RES+1)/2
N=MR-I
M1=N*64
/CONV(NR,1,0,64,M1)
FR=MR*RES
/WRITE('EXACT FREQUENCY',FR)
FA=6.28318*MR*RES/1000000.0
/ARITH("TAPE",2,7,FA)
/ARITH(1,3,2,2)
/SCREEN(3,0,1,24)
END
```

Computer Programmes A1 - A5

These programmes form the suite designed for the CAI-LSI mini computer in the Noise Department,Rolls Royce (D.E.D.). They form a complete package for Polar Correlation analysis.

Computer Programme A1 POCO

```
C      TELESCOPE PROGRAM
C      MASTER XØPOCO 2/6/77
       COMMON IBUF(8192),A(128),B(128),IBR(128),IBI(128),ISIN(128),
      1NAME(4),RES(32),
      2IGUF(50),NTEST(2),NTAPE,COND,PRIVEL,
      3PRIDIA,TEMP,WINDVE,WINDDI,PRAD,
      4NMIC,NSUB,NSMIC(5),DEL(5),TDCAL(32),REFANG,MICSUB(5,15),
      5AFREQ,IFBAND,IBT,SRATE,ITL,ISAMP,
      6SAMP,NCHAN,NGULP,NOMIC(8),NORUN,NOSUB,ICHAN,NOSPAR(4)
C
1      CALL PLOT(-1,Ø,Ø)
       WRITE (1,1ØØ)
       WRITE(1,99)
1ØØ    FORMAT ('POLAR CORRELATION PROGRAM VERSION 1',//,
      1'TYPE IN LETTER OF OPTION REQUIRED',//,
      2'I) CALIBRATE STORE',/,
      3'L) ACQUIRE DATA TO DISK',/,'A) ANALYSE DATA',/)
99     FORMAT('C) CALCULATE SOURCE DISTRIBUTION',/,
      5'S) SCREEN PLOT RESULTS',/,'H) HARD COPY RESULTS',/,
      6'P) PLOT SPECTRA FOR EACH MIC',/,'X) EXIT')
       ND=5
       READ(1,1Ø1)NEXT
1Ø1    FORMAT(A1)
       CALL MATCH(NEXT,'I','L','A','C','S','H','P','X',NEXT)
       GO TO (1,199,2ØØ,3ØØ,4ØØ,5ØØ,6ØØ,7ØØ,1ØØØ),NEXT
7ØØ    WRITE(Ø,7Ø1)
7Ø1    FORMAT('XØSPEC')
1ØØØ   CALL EXIT
1Ø2    FORMAT(F1Ø.4)
1Ø3    FORMAT(I7)
1Ø4    FORMAT(3A1)
C
199    WRITE(1,198)
198    FORMAT(///,'C) RE-CALIBRATE STORE',/,
      1'R)READ CALIBRATION FROM DISK')
       READ(1,1Ø1)NEXT
       CALL MATCH(NEXT,'C','R',NEXT)
       GO TO (1,19Ø,191),NEXT
19Ø    WRITE(Ø,192)
192    FORMAT('XØCALI')
191    CALL FILEOP('R')
       CALL RBDISK(IGUF)
       GO TO 19Ø
2ØØ    WRITE(Ø,2Ø1)
2Ø1    FORMAT('XØPLOG')
C      ANALYSIS SECTION
C
3ØØ    WRITE(Ø,35Ø)
35Ø    FORMAT('XØPANA')
C
C       CALCULATE SINE TABLE FOR TRANS
C
4ØØ    LENGTH=128
       LSIN=LENGTH/4
       DO 2Ø3 I=1,LSIN
       THETA=3.14159/FLOAT(2*LSIN)
2Ø3    ISIN(I)=IFIX(32767.9*SIN(FLOAT(I-1)*THETA))
C
C      CALCULATE SOURCE DISTRIBUTION.
C
```

```
        EAD DATA FROM FILE
C
C       NAME FILES
C
        WRITE(1,451)
451     FORMAT('READ IN 3 CHARACTER TEST NAME TO BE ANALYSED',/)
        READ(1,104)(NAME(I),I=1,3)
        WRITE(1,454)
454     FORMAT('READ IN NO. OF FILES TO BE ANALYSED')
        READ(1,103)NF
        NAME(4)=27
        CALL ANFILE('R',NAME)
        CALL RBDISK(IGUF)
C
C       ANALYSE DATA
C
C       SET PARAMETERS FOR SOURCE DISTRIBUTIOON
        WRITE (1,401)
401     FORMAT('TYPE FREQUENCY REQUIRED=')
        READ (1,103)NFREQ
404     WRITE (1,403)
403     FORMAT('DEFINE EXTREME LIMITS OF SOURCE',/,
       1'DISTRIBUTION REQUIRED (IN METRES)',/,'UPSTREAM LIMIT=')
        READ (1,102)ALIMU
        WRITE(1,473)
473     FORMAT('DOWNSTREAM LIMIT=')
        READ(1,102)ALIMD
        IF (ALIMU-ALIMD)406,404,405
405     X=ALIMU
        ALIMU=ALIMD
        ALIMD=X
406     ALT=ALIMD-ALIMU
C
C       CALCULATE SUBARRAY TO BE USED & ALIASING LENGTH
        INF=IFIX(FLOAT(NFREQ)/FLOAT(IFBAND)+0.5)
        PIF=6.283185*FLOAT(INF*IFBAND)/1000000.0
        NFREQ=INF*IFBAND
        ISUBNO=0
        X=100.0*ALT
        ALANDA=340.0/FLOAT(NFREQ)
        DO 407 J=1,NSUB
        AXE=ALANDA/DEL(J)
        IF(AXE-ALT)407,408,408
408     IF(AXE-X)409,407,407
409     X=AXE
        ISUBNO=J
407     CONTINUE
        IF(ISUBNO)404,404,410
410     ALIAS=X
        APP=FLOAT(NSMIC(ISUBNO))*DEL(ISUBNO)
        RESOL=ALANDA/APP
        N1=NSMIC(ISUBNO)
C
C       EXTRACT DATA FROM IBUF FOR DEFINED
C       MIC NOS IN MICSUB((ISUBNO,N1)
C       AND CALCULATE SOURCE DISTRIBUTION
C
        ITL2=ITL/2
        CALL CONSTANT(A,128,0.0)
        CALL CONSTANT(B,128,0.0)
```

```
      F=2.0*DEL(ISUBNO)
      A(1)=0.5*F
      SN=FLOAT(N1)
      IT=1
      DO 411 J=2,N1
      IM=MICSUB(ISUBNO,J)
C     APPLY WINDOW  FUNCTION
      FX=F*(1.0-FLOAT(J)/SN)
C     APPLY TIME DELAY CALIBRATIION
      TR=COS(PIF*TDCAL(IM))
      TI=SIN(PIF*TDCAL(IM))
      CALL RDATA(IM,IT,NF,INF,X1,Y1,ZZZ)
      IT=2
      X1=X1*FX
      Y1=Y1*FX
      A(J)=TR*X1-TI*Y1
      B(J)=TI*X1+TR*Y1
411   CONTINUE
      DO 204 I=1,128
      IBR(I)=IFIX(A(I)*32000.)
204   IBI(I)=IFIX(32000.*B(I))
      CALL TRANS(IBR,IBI,ISIN,LENGTH,IHALVE)
      DO 205 I=1,128
      A(I)=FLOAT(IBR(I))/32000.0
205   CONTINUE
C
C     DEFINE RESULTS ARRAY
C     USING LINEAR INTERPOLATION
C
      SDSP=ALIAS/128.0
      DO 450 J=1,128
      X=ALIMU+(ALT/128.0)*FLOAT(J-1)
      Y=X/SDSP
      J2=IFIX(Y)
      Y0=FLOAT(J2)*SDSP
      D=(X-Y0)/SDSP
      IF(J2)414,415,416
416   J2=J2+1
      IF(J2-128)417,418,419
419   J2=J2-128
417   J1=J2+1
      GO TO 420
418   J1=1
      GO TO 420
415   J2=1
      IF(Y)422,422,421
421   J1=2
      GO TO 420
414   J2=J2+1
      D=-D
423   J2=J2+128
      J1=J2-1
      IF(J2-1)423,422,420
422   J1=128
420   B(J)=A(J2)+(A(J1)-A(J2))*D
450   CONTINUE
      AMAX=0.0
      DO 459 J=1,128
      AXXX=B(J)
      IF(AXXX-AMAX)459,459,460
```

```
.460    AMAX=A
 459    CONTINUE
        DO 461 J=1,128
 461    B(J)=B(J)/(AMAX*2.0)
        GO TO 1
 500    ND=1
        CALL PLOT(-1,0,0)
 600    ND1=ND+1
 C      PRINT INPUT DATA
        CALL NEWPAGE(ND)
        CALL PTEXT(ND1,24,5)
        WRITE(ND1,502)
 502    FORMAT('INPUT DATA FROM',/,)
        CALL OUTSTRING(ND,IGUF,2,48)
        WRITE(ND,602)NTEST,NTAPE,NFREQ,IFBAND,RESOL,ALIAS
        WRITE(ND,503)
 503    FORMAT(5X,'MIC NO.',5X,'DISPLACEMENT',5X,'COHERENCE',5X,'PHASE'
       15X,'P.S.D.')
        IT=1
        DO 504 J=1,N1
        IM=MICSUB(ISUBNO,J)
        CALL RDATA(IM,IT,NF,INF,X1,Y1,PSD)
        IT=2
        COH=SQRT(X1*X1+Y1*Y1)
        PHA=ATAN2(Y1,X1)
        IF(PSD)515,515,513
 513    PSD=10.0*ALOG10(PSD)
        GO TO 516
 515    PSD=0.0
 516    D=DEL(ISUBNO)*FLOAT(J-1)
        WRITE(ND,505)J,D,COH,PHA,PSD
 504    CONTINUE
 505    FORMAT(8X,I2,9X,F7.5,10X,F6.4,6X,F7.4,5X,F5.1)
        WRITE(1,1001)
1001    FORMAT('TYPE SPACE TO CONTINUE')
        CALL IPCH(1,K)
        IF(K-' ')1,550,1
 550    CALL NEWPAGE(ND)
        CALL PTEXT(ND1,24,5)
        WRITE(ND1,601)
 601    FORMAT('SOURCE DISTRIBUTION FROM')
        CALL NEWLINE(ND1)
        CALL OUTSTRING(ND,IGUF,2,48)
        WRITE(ND,602)NTEST,NTAPE,NFREQ,IFBAND,RESOL,ALIAS
 602    FORMAT(/,15X,'TEST NO=',2A2,15X,'TAPE NO=',I4,
       1/,15X,'FREQUENCY=',I7,10X,'BANDWIDTH=',I5,
       2/,15X,'RESOLUTION=',F7.3,9X,'ALIASING LENGTH=',F7.3)
        NG=1
        ILINE=37
        NG1=1
        IX0=IFIX(128.0*ALIMU/ALT)
        IX0=-IX0
        IF(IX0)615,616,616
 615    IX0=0
 616    INC=8
        STEP=ALT/FLOAT(INC)
        LEN=128
        DO 610 I=1,128
 610    IBR(I)=IFIX(B(I)*32000.0)
        CALL SGPLOT(NG,IBR,LEN,INC,IX0,NG1,ND)
```

```
      DO 611 I=1,INC
      J=(I*55/INC)+1
      X=ALIMU+FLOAT(I-1)*(ALT/FLOAT(INC))
      CALL PTEXT(ND1,J,ILINE)
      WRITE(ND1,603)X
603   FORMAT(F6.2)
611   CONTINUE
      WRITE(ND1,604)
604   FORMAT('  METERS')
      WRITE(1,1001)
      CALL IPCH(1,K)
      IF(ND-2)1,1,501
C      PRINT OUTPUT DATA
501   CALL NEWPAGE(ND1)
      CALL PTEXT(ND1,24,5)
      WRITE(ND,601)
      CALL OUTSTRING(ND,IGUF,2,48)
      WRITE(ND,602)NTEST,NTAPE,NFREQ,IFBAND,RESOL,ALIAS
      WRITE(5,506)
      Y=0
      D=2.0*SDSP/ALANDA
506   FORMAT(5X,'LOCATION',5X,'SOURCE LEVEL',5X,'INTEGRATED LEVEL')
      DO 507 J=2,128
      X=ALIMU+FLOAT(J-1)*(ALT/128.0)
      Y=Y+(B(J)+B(J-1))/D
      WRITE(5,508)X,B(J),Y
507   CONTINUE
508   FORMAT(5X,F7.3,7X,F7.3,13X,F7.3)
      GO TO 1
      END
      SUBROUTINE ANFILE(L,NAME)
      DIMENSION NAME(4)
10    IH=1
      IF(L-'R')2,3,2
3     WRITE(1,4)
      GO TO 5
2     WRITE(1,6)
5     WRITE(1,7)NAME
4     FORMAT(/,'READ')
6     FORMAT(/,'WRITE')
7     FORMAT('FILE CALLED  ',4A1,'  ON HANDLER 1')
      ASSIGN 9999 TO LAB
      CALL ERTRAP(IEMESS,LAB)
      WRITE(0,1)L,IH,NAME
1     FORMAT(A1,I1,4A1,'D')
      RETURN
9999  WRITE(1,9996)
9996  FORMAT('STICK IN ANOTHER DISK',/,'TYPE SPACE TO CONTINUE')
      CALL IPCH(1,ICH)
      IF(ICH-' ')9998,10,9998
9998  CALL EXIT
      END
      SUBROUTINE FILEOP(L)
      DIMENSION NAME(4)
      WRITE(1,1)
1     FORMAT('TYPE IN 3 CHARACTER TEST NAME')
      IF (L-'R')10,11,10
11    WRITE (1,2)
2     FORMAT('TO BE READ')
      GO TO 20
```

```
10      WRITE (1,3)
3       FORMAT('TO BE WRITTEN')
20      READ(1,4)(NAME(J),J=1,3)
        WRITE(1,8)
8       FORMAT(/,'TAKE NO=')
        READ(1,7)IT
        NAME(4)=IT
        WRITE(1,6)
6       FORMAT(/,'  HANDLER NO. =')
        READ(1,7)IH
7       FORMAT(I3)
4       FORMAT(3A1)
        WRITE (0,5)L,IH,NAME
5       FORMAT(A1,I1,4A1,'D')
        RETURN
        END
C
        SUBROUTINE RDATA(MICNO,IT,NTAKE,INFREQ,X,Y,Z)
C       EXTRACTS DATA VALUES X,Y FROM CORRECT FILE FOR FREQ.
C       LOCATION INFREQ, AND MIC. NO.   MICNO;
C       IT=NUMBER OF CALLS TO ROUTINE+1
C       NTAKE=NO. OF FILES IN NAME
        COMMON IBUF(8192),A(128),B(128),IBR(128),IBI(128),ISIN(128),
       1NAME(4),RES(32),
       2IGUF(50),NTEST(2),NTAPE,COND,PRIVEL,
       3PRIDIA,TEMP,WINDVE,WINDDI,PRAD,
       4NMIC,NSUB,NSMIC(5),DEL(5),TDCAL(32),REFANG,MICSUB(5,15),
       5AFREQ,IFBAND,IBT,SRATE,ITL,ISAMP,
       6SAMP,NCHAN,NGULP,NOMIC(8),NORUN,NOSUB,ICHAN,NOSPAR(4)
C
        NTIME=NAME(4)-26
        IF(IT-1)5,5,6
5       NTIME=1
7       NAME(4)=NTIME+26
        CALL ANFILE('R',NAME)
        CALL RBDISK(IGUF)
        READ(4)IBUF
6       DO 1 I1=1,NCHAN
        IF(NOMIC(I1)-MICNO)1,2,1
1       CONTINUE
        NTIME=NTIME+1
        IF(NTIME-NTAKE)7,7,8
8       WRITE(1,3)
        CALL EXIT
3       FORMAT('DATA NOT AVAILABLE')
2       ITL2=ITL/2
        LOC=ITL2*(I1-1)+INFREQ
        X=FLOAT(IBUF(LOC))/32000.0
        Y=FLOAT(IBUF(LOC+1024))/32000.0
        Z=FLOAT(IBUF(LOC+2048))/32000.0
        RETURN
        END
        SUBROUTINE RBDISK(IG)
        DIMENSION IG(300)
        READ(4)IG
        RETURN
        END
        SUBROUTINE WBDISK(IG)
        DIMENSION IG(300)
        WRITE (4)IG
```

```
      RETURN
      END
      SUBROUTINE SGPLOT(NG,IY,NP,INC,IX0,NG1,ND)
      DIMENSION IY(128)
C      PLOTS UP TO 128 POINTS AT EQUAL INCREMENTS
C     NG= NUMBER OF GRAPHS PER PAGE
C     IY()=DATA
C     NP=NUMBER OF POINTS
C     INC=NUMBER OF DIVISONS ON X-AXIS
C     IX0=LOCATION OF ORIGIN
C     NG1=GRAPH NUMBER
C     ND=1,2 FOR SCREEN...5,6 FOR PLOTTER
C
      IXX=IFIX(48000.0*(FLOAT(IX0)/FLOAT(NP))-24000.0)
      Y0=FLOAT(2*NG1-1)/FLOAT(NG)-1.0
      IY0=-IFIX(32000.0*Y0)
      IYMAX=IY0+16000/NG
      IY0=IY0-16000/NG
      IC=24000/(NP)
      IP=24000/INC
C     PLOT X-AXIS
      CALL PICTURE(ND,0,-24000,IY0)
      CALL PICTURE(ND,1,24000,IY0)
C      MARK DIVISIONS ON X-AXIS
      DO 103 J=1,INC
      IX=12000-J*IP
      IX=IX*2
103   CALL PICTURE(ND,'+',IX,IY0)
C     PLOT Y-AXIS
      CALL PICTURE(ND,0,IXX,IYMAX)
      CALL PICTURE(ND,1,IXX,IY0)
      IY1=IFIX(FLOAT(IY(1))/FLOAT(NG))+IY0
      CALL PICTURE(ND,0,-24000,IY1)
      CALL PICTURE(ND,4,-24000,IY1)
      DO 104 J=2,NP
      IX=(2*J-NP)*IC
      IY1=IFIX(FLOAT(IY(J))/FLOAT(NG))+IY0
104   CALL PICTURE(ND,1,IX,IY1)
      CALL PICTURE(ND,3,IX,IY1)
      RETURN
      END
```

Computer Programme A2 CALI

```
C       MASTER X0CAL
C
C       POLAR CORRELATION PARAMETER SETTING PROG,
C      VERSION 1 - S.G. 2/6/77
C
       COMMON IGUF(50),NTEST(2),NTAPE,COND,PRIVEL,
      1PRIDIA,TEMP,WINDVE,WINDDI,PRAD,
      2NMIC,NSUB,NSMIC(5),DEL(5),TDCAL(32),REFANG,MICSUB(5,15),
      3AFREQ,IFBAND,IBT,SRATE,ITL,ISAMP,
      4SAMP,NCHAN,NGULP,NOMIC(8),NORUN,NOSUB,ICHAN,NOSPAR(4)
C
       CALL PLOT(-1,0,0)
       WRITE(1,10)
10     FORMAT('PARAMETER SETTING PROGRAM FOR POLAR CORRELATION',
      11//,'VERSION ONE, STANDARD MICROPHONE ARRAY',//,
      2'INITIAL SET UP? (Y OR N)')
       READ(1,11)INIT
11     FORMAT (A1)
       CALL MATCH(INIT,'Y',INIT)
       GO TO (100,1),INIT
C
C      WRITE OUT ALL CONSTANTS.
C
100    CALL PLOT(-1,0,0)
       WRITE (1,12)NTEST,NTAPE
12     FORMAT(/,'1)TEST IDENTIFICATION',//,'TEST NO =',2A2,
      1/,'TAPE NO =',I5,/,'TEST DESCRIPTION =',/)
       CALL OUTSTRING (1,IGUF,0,50)
       WRITE(1,13)WINDVE,WINDDI,PRAD
13     FORMAT(/,'2)WIND SPEED DATA',//,'WIND SPEED ='
      1,F5.1,' METERS/SEC',/,'WIND DIRECTION RE AXIS =',F5.1,
      2' DEGREES',/,'POLAR ARC RADIUS =',F5.1,' METERS')
C
       REFANG=90.0-REFANG
       WRITE(1,300)
300    FORMAT(///,'TYPE SPACE FOR NEXT PAGE')
       CALL IPCH(1,J)
       CALL PLOT(-1,0,0)
       WRITE(1,14)NMIC,NSUB,REFANG
14     FORMAT(/,'3)MICROPHONE ARRAY CALIBRATION',//,
      1'NO OF MICROPHONES=',I2,/,'NO OF SUB-ARRAYS='
      2,I1,/,'ANGLE OF REFERENCE MICROPHONE RE JET AXIS='
      3,F5.1,' DEGREES')
       REFANG=90.0-REFANG
       WRITE(1,15)
15     FORMAT(/,'NO OF MICS IN SUB-ARRAYS AND ANGULAR',/,
      1'SEPARATIONS IN SINE (ALPHA)',//,
      2'SUB-ARRAY ',10X,' NO OF MICS ',10X,' ANG. SEP.',/)
       DO 200 I=1,NSUB
200    WRITE(1,16)I,NSMIC(I),DEL(I)
16     FORMAT(4X,I1,19X,I2,17X,F7.5)
       WRITE(1,45)(I,I=1,NSUB)
45     FORMAT(/,'MICROPHONE IDENTIFICATION TABLE',/,
      1'  GIVES MIC. IDENTS. IN EACH SUB-ARRAY',//,
      23X,'SUBARRAY NO.',5(9X,I1))
       WRITE(1,46)
46     FORMAT(/,3X,'SUBARRAY',/,3X,'LOCATION')
       DO 48 I=1,15
48     WRITE(1,47)I,(MICSUB(J,I),J=1,NSUB)
47     FORMAT(9X,I2,5X,5(8X,I2))
```

```
      WRITE(1,300)
      CALL IPCH(1,J)
      CALL PLOT(-1,0,0)
      WRITE(1,17)
17    FORMAT(/,'4)TIME DELAY CALIBRATION FOR EACH MIC',
     1' IN MICROSECS',/,'MIC NO    TIME DELAY')
      DO 201 I=1,NMIC
201   WRITE(1,18)I,TDCAL(I)
18    FORMAT(2X,I2,6X,F10.1)
      WRITE(1,300)
      CALL IPCH(1,J)
      CALL PLOT(-1,0,0)
      WRITE(1,19)AFREQ,IFBAND,IBT,ITL,SAMP
19    FORMAT(/,'5)DATA ANALYSIS CONSTANTS',//,'MAXIMUM FREQ='
     1,F9.1,/,'BANDWIDTH=',I5,/,'NO OF DEGREES OF ',
     2'FREEDOM=',I4,/,'TRANSFORM LENGTH=',I3,
     3/,'NO. OF SAMPLES PER CHANNEL=',F10.1)
      WRITE(1,20)NCHAN,(NOMIC(I),I=1,NCHAN)
20    FORMAT(/,'6)INPUT DATA DEFINITION',//,
     1'NO OF CHANNELS TO BE ACQUIRED =',I2,/,
     3'MICROPHONE IDENTIFIICATION NUMBERS ARE:',/,10(3X,I2))
      TIME=3.0*SAMP/FLOAT(NGULP)
      WRITE(1,40)TIME
40    FORMAT ('THIS WILL TAKE APPROXIMATELY',F10.4,/,
     1'SECONDS TO ACQUIRE DATA ONTO DISK')
      WRITE (1,21)
21    FORMAT (///,'TO CHANGE A PARAMETER, TYPE THE',
     1' CORRESPONDING CHOICE NUMBER',/,
     2'TYPE 0 TO PROCEED WITH COMPUTATION',/,'CHOICE=')
      READ (1,22)II
22    FORMAT (I1)
      INIT=1
      II=II+1
      GO TO (99,1,2,3,4,5,6),II
C
1     WRITE (1,23)
23    FORMAT ('1)TEST DESCRIPTION',//,'TYPE TEST NUMBER(4 CHAR)=')
500   FORMAT('     TAPE NUMBER=')
      READ(1,516)NTEST
516   FORMAT(2A2)
      WRITE(1,500)
      READ(1,24)NTAPE
24    FORMAT (I5)
      WRITE (1,25)
25    FORMAT ('TYPE PLACE, DATE, NATURE OF TEST ETC (46 CHAR)')
      IGUF(1)=:8DA0
      CALL RECIN(1,IGUF,2,48,I)
      GO TO (100,2),INIT
C
2     WRITE (1,26)
26    FORMAT ('2)WIND SPEED DATA',//,
     1'TYPE WIND SPEED IN METERS/SEC=')
501   FORMAT(/,' WIND DIRECTION RE-AXIS (DEGREES)=')
502   FORMAT(/,' POLAR ARC RADIUS (METERS)=')
      READ (1,27)WINDVE
      WRITE(1,501)
      READ(1,27)WINDDI
      WRITE(1,502)
      READ(1,27)PRAD
27    FORMAT (F10.0)
```

```
                G
       O TO (100,3),INIT
C
3      CALL PLOT(-1,0,0)
       WRITE (1,28)
28     FORMAT (///,'3) MICROPHONE ARRAY CALIBRATION',//,
      1'NO. OF MICROPHONES(<32)=')
503    FORMAT(/,' NO. OF SUB-ARRAYS(<=5)=')
504    FORMAT(/,'ANGLE OF REF. MICROPHONE RE JET AXIS (DEGREES)=')
       READ (1,24)NMIC
       WRITE(1,503)
       READ(1,24)NSUB
       WRITE(1,504)
       READ(1,27)REFANG
       REFANG=90.0-REFANG
       WRITE (1,505)
505    FORMAT(/,'TYPE IN NO OF MICS IN SUB-ARRAYS(<=15) AND ANGULAR',/,
      1'SEPARATIONS IN SINE (ALPHA)')
       DO 203 I=1,NSUB
       WRITE (1,30)I
30     FORMAT (/,'DATA FOR SUB ARRAY NO ',I2,/,'NO. OF MICS=')
       READ (1,24)NSMIC(I)
       WRITE(1,506)
203    READ(1,27)DEL(I)
506    FORMAT(/,'ANGULAR SEPARATION=')
       WRITE(1,507)
507    FORMAT(//,'DEFINE MICROPHONE IDENT. NUMBERS IN ',/,
      1'EACH SUBARRAY')
       DO 509 I=1,NSUB
       WRITE(1,508)I
508    FORMAT(/,'TYPE IN MICROPHONES FOR SUB-ARRAY NO.',I2)
       NN=NSMIC(I)
       DO 509 J=1,NN
       WRITE(1,510)J
510    FORMAT(/,'MICROPHONE IDENT. NO.  AT SUB LOCATION',
      1I2,'=')
       READ(1,24)MICSUB(I,J)
509    CONTINUE
       GO TO (100,4),INIT
C
4      CALL PLOT(-1,0,0)
       WRITE (1,17)
       DO 204 I=1,NMIC
       WRITE (1,514)I
514    FORMAT(/,2X,I2,10X,'=')
204    READ (1,27)TDCAL(I)
       GO TO (100,5),INIT
C
5      CALL PLOT(-1,0,0)
       WRITE (1,33)
33     FORMAT (///,'5)DATA ANALYSIS CONSTANTS',//,
      1'TYPE MAXIMUM FREQUENCY REQUIRED( >1000.0HZ)=')
511    FORMAT(/,' FREQUENCY BANDWIDTH=')
512    FORMAT(/,'NO. OF DEGREES OF FREEDOM=')
       READ (1,27)AFREQ
       WRITE(1,511)
       READ(1,24)IFBAND
       WRITE(1,512)
       READ(1,24)IBT
       I1=IFIX(2.5*AFREQ/2500.0)
       CALL IPWR2(I1,1000,1,ISAMP)
```

```
      SRATE=FLOAT(I1)*2500.0
      AFREQ=SRATE/2.5
      ITL=IFIX(SRATE/FLOAT(IFBAND))
      CALL IPWR2(ITL,256,16,I2)
      IFBAND=IFIX(SRATE/FLOAT(ITL))
126   SAMP=FLOAT(ITL)*FLOAT((IBT+1)/2)
      GO TO (100,6),INIT
C
6     WRITE(1,36)
36    FORMAT(///,'6)INPUT DATA DEFINITION',//,
     1'TYPE NUMBER OF CHANNELS TO BE ACQUIRED=')
      READ(1,24)NCHAN
      IF(NCHAN-8)42,42,6
42    WRITE(1,38)
38    FORMAT(/,'MICROPHONE IDENTIFICATION NUMBERS FOR EACH CHANNEL')
      DO 205 I=1,NCHAN
      WRITE(1,513)I
513   FORMAT(/,'CHANNEL NO. ',I2,'=')
205   READ(1,24)NOMIC(I)
      I2=1
      I1=NCHAN
      CALL IPWR2(I1,8,1,ICHAN)
127   NGULP=32767/(2**ICHAN)
      GO TO 100
C
99    WRITE(0,41)
41    FORMAT('X0POCO')
      STOP
      END
      SUBROUTINE IPWR2(I22,IMAX,ISTART,ILOG)
      I11=I22
      ILOG=0
      I22=ISTART
3     IF(I11-I22)1,1,2
2     I22=I22*2
      ILOG=ILOG+1
      IF(I22-IMAX)3,1,1
1     RETURN
      END
```

Computer Programme A3 PLOG

```
C      TELESCOPE PROGRAM - POLAR CORRELATION SUITE
C      PLOG 25/5/77        16K    GULP
C      LOGS A NUMBER OF MICROPHONE CHANNELS TO DISK
C      DATA IS IN DESCENDING ORDER AS INPUT FROM ADC
C      AND NEEDS UNPACKING BY 'FISH'
C
       COMMON IBUF(16384),
C    THE FOLLOWING VARIABLES LIVE AT THE TOP OF COMMON
      1 IGUF(50),NTEST(2),NTAPE,COND,PRIVEL,
      2 PRIDIA,TEMP,WINDVE,WINDDI,PRAD,
      3 NMIC,NSUB,NSMIC(5),DEL(5),TDCAL(32),REFANG,MICSUB(5,15),
      4 AFREQ,IFBAND,IBT,SRATE,ITL,ISAMP,
      5 SAMP,NCHAN,NGULP,NOMIC(8),NORUN,NOSUB,ICHAN,NOSPAR(4)
C
       CALL PLOT(-1,0,0)
1      WRITE (1,100)
100    FORMAT ('POLAR CORRELATION  DATA LOGGING PROGRAM-VERSION 1 ',
      1/,'  23/5/77        16K    GULP')
C      LOG DATA TO DISK
204    CALL FILEOP('W',IT)
       NORUN=IT
       CALL WBDISK(IGUF)
C      ISAMP =SPEED CODE    SRATE=2500*2**ISAMP
C      SRATE=SAMPLE RATE ON EACH CHANNEL
C      NCHAN=NO. OF CHANNELS TO BE AQUIRED
C      NGULP=NO. OFF SAMPLES /CHAN/GULP OF  16384
C      SAMP=NO. OF SAMPLES REQUIRED/CHAN
       ICI=2**ICHAN
       WRITE(1,101)ICI
101    FORMAT('NUMBER OF CHANNELS BEING LOGGED=',I2,
      1//,'ENSURE STORE HAS BEEN CALIRATED WITH CORRECT CHANNEL NOS',///
       WRITE(1,201)
201    FORMAT('  INPUT SIGNALS WILL BE PRESENTED ON THE SCREEN',//,
      1'TYPE CHARACTERS  A,B,C,D,....TO VIEW EACH CHANNEL',/,
      2'TYPE SPACE TO CONTINUE')
       CALL IPCH(1,J)
       CALL ADCV(ISAMP,ICH)
       IF(ICH-' ')1,216,1
216    N=0
       ICHA=ICHAN-1
212    CALL ADCU(IBUF,16384,ICHA,ISAMP)
211    WRITE(4)IBUF
       N=N+NGULP
       WRITE(1,221)N
221    FORMAT(/,'NO. OF SAMPLES LOGGED =',I5)
       IF(IFIX(SAMP)-N)215,215,212
215    ENDFILE 4
       WRITE(0,220)
220    FORMAT('X0POCO')
       END
C
       SUBROUTINE FILEOP(L,IT)
       DIMENSION NAME(4)
       WRITE(1,1)
1      FORMAT('TYPE IN 3 CHARACTER TEST NAME')
       IF (L-'R')10,11,10
11     WRITE (1,2)
2      FORMAT('TO BE READ')
       GO TO 20
10     WRITE (1,3)
```

```
3       FORMAT('TO BE WRITTEN')
20      READ(1,4)(NAME(J),J=1,3)
        WRITE(1,8)
8       FORMAT(/,'TAKE NO=')
        READ(1,7)IT
        NAME(4)=IT
        WRITE(1,6)
6       FORMAT(/,'HANDLER NO. =')
        READ(1,7)IH
7       FORMAT(I3)
4       FORMAT(3A1)
        WRITE (0,5)L,IH,NAME
5       FORMAT(A1,I1,4A1,'D')
        RETURN
        END
C
        SUBROUTINE RBDISK(IG)
        DIMENSION IG(300)
        READ(4)IG
        RETURN
        END
        SUBROUTINE WBDISK(IG)
        DIMENSION IG(300)
        WRITE (4)IG
        RETURN
        END
```

Computer Programme A4 PANA

```
C      TELESCOPE PROGRAM - POLAR CORRELATION SUITE
C      MASTER XØPANA 2/6/77
C      THIS PROG ANALYSES POLAR CORRELATION DATA
C      DATA INPUT FROM FILE CREATED BY PLOG
C      FOR MICROPHONES DEFINED IN NOMIC(   )
C      OUTPUT THE COHERENCE(COMPLEX) BETWEEN THESE
C      MICROPHONES AND REFERENCE
C
       COMMON IBUF(8192),CSDR(1Ø24),CSDI(1Ø24),PSD(1Ø24),DUM(128),
      1IA(256),IB(256),IC(256),ID(256),NAME(4),ISIN(256),
      3IGUF(5Ø),NTEST(2),NTAPE,COND,PRIVEL,
      4PRIDIA,TEMP,WINDVE,WINDDI,PRAD,
      5NMIC,NSUB,NSMIC(5),DEL(5),TDCAL(32),REFANG,MICSUB(5,15),
      6AFREQ,IFBAND,IBT,SRATE,ITL,ISAMP,
      7SAMP,NCHAN,NGULP,NOMIC(8),NORUN,NOSUB,ICHAN,NOSPAR(4)
C
       CALL PLOT(-1,Ø,Ø)
1      WRITE (1,1ØØ)
1ØØ    FORMAT ('POLAR CORRELATION PROGRAM VERSION 1',//,
      1'DATA ANALYSIS PROGRAM  -DEFINES COHERENCE AND PHASE')
C
C
C
C      NAME FILES
C
3ØØ    WRITE(1,35Ø)
35Ø    FORMAT('READ IN 3 CHARACTER TEST NAME TO BE ANALYSED',/)
       READ(1,1Ø4)(NAME(I),I=1,3)
1Ø4    FORMAT(3A1)
       WRITE(1,2Ø4)
2Ø4    FORMAT('READ IN NO. OF FILES TO BE ANALYSED')
       READ(1,3Ø1)NF
3Ø1    FORMAT(I5)
C
C      DATA ANALYSIS
C
3Ø9    DO 349 N1=1,NF
C      OPEN I/P FILE NO N1
       NAME(4)=N1
       CALL ANFILE('R',NAME)
       CALL RBDISK(IGUF)
C
C      ICSDR=REAL PPART OF CSD
C      ICSDI=IMAG PART OF CSD
C      IPSD=P.S.D.
C      ITL=TRANNSFORM LENGTH
C      ITL2=HALF TRANSFORM LENGTH
C
C      ZERO SPECTRA ARRAYS
       IZERO=Ø
       I1Ø24=1Ø24
       CALL CONSTANT(CSDR,I1Ø24,Ø.Ø)
       CALL CONSTANT(CSDI,I1Ø24,Ø.Ø)
       CALL CONSTANT(PSD,I1Ø24,Ø.Ø)
       CALL CONSTANT(DUM,128,Ø.Ø)
C
C       CALCULATE SINE TABLE FOR TRANS
C
       LSIN=ITL/4
       DO 2Ø3 I=1,LSIN
```

```
      THETA=3.14159/FLOAT(2*LSIN)
203   ISIN(I)=IFIX(32767.9*SIN(FLOAT(I-1)*THETA))
C
      ITL2=ITL/2
CC    CALL SCROG(PSD,ITL2)
CC    CALL SCROG(CSDR,ITL2)
CC    CALL SCROG(CSDI,ITL2)
      NCH=2**ICHAN
      NSTEP=16384/NCH
      ANUM=FLOAT(NSTEP)
C
C     START GULP LOOP
C     NSTEP=NO. OF SAMPLES/CHAN/8192 WORD GULP
C     READ IN 16384 DATA SAMPLES FROM I/P FILE
      NDOS=(NSTEP-ITL2)/ITL
      NREAD=IFIX(SAMP/ANUM)
      DO 310 J1=1,NREAD
      READ(4)IBUF
C      ANALYSE EACH SECTION
      DO 310 J2=1,NDOS
      IFIRST=ITL*(J2-1)+1
      IF2=IFIRST+ITL2
C      ANALYSE EACH CHANNEL
      DO 310 N2=1,NCHAN
      ICS=(N2-1)*ITL2+1
C
C     READ INPUT DATA INTO WORK ARRAYS
C     IA,IB=WORK ARRAYS
C     IBUF=DATA ARRAY
C     N2=CHAN NO
C     NCH=TOTAL NO OF CHAN    (NCH=2**ICHAN)
C     IFIRST=FIRST SAMPLE OF SECTION
C     SUBROUTINE FISH EXTRACTS REQUIRED DATA FROM IBUF
C
      CALL FISH(IBUF,8192,NCH,N2,IFIRST,IA,ITL)
      CALL FISH(IBUF,8192,NCH,N2,IF2,IB,ITL)

C
C     TRANS=FFT ROUTINE  LENGTH=ITL,NO.OF HALVINGS=IHALVE
      CALL TRANS(IA,IB,ISIN,ITL,IHALVE)
      IXIX=32000/ITL
      IXIX=2*IXIX
CC    CALL SING(ISIN,ITL2,100,ICHY,IXIX)
CC    CALL SING(IA,ITL,100,ICHY,IXIX)
CC    CALL SING(IB,ITL,100,ICHY,IXIX)
      IH1=IHALVE
C
      IF (N2-1)316,316,317
C
C     MOVE IA & IB TO IC & ID FOR FIRST CHAN
      I1111=1
316   CALL MOVEDATA(IA,I1111,IC,I1111,ITL)
      CALL MOVEDATA(IB,I1111,ID,I1111,ITL)
C
CC    CALL SING(IC,ITL,100,ICHY,IXIX)
CC    CALL SING(ID,ITL,100,ICHY,IXIX)
C
      IG1=IHALVE
317   CALL CMULAD(IA,IB,IH1,IC,ID,IG1,CSDR(ICS),CSDI(ICS),ITL)
CC    CALL SCROG(CSDR(ICS),ITL2)
```

```
CC      CALL SCROG(CSDI(ICS),ITL2)
        CALL CMULAD(IA,IB,IH1,IA,IB,IH1,PSD(ICS),DUM,ITL)
CC      CALL SCROG(PSD(ICS),ITL2)
CC      CALL SCROG(DUM,ITL2)
310     CONTINUE
323     NT=NCHAN*ITL2
        AMAX=0.0
        DO 330 I=1,NT
        BMAX=ABS(PSD(I))
        IF(BMAX-AMAX)330,330,331
331     AMAX=BMAX
330     CONTINUE
CC      CALL SCROG(CSDR,NT)
CC      CALL SCROG(CSDI,NT)
CC      CALL SCROG(PSD,NT)
        N=0
        DO 320 I=1,NT
        N=N+1
        PSD(I)=PSD(I)/AMAX
        IF(N-ITL2)321,321,322
321     X=SQRT(PSD(I)*PSD(N))
        IF(X-0.1E-3)324,324,325
322     N=1
324     IBUF(I)=0
        IBUF(I+1024)=0
        IBUF(I+2048)=0
        GO TO 320
325     X1=CSDR(I)/(X*AMAX)
        X2=CSDI(I)/(X*AMAX)
        X3=PSD(I)
        IBUF(I+2048)=IFIX(32000.*X3)
        IBUF(I)=IFIX(32000.*X1)
        IBUF(I+1024)=IFIX(32000.*X2)
320     CONTINUE
        NAME(4)=NAME(4)+26
        CALL ANFILE('W',NAME)
        CALL WBDISK(IGUF)
        WRITE(4)IBUF
        ENDFILE 4
349     CONTINUE
        WRITE (0,400)
400     FORMAT('X0POCO')
        END
C
        SUBROUTINE SCROG(ARR,L)
        DIMENSION ARR(1024)
        IXI=64000./FLOAT(L)
        AMAX=0.00001
        DO 1 I=1,L
        A=ABS(ARR(I))
        IF(A-AMAX)1,1,2
 2      AMAX=A
 1      CONTINUE
        WRITE(1,4)AMAX
 4      FORMAT(E12.4)
        IPEN=0
        IX=-32000
        DO 3 I=1,L
        IY=32000.*ARR(I)/AMAX
        CALL PLOT(IPEN,IX,IY)
```

```
      IX=IX+IXI
 3    IPEN=1
      CALL IPCH(1,ICH)
      RETURN
      END
C
      SUBROUTINE ANFILE(L,NAME)
      DIMENSION NAME(4)
10    IH=1
      IF(L-'R')2,3,2
3     WRITE(1,4)
      GO TO 5
2     WRITE(1,6)
5     WRITE(1,7)NAME
4     FORMAT(/,'READ')
6     FORMAT(/,'WRITE')
7     FORMAT('FILE CALLED  ',4A1,'  ØN HANDLER 1')
      ASSIGN 9999 TO LAB
      CALL ERTRAP(IEMESS,LAB)
      WRITE(Ø,1)L,IH,NAME
1     FORMAT(A1,I1,4A1,'D')
      RETURN
9999  WRITE(1,9996)
9996  FORMAT('STICK IN ANOTHER DISK',/,'TYPE SPACE TO CONTINUE')
      CALL IPCH(1,ICH)
      IF(ICH-' ')9998,10,9998
9998  CALL EXIT
      END
C
      SUBROUTINE RBDISK(IG)
      DIMENSION IG(3ØØ)
      READ(4)IG
      RETURN
      END
      SUBROUTINE WBDISK(IG)
      DIMENSION IG(3ØØ)
      WRITE (4)IG
      RETURN
      END
```

Computer Programme A5 SPECTRA

```
C      MASTER SPECTRA 30/5/77
C     PLOTS CROSS SPECTRA (REAL AND IMAG.) WITH
C     MIC NO  1 FOR SPECIFIED MICROPHONES
       COMMON IBUF(8192),IA(128),IB(128),
      2IFREQ(18),RES(18,36),ALIAS(18),RESOL(18),
      3IGUF(50),NTEST(2),NTAPE,COND,PRIVEL,
      4PRIDIA,TEMP,WINDVE,WINDDI,PRAD,
      5NMIC,NSUB,NSMIC(5),DEL(5),TDCAL(32),REFANG,MICSUB(5,15),
      6AFREQ,IFBAND,IBT,SRATE,ITL,ISAMP,
      7SAMP,NCHAN,NGULP,NOMIC(8),NORUN,NOSUB,ICHAN,NOSPAR(4)
C
       CALL PLOT(-1,0,0)
191    CALL FILEOP('R')
       CALL RBDISK(IGUF)
       READ(4)IBUF
108    WRITE(1,419)
419    FORMAT('TYPE IN CHANNEL NO.')
       READ(1,103)N
103    FORMAT(I7)
       DO 100 I=1,NCHAN
       IF(NOMIC(I)-N)100,101,100
100    CONTINUE
       GO TO 1000
101    IMIC=I
       ITL2=ITL/2
       ISEC=ITL2*(IMIC-1)
       NT=NCHAN*ITL2
       I2=ISEC+1024
       I3=ISEC+2048
       DO 102 J=1,ITL2
       IA(J)=IBUF(I3+J)
       X=FLOAT(IBUF(ISEC+J))/32000.0
       Y=FLOAT(IBUF(I2+J))/32000.0
       Z=SQRT(X*X+Y*Y)
       IB(J)=IFIX(32000.0*Z)
102    CONTINUE
       NG=2
       INC=8
       IX0=0
       NG1=1
       ND=1
       CALL PLOT(-1,0,0)
       WRITE(1,106)N
106    FORMAT(/,15X,'POWER SPECTRAL DENSITY AND COHERENCE(AMPLITUDE
      1/,20X,'BETWEEN MIC. NO 1 AND MIC NO.  ',I2)
       CALL SGPLOT(NG,IA,ITL2,INC,IX0,NG1,ND)
       NG1=2
       CALL SGPLOT(NG,IB,ITL2,INC,IX0,NG1,ND)
1000   CALL PTEXT(ND,1,45)
       WRITE(1,107)
107    FORMAT('TYPE  0 TO EXIT,  1 TO RE-VIEW')
       READ(1,103)IYES
       IF(IYES)109,109,108
109    WRITE(0,110)
110    FORMAT('X0POCO')
       END
       SUBROUTINE SGPLOT(NG,IY,NP,INC,IX0,NG1,ND)
       DIMENSION IY(128)
C      PLOTS UP TO 128 POINTS AT EQUAL INCREMENTS
C     NG= NUMBER OF GRAPHS PER PAGE
```

```
C       IY()=DATA
C       NP=NUMBER OF POINTS
C       INC=NUMBER OF DIVISONS ON X-AXIS
C       IX0=LOCATION OF ORIGIN
C       NG1=GRAPH NUMBER
C       ND=1,2 FOR SCREEN...5,6 FOR PLOTTER
C
        IXX=IFIX(32000.0*(FLOAT(IX0)/FLOAT(NP)))-16000
        Y0=FLOAT(2*NG1-1)/FLOAT(NG)-1.0
        IY0=-IFIX(32000.0*Y0)
        IYMAX=IY0+16000/NG
        IY0=IY0-16000/NG
        IC=16000/(NP)
        IP=32000/INC
C       PLOT X-AXIS
        CALL PICTURE(ND,0,-16000,IY0)
        CALL PICTURE(ND,1,16000,IY0)
C        MARK DIVISIONS ON X-AXIS
        DO 103 J=1,INC
        IX=16000-J*IP
103     CALL PICTURE(ND,'+',IX,IY0)
C       PLOT Y-AXIS
        CALL PICTURE(ND,0,IXX,IYMAX)
        CALL PICTURE(ND,1,IXX,IY0)
        IY1=IFIX(FLOAT(IY(1))/FLOAT(NG))+IY0
        CALL PICTURE(ND,0,-16000,IY1)
        DO 104 J=2,NP
        IX=(2*J-NP)*IC
        IY1=IFIX(FLOAT(IY(J))/FLOAT(NG))+IY0
104     CALL PICTURE(ND,1,IX,IY1)
        RETURN
        END
        SUBROUTINE FILEOP(L)
        DIMENSION NAME(4)
        WRITE(1,1)
1       FORMAT('TYPE IN 3 CHARACTER TEST NAME')
        IF (L-'R')10,11,10
11      WRITE (1,2)
2       FORMAT('TO BE READ')
        GO TO 20
10      WRITE (1,3)
3       FORMAT('TO BE WRITTEN')
20      READ(1,4)(NAME(J),J=1,3)
        WRITE(1,8)
8       FORMAT(/,'TAKE NO=')
        READ(1,7)IT
        NAME(4)=IT+26
        WRITE(1,6)
6       FORMAT(/,'HANDLER NO. =')
        READ(1,7)IH
7       FORMAT(I3)
4       FORMAT(3A1)
        WRITE (0,5)L,IH,NAME
5       FORMAT(A1,I1,4A1,'D')
        RETURN
        END
C
        SUBROUTINE REDISK(IG)
        DIMENSION IG(300)
        READ(4)IG
```

```
RETURN
END
SUBROUTINE WBDISK(IG)
DIMENSION IG(300)
WRITE (4)IG
RETURN
END
```

FIG.1.1.

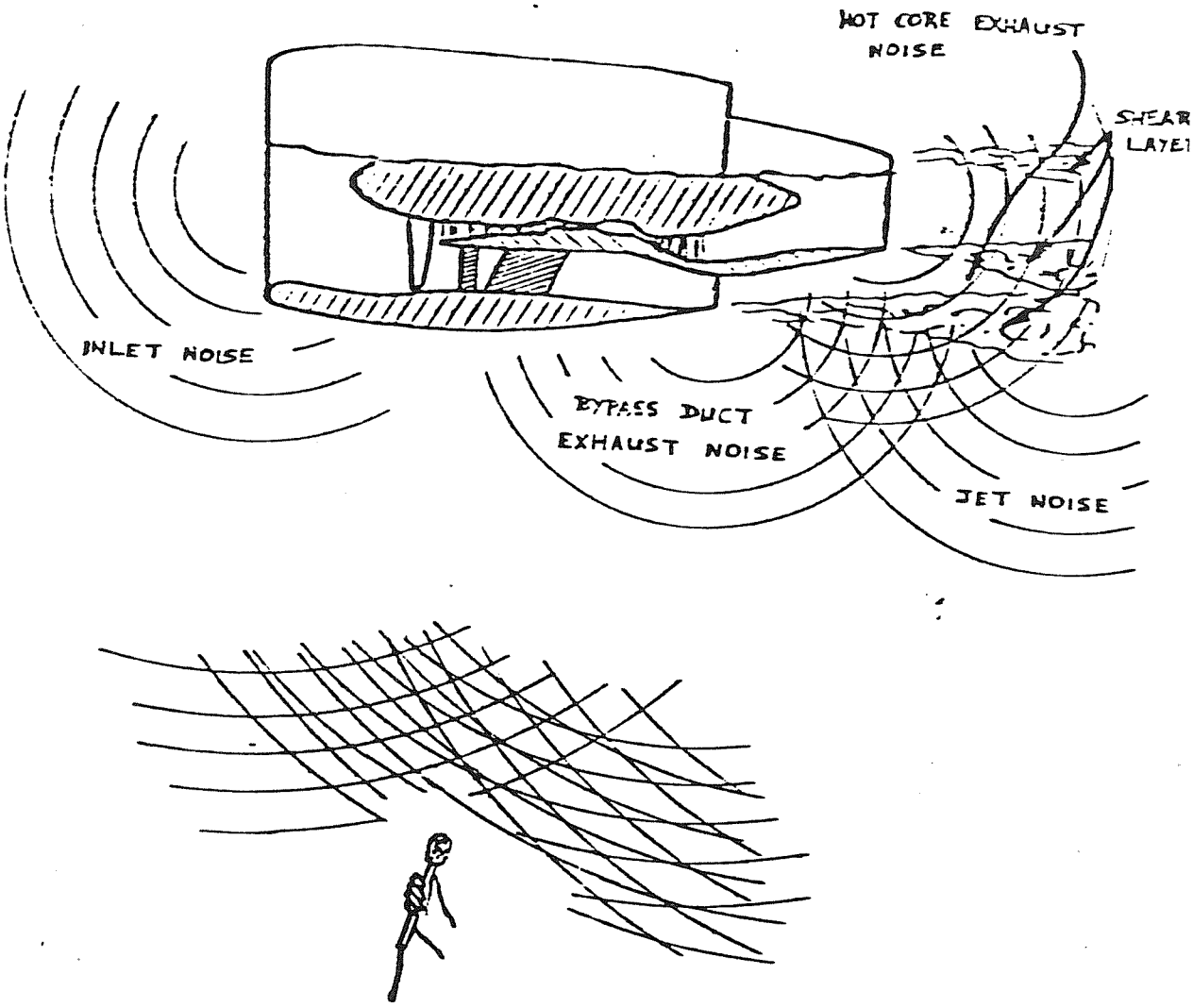

JET ENGINE NOISE SOURCES

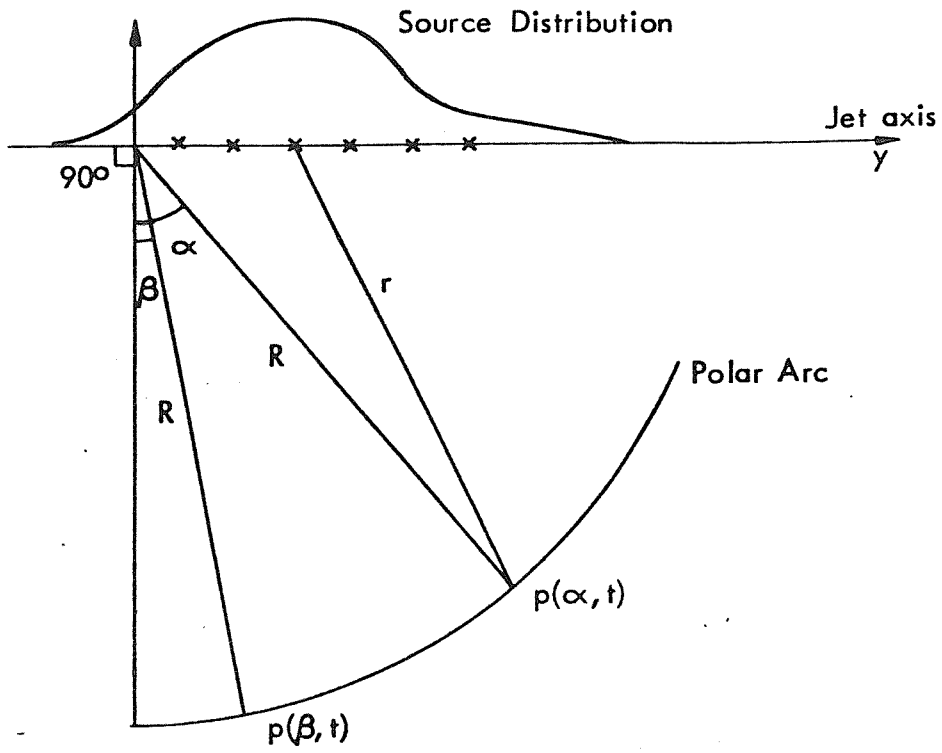

FIG. 2.1. THE PRINCIPLE OF THE WAVENUMBER SPECTRUM

FIG. 2.2.

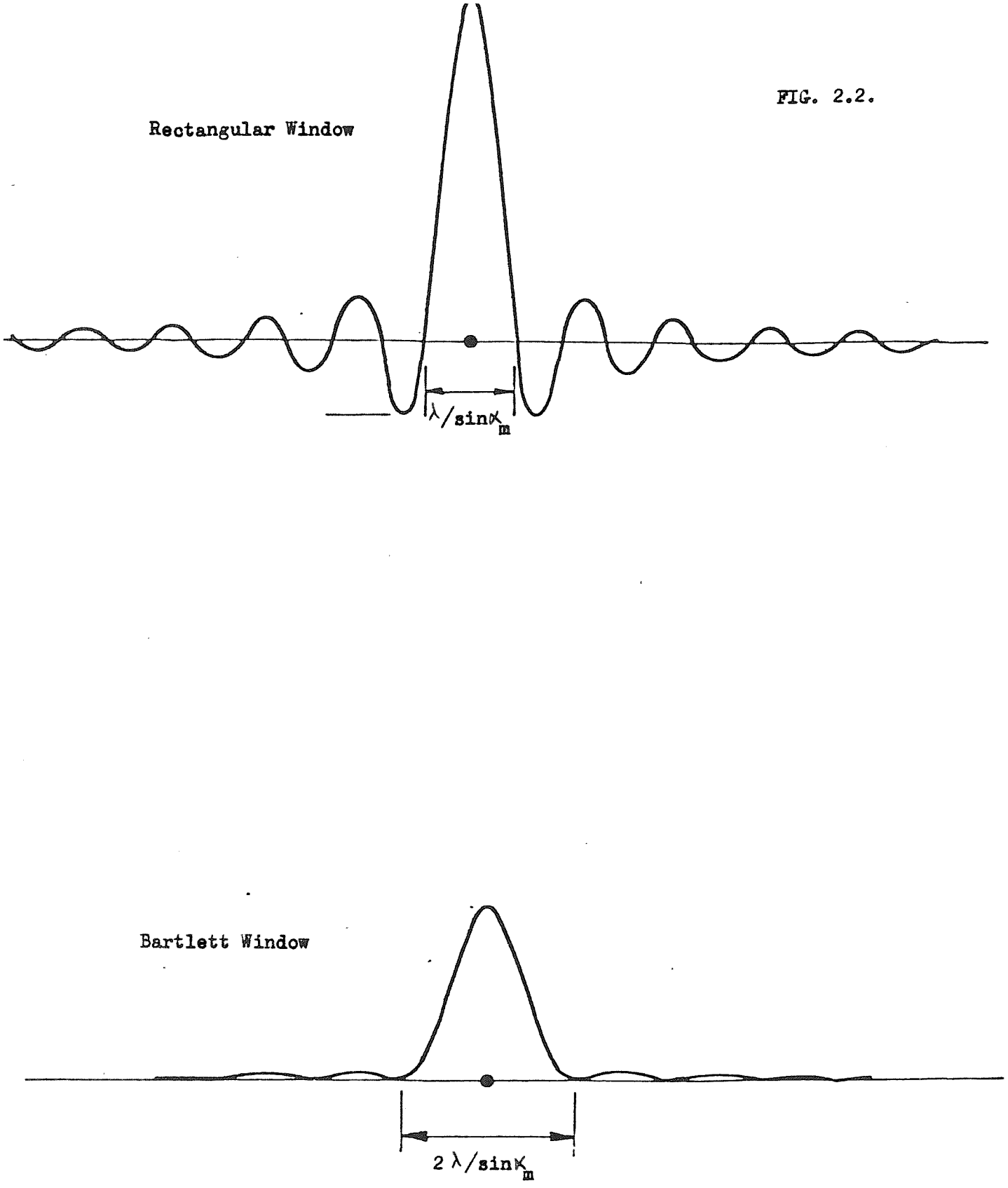

EXAMPLES OF WINDOW FUNCTIONS

FIG. 2.3.

Evaluation of the far field path length approximation for different values of error parameter ϕ

———	$\phi = 0$
—△—	$\phi = 0.392$
—+—	$\phi = 0.785$
—x—	$\phi = 1.13$

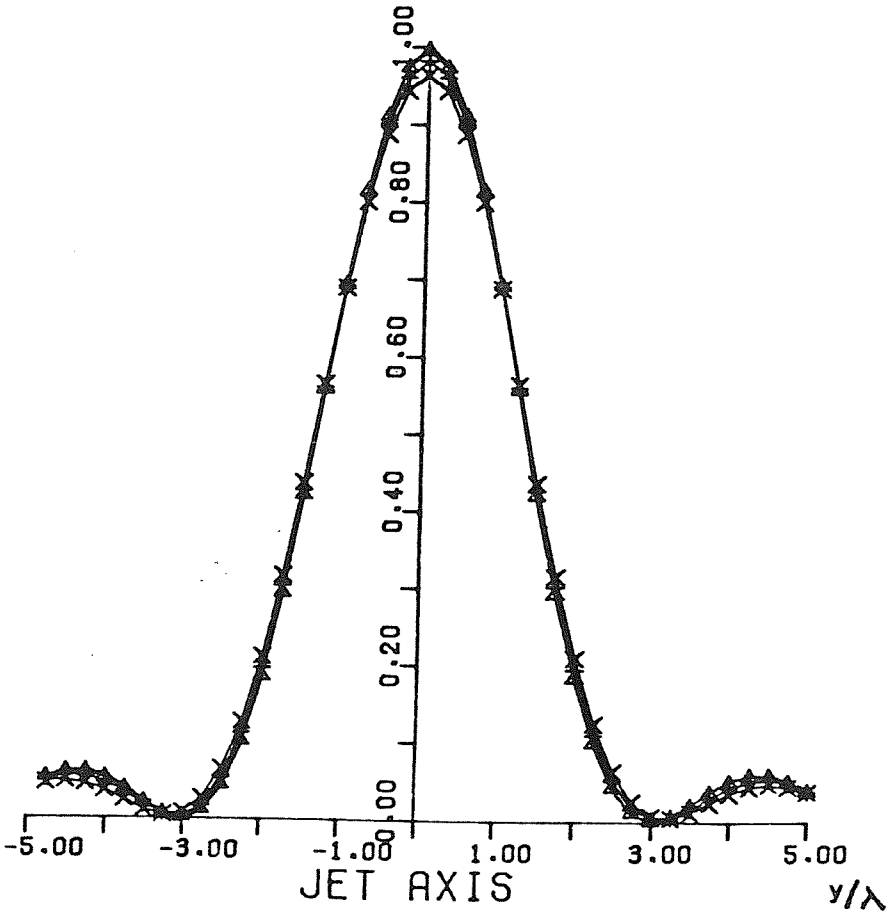

FIG. 2.4.

Evaluation of the far field path length approximation for different values of the error parameter ϕ

——— $\phi = 0$

—△— $\phi = 1.57$

—+— $\phi = 3.142$

—x— $\phi = 4.52$

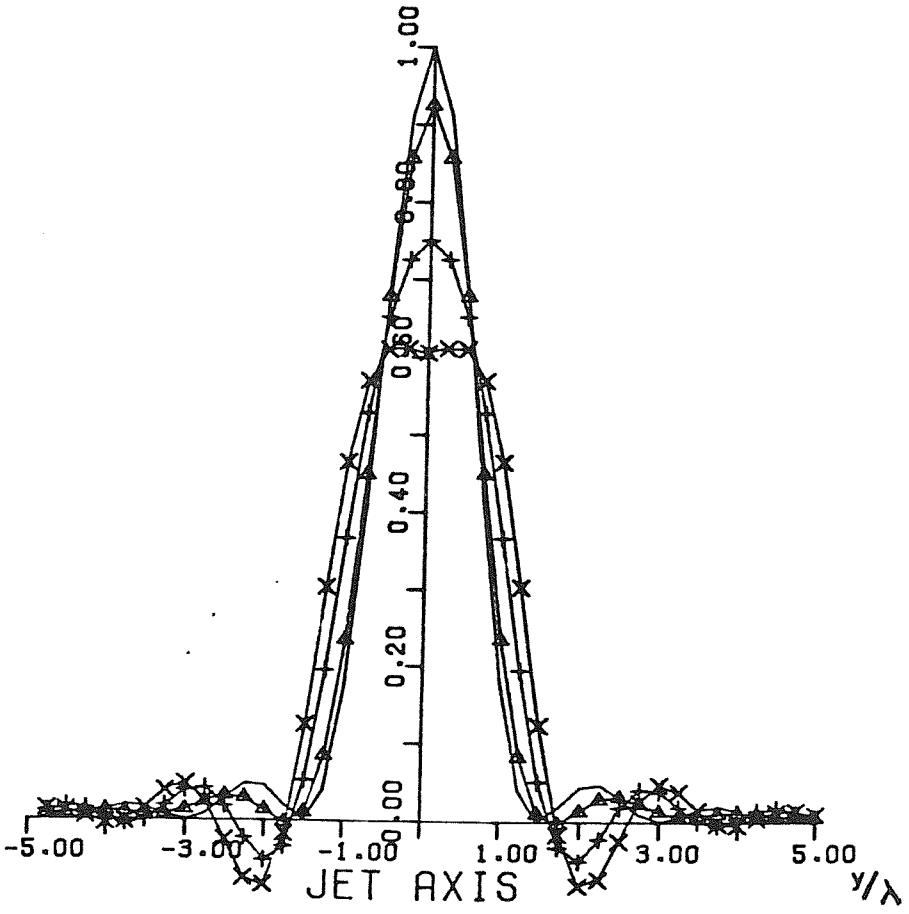

FIG. 2.5.

Evaluation of the far field path length approximation for different values of the error parameter ϕ

——— $\phi = 0$

—△— $\phi = 3.53$

—+— $\phi = 7.06$

—x— $\phi = 10.17$

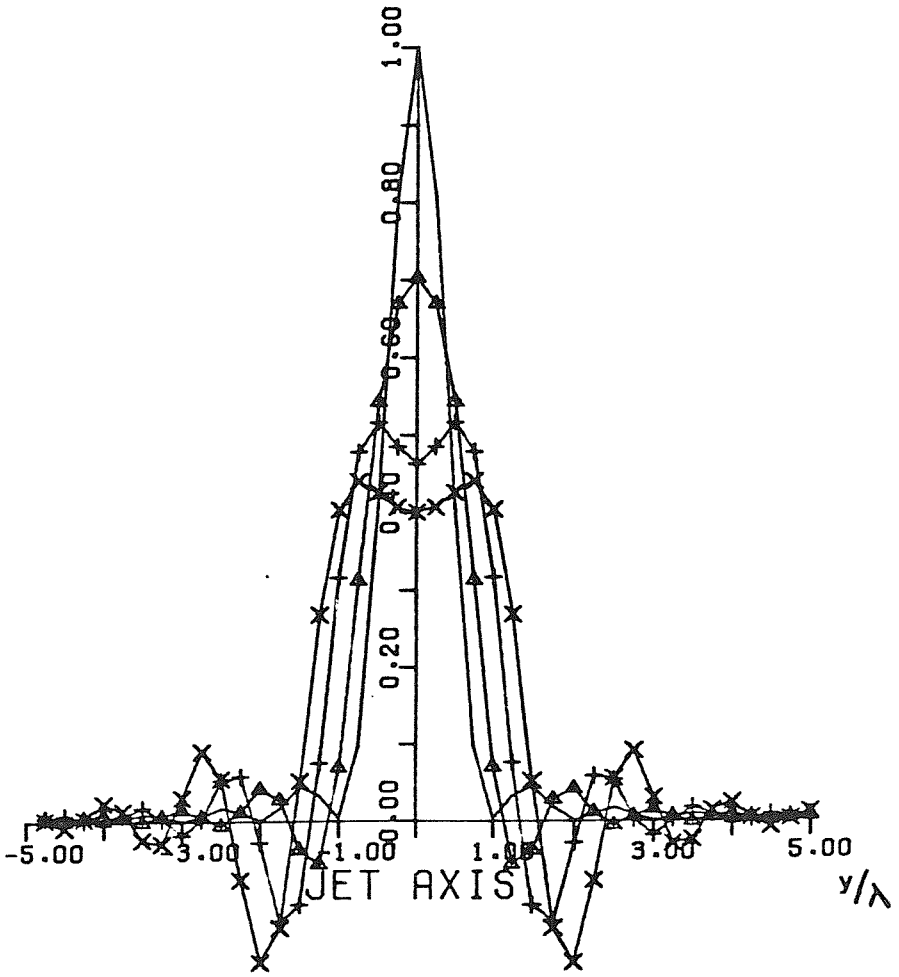

FIG. 2.6.

Source Images of an off axis source

$\alpha_m = 10^o$

——— $z/\lambda = 0$

—△— $z/\lambda = 5$

—+— $z/\lambda = 10$

—x— $z/\lambda = 15$

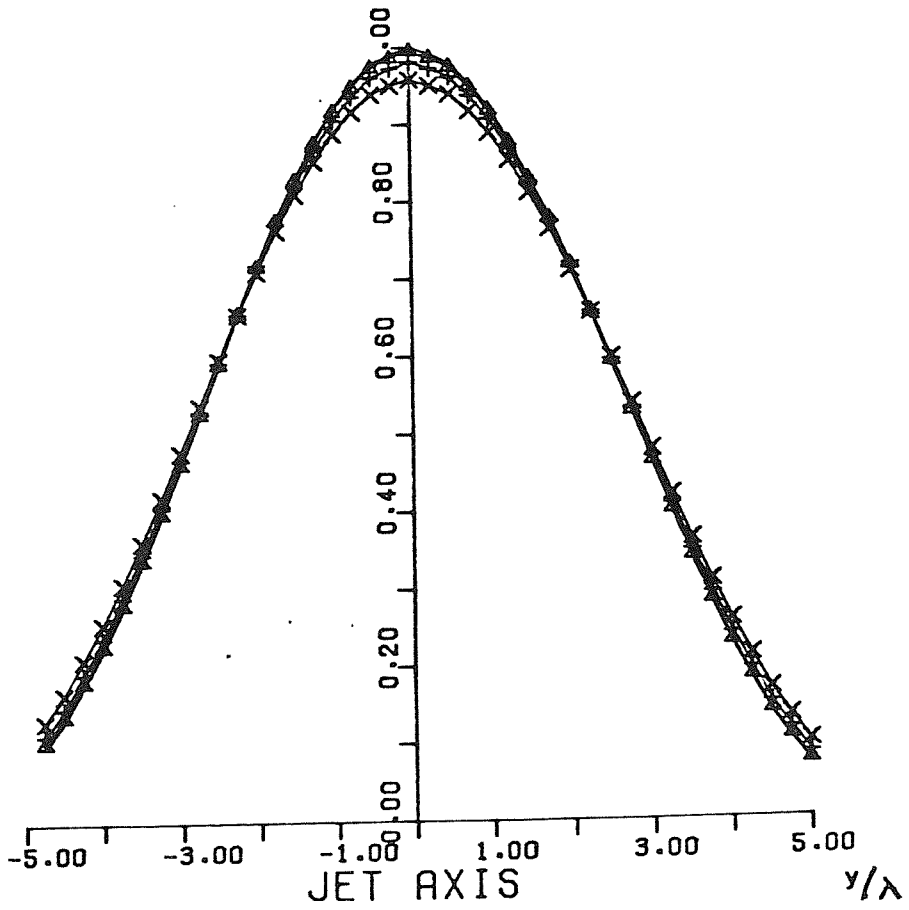

FIG. 2.7.

Source Images of an off axis source

$\alpha_m = 30^\circ$

——— $z/\lambda = 0$

—△— $z/\lambda = 5$

—+— $z/\lambda = 10$

—x— $z/\lambda = 15$

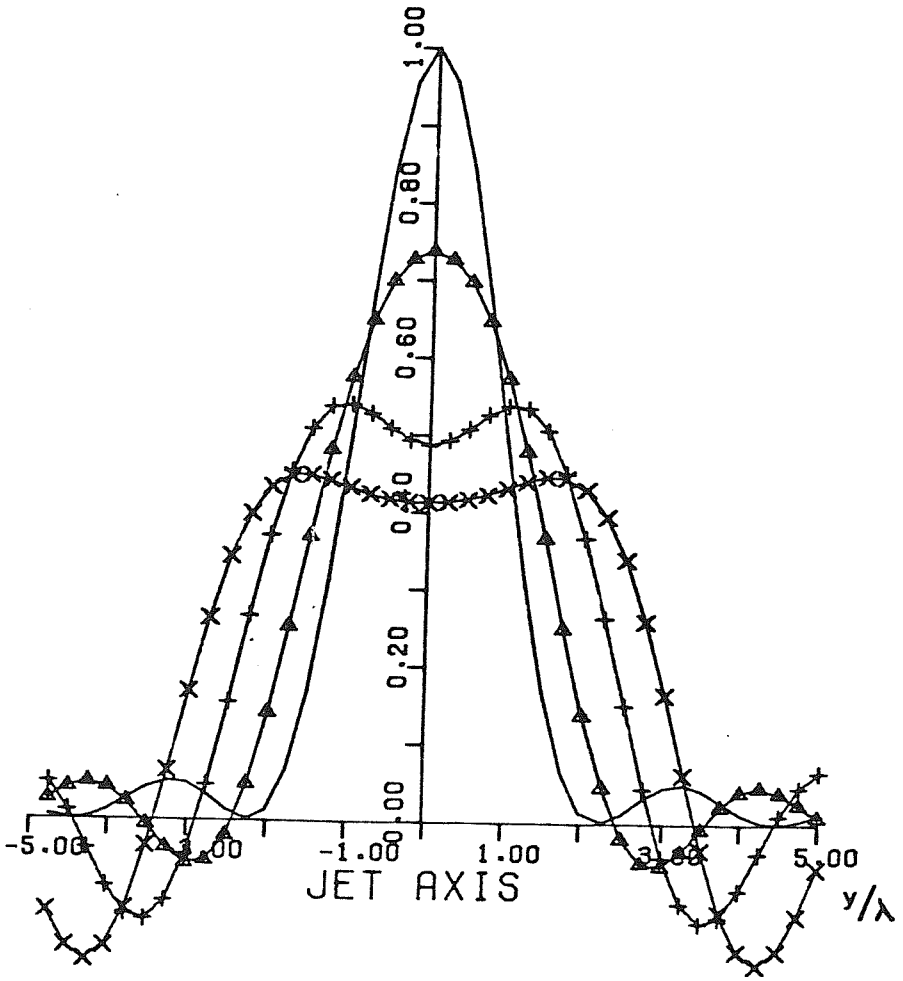

FIG. 2.8.

Source Images of an off axis source

$\alpha_m = 60^\circ$

——— $z/\lambda = 0$

—△— $z/\lambda = 5$

—+— $z/\lambda = 10$

—x— $z/\lambda = 15$

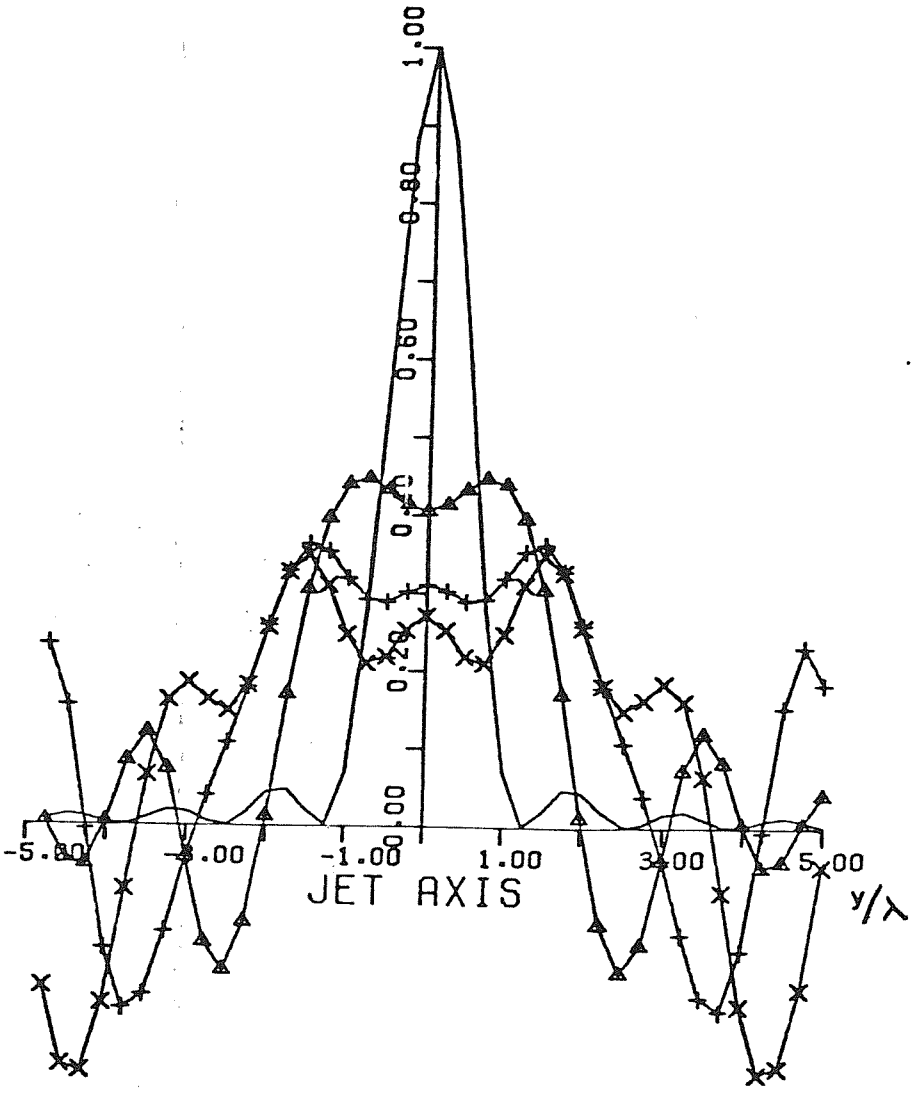

FIG. 2.9.

Source Image for omnidirectional source
in the presence of dominant jet noise

Jet noise directionality = $(1 - 0.7 \sin\alpha)^{-n}$

——— n = 1 $\alpha_m = 30^\circ$

△ n = 2

\+ n = 3

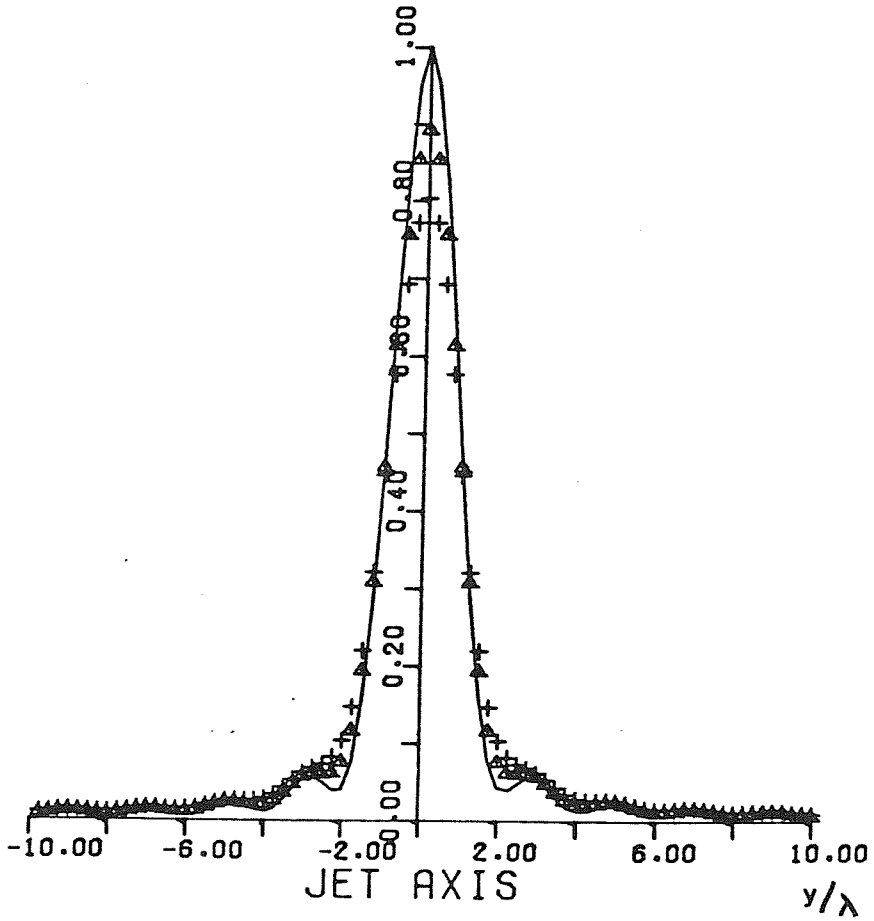

FIG. 2.10.

Source Image of omnidirectional point source in the presence of jet noise of equal significance

Jet noise directionality = $(1 - 0.7 \sin\alpha)^{-n}$

——— n = 1 $\qquad \alpha_m = 30^o$

△ n = 2

\+ n = 3

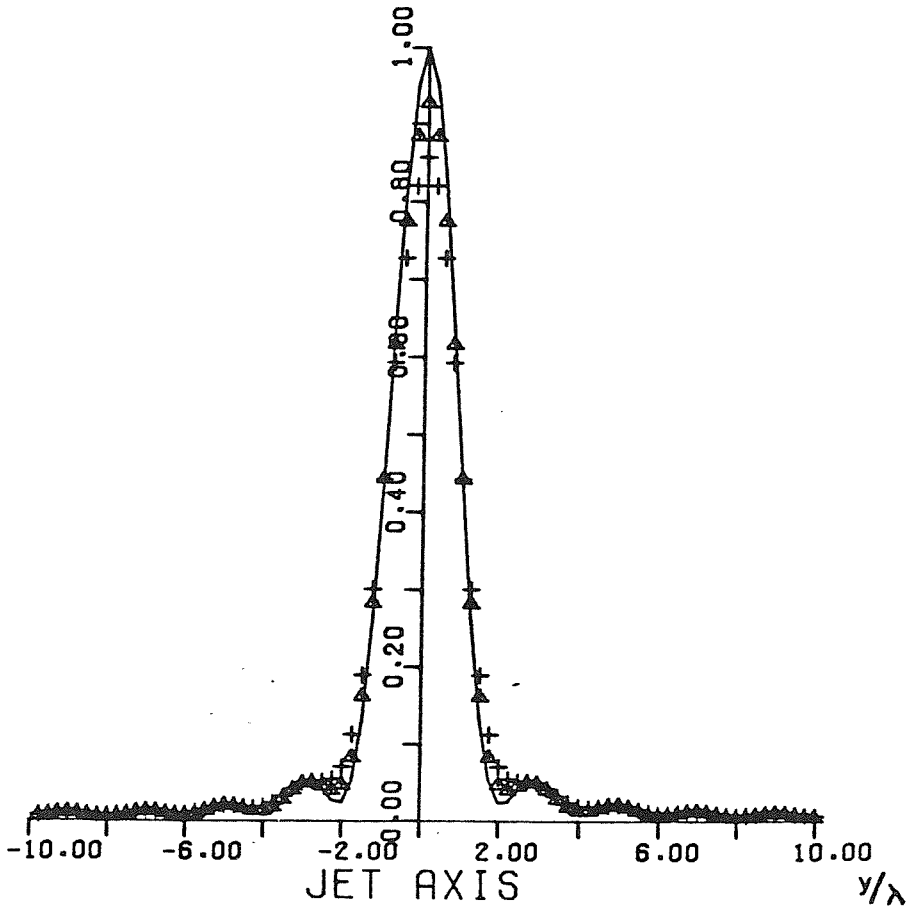

FIG. 2.11.

Source Image for a region of jet noise in the presence of an omnidirectional source of equal significance

Jet noise directionality = $(1 - 0.7 \sin\alpha)^{-n}$

——— n = 1 $\alpha_m = 30^\circ$

△ n = 2

\+ n = 3

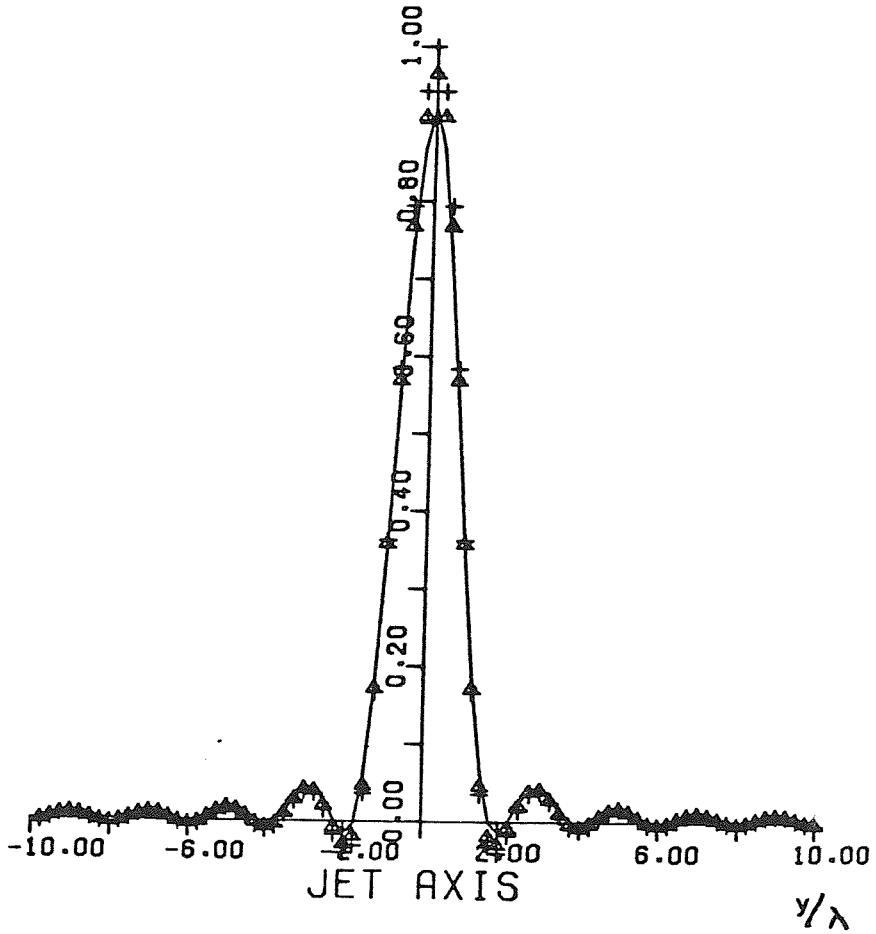

FIG. 3.1.

BASIC PRINCIPLE OF THE WAVENUMBER SPECTRUM

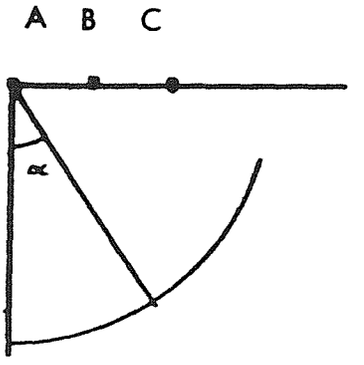

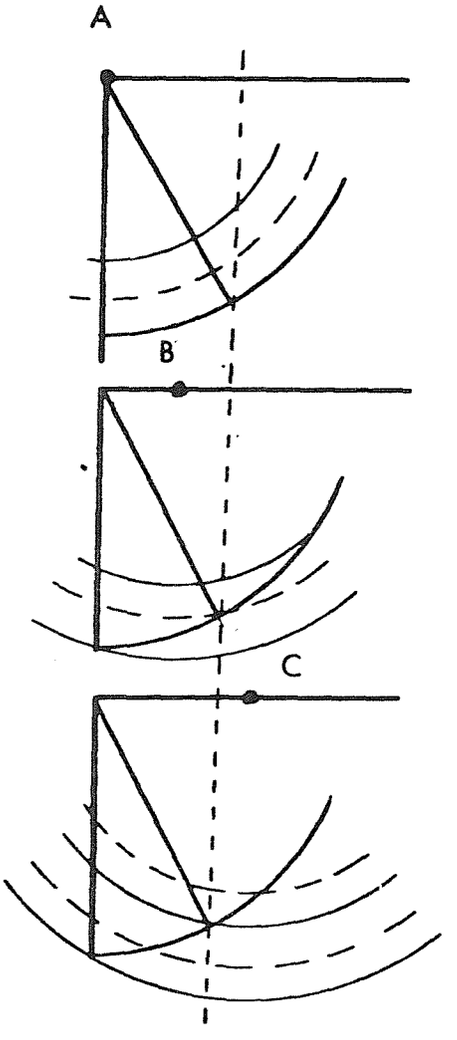

Frozen time wavefields for harmonic sources at A, B and C.

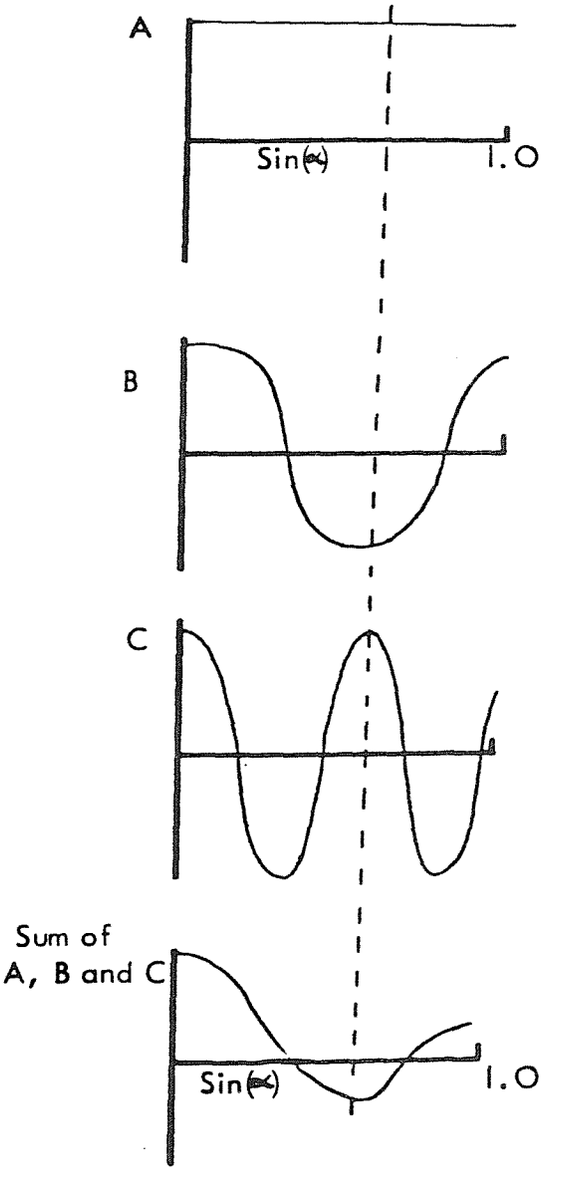

Amplitude Variation with Sin(∝) on polar arc.

FIG. 3.2.

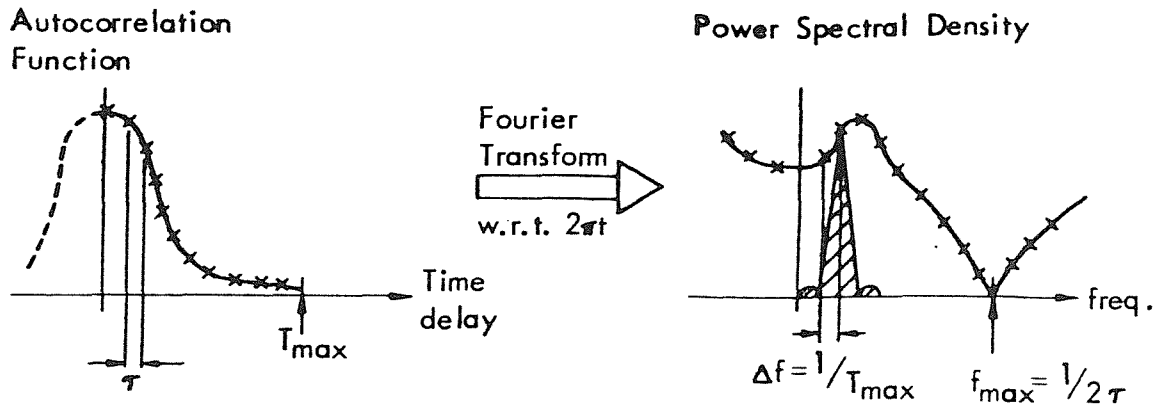

Far field C.P.S.D.

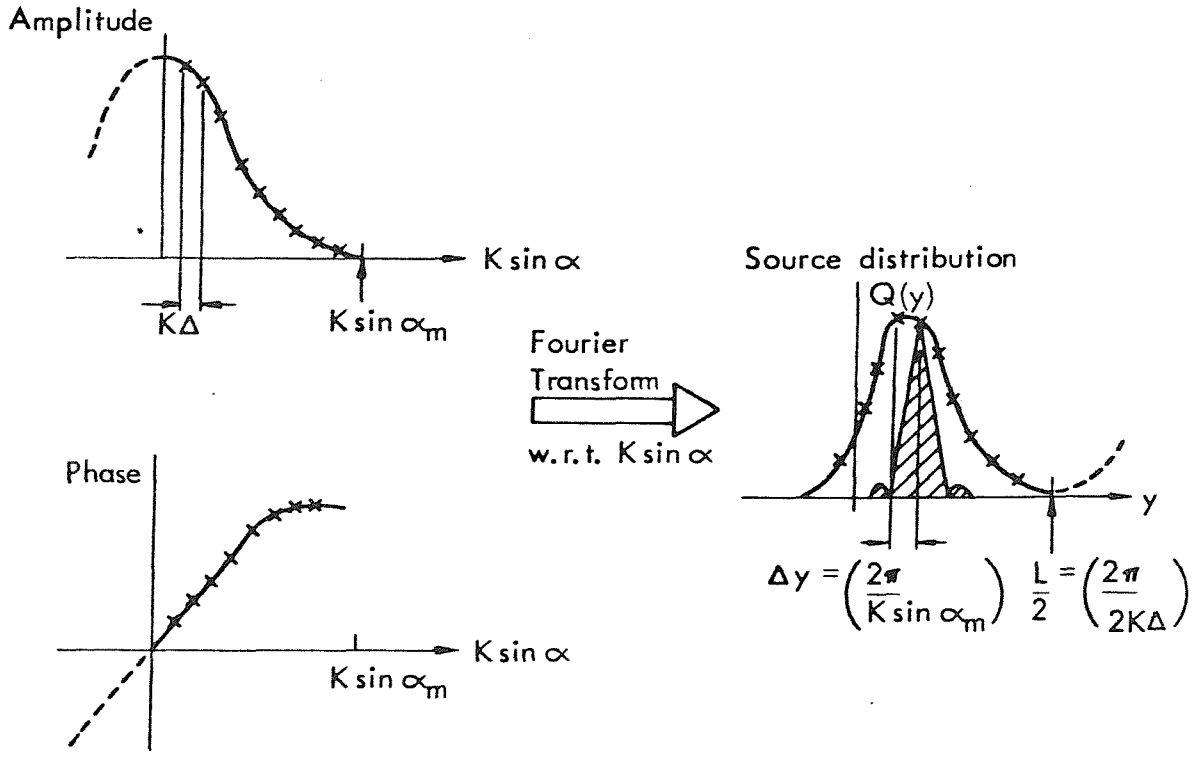

THE ANALOGY BETWEEN THE EVALUATION OF A POWER SPECTRAL DENSITY FUNCTION, AND THE EVALUATION OF THE SOURCE DISTRIBUTION.

FIG.3.3.

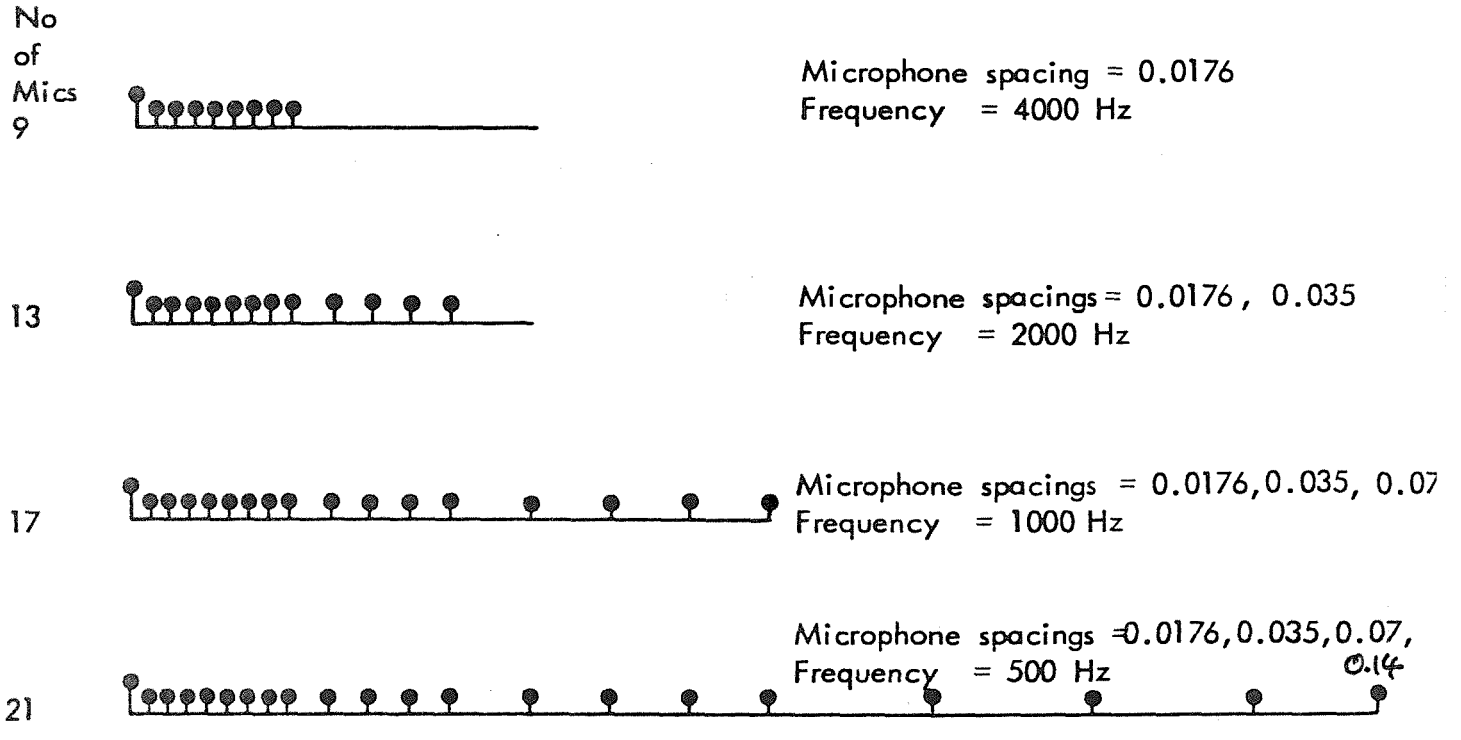

. EXAMPLE OF REDUCED GRADED MICROPHONE ARRAY.

Length of source distribution = 16 ft
Minimum separation = 3ft

Microphone spacings in units of $k\sin\alpha$

FIG. 3.4.

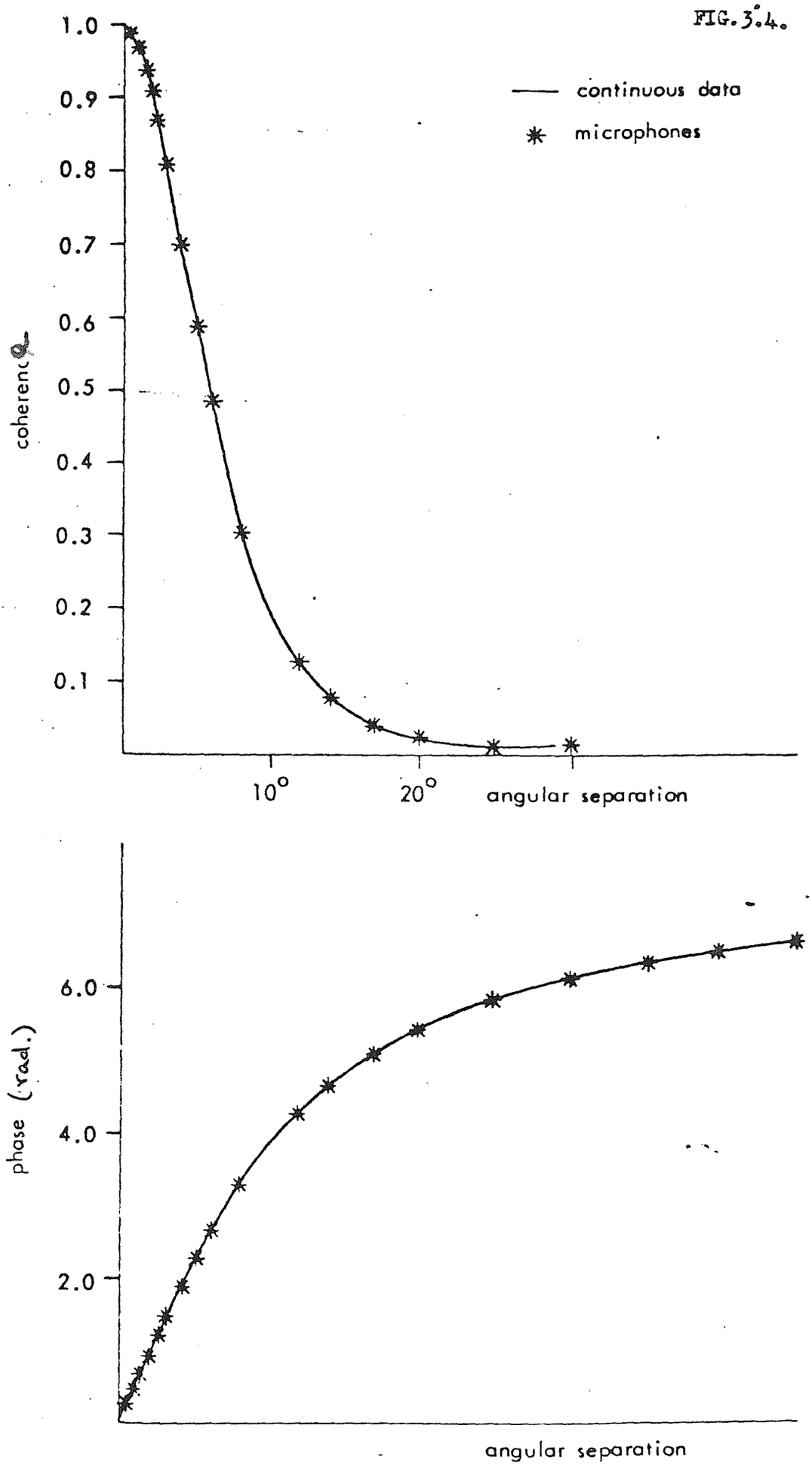

AMPLITUDE AND PHASE DATA FOR CONTINUOUS SOURCE DISTRIBUTION

FIG.3.5.

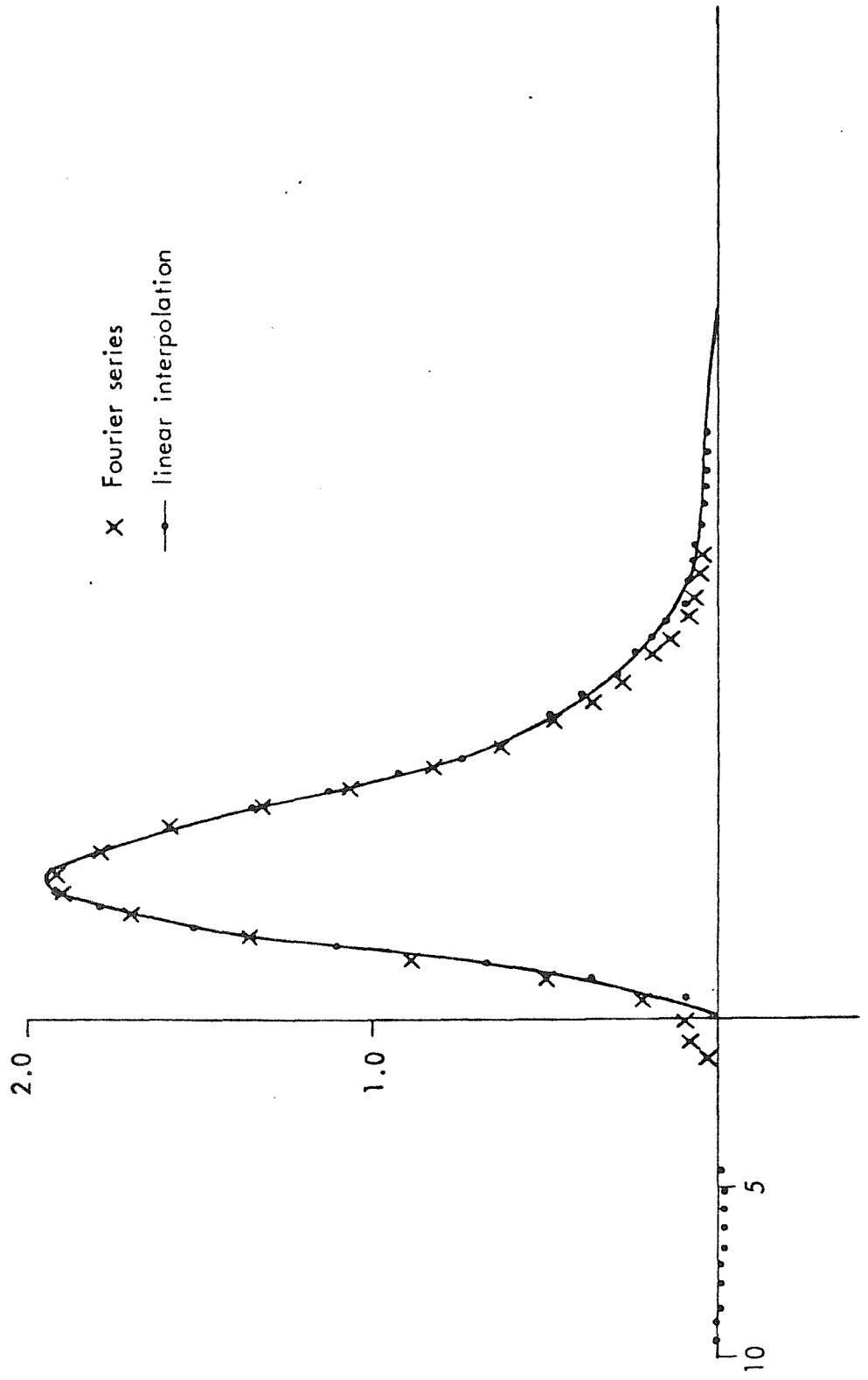

TRANSFORM OF CONTINUOUS SOURCE DISTRIBUTION

FIG. 3.6.

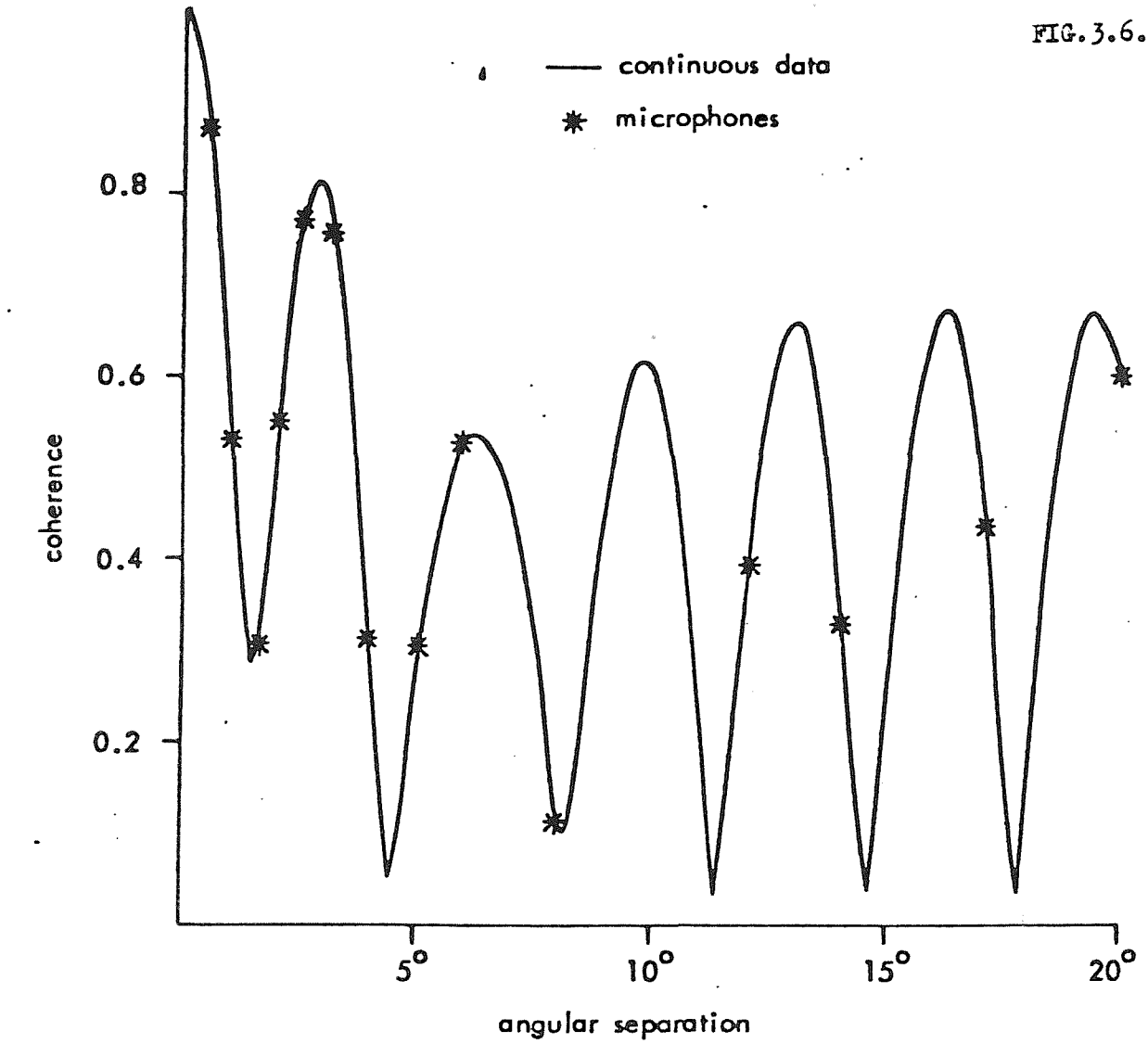

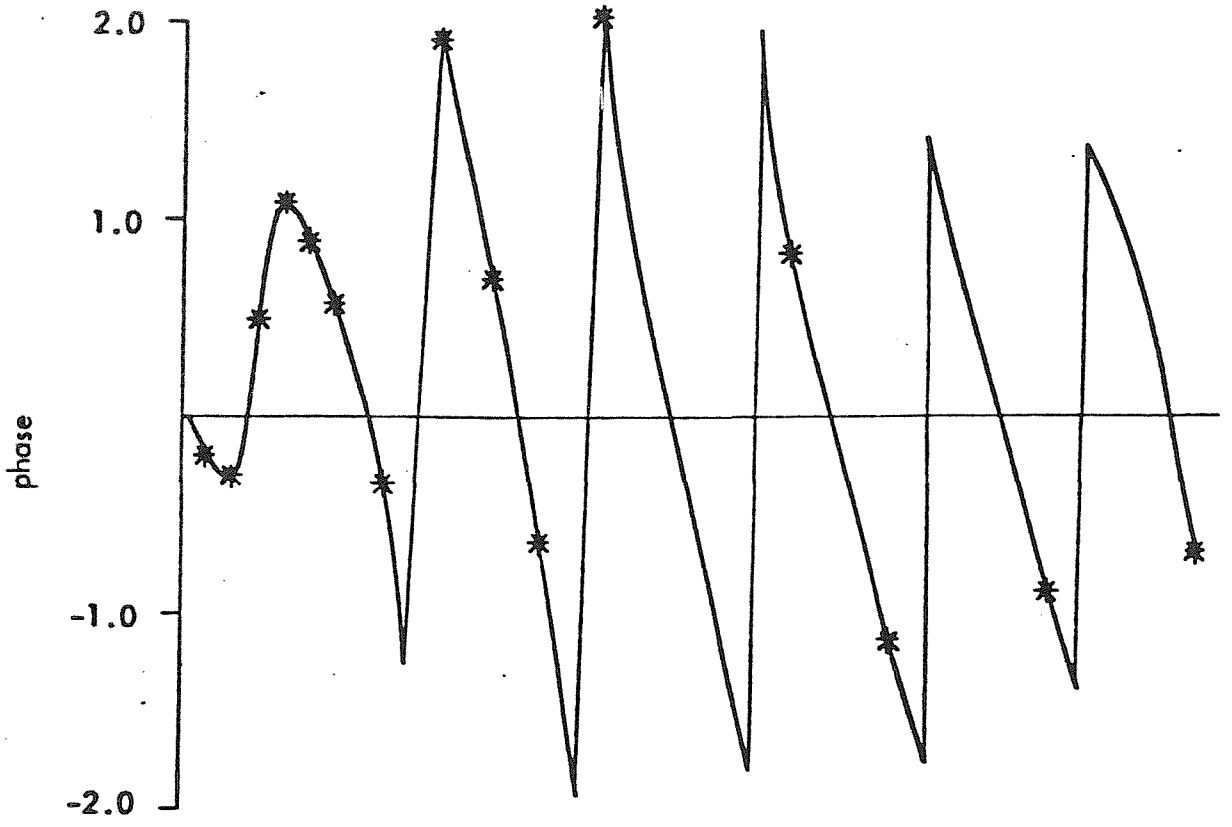

AMPLITUDE AND PHASE DATA FOR CONTINUOUS SOURCE DISTRIBUTION PLUS TWO POINT SOURCES

FIG.3.7.

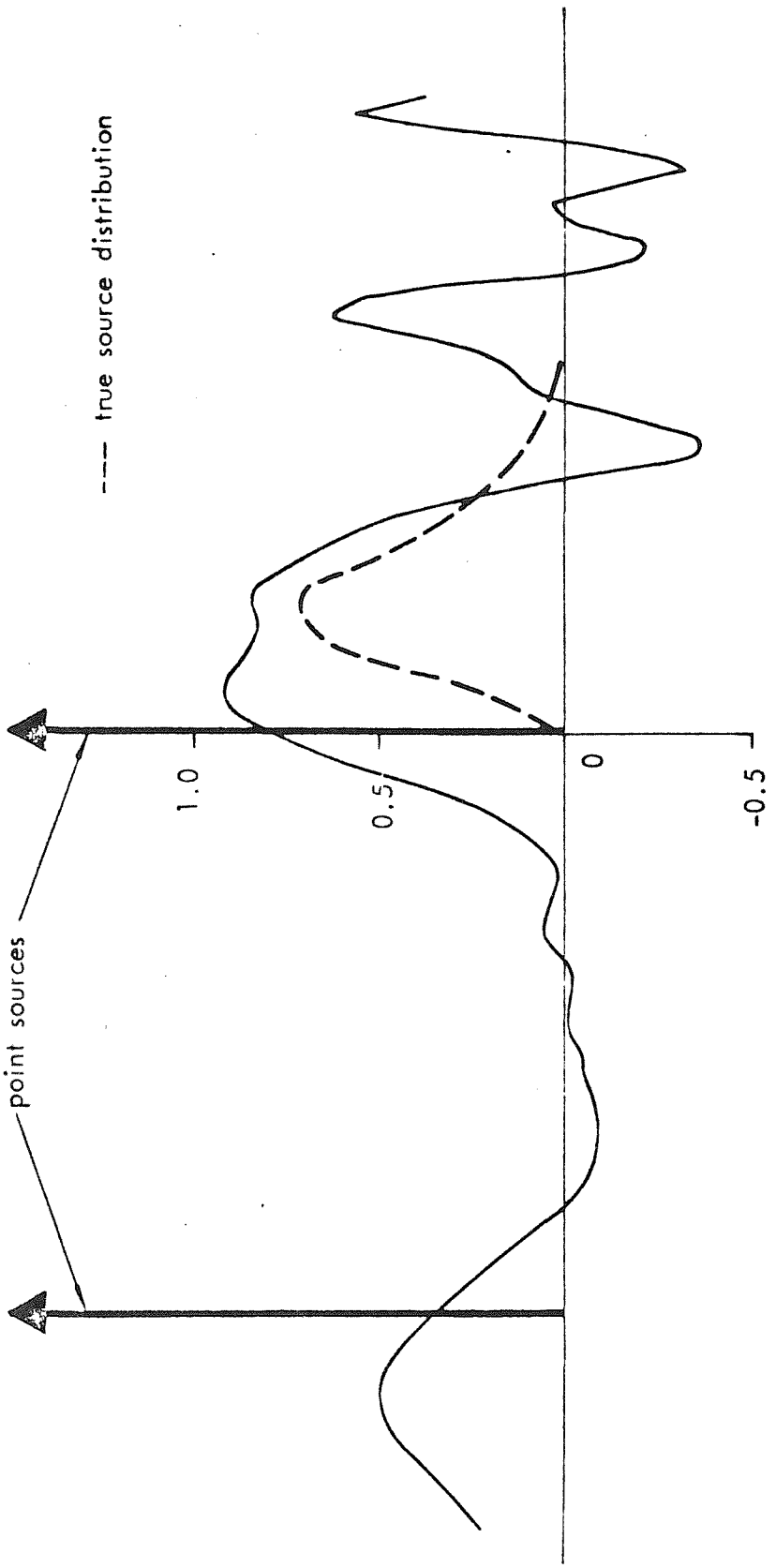

TRANSFORM OF CONTINUOUS SOURCE DISTRIBUTION WITH TWO POINT SOURCES USING LINEAR INTERPOLATION

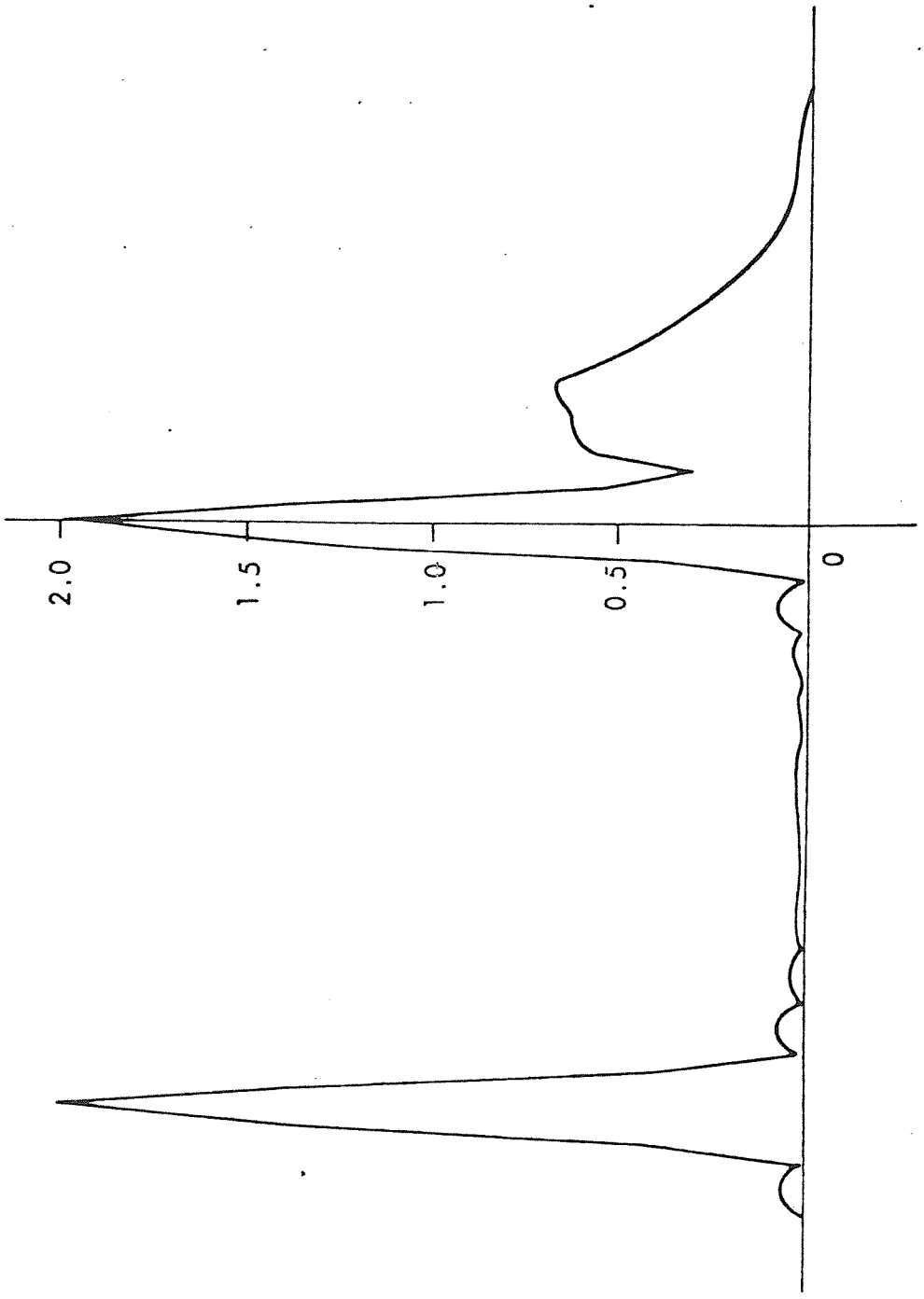

TRANSFORM OF CONTINUOUS SOURCE DISTRIBUTION WITH TWO POINT SOURCES USING A FOURIER SERIES SOLUTION

FIG.3.9.

ERROR ANALYSIS: COMPARISON OF THEORY WITH PRACTICE

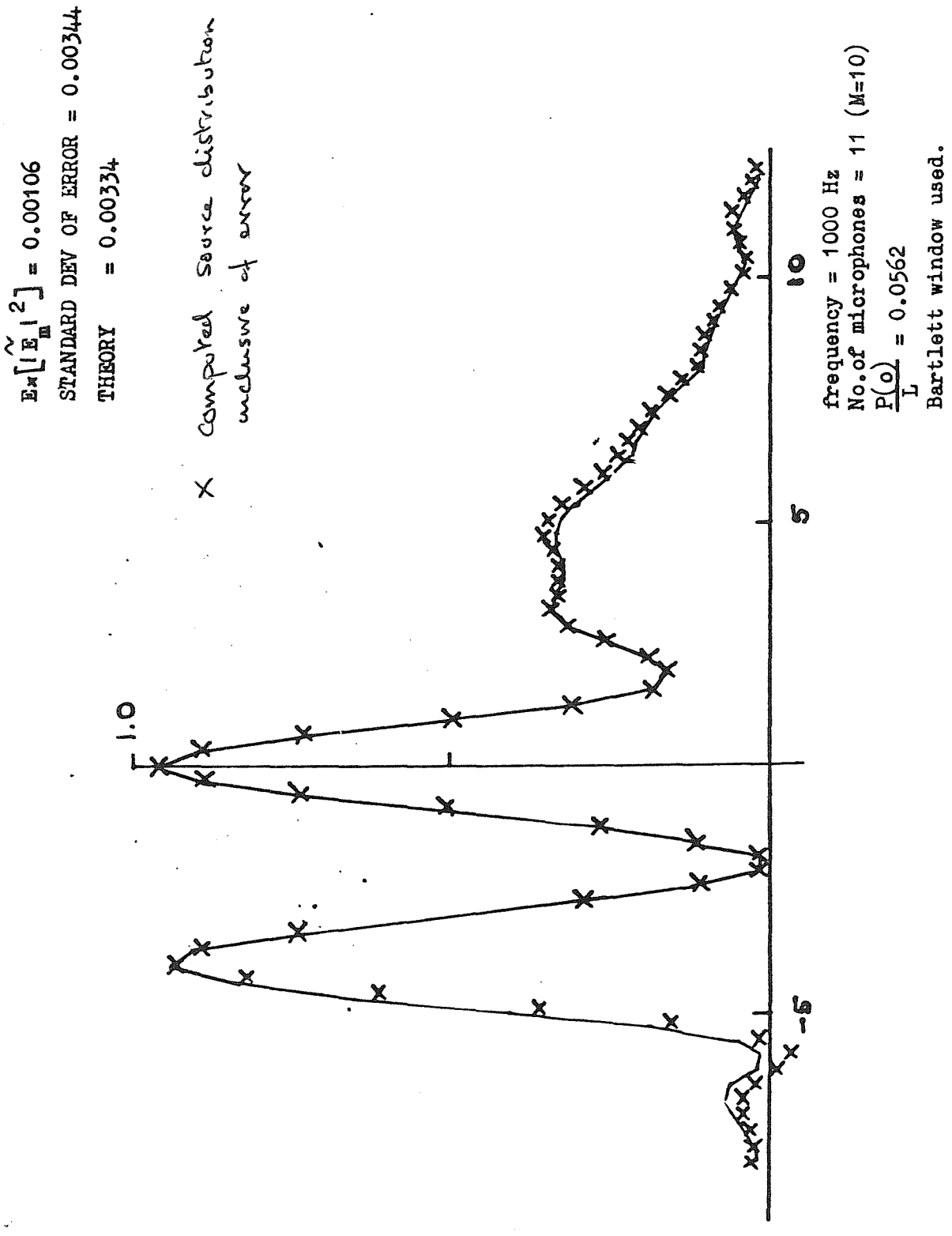

FIG.3.10.

ERROR ANALYSIS: COMPARISON OF THEORY WITH PRACTICE

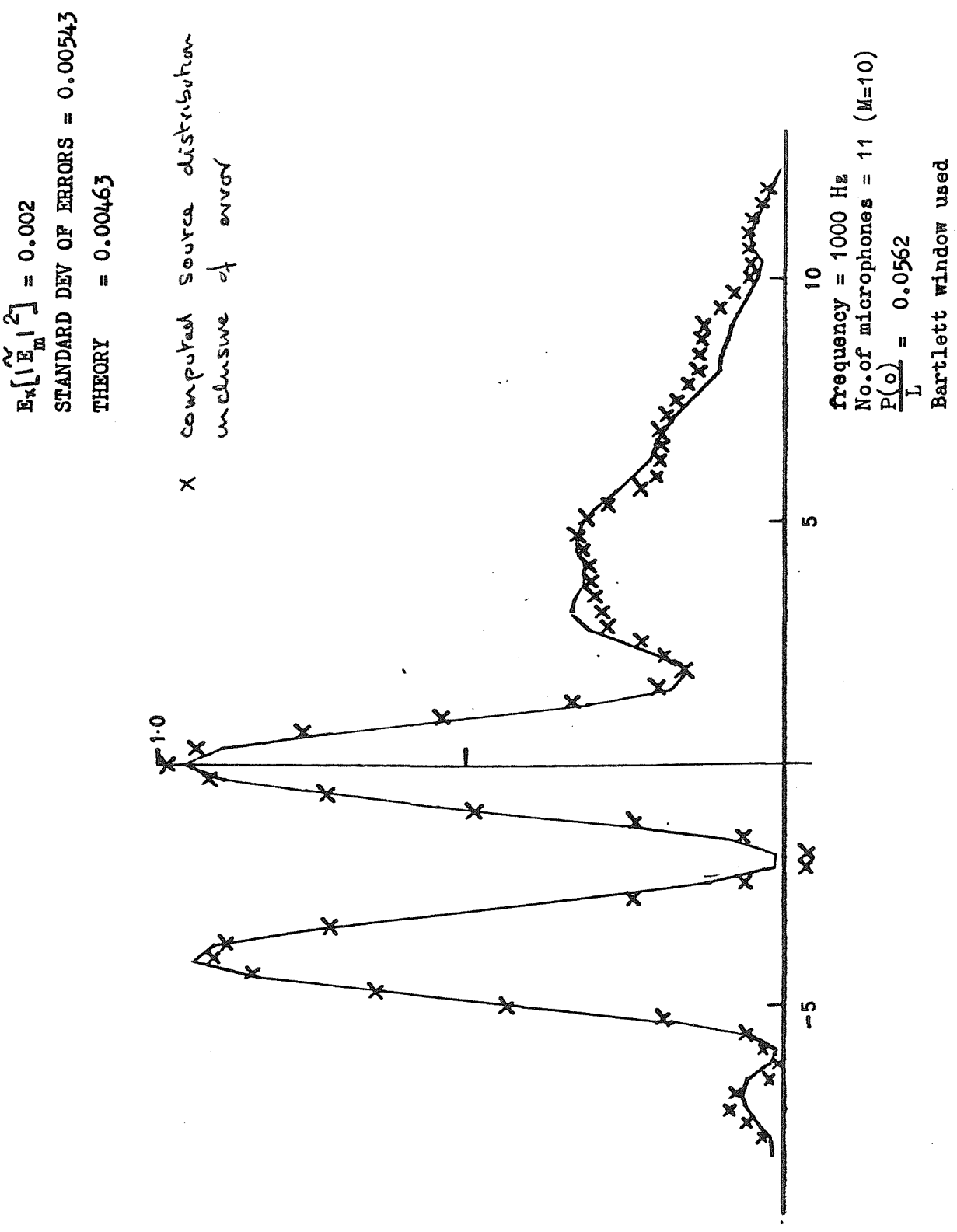

FIG. 3.11.

ERROR ANALYSIS: COMPARISON OF THEORY WITH PRACTICE

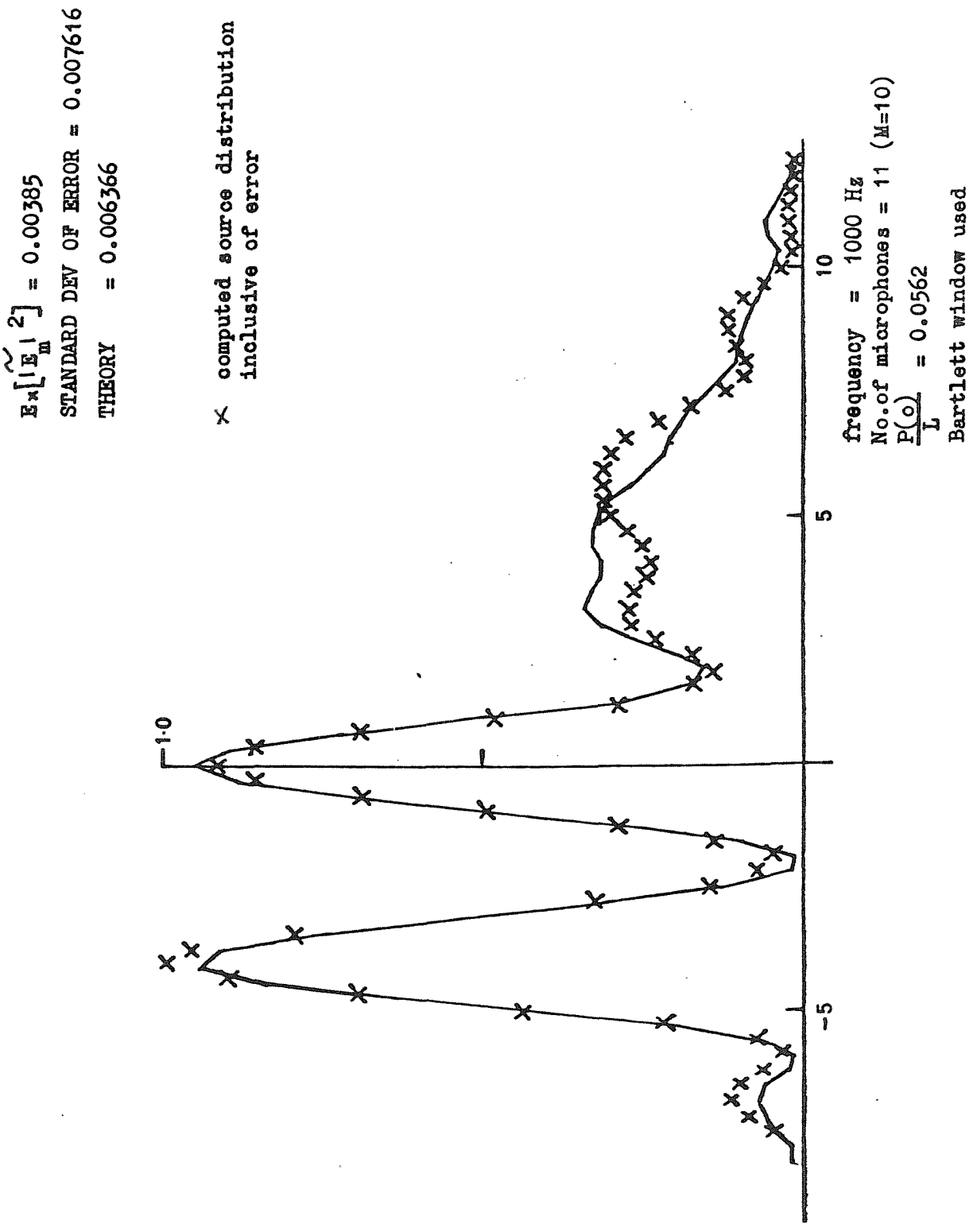

FIG.3.12.

ERROR ANALYSIS: COMPARISON OF THEORY WITH PRACTICE

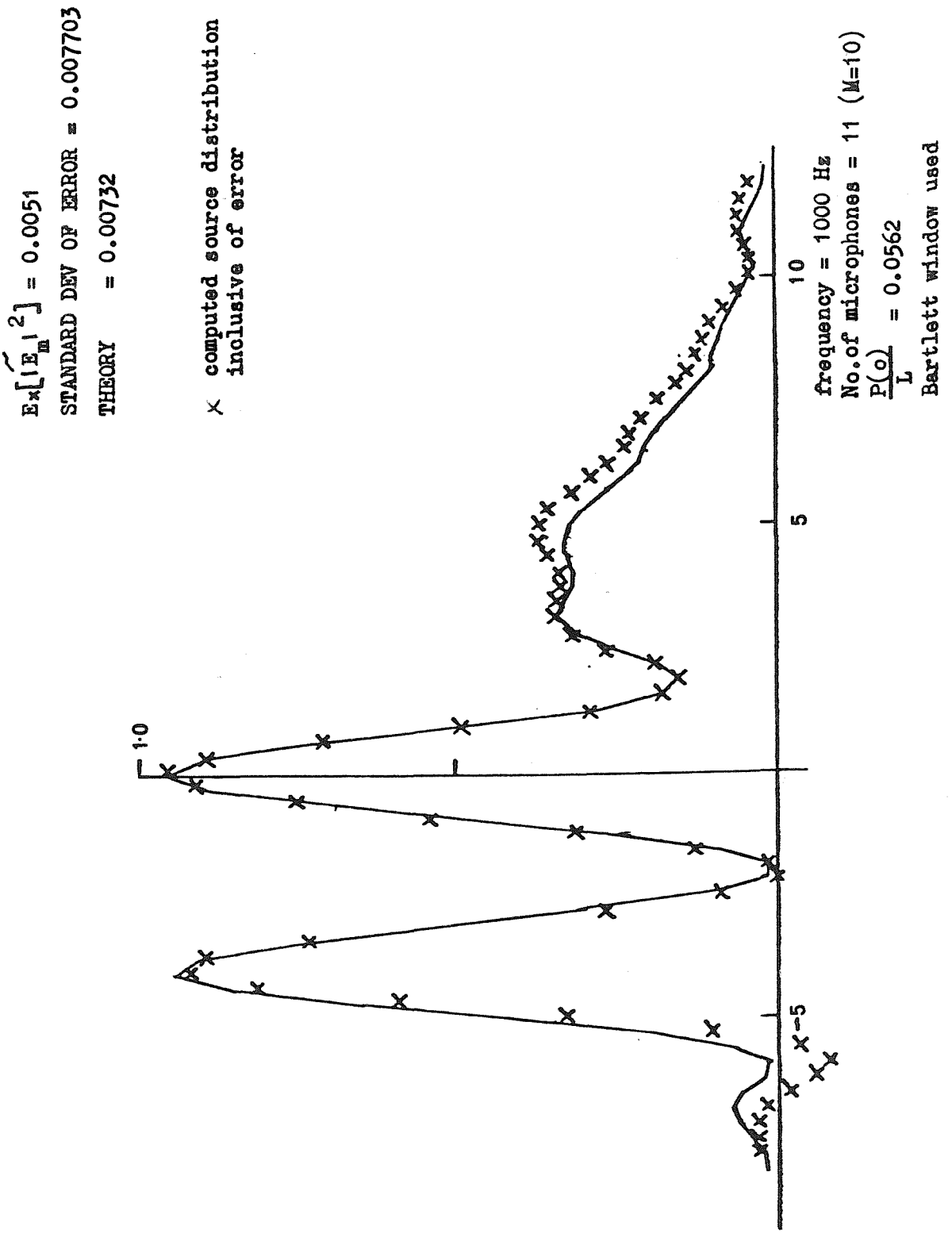

FIG.3.13.

ERROR ANALYSIS: COMPARISON OF THEORY WITH PRACTICE

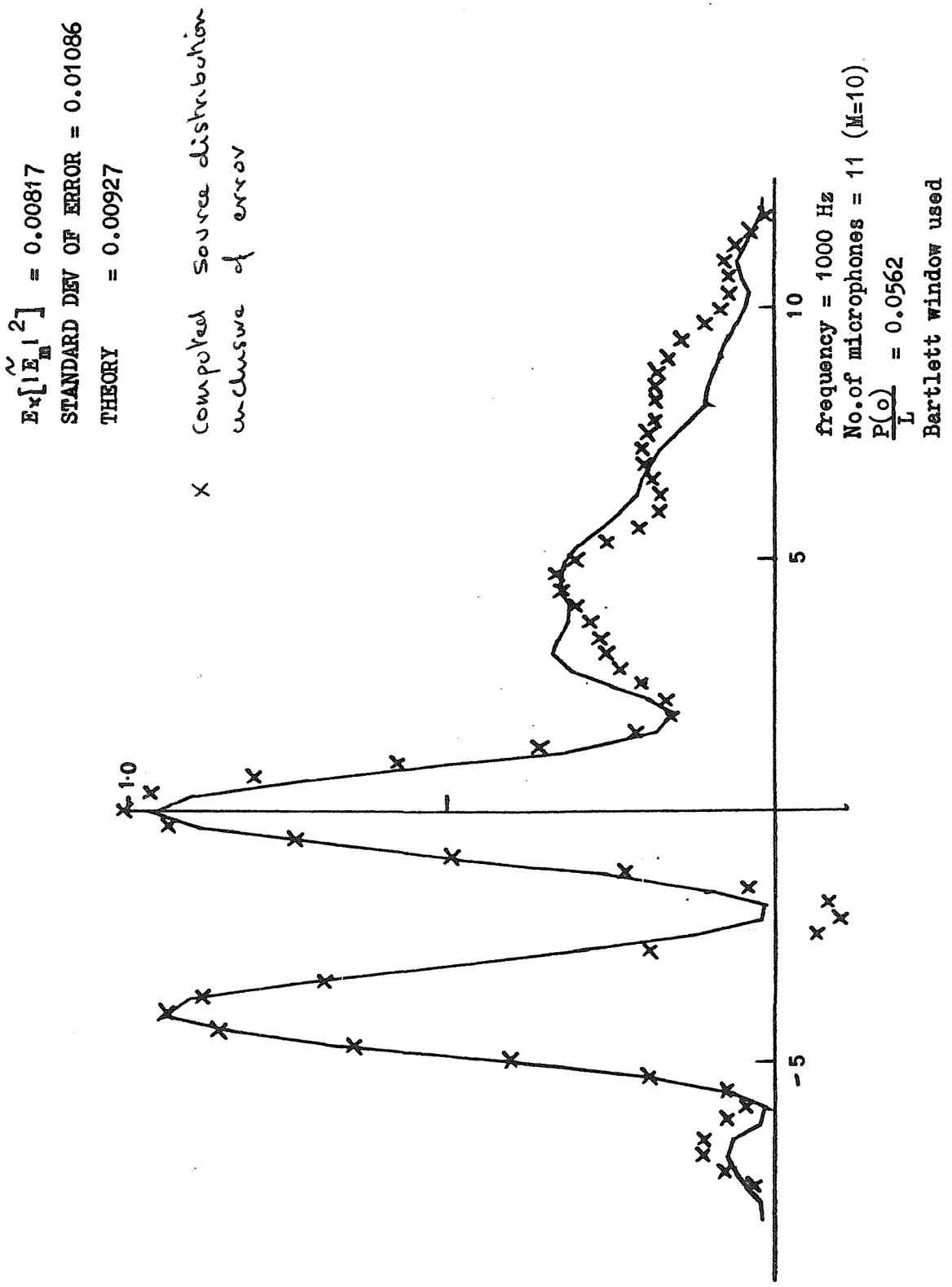

FIG. 3.14.

ERROR ANALYSIS: COMPARISON OF THEORY WITH PRACTICE

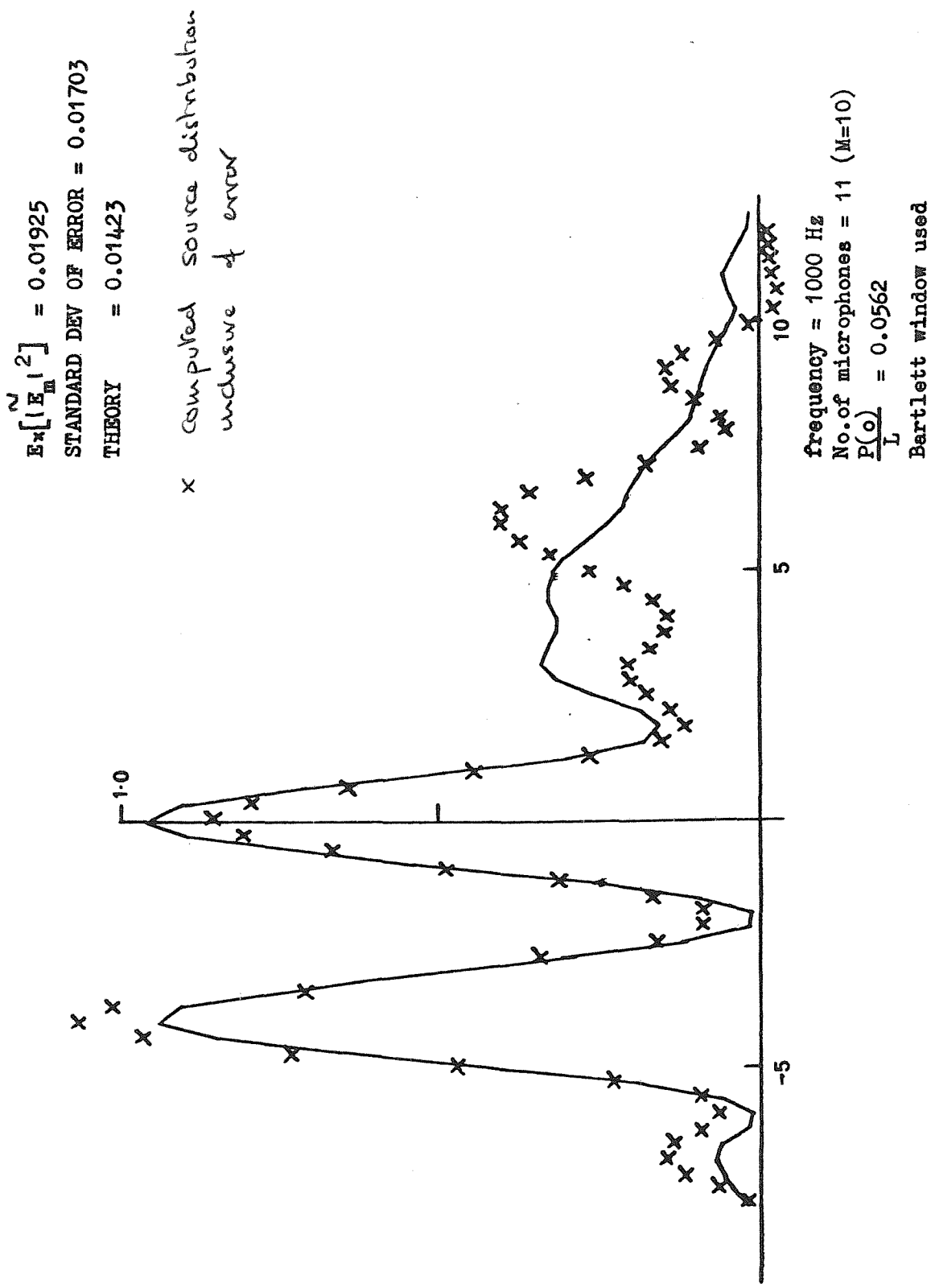

FIG.3.15.

TRANSMISSION OF ERRORS TO SOURCE DISTRIBUTION

A COMPARISON OF THEORY TO PRACTICE

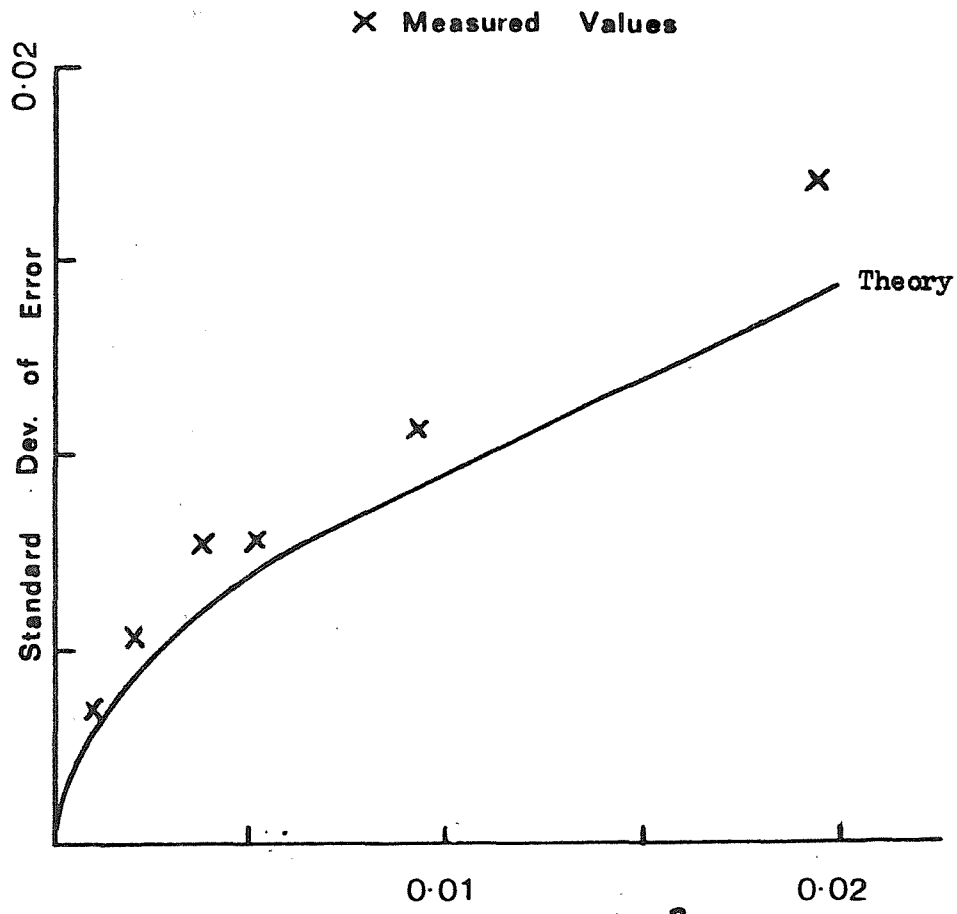

$$\text{Theory} = \frac{P(o)}{L} \quad \frac{Ex\left[|\tilde{E}_m|^2\right]}{2Y_{\mathcal{B}}(M)}$$

$$\frac{P(o)}{L} = 0.0562 \qquad Y_{\mathcal{B}}(M) = 3/20$$

FIG. 3.16

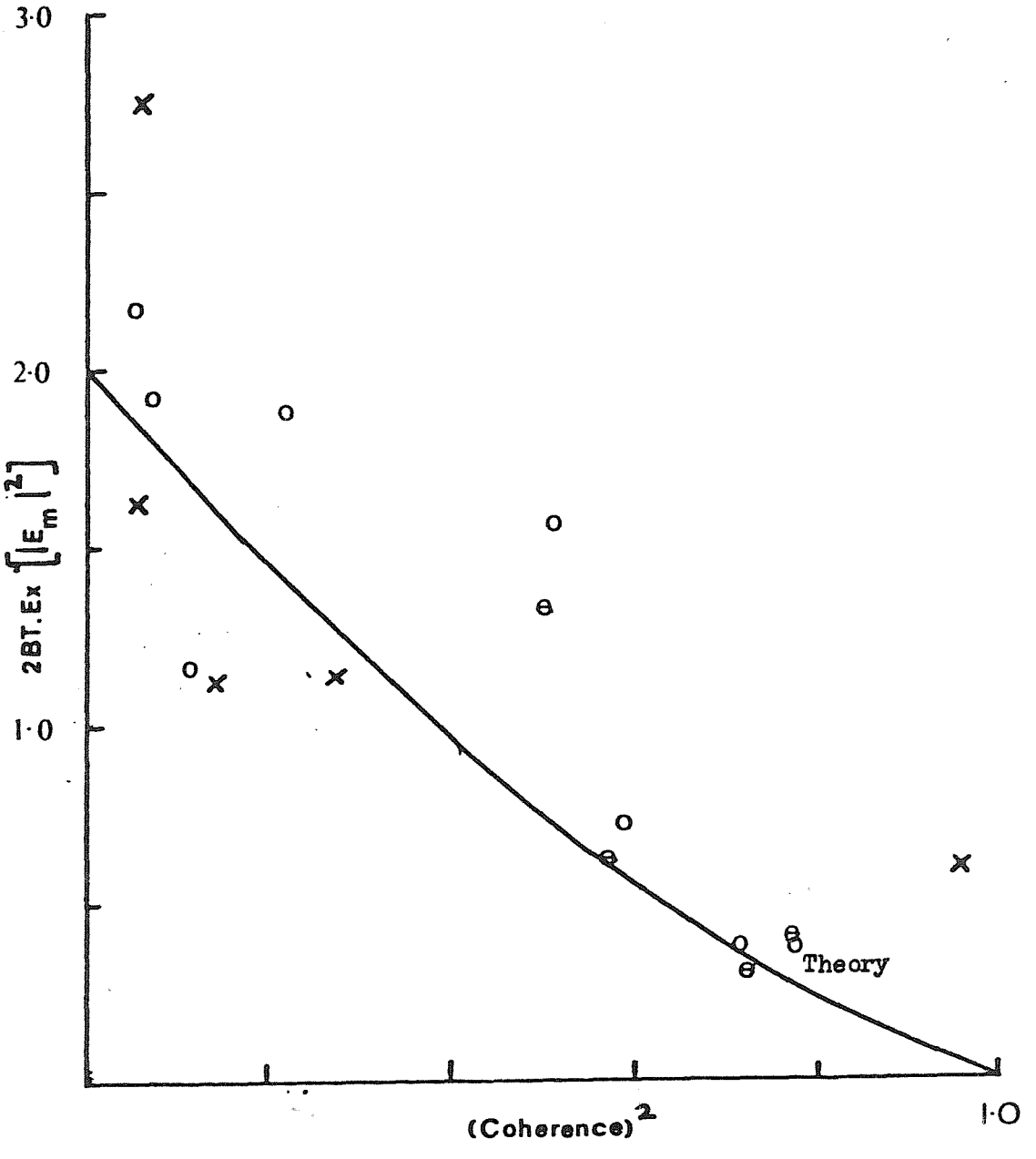

COMPARISON OF MEASURED ERRORS WITH THEORY

× BT=48

o BT=98

⊖ BT=248

ANALOG METHOD

FIGURE 4.1

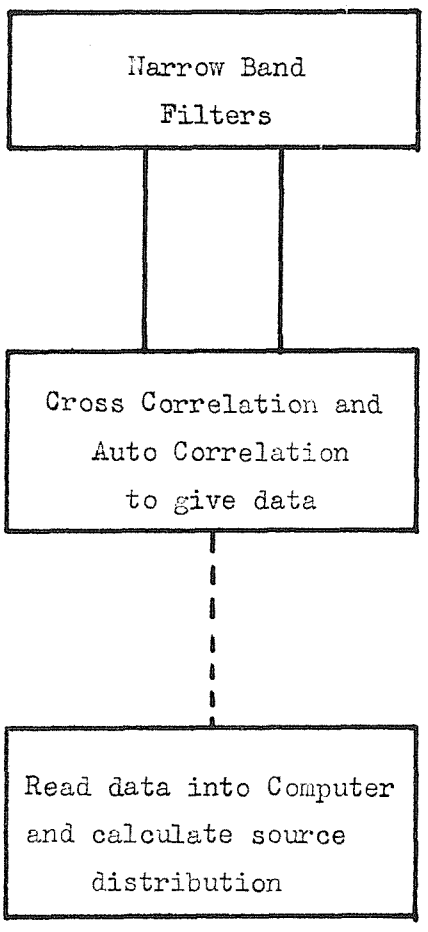

H.P. Correlator

Computer

Problems

Operator time required to carry out the number of correlations required (3 x No. of microphones)

Time = $\frac{1}{4}$ day per frequency

Advantages

The operator is in control of the data at all stages, therefore snags may be easily traced. Proved to be very useful in the development stages of the technique.

ANALOG/DIGITAL METHOD

FIGURE 4.2

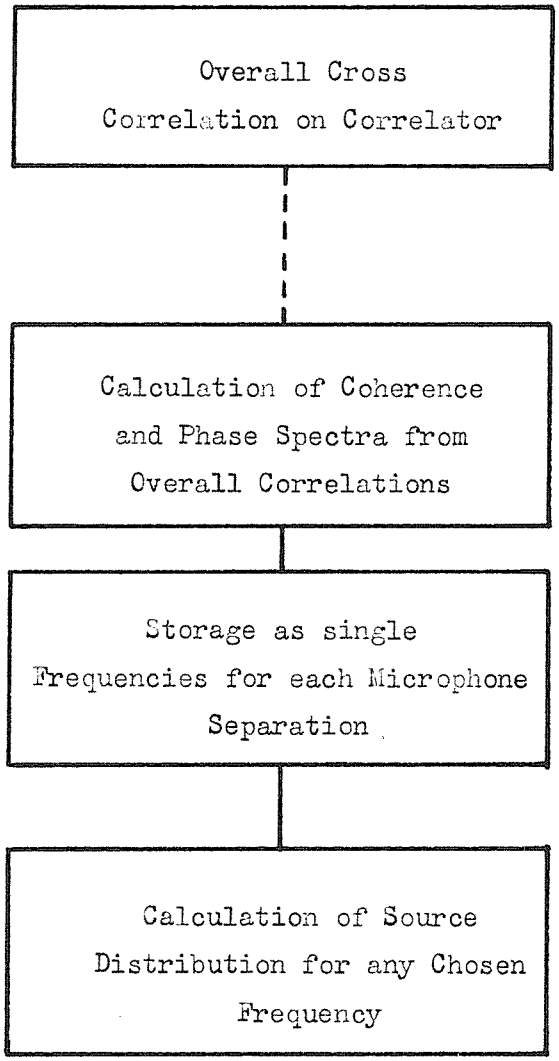

Problems

Operator time required to carry out the correlations
(4 x No. of microphones)

Time = $\frac{1}{2}$ day spectrum

Advantages

Small storage requirement and the A/D conversion problem is eliminated.

DIGITAL COMPUTER METHOD

FIGURE 4.3

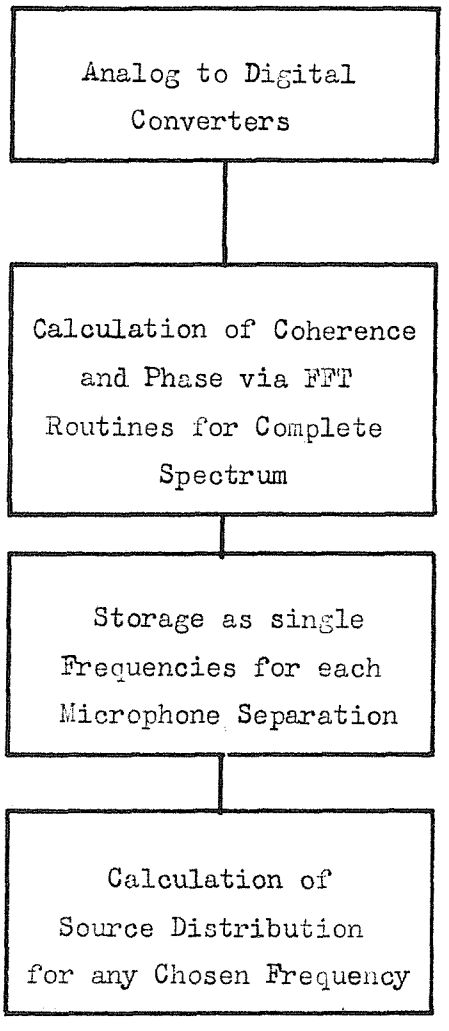

Sample rate 4,000/ sec. on each channel

Computer (PDP 1150)

Storage requirement
= 32 K x 2 x 21
= 1344 K. at 62.5 Hz bandwidth

Problems

To obtain high accuracy at low coherence levels a large number of statistical degrees of freedom are required ($\sim$ 600). This requires 10K samples per channel per angle.

Advantage

Operator time = 2 hrs/spectrum (defined by A/D converter time)

LAYOUT OF EQUIPMENT FOR CALCULATION OF C.P.S.D. USING NARROW BAND CROSS CORRELATION

FIGURE 4.4

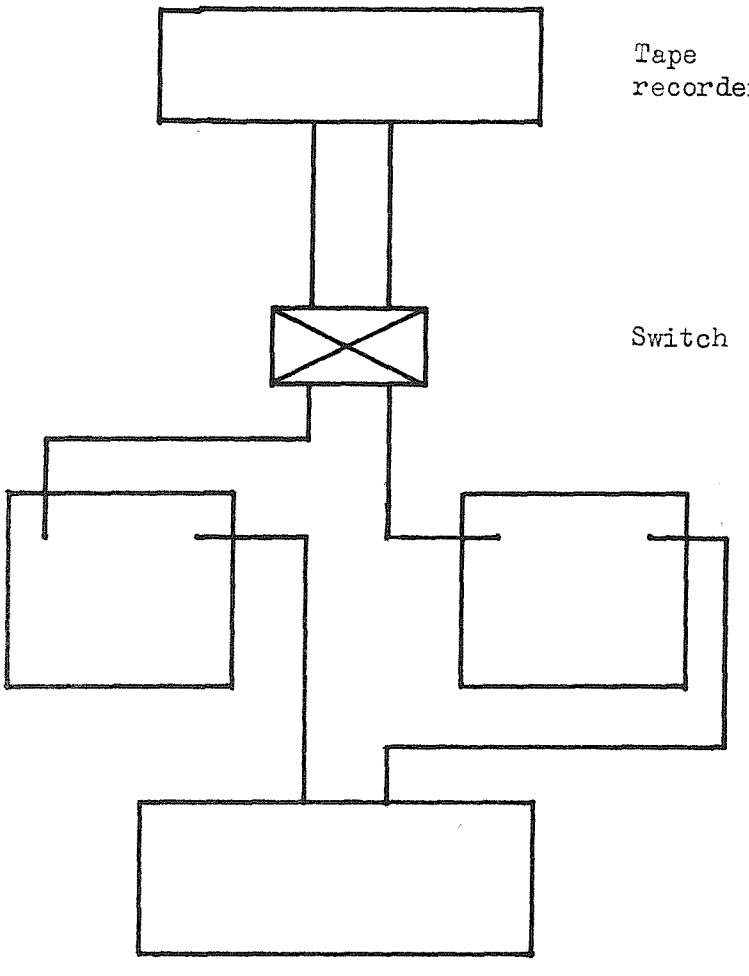

LAYOUT OF EQUIPMENT FOR CALCULATION OF C.P.S.D. USING OVERALL CROSS CORRELATION

FIGURE 4.5

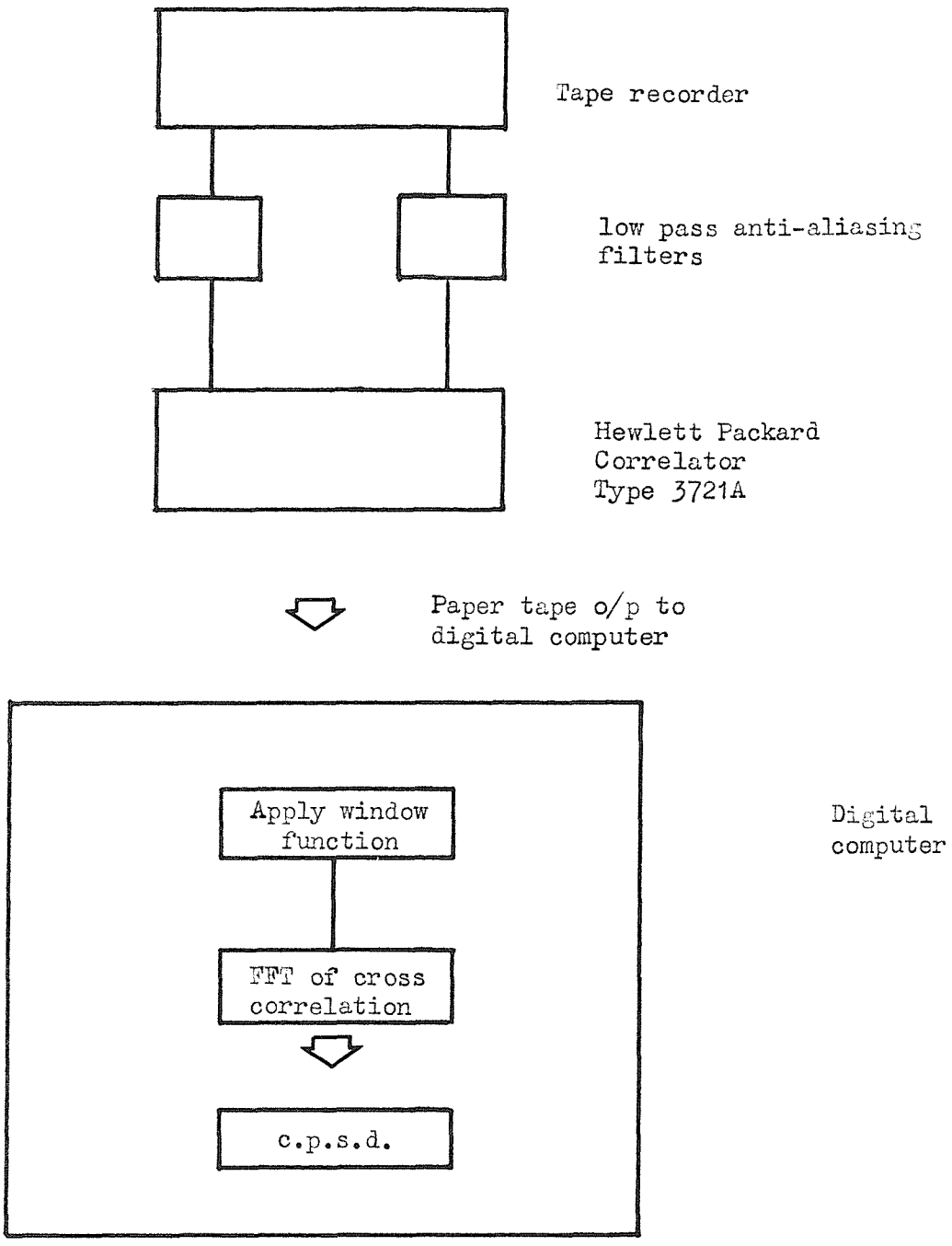

PRINCIPLE OF THE PROGRAMME SUITE ON THE ISVR PDP 11/50 FOR POLAR CORRELATION

FIGURE 4.6

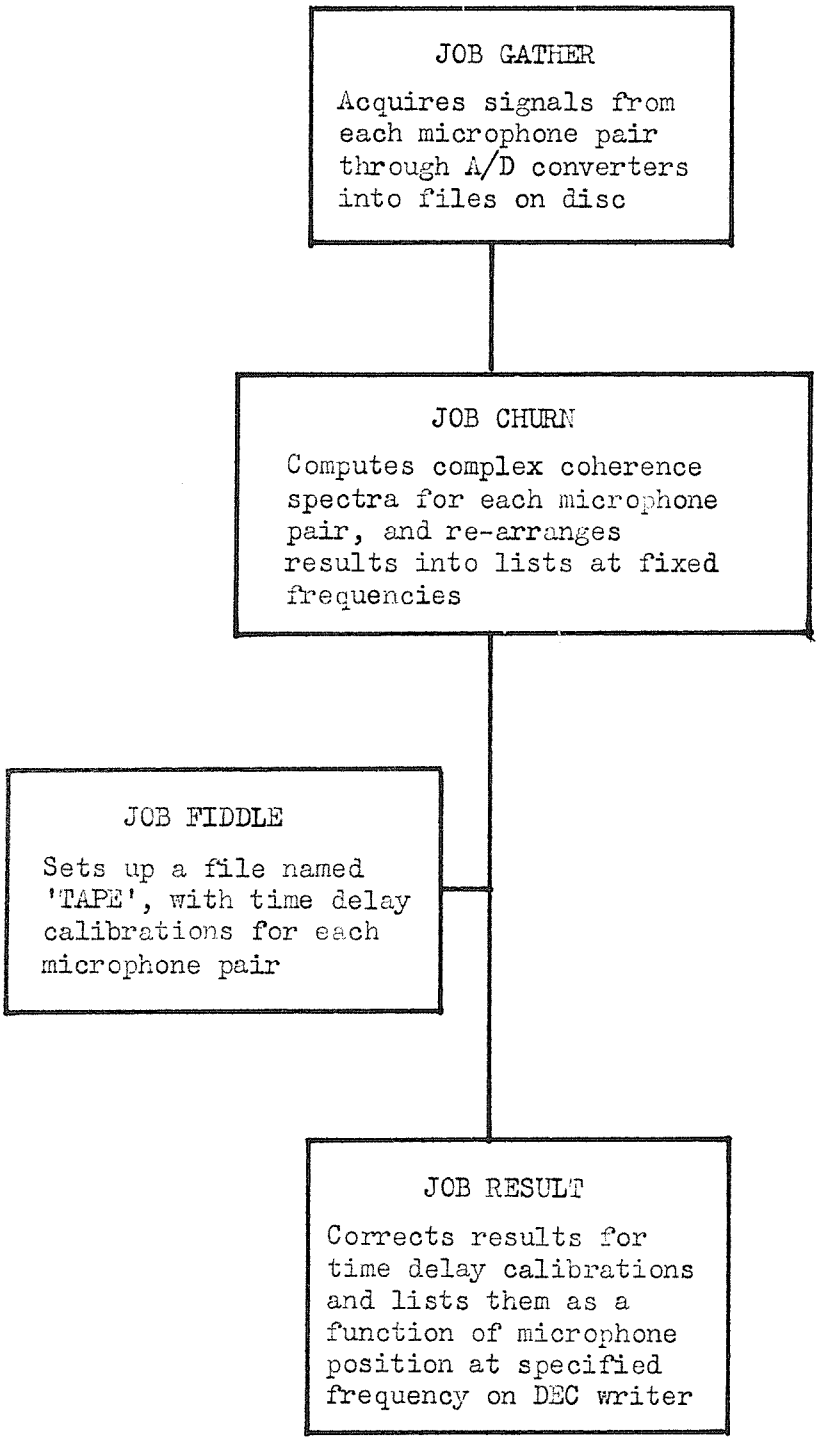

BLOCK DIAGRAM OF PROGRAMMES ON THE ALPHA COMPUTER FIGURE 4.7

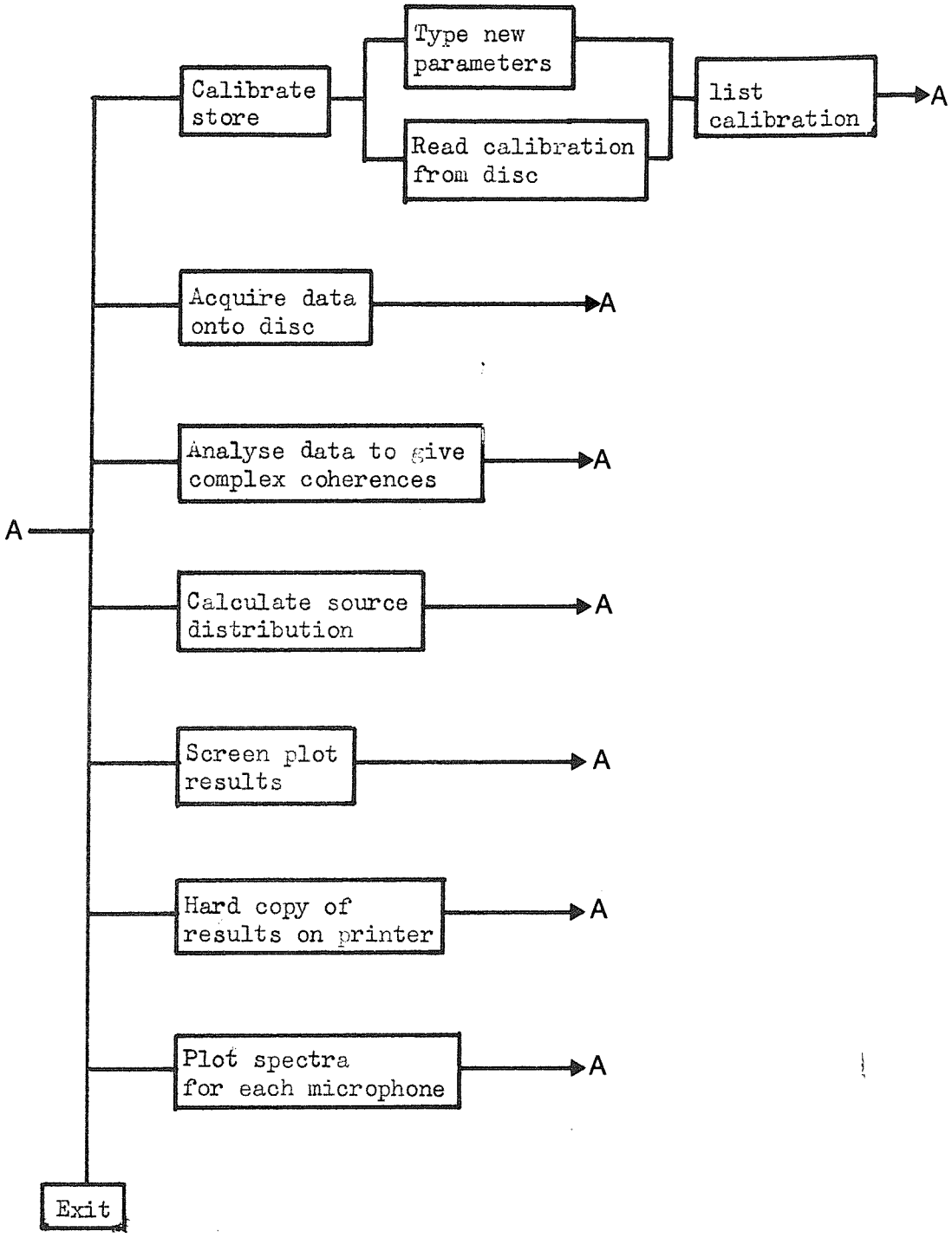

FLOW CHART FOR COMPUTER PROGRAMME PANA

FIGURE 4.8

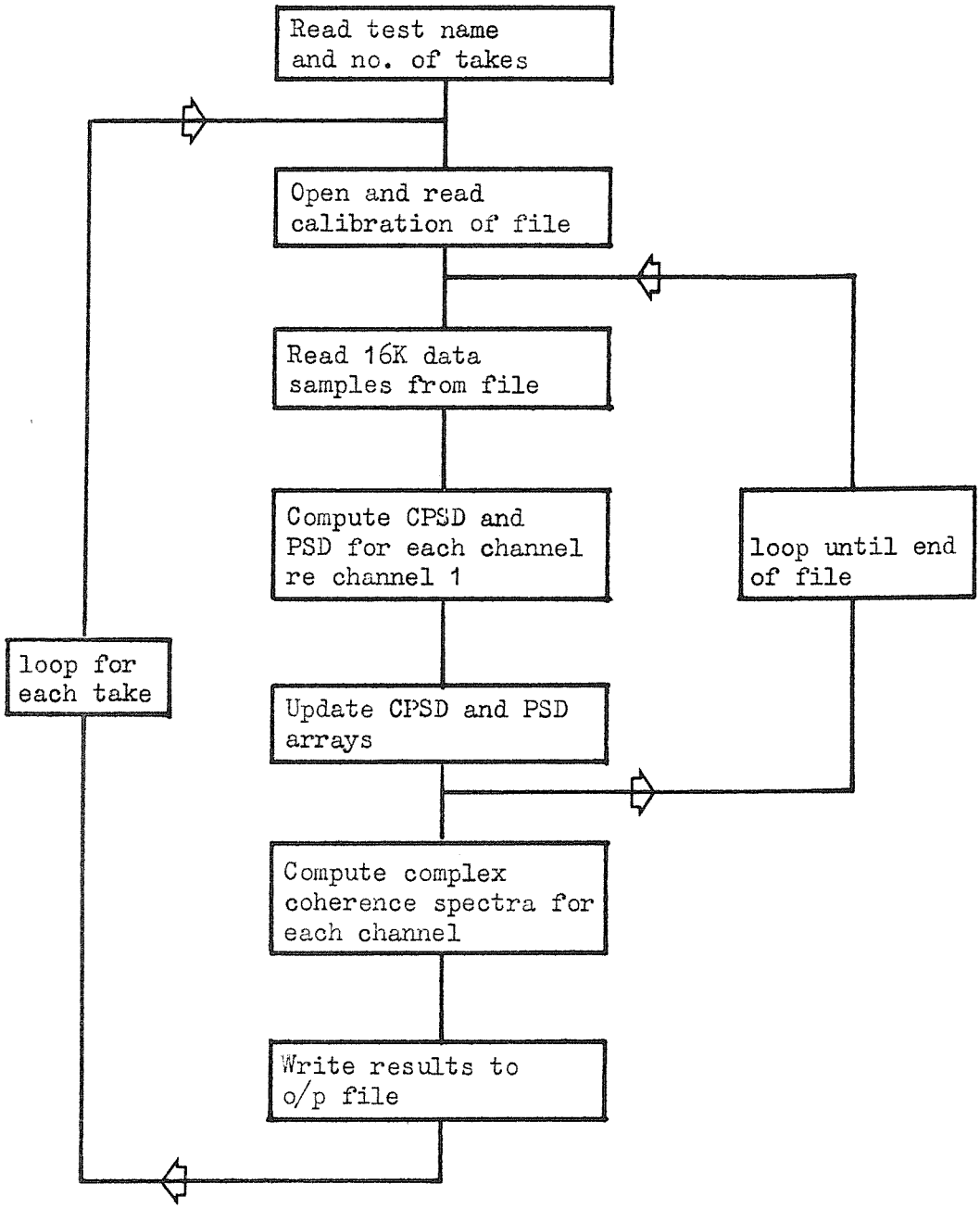

FLOW CHART FOR THE CALCULATION OF C.P.S.D. IN PANA

FIGURE 4.9

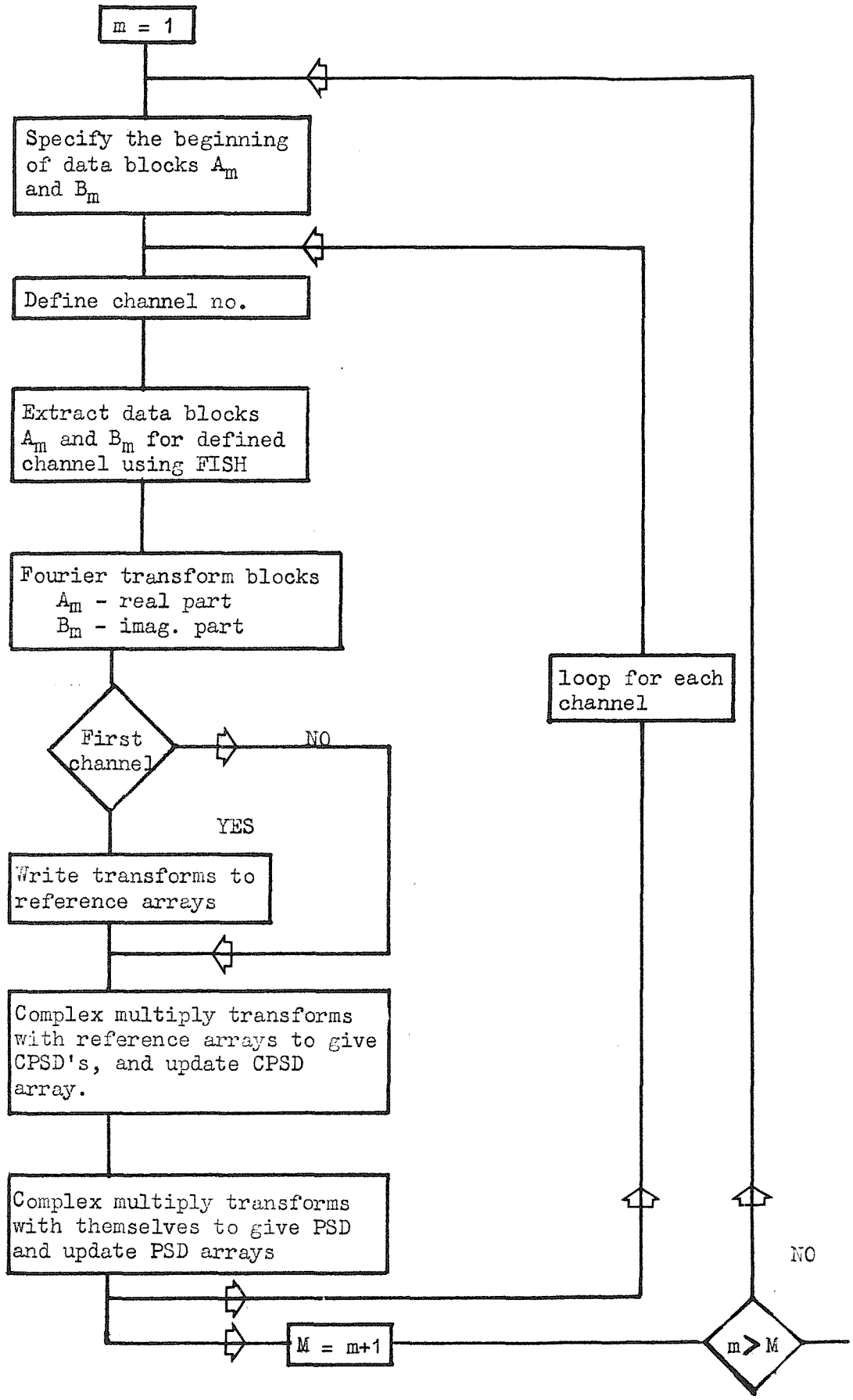

CALCULATION OF SOURCE DISTRIBUTION

FIGURE 4.10

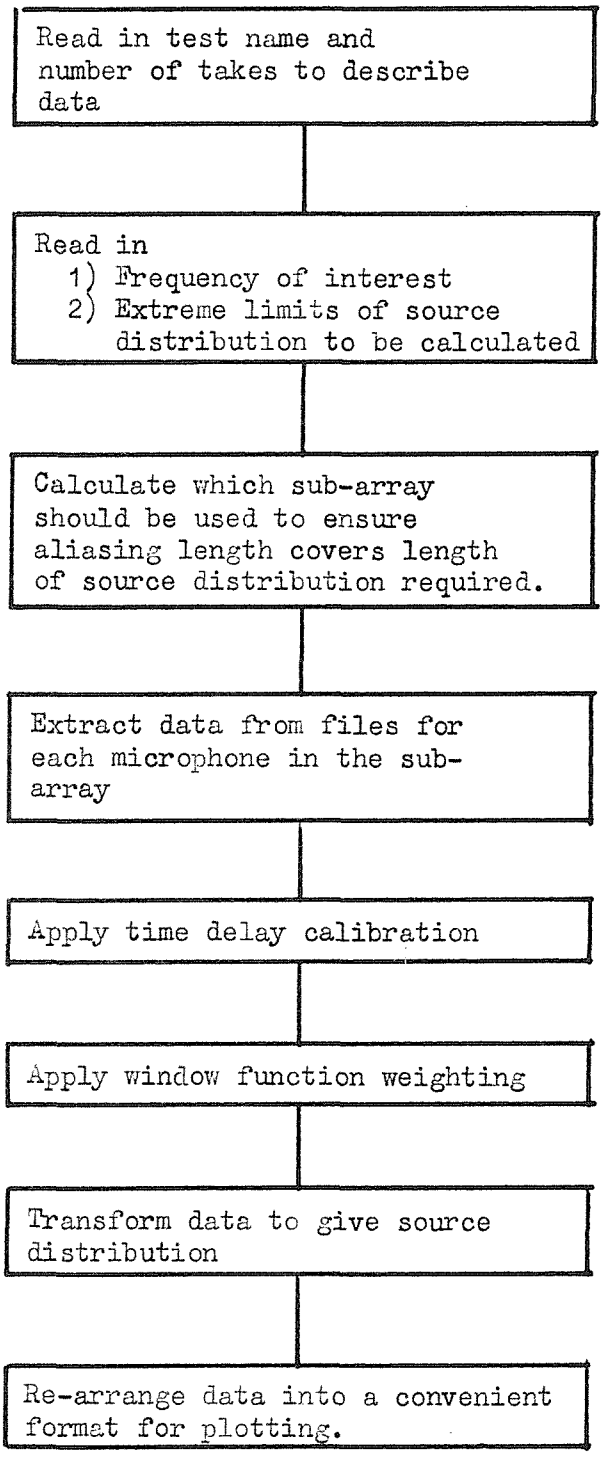

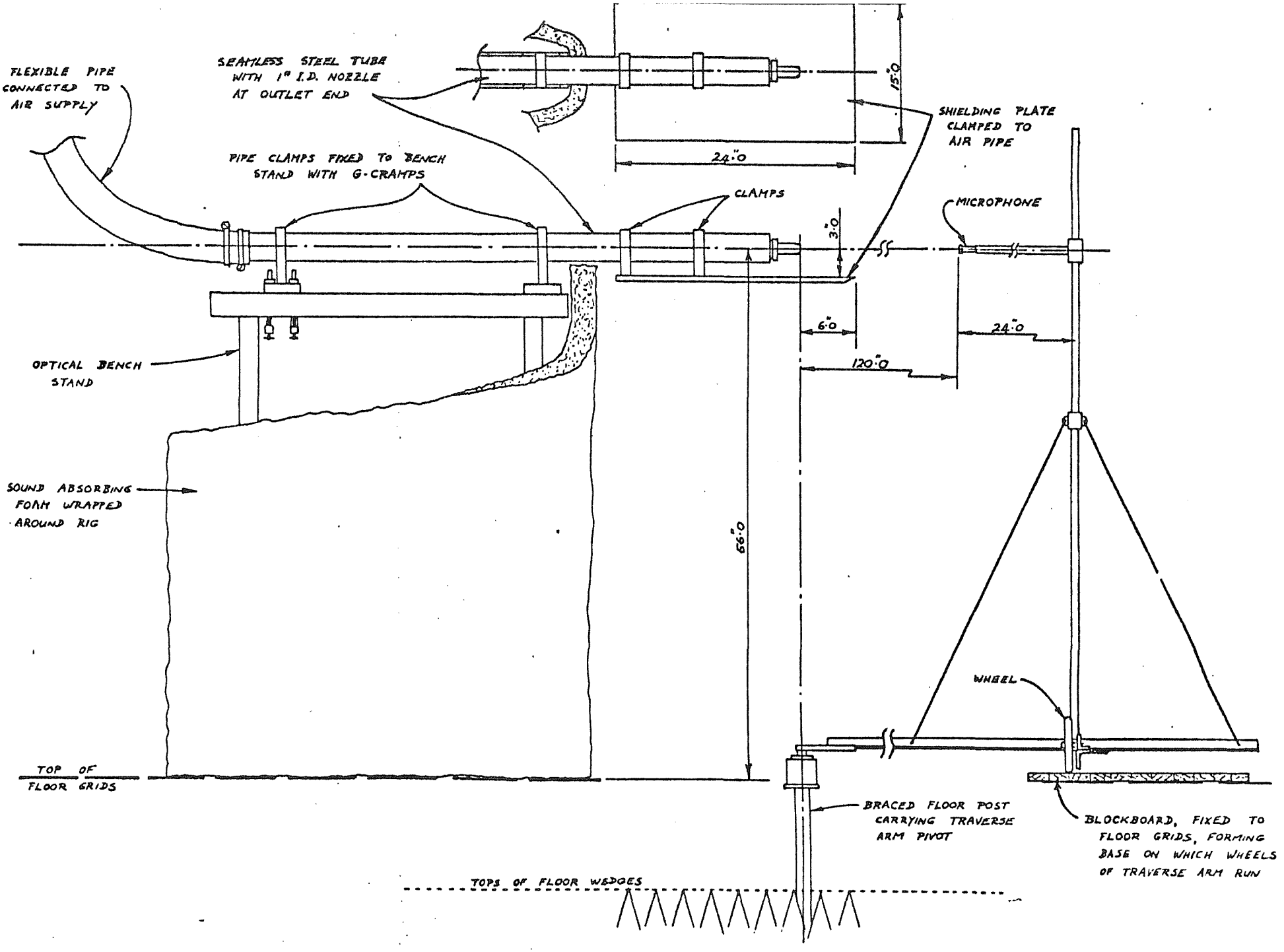

FIG. 5.1.

GENERAL ARRANGEMENT OF HORIZONTAL JET RIG IN I.S.V.R. ANECHOIC CHAMBER

FIG. 5.2.

SOURCE DISTRIBUTION FROM 1 INCH COLD JET

_____ Rear Arc Measurement

—△— Forward Arc Measurement

Aliasing Length = 125.5 in.

Resolution = 12.5 in.

Frequency = 1293.0 Hz

Strouhal No. = 0.25

U_J/a_o = 0.4

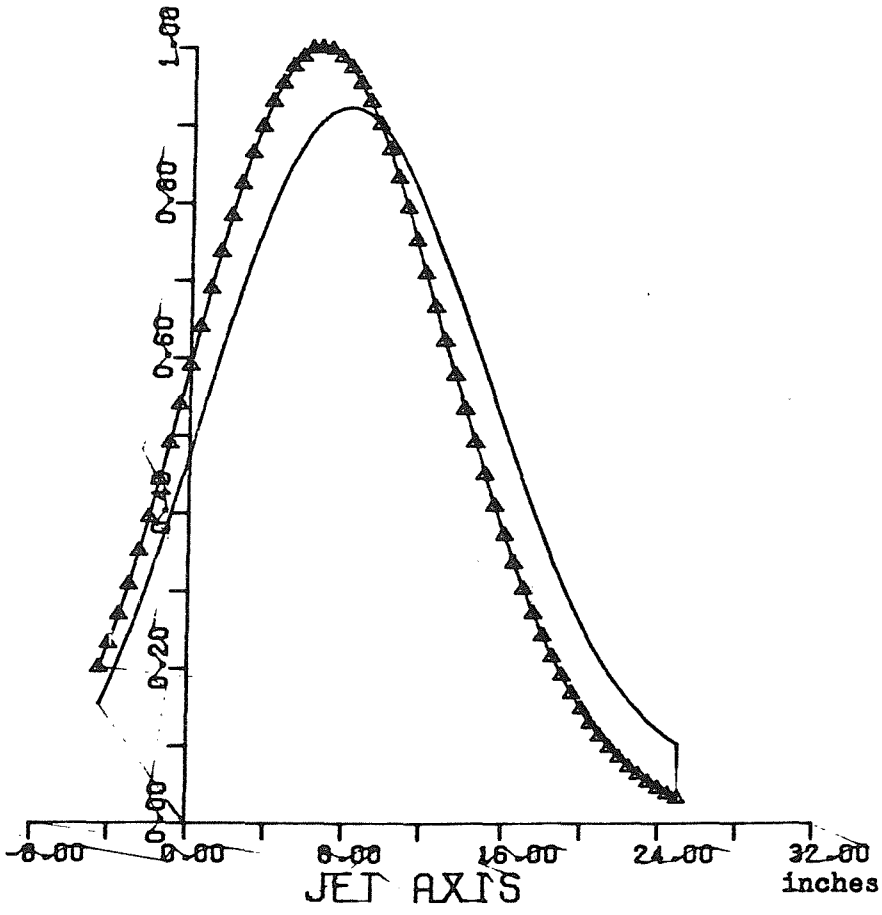

FIG.5.3.

SOURCE DISTRIBUTION FROM 1 INCH COLD JET

_____ Rear Arc Measurement

—△— Forward Arc Measurement

Aliasing Length = 62.75 in.

Resolution = 6.27 in.

Frequency = 2586.0 Hz

Strouhal No. = 0.5

U_J/a_o = 0.4

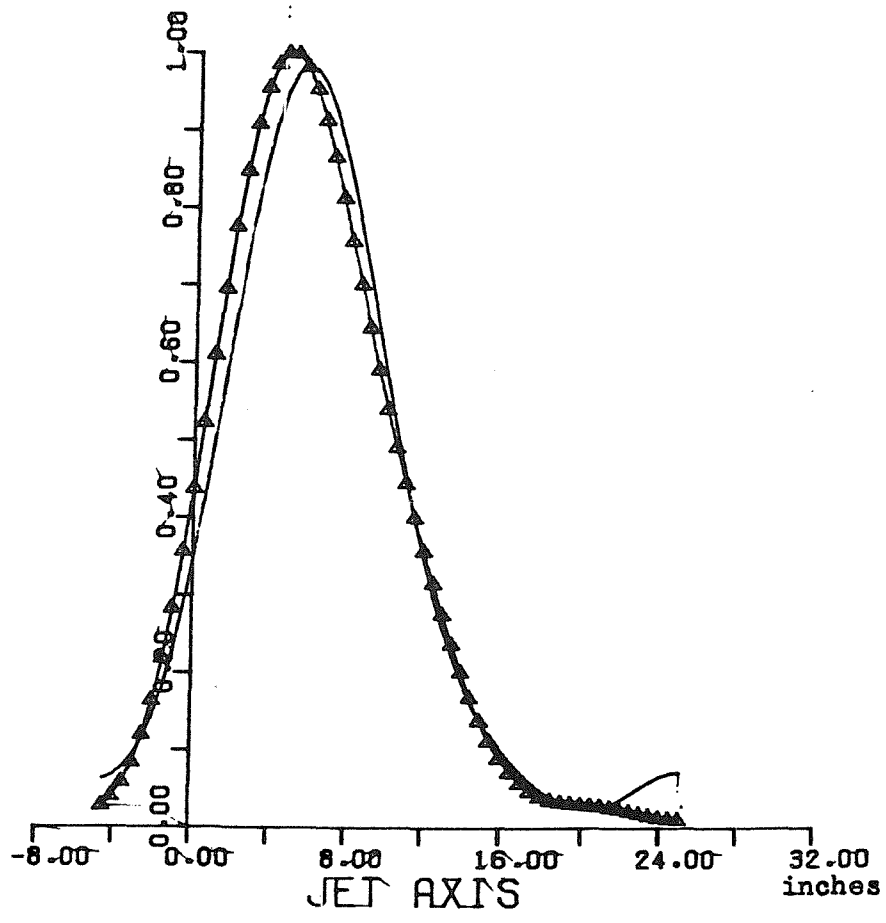

FIG. 5.4.

SOURCE DISTRIBUTION FROM 1 INCH COLD JET

_____ Rear Arc Measurement

—△— Forward Arc Measurement

Aliasing Length = 28.95 in.

Resolution = 2.89 in.

Frequency = 5603.0 Hz

Strouhal No. = 1.0

U_J/a_o = 0.4

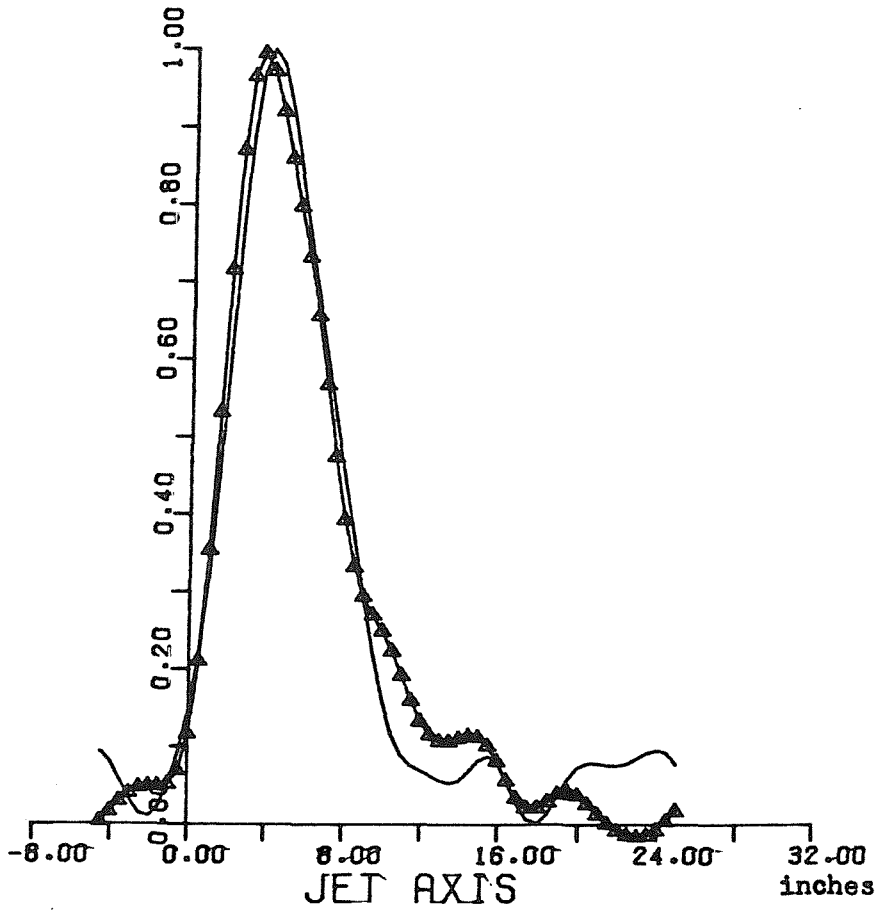

FIG.5.5.

SOURCE DISTRIBUTION FROM 1 INCH COLD JET

——— Rear Arc Measurement

—△— Forward Arc Measurement

Aliasing Length = 30.11 in.

Resolution = 3.0 in.

Frequency = 10775.0 Hz

Strouhal No. = 2.0

U_J/a_o = 0.4

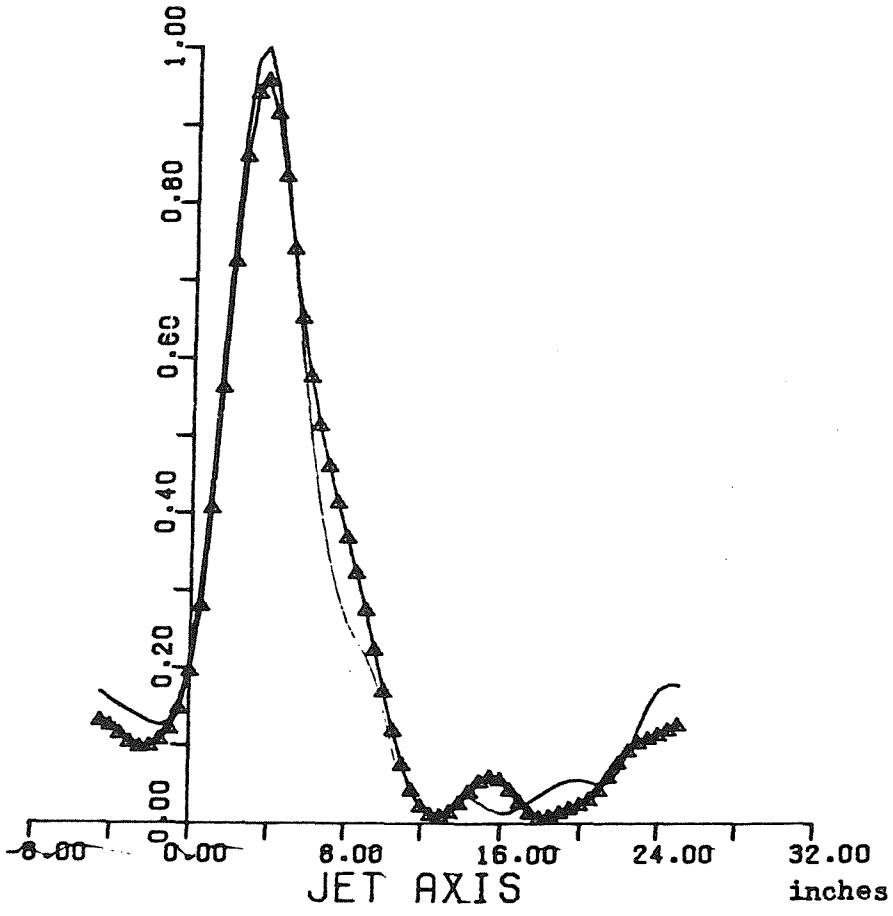

FIG.5.6.

SOURCE DISTRIBUTION FROM 1 INCH COLD JET

_____ Rear Arc Measurement

—△— Forward Arc Measurement

Aliasing Length = 125.5 in.

Resolution = 12.55 in.

Frequency = 1293.0 Hz

Strouhal No. = 0.12

U_J/a_o = 0.8

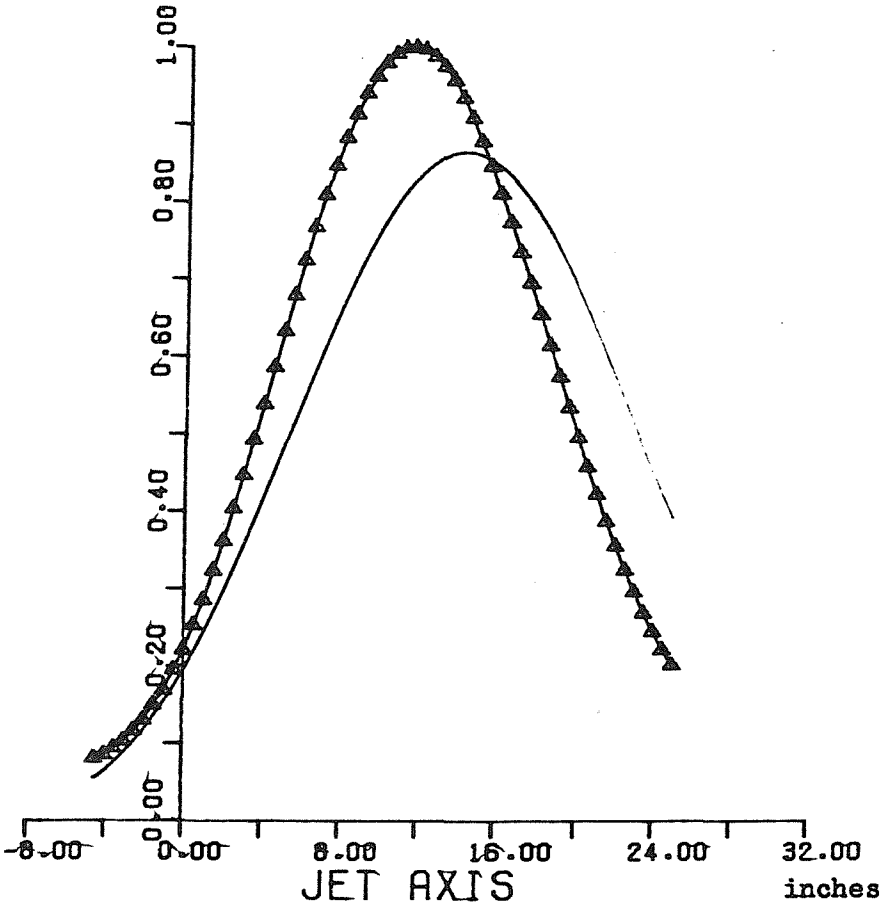

FIG.5.7.

SOURCE DISTRIBUTION FROM 1 INCH COLD JET

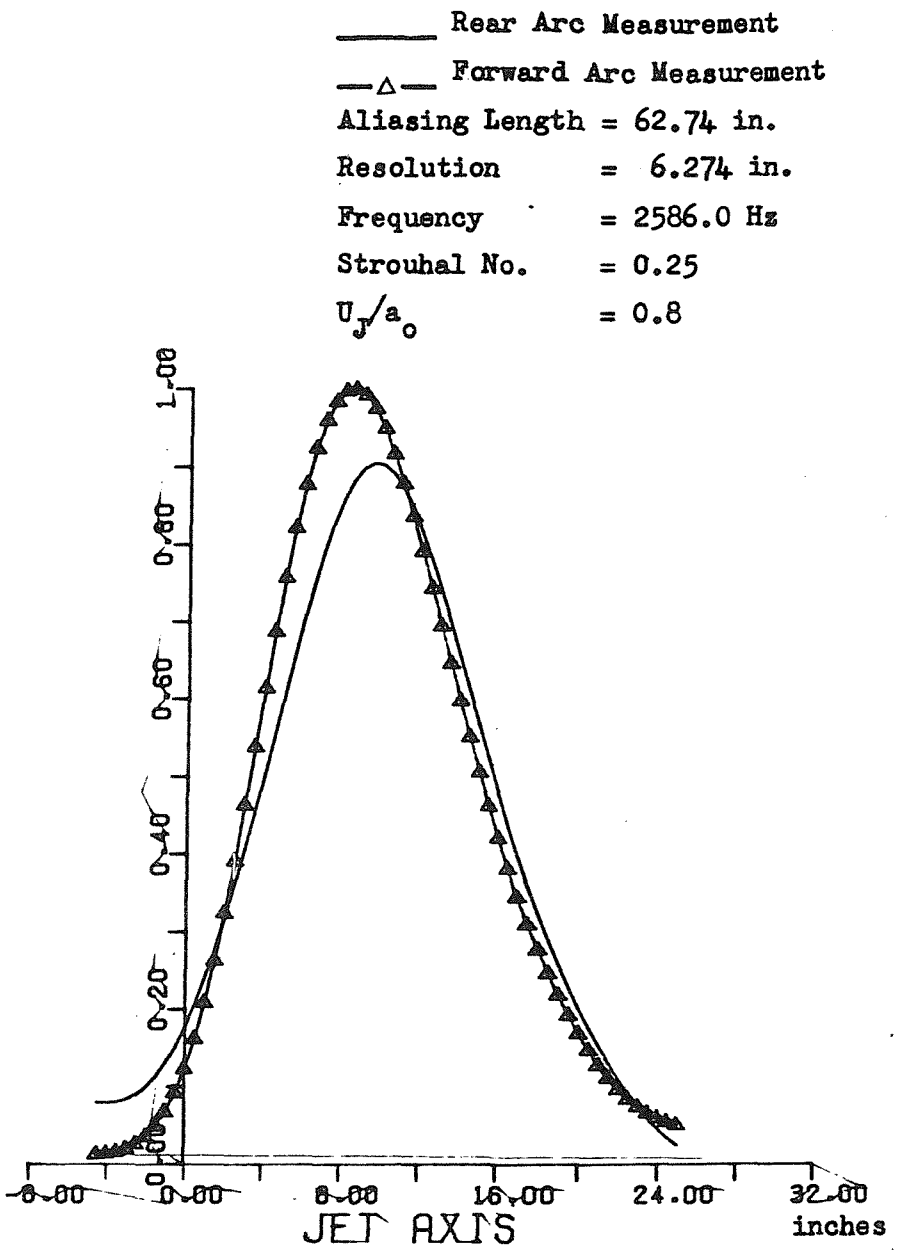

SOURCE DISTRIBUTION FROM 1 INCH COLD JET

——— Rear Arc Measurement

—△— Forward Arc Measurement

Aliasing Length = 28.95 in.

Resolution = 2.896 in.

Frequency = 5603 Hz

Strouhal No. = 0.5

U_J/a_o = 0.8

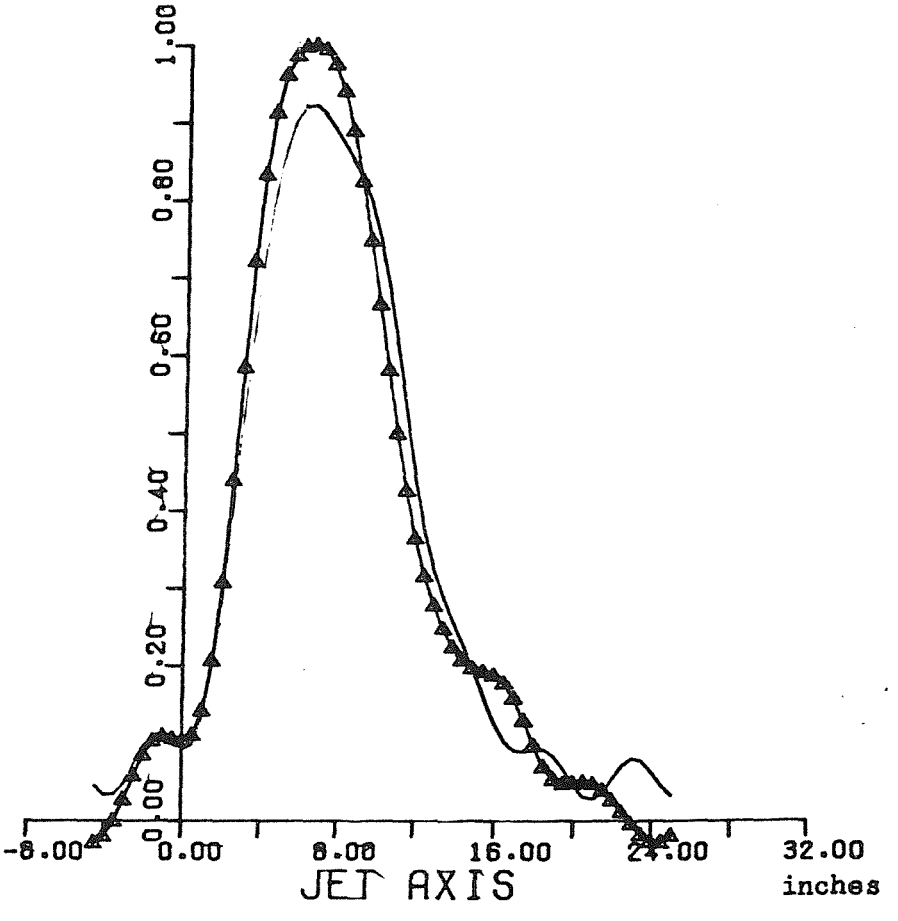

FIG. 5.9.

SOURCE DISTRIBUTION FROM 1 INCH COLD JET

_____ Rear Arc Measurement

—△— Forward Arc Measurement

Aliasing Length = 30 in.

Resolution = 3 in.

Frequency = 10775.0 Hz

Strouhal No. = 1.0

U_J/a_o = 0.8

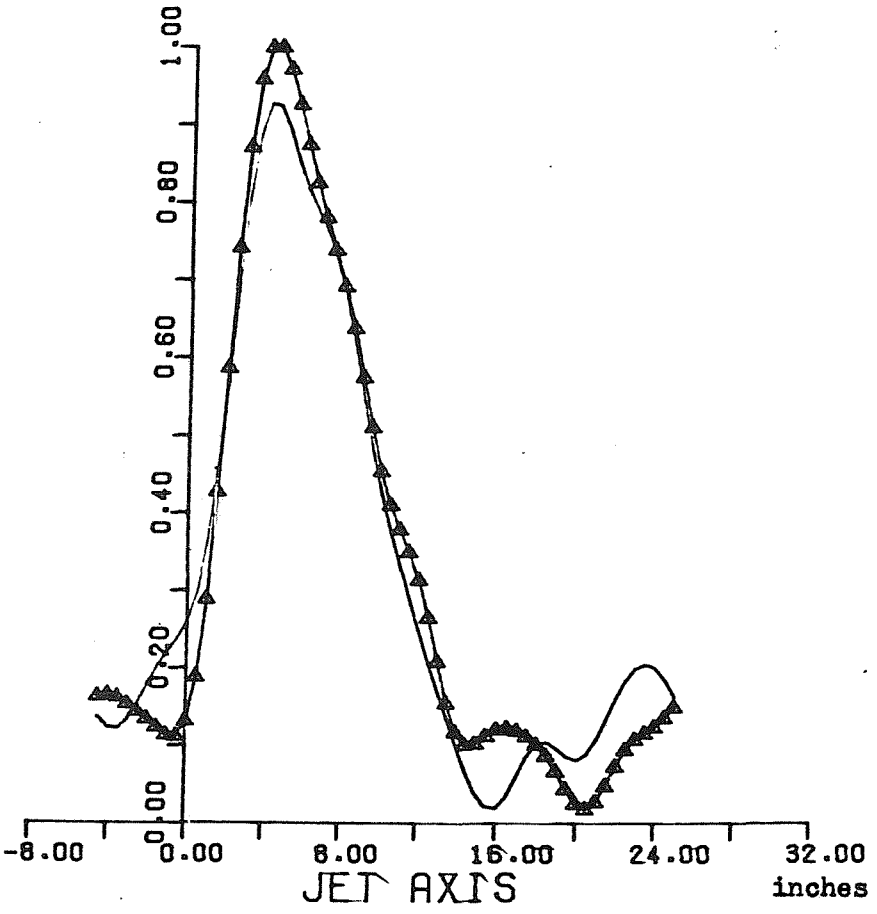

FIG.5.10.

SOURCE DISTRIBUTION FROM 1 INCH COLD JET

COMPARISON BETWEEN MODEL OF SOURCE DISTRIBUTION AND MEASUREMENTS

——— Measured Source Image U_J/a_o = 0.8; Strouhal No. = 0.48

△ Model of distribution (see eq.5.2.1)

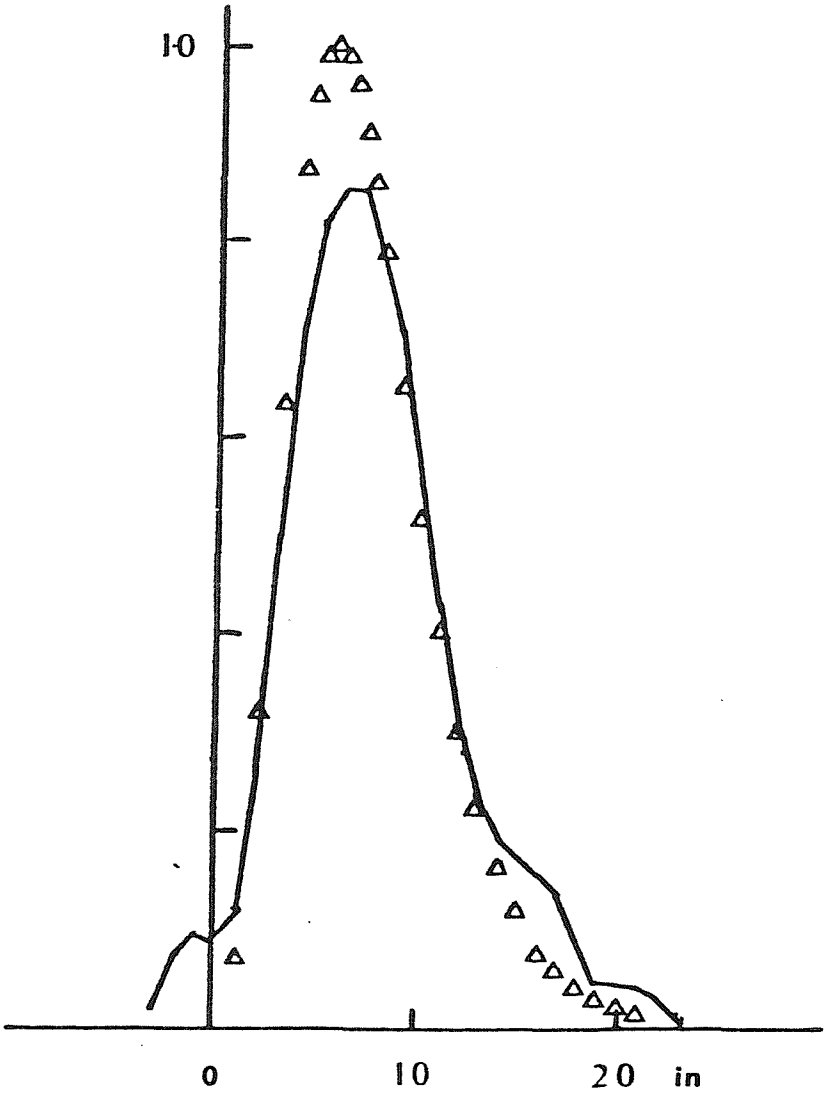

FIG.5.11.

MEASURED TIME DELAYS FROM LOUDSPEAKER TESTS

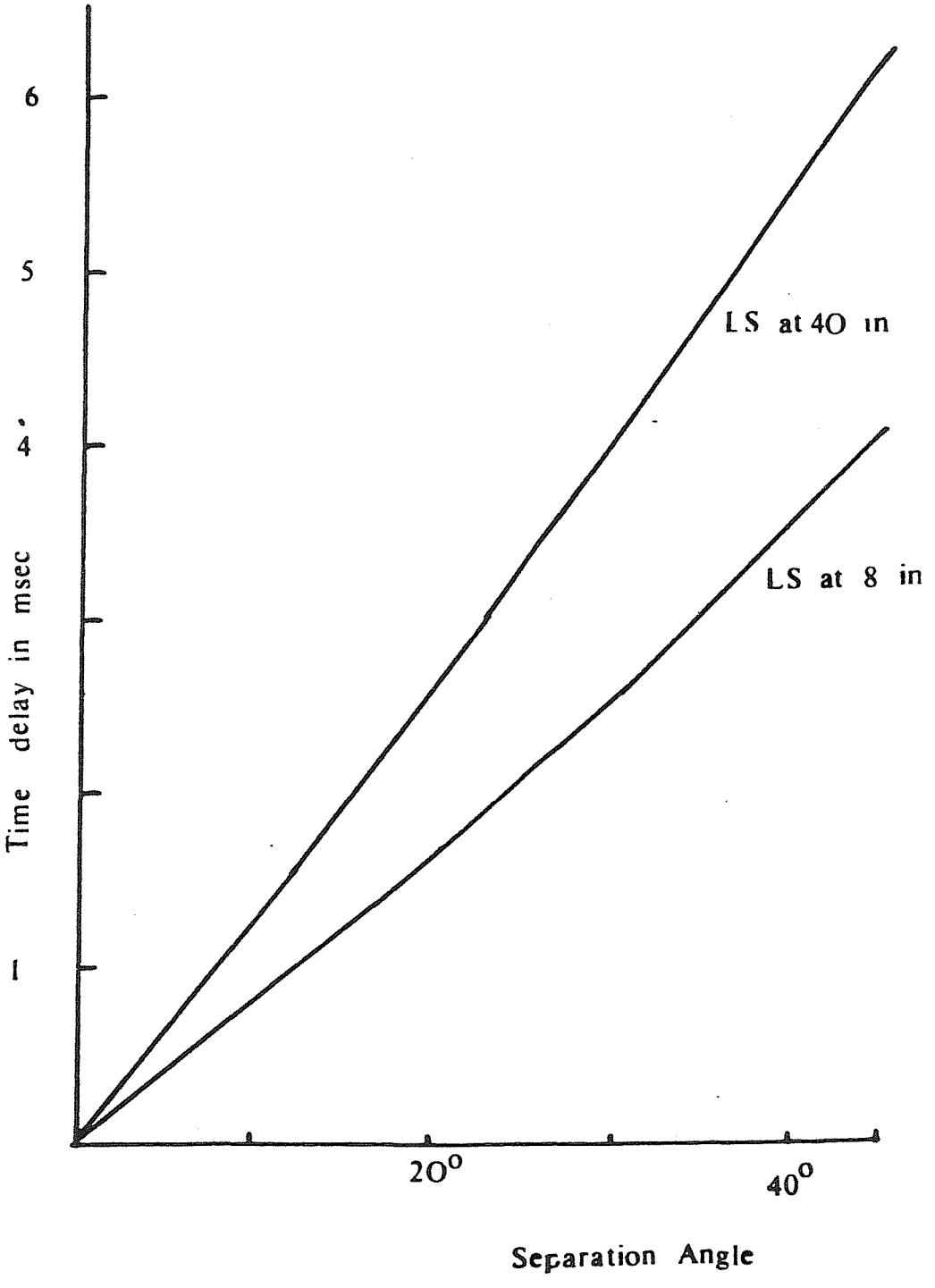

FIG.5.12.

TIME DELAY CORRECTION FACTORS FOR POLAR ARC CENTRE MISALIGNMENT

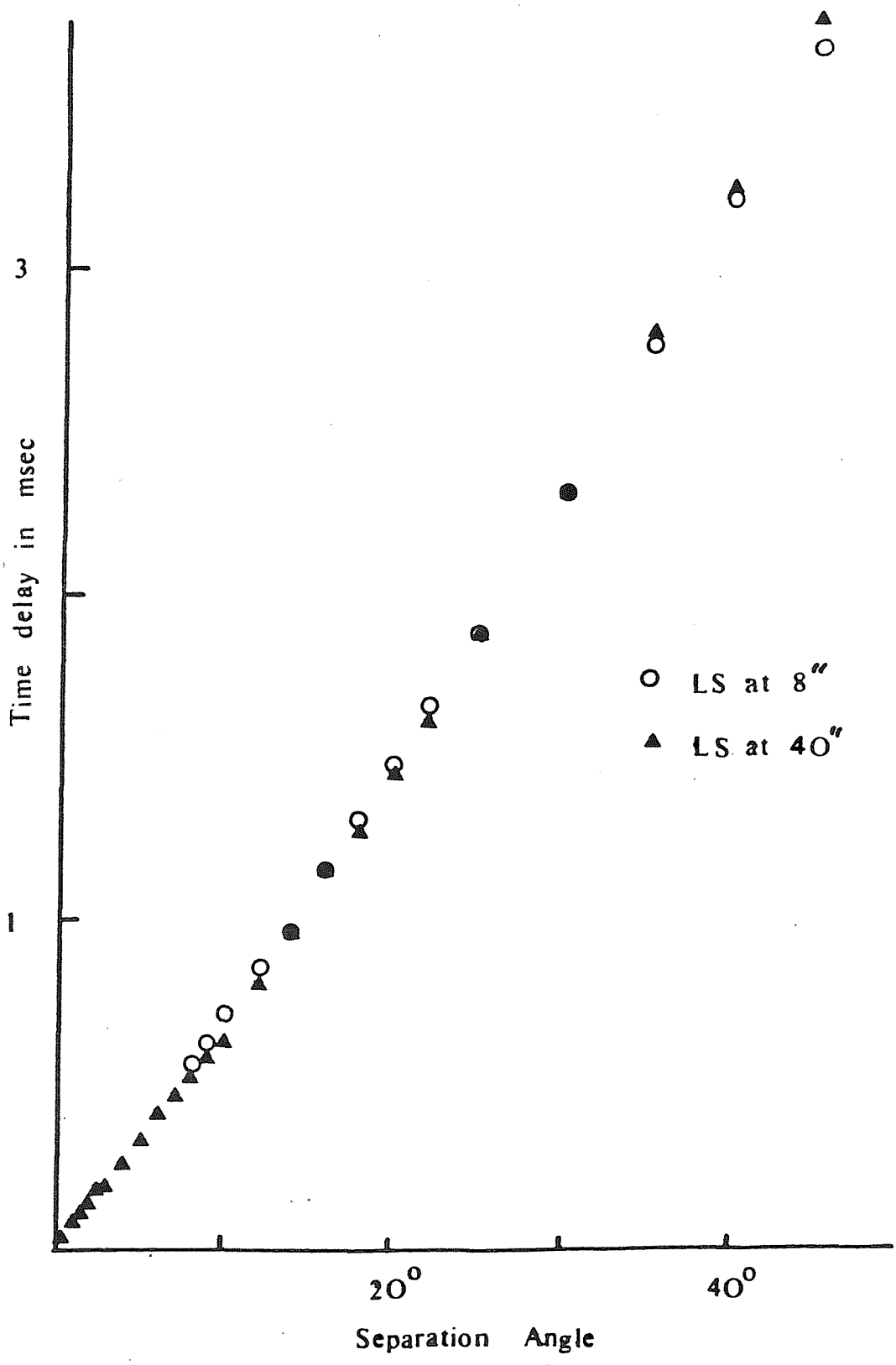

FIG.5.13.

SPECTRA AT 92° TO JET AXIS

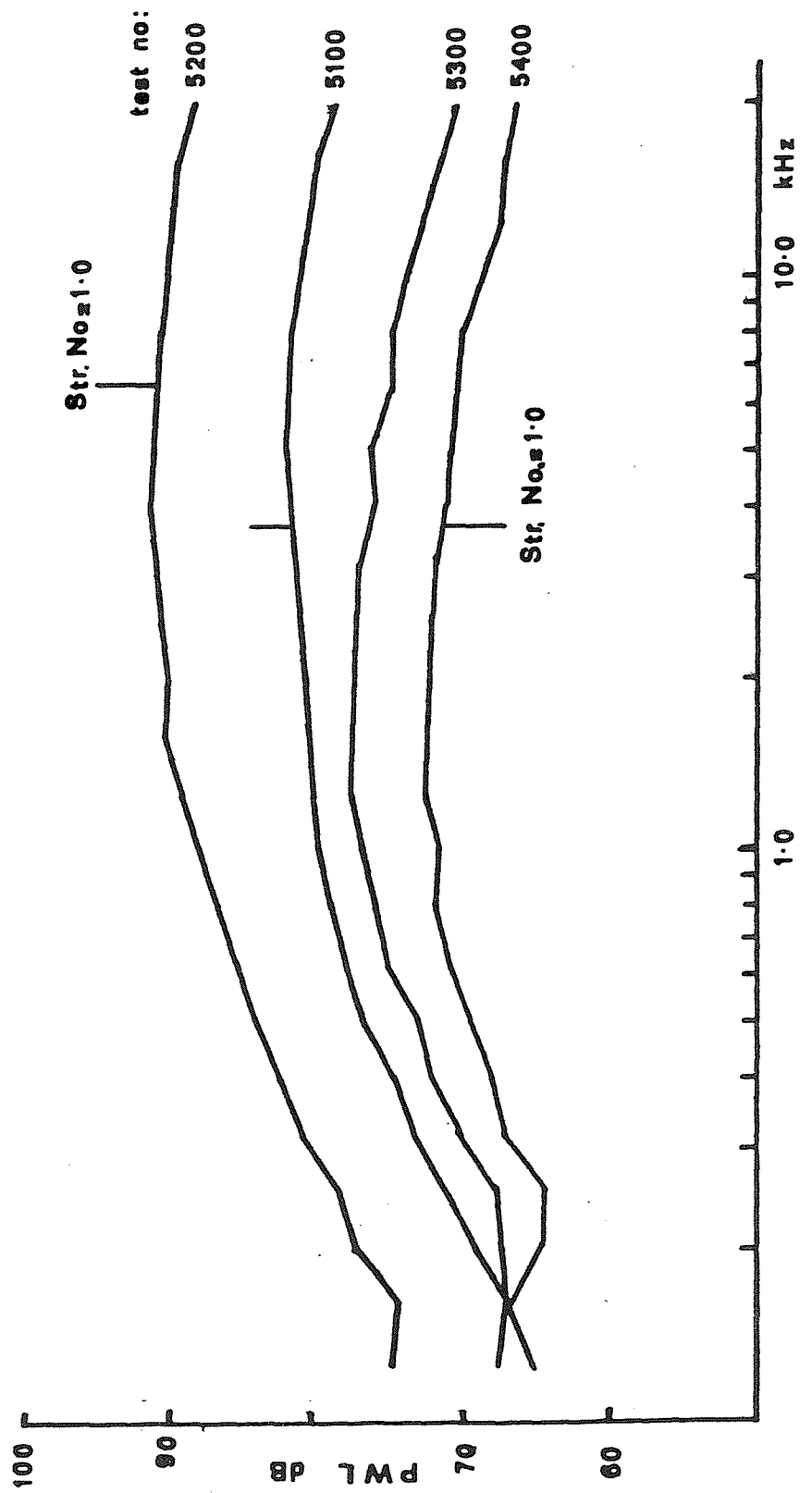

FIG.5.14.

RESULTS FROM NOISE TESTS FACILITY AT NGTE

Vp = 307 m/s
(12.09 x 10^3 in/sec)

Temp = 880°K

—■— Frequency= 1070 Hz
Resolution= 76.9 in

——— Frequency= 3569 Hz
Resolution= 23 in

—▲— Frequency= 7140 Hz
Resolution= 11.5 in

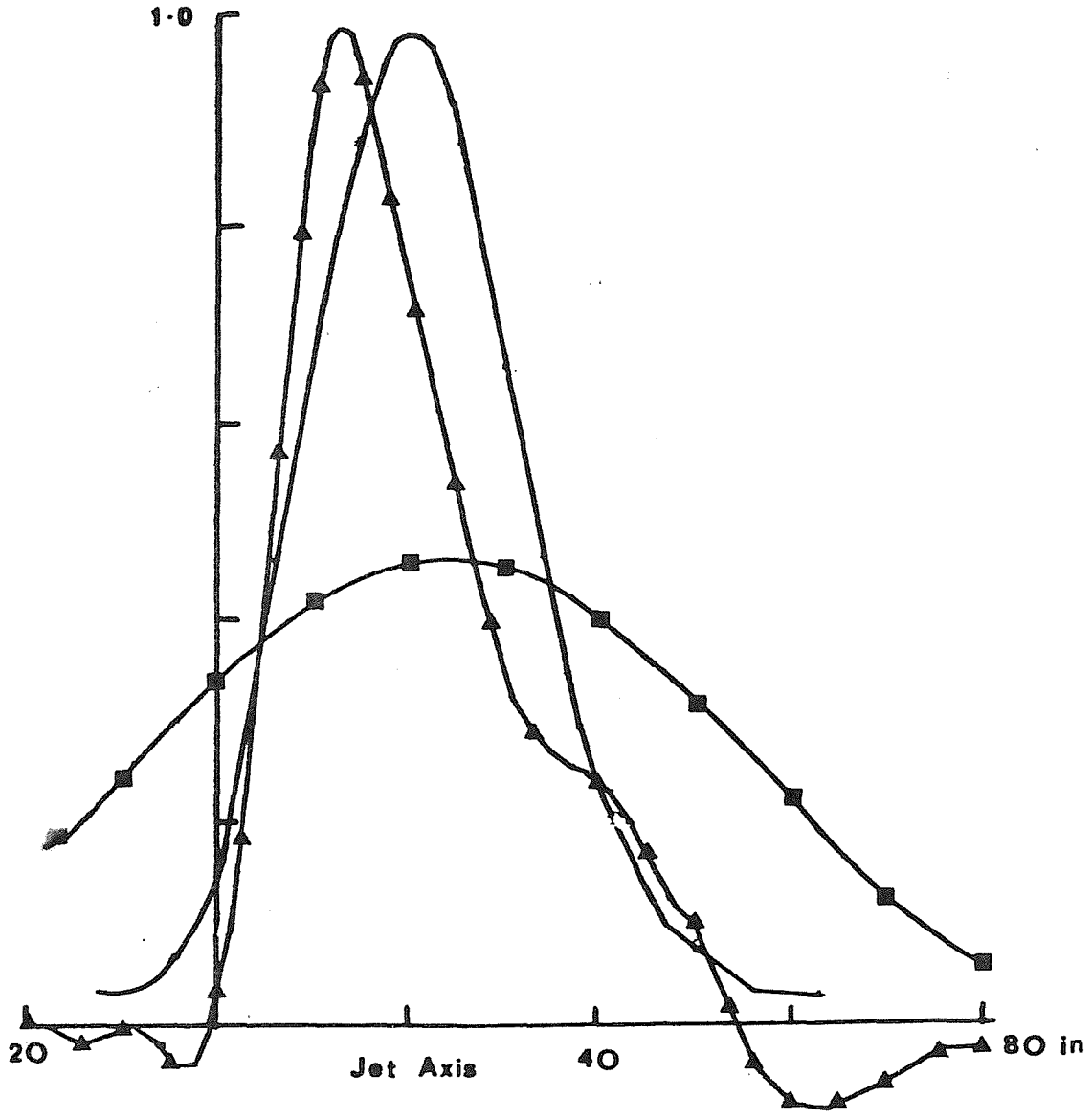

FIG.5.15.

RESULTS FROM NOISE TEST FACILITY AT NGTE

Vp = 507 m/s
(19.96 x 10^3 in/sec
Temp = 880°K

Frequency= 1848 Hz
Resolution= 44.5 in

Frequency= 6161 Hz
Resolution= 13.35 in

Frequency= 12322 Hz
Resolution= 6.678 in

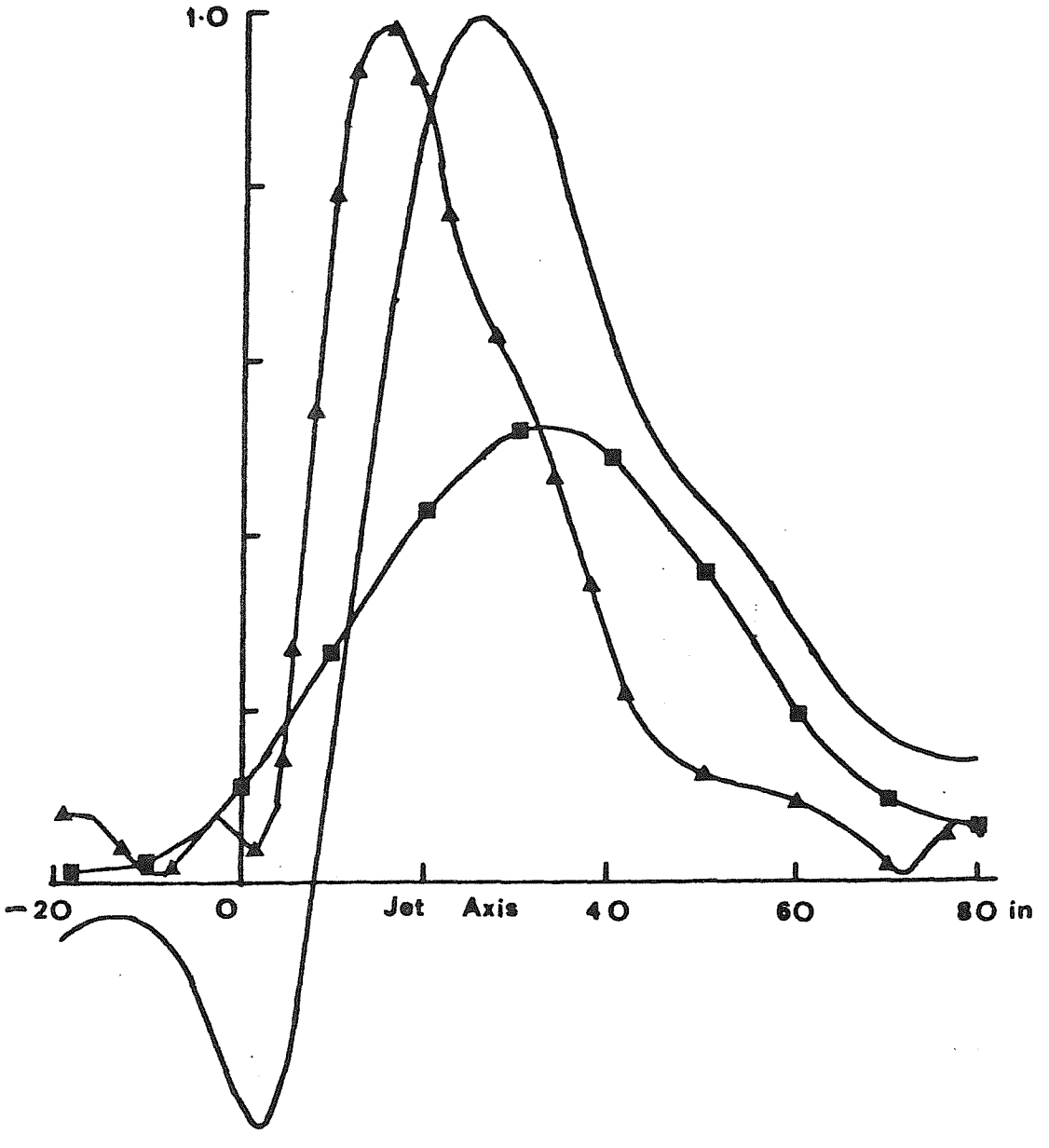

FIG.5.16.

RESULTS FROM NOISE TEST FACILITY AT NGTE

Vp = 307 m/s
Nozzle Diameter = 3.4 in.
Frequency = 1070 Hz
Resolution = 20 in.
Aliasing Length = 140.4 in.
Strouhal No. = 0.3

——— T = 300°K, V_s = 0
—△— T = 880°K, V_s = 0
—+— T = 880°K, V_s = 60 m/s

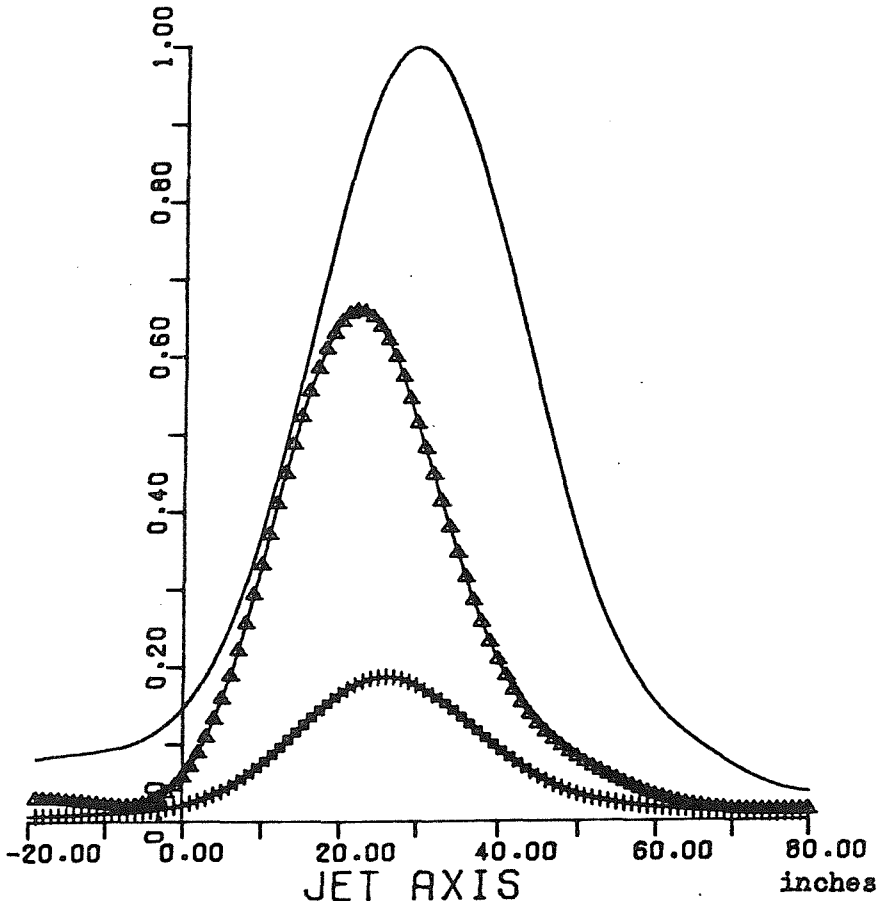

RESULTS FROM NOISE TEST FACILITY AT NGTE

Vp = 307 m/s
Nozzle Diameter = 3.4 in
Frequency = 3569.0
Resolution = 138.33 in.
Aliasing Length = 11.52 in.
Strouhal No. = 1.0

——— T = 300°K, V_s = 0
—△— T = 880°K, V_s = 0
—+— T = 880°K, V_s = 6- m/s

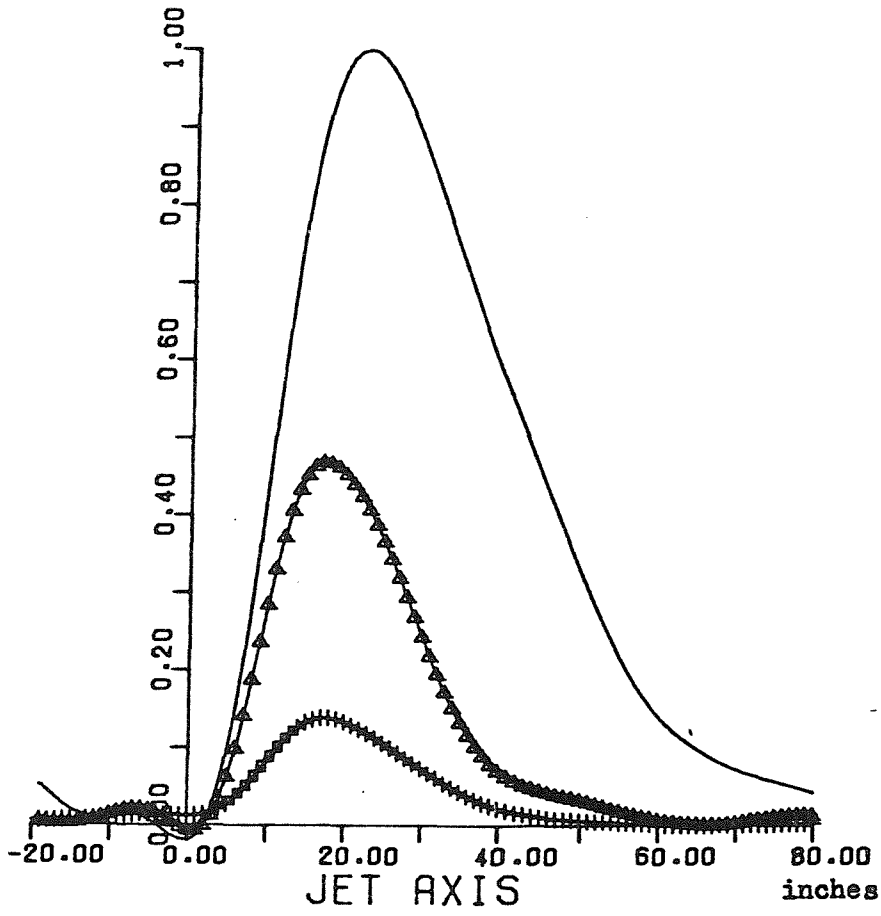

FIG.5.18.

RESULTS FROM NOISE TEST FACILITY AT NGTE

Vp = 307 m/s
Nozzle Diameter = 3.4in
Frequency = 7140 Hz
Resolution = 11.52 in.
Aliasing Length = 138.3 in.
Strouhal No. = 2.0

——— T = 300°K, V_s = 0
—△— T = 880°K, V_s = 0
—+— T = 880°K, V_s = 60 m/s

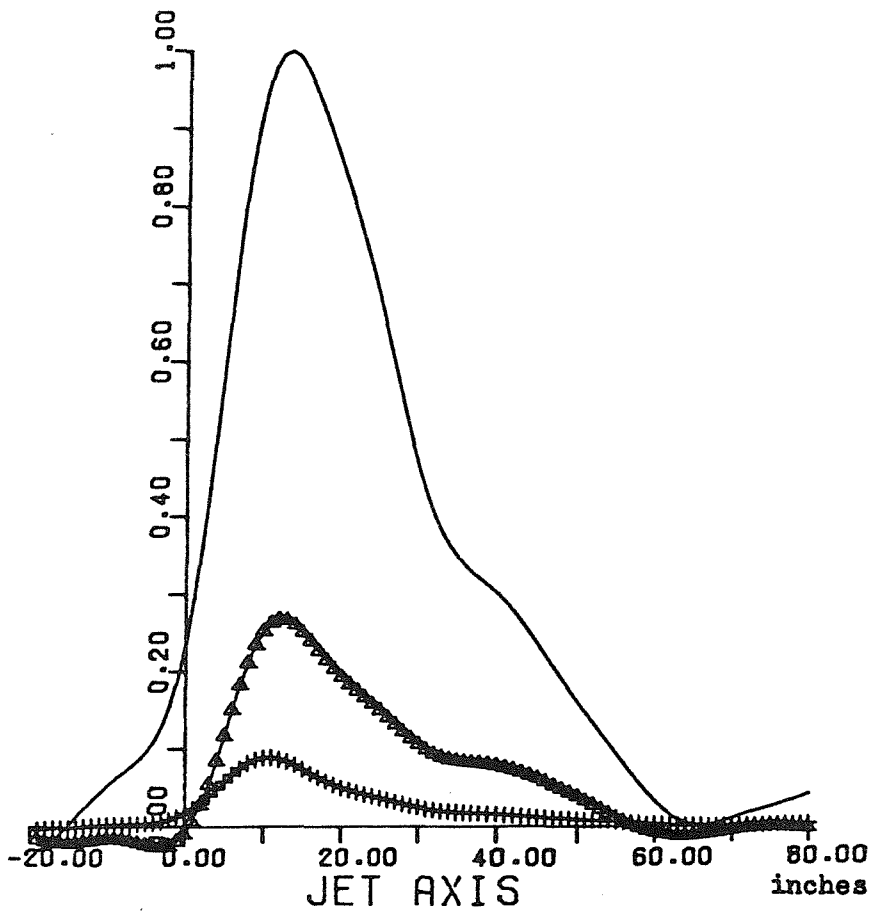

FIG.6.1.

SCALED DIAGRAM OF ENGINE

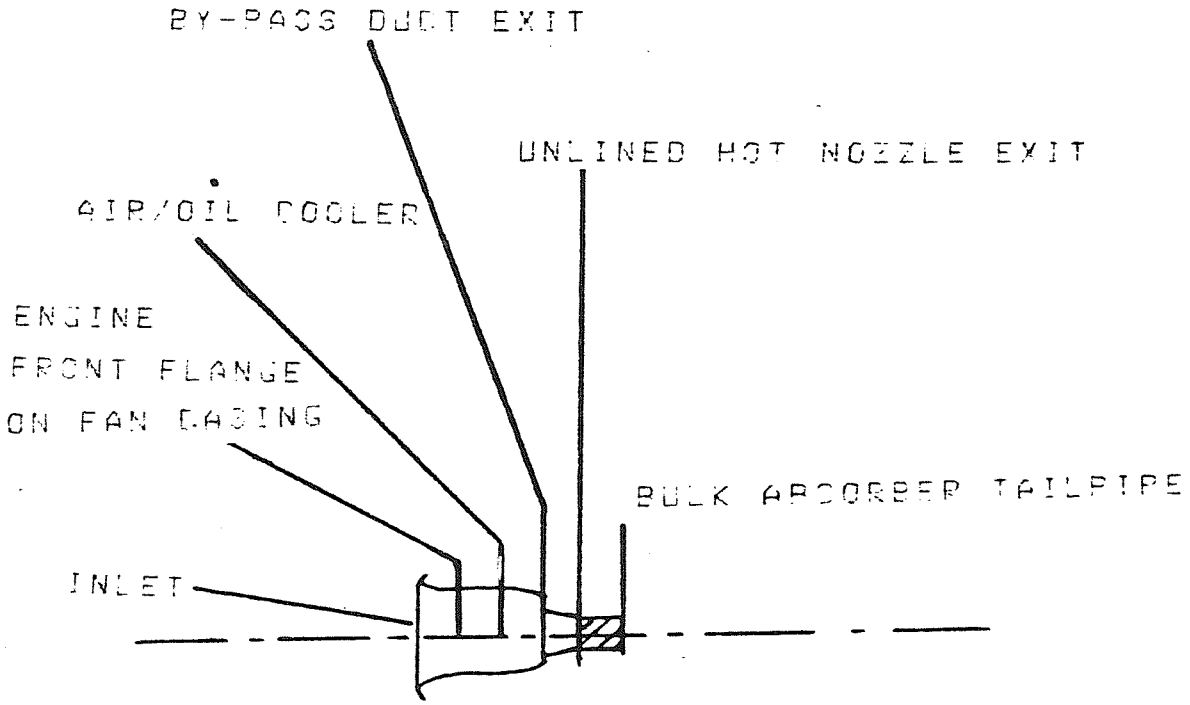

FIG.6.2.

RESULTS FROM RB.211 Q.E.D.

250 Hz **60% N.L.**

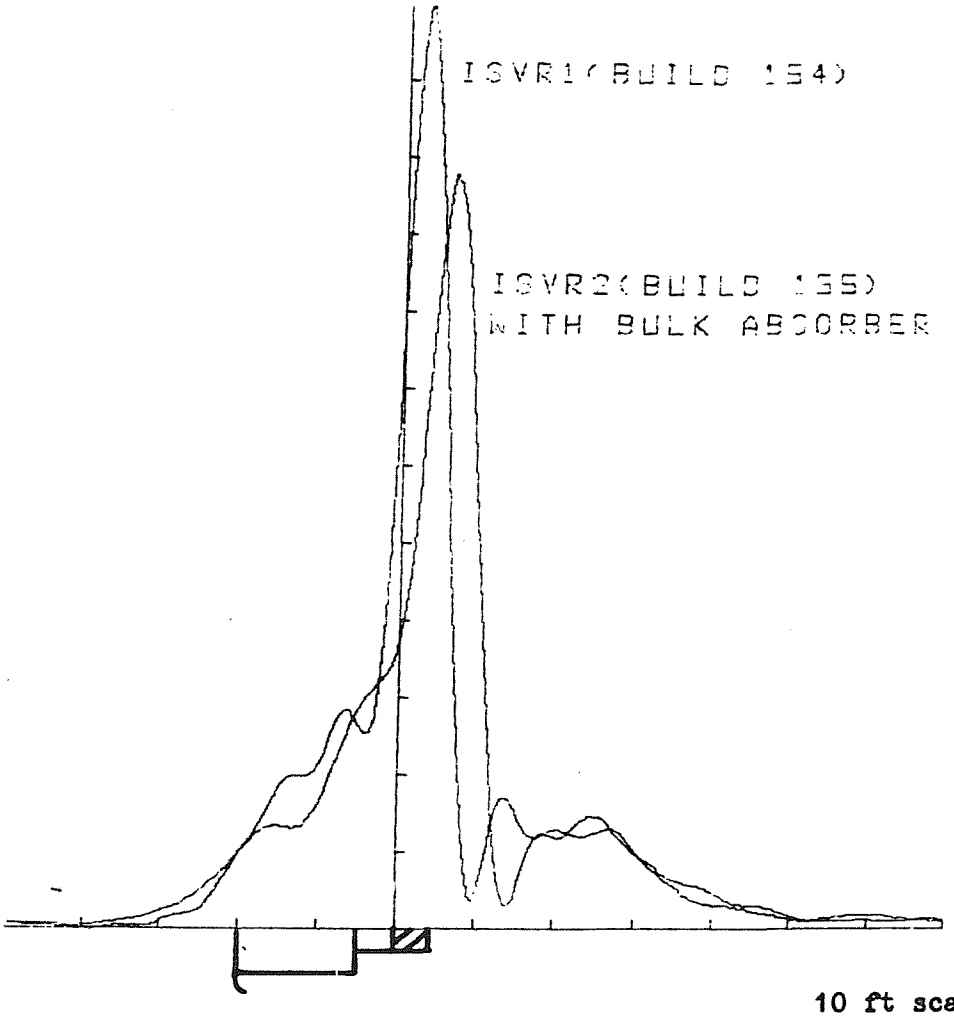

10 ft scale

FIG.6.3.

RESULTS FROM RB.211 Q.E.D.

250 Hz 90% N.L.

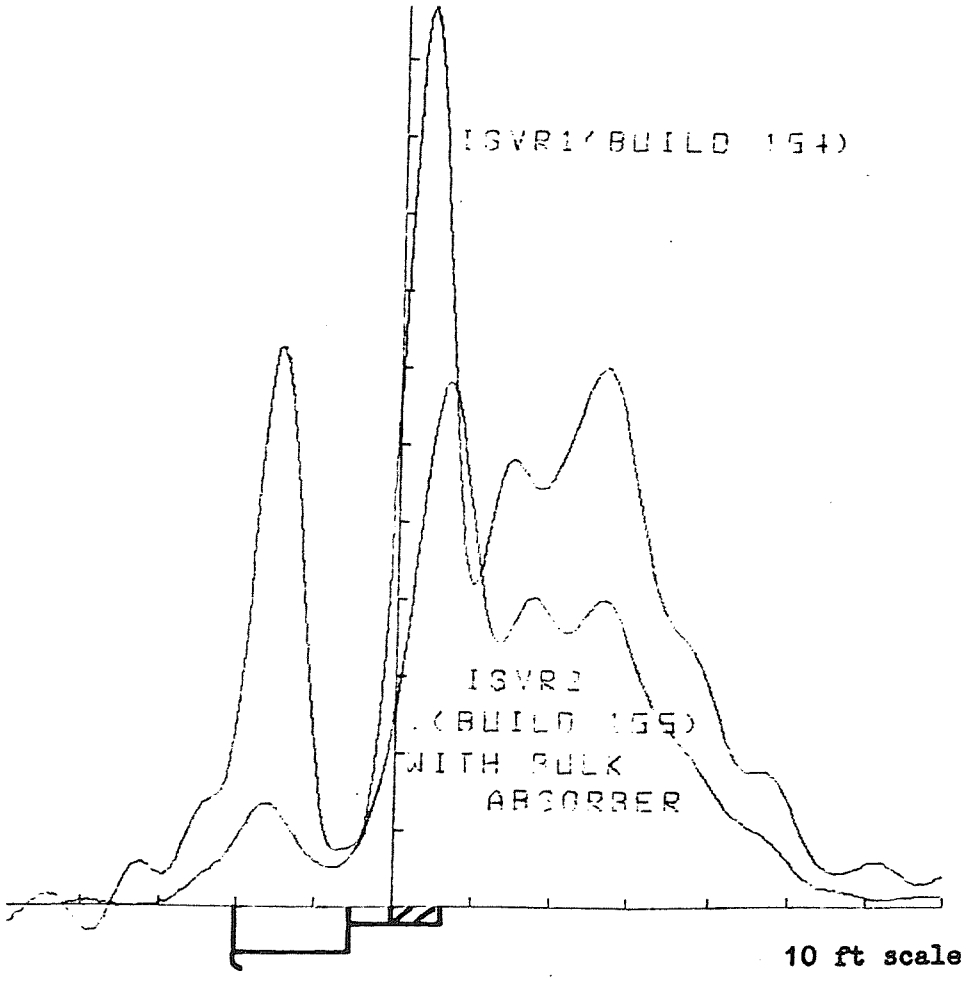

FIG.6.4.

RESULTS FROM RB.211 Q.E.D.

500 Hz 60% N.L.

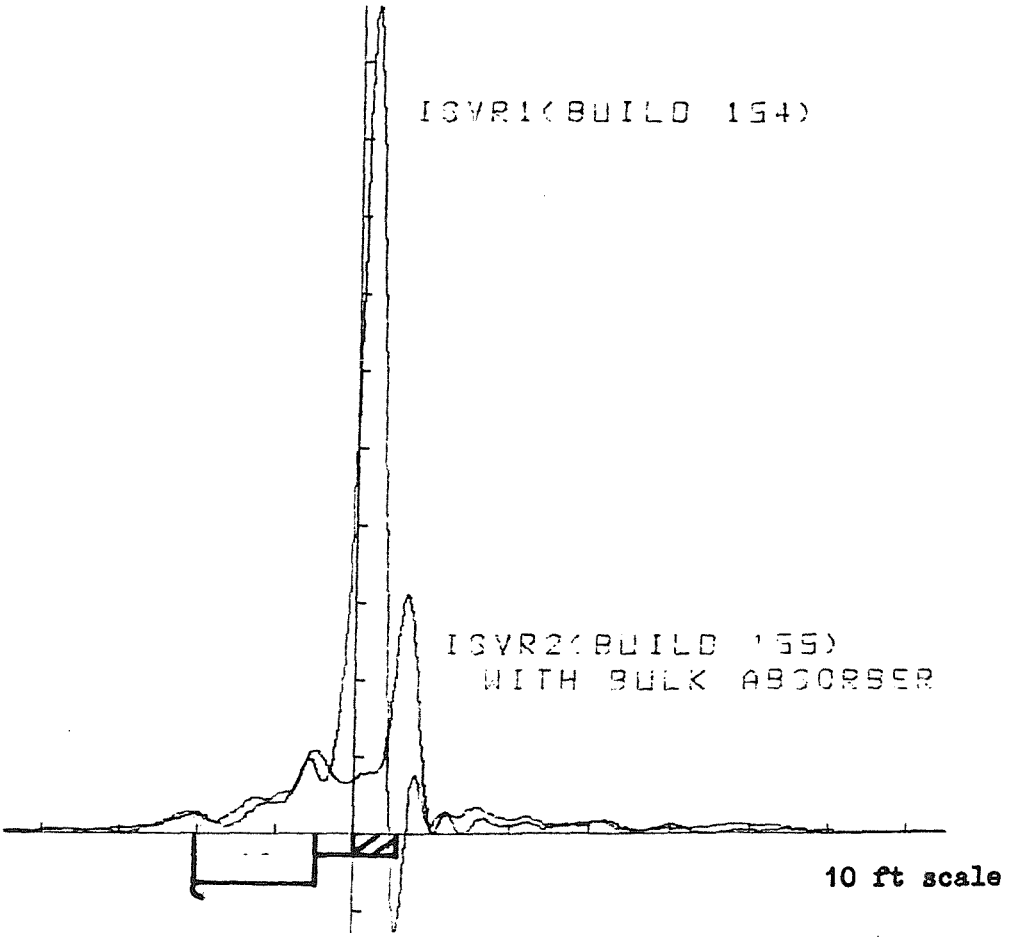

FIG.6.5.

RESULTS FROM RB.211 Q.E.D.

500 Hz 90% N.L.

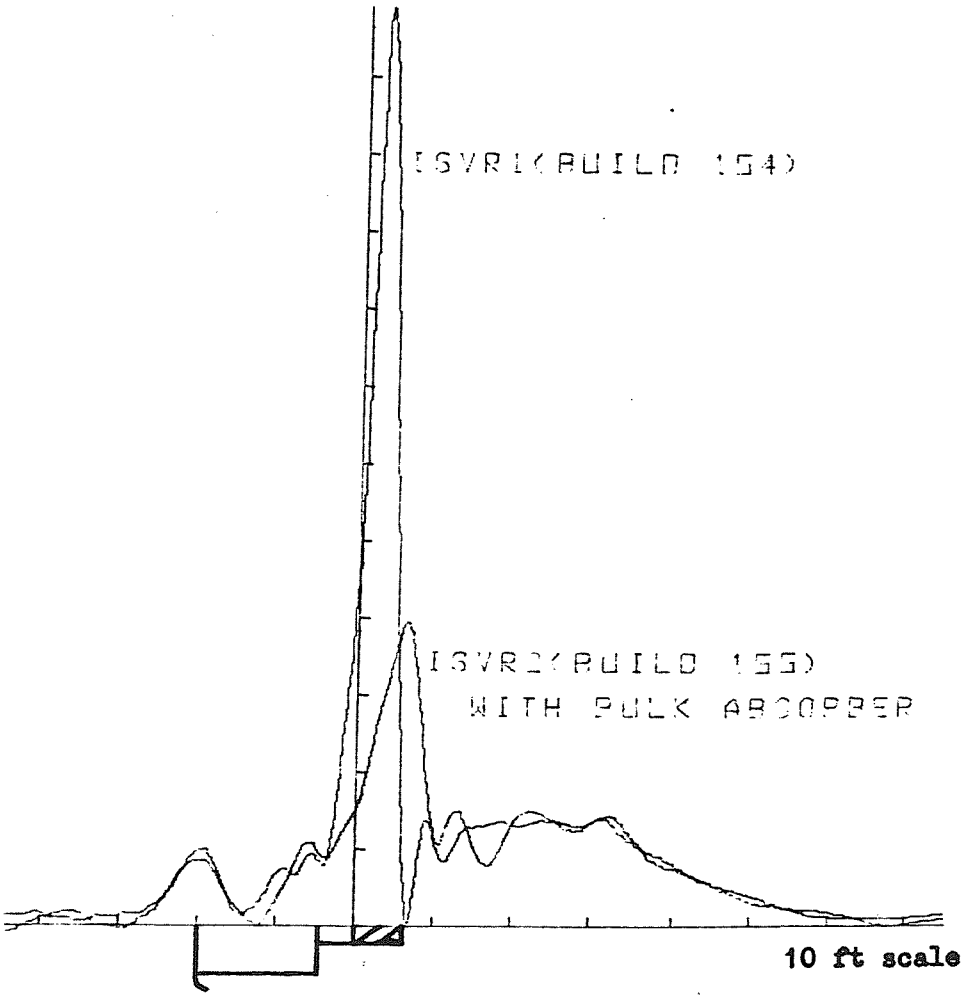

FIG.6.6.

RESULTS FROM RB.211 Q.E.D.

1000 Hz **60% N.L.**

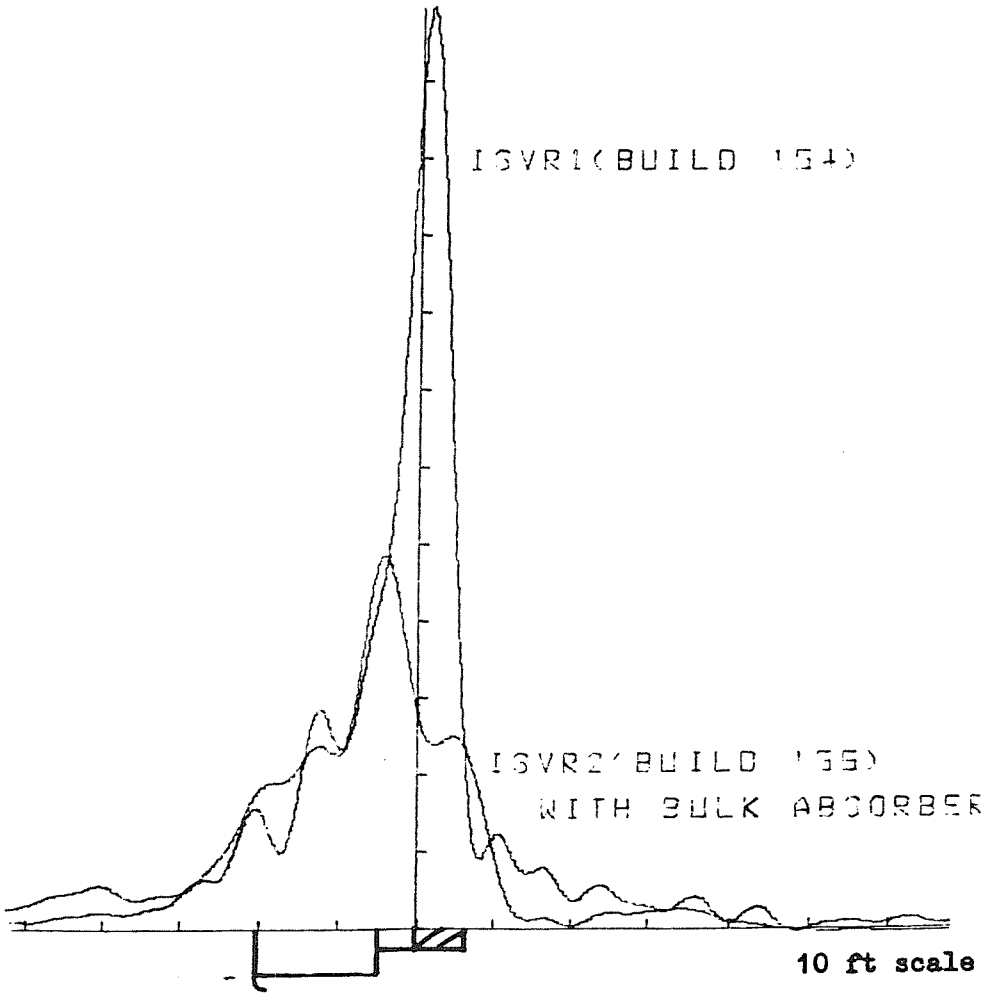

FIG.6.7.

RESULTS FROM RB.211 Q.E.D.

1000 Hz **90% N.L.**

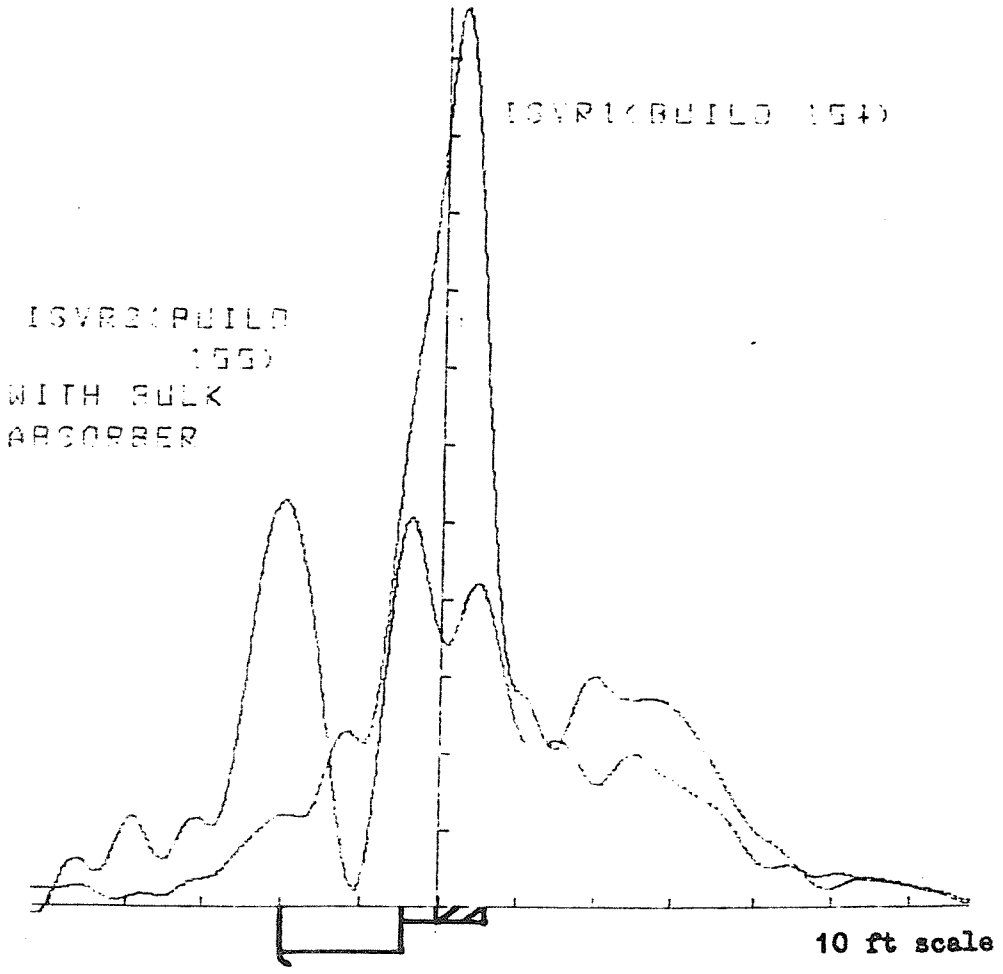

FIG.6.8.

RESULTS FROM RB.211 Q.E.D.

2250 Hz 60% N.L.

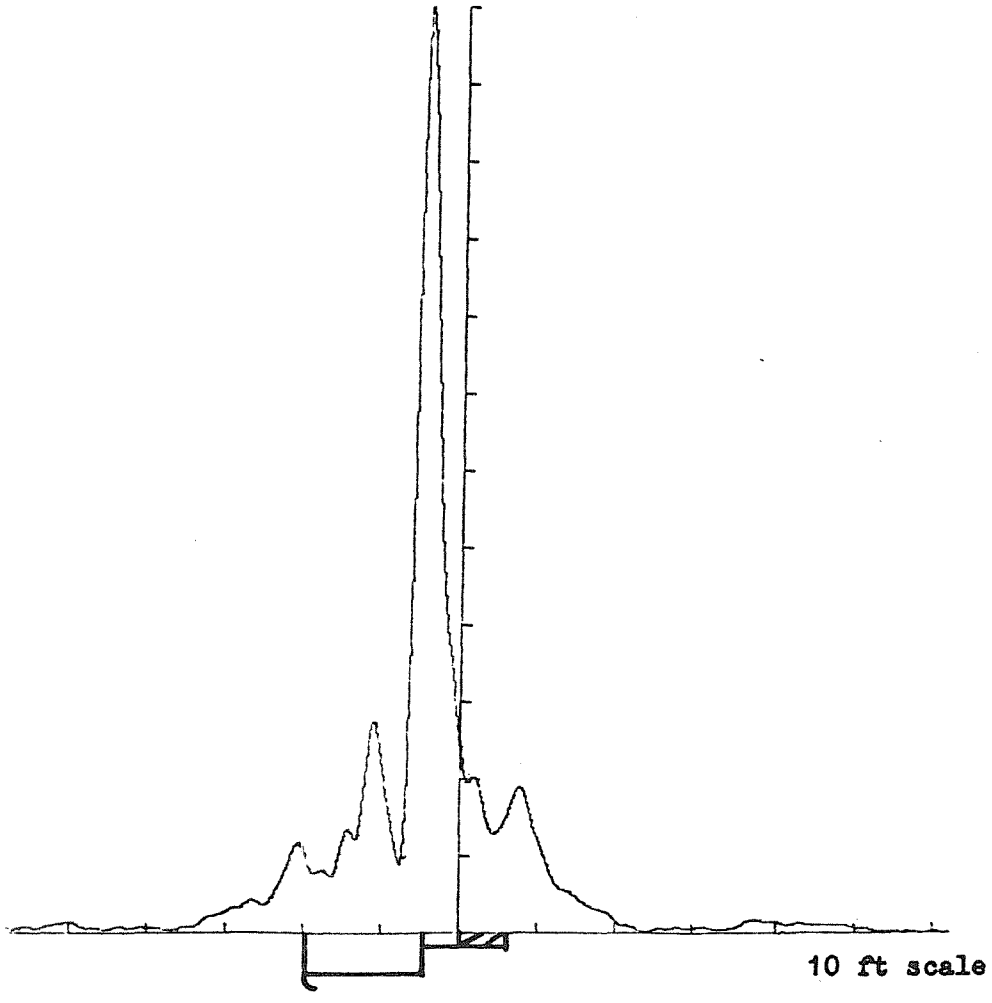

FIG.6.9.

FIG.

RESULTS FROM RB.211 Q.E.D.

3380 Hz 90% N.L.

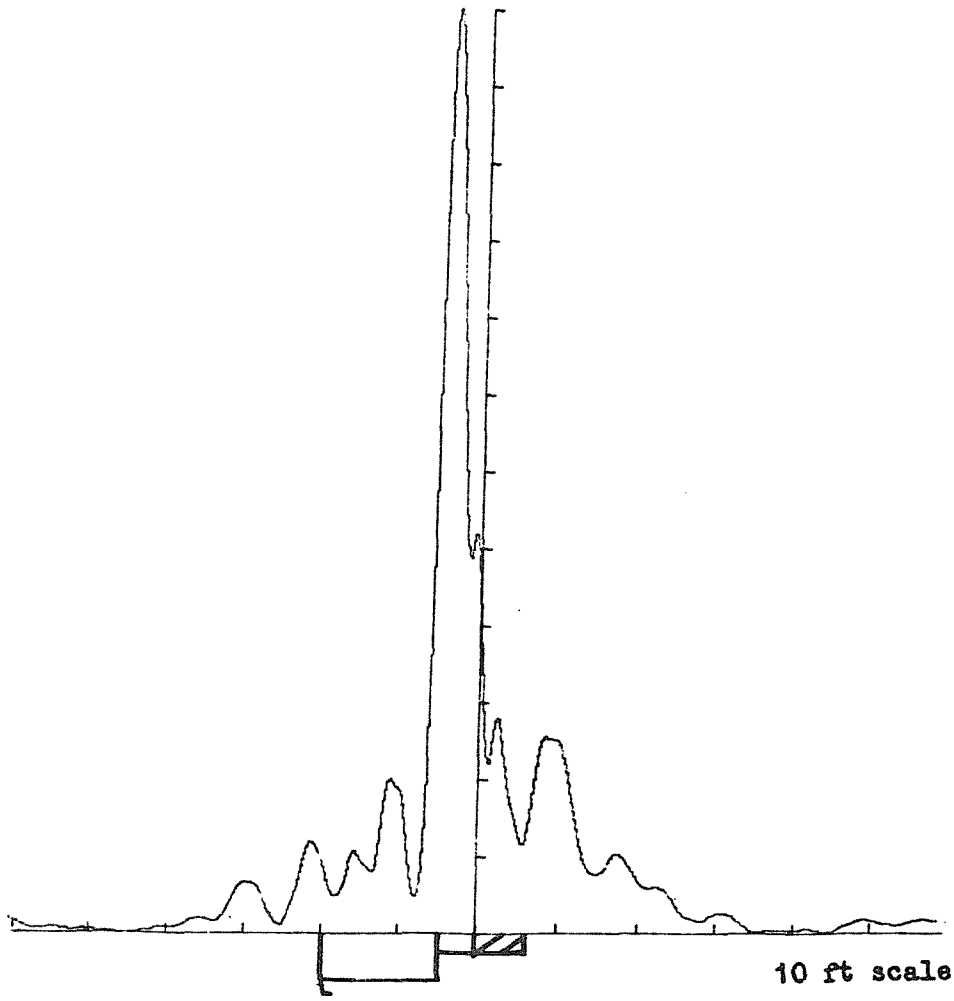

FIG.6.10.

RESULTS FROM RB.211 Q.E.D.

500 Hz 75% N.L.

(40° Aperture)

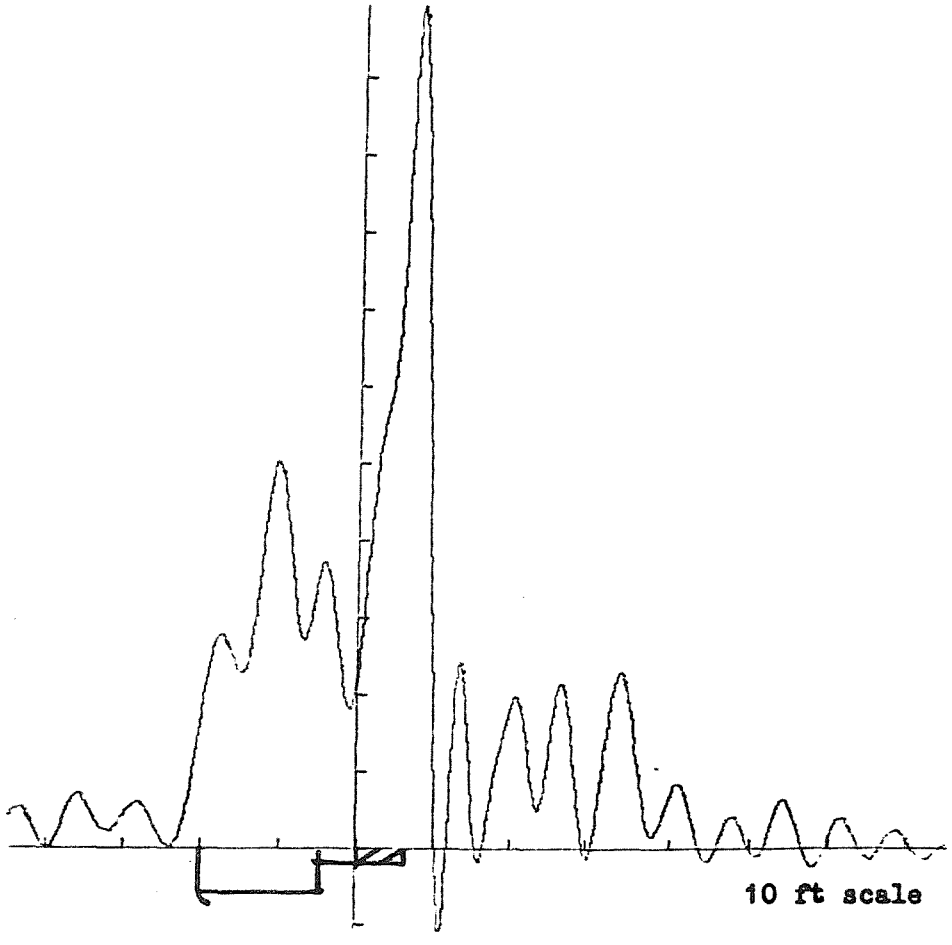

FIG.6.11.

RESULTS FROM RB.211 Q.E.D.

500 Hz 75% N.L.

(20° Aperture)

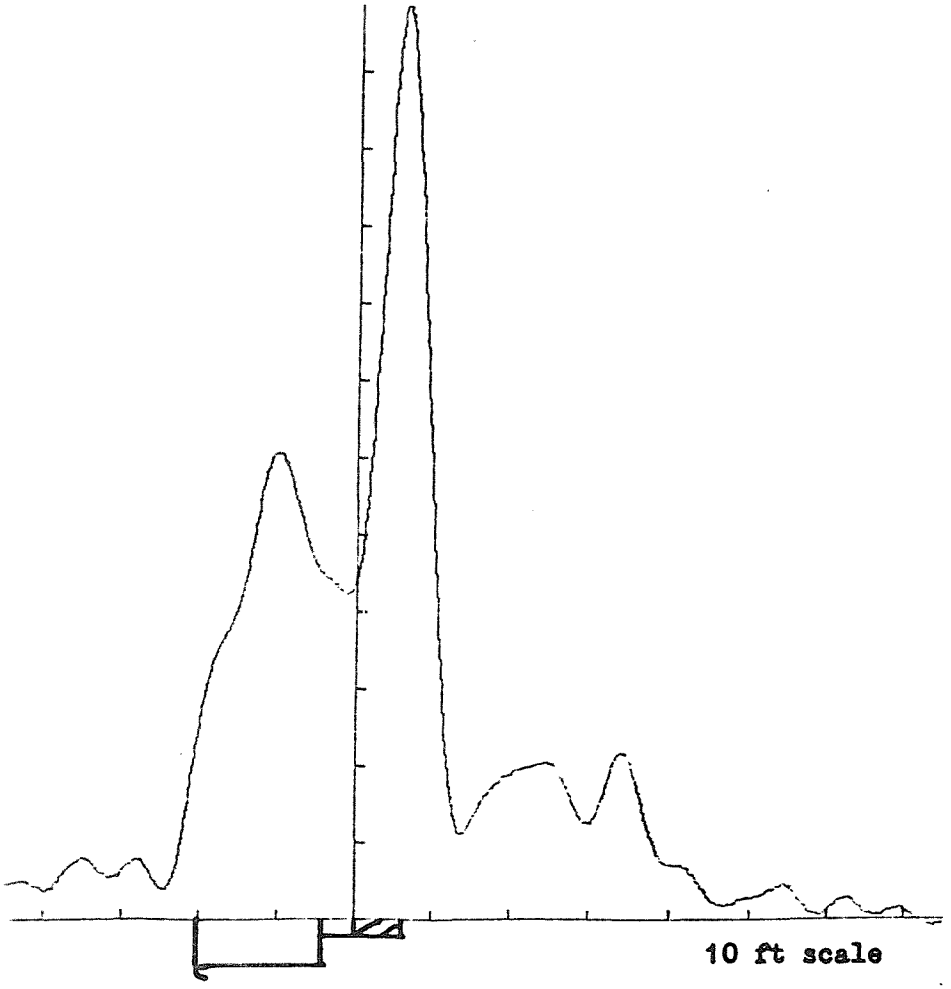

FIG.6.12.

RESULTS FROM RB.211 Q.E.D.

500 Hz 75% N.L.

(10° Aperture)

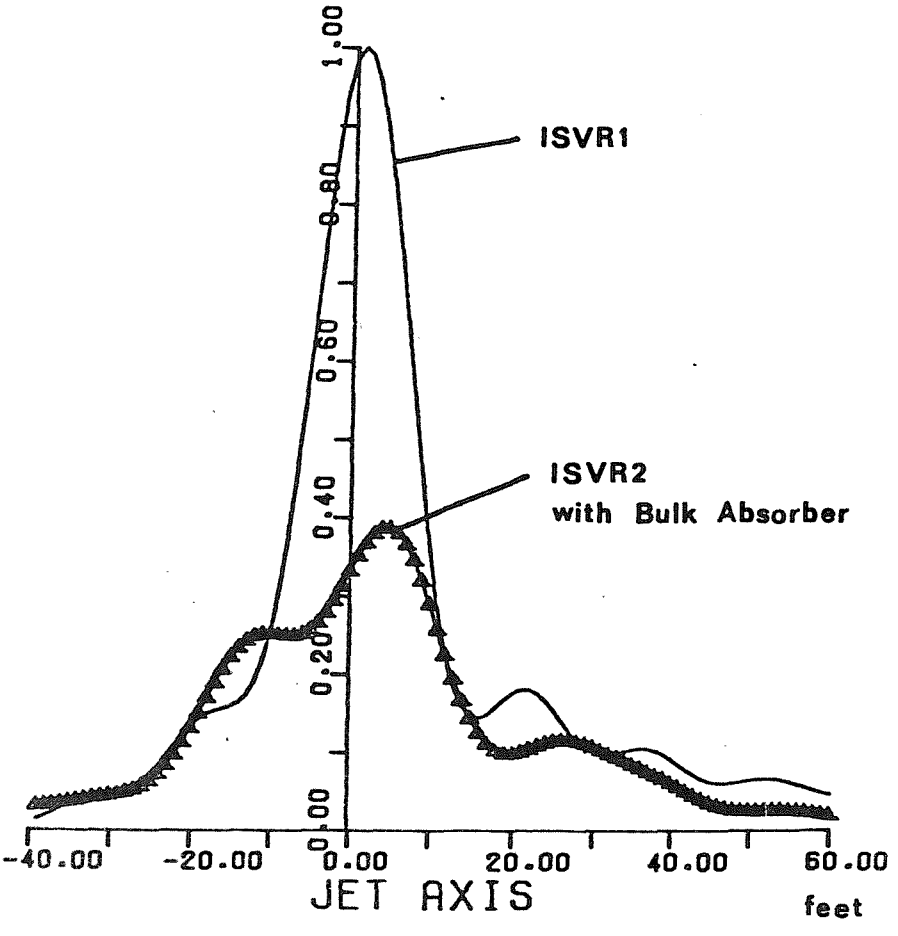

FIG.6.13.

INTEGRATED BARTLETT WINDOW FUNCTION

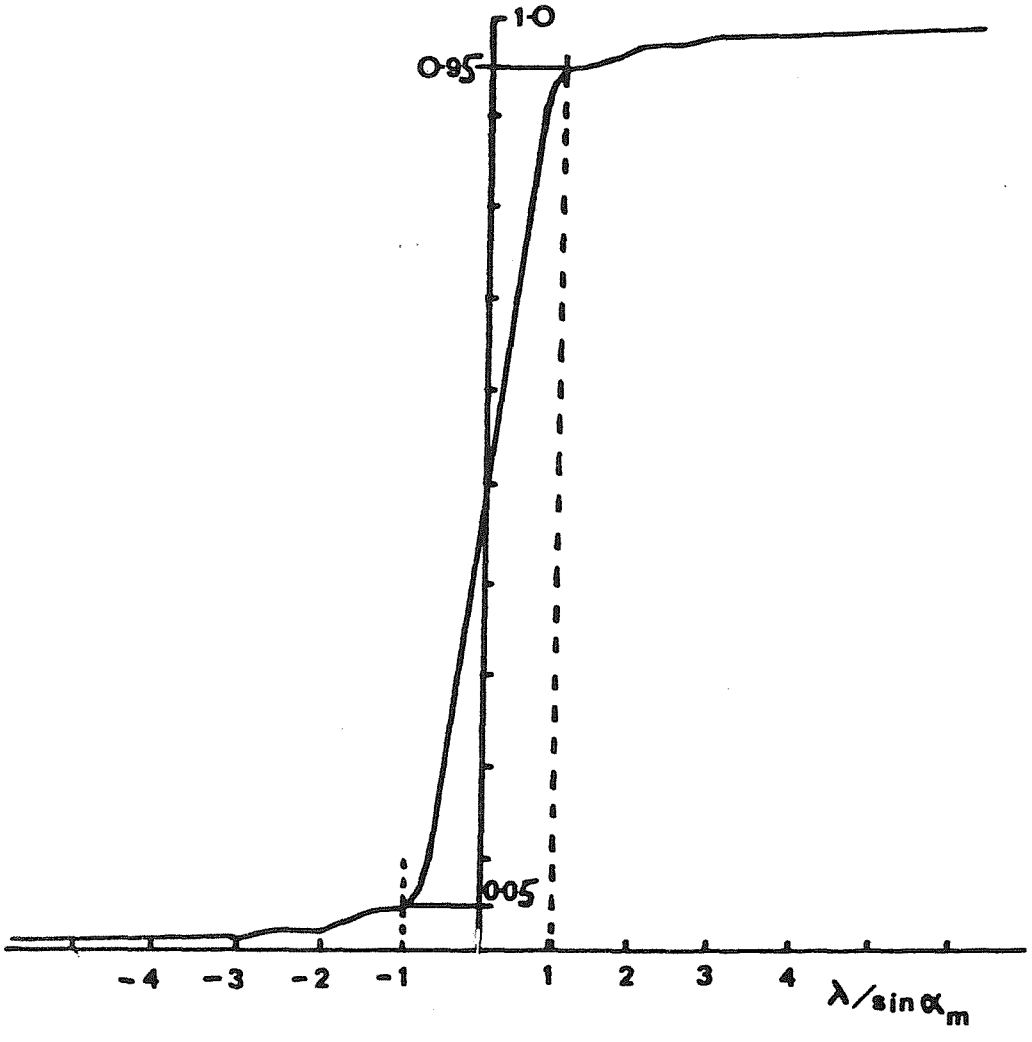

FIG.6.14.

COMPARISON OF MEASURED LEVELS

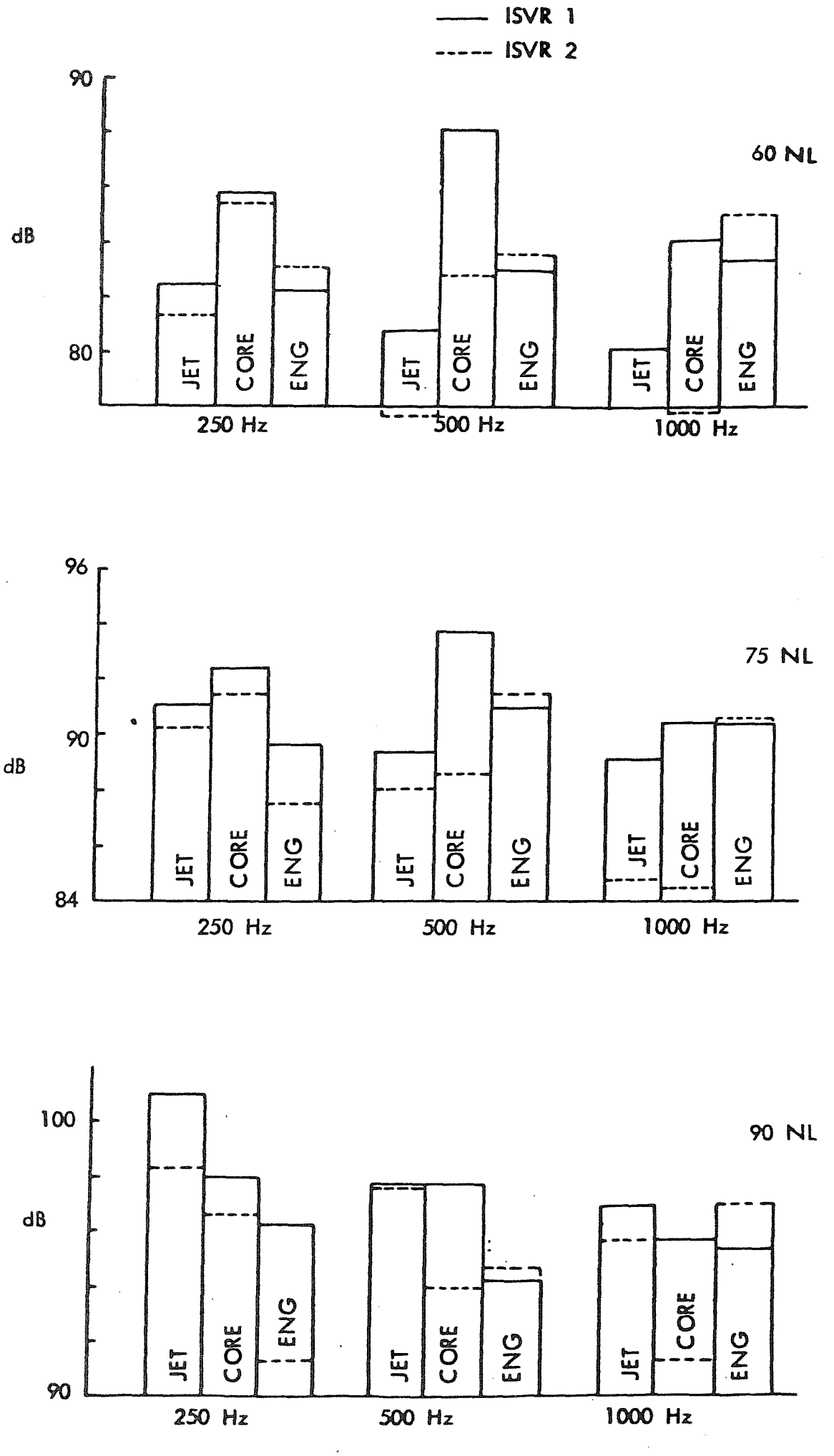

FIG. 6.15.

Attenuation of Tailpipe Noise by Bulk Absorber vs. frequency

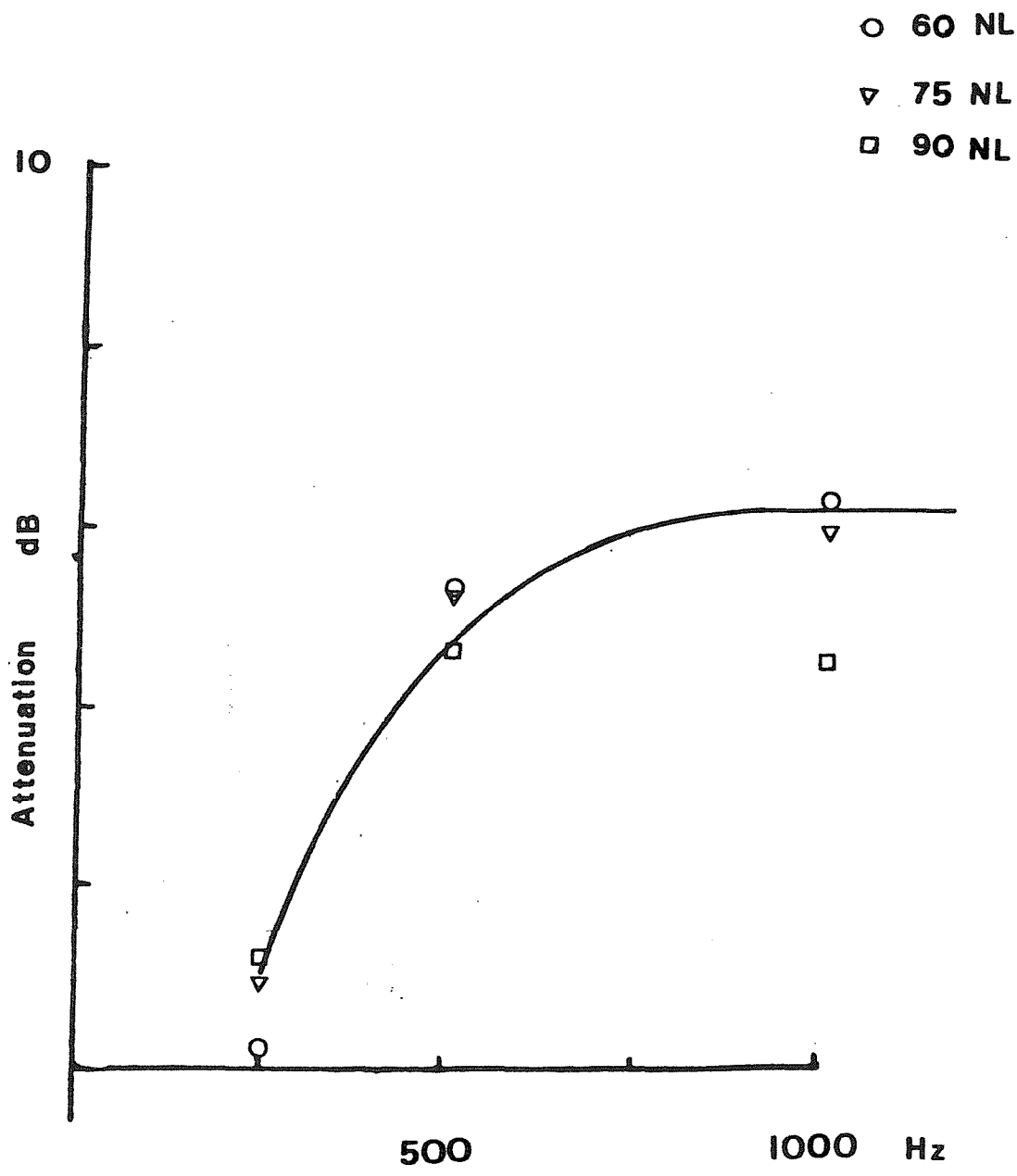

FIG.6.16.

Measured Levels of Jet Noise vs. Engine Condition

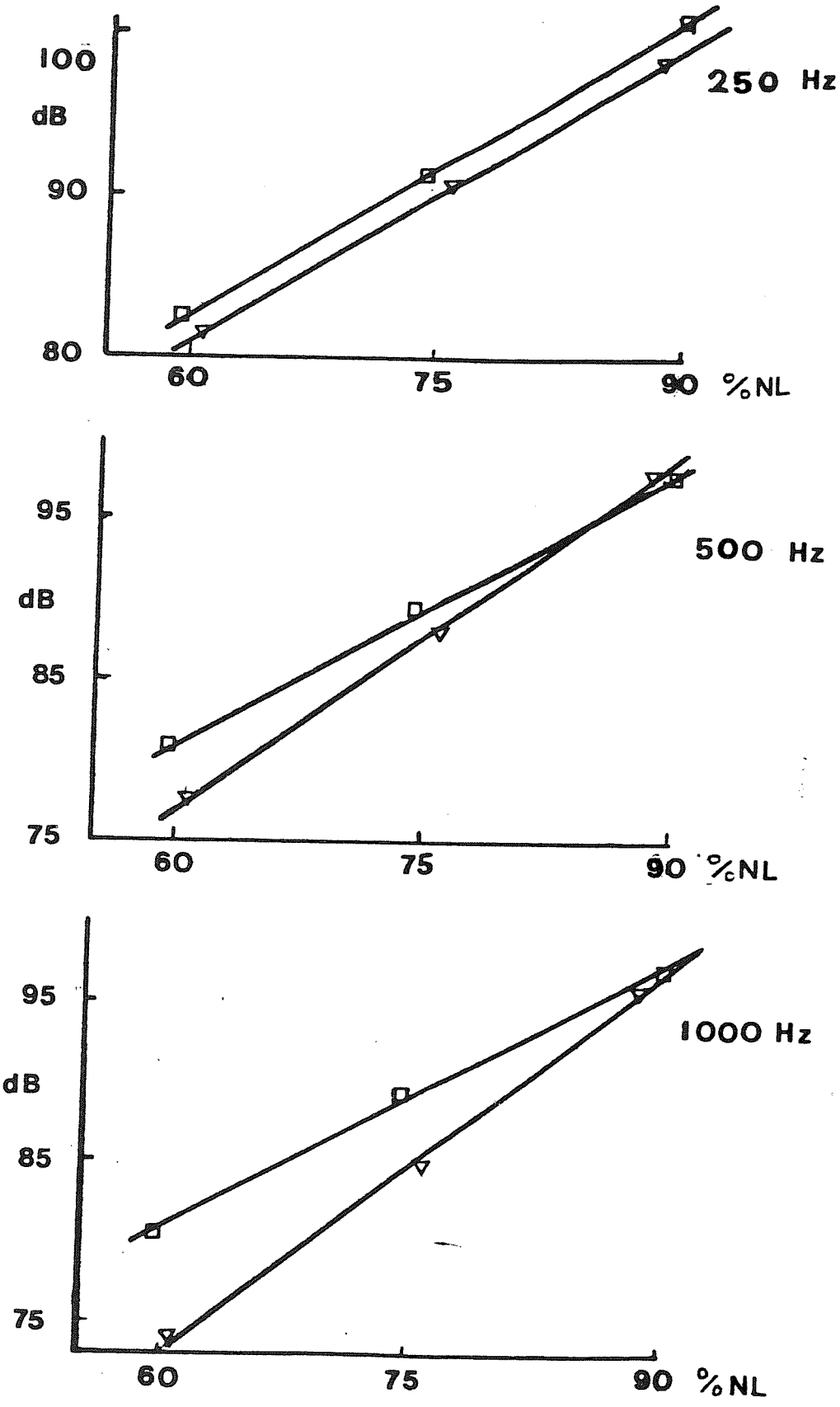

FIG.6.17.

ATTENUATION OF JET NOISE
BY BULK ABSORBER VS FREQUENCY